

Measurements and Predictions of HF Ground Wave Radio Propagation Over Irregular, Inhomogeneous Terrain

J.E. Adams
J.C. Carroll
E.A. Costa
D.R. Ebaugh, Jr.
J.R. Godwin
E.J. Haakinson
D.H. Layton
D. Smith



U.S. DEPARTMENT OF COMMERCE
Malcolm Baldrige, Secretary

David J. Markey, Assistant Secretary
for Communications and Information

July 1984



TABLE OF CONTENTS

	Page
ABSTRACT	1
1. INTRODUCTION	2
1.1 Background and Objectives	2
1.2 Approach for Measurements and Analysis	2
1.3 Scope	4
2. MEASUREMENT FREQUENCIES AND CONDITIONS	5
3. MEASUREMENT SITE AND PATHS	5
3.1 Selected Site	5
3.2 Path Descriptions and Features	5
4. TERRAIN AND OBSTACLE EFFECTS DISCUSSION	9
5. PROPAGATION MEASUREMENT RESULTS	13
5.1 Measurement Description	13
5.2 Raw Signal Level Measurements	16
5.3 Processed Measurements and Computed Path Loss Results	16
6. GROUND CONSTANT CALCULATIONS	49
6.1 Background	49
6.2 Experimental Results	49
7. HF GROUND WAVE PREDICTIONS	51
7.1 Background	51
7.2 Inputs to the Model	51
7.3 Predictions	58
8. ANALYSIS OF MEASURED AND PREDICTED PROPAGATION LOSSES	59
8.1 Measured Propagation Losses	69
8.2 Measured Ground Constants	72
8.3 Predicted Propagation Losses	76
9. CONCLUSIONS	77
10. REFERENCES	79
APPENDIX A: THE PROPAGATION MEASUREMENT SYSTEM AND PROCEDURE	80
A.1 Introduction	80
A.2 Transmitter System	80
A.3 Receiver System	89

TABLE OF CONTENTS (Cont.)

APPENDIX B: GROUND CONSTANTS MEASUREMENT	104
B.1 Introduction	104
B.2 Operation	104
B.3 Equipment Description	113
B.3.1 Antenna Design	113
B.3.2 Receiver Design	115
B.3.3 Transmitter and Transmitter Antenna	123
B.3.4 Power Supplies	123
B.4 Measurement Process	123
B.5 References	126
APPENDIX C: AUTOMATED GROUND CONSTANTS MEASUREMENT INSTRUMENTATION	127
C.1 Introduction	127
C.2 Antenna Design	129
C.3 Receiver Design	133
C.4 Analog-to-Digital Conversion	133
C.5 Fiber Optic Link	135
C.6 Power Supplies	135
C.7 Antenna Rotation Control	135
C.8 Program Control and Data Reduction	137
C.9 References	137
APPENDIX D: MONOPULSE RECEIVER	137

LIST OF FIGURES

Figure		Page
1.	Transmitter site at Boulder, Colorado.	6
2.	Transmitter van and antenna.	7
3.	Topographic map showing transmitter site and measurement paths.	8
4.	Photograph of a portion of the East Path.	10
5.	Terrain profiles from a digitized terrain data base for the East and South Paths.	11
6.	Terrain profile for the North Path.	12
7.	Relative permittivity and conductivity as a function of frequency (CCIR, 1982a).	14
8.	Skin depth as a function of frequency (CCIR, 1982a).	15
9.	Scatter plots of measured signal levels along the East Path, 5.25 and 7.50 MHz.	17
10.	Scatter plots of measured signal levels along the East Path, 11.5 and 28.0 MHz.	18
11.	Plots of the median noise power at 5.25 and 11.5 MHz along the East Path measured at the input to the spectrum analyzer in a 1 kHz bandwidth with a system sensitivity of -110 dBm.	19
12.	Plot of the median noise power at 28 MHz along the East Path measured at the input to the spectrum analyzer in a 1 kHz bandwidth with a system sensitivity of -110 dBm.	20
13.	Plots of median received signal level measured along the South Path at 5.25 MHz.	21
14.	Plots of median received signal level measured along the South Path at 7.50 MHz.	22
15.	Plots of median received signal level measured along the South Path at 11.50 MHz.	23
16.	Plots of median received signal level measured along the South Path at 28.00 MHz.	24
17.	Plots of median received signal level measured along the East Path with no snow cover at 5.25 MHz.	25
18.	Plots of median received signal level measured along the East Path with no snow cover at 7.50 MHz.	26

19.	Plots of median received signal level measured along the East Path with no snow cover at 11.50 MHz.	27
20.	Plots of median received signal level measured along the East Path with no snow cover at 28.00 MHz.	28
21.	Plots of median received signal level measured along the East Path with snow cover at 5.25 MHz.	29
22.	Plots of median received signal level measured along the East Path with snow cover at 7.50 MHz.	30
23.	Plots of median received signal level measured along the East Path with snow cover at 11.50 MHz.	31
24.	Plots of median received signal level measured along the East Path with snow cover at 28.00 MHz.	32
25.	Plots of median, upper, and lower decile path loss measured along the South Path at 5.25 MHz.	33
26.	Plots of median, upper, and lower decile path loss measured along the South Path at 7.50 MHz.	34
27.	Plots of median, upper, and lower decile path loss measured along the South Path at 11.50 MHz.	35
28.	Plots of median, upper, and lower decile path loss measured along the South Path at 28.00 MHz.	36
29.	Plots of median, upper, and lower decile path loss measured along the East Path without snow cover at 5.25 MHz.	37
30.	Plots of median, upper, and lower decile path loss measured along the East Path without snow cover at 7.50 MHz.	38
31.	Plots of median, upper, and lower decile path loss measured along the East Path without snow cover at 11.50 MHz.	39
32.	Plots of median, upper, and lower decile path loss measured along the East Path without snow cover at 28.00 MHz.	40
33.	Plots of median, upper, and lower decile path loss measured along the East Path with snow cover at 5.25 MHz.	41
34.	Plots of median, upper, and lower decile path loss measured along the East Path with snow cover at 7.50 MHz.	42
35.	Plots of median, upper, and lower decile path loss measured along the East Path with snow cover at 11.50 MHz.	43
36.	Plots of median, upper, and lower decile path loss measured along the East Path with snow cover at 28.00 MHz.	44

37.	Plots of median, upper, and lower decile path loss measured along the North Path at 5.25 and 7.50 MHz.	45
38.	Plots of median, upper, and lower decile path loss measured along the North Path at 11.50 and 28.00 MHz.	46
39.	Plots of median, upper, and lower decile path loss measured along the Mountain Path at 5.25 and 7.50 MHz.	47
40.	Plots of median, upper, and lower decile path loss measured along the Mountain Path at 11.50 and 28.00 MHz.	48
41.	Elliptical polarization of the electric vector at the surface of an earth that is not a perfect conductor.	50
42.	Site map for wave-tilt measurements.	52
43.	28 MHz wave-tilt measurement results plotted on families of constant relative permittivity and conductivity curves.	54
44.	11.54 MHz wave-tilt measurement results plotted on families of constant relative permittivity and conductivity curves.	55
45.	7.5 MHz wave-tilt measurement results plotted on families of constant relative permittivity and conductivity curves.	56
46.	5.25 MHz wave-tilt measurement results plotted on families of constant relative permittivity and conductivity curves.	57
47.	Predicted and measured median loss for the East Path at 5.25 and 7.5 MHz.	60
48.	Predicted and measured median loss for the East Path at 7.5 and 11.5 MHz.	61
49.	Predicted and measured median loss for the East Path at 11.5 and 28 MHz.	62
50.	Predicted and measured median loss for the East Path at 28 MHz.	63
51.	Predicted and measured median loss for the South Path at 5.25 and 7.5 MHz.	64
52.	Predicted and measured median loss for the South Path at 11.5 and 28 MHz.	65
53.	Predicted and measured median loss for the South Path at 28 MHz.	66
54.	Predicted and measured median loss for the North Path at 5.25 and 7.5 MHz.	67
55.	Predicted and measured median loss for the North Path at 11.5 and 28 MHz.	68

56.	Signal level variation over a short distance 1.1 to 2.1 km from the transmitter at 7.5 MHz.	73
57.	Signal level variation over a short distance 1.0 to 2.0 km from the transmitter at 11.5 MHz.	74
58.	Signal level variation over a short distance 15.3 to 16.3 km from the transmitter at 7.5 MHz.	75
A-1.	Ground wave measurement system block diagram.	81
A-2.	Transmitter system block diagram.	81
A-3.	Adjustable length vertical monopole transmitter antenna with ground screen.	83
A-4a.	Transmitter site map. Location of antenna, ground screen, roads, and buildings.	84
A-4b.	Location of electrical lines.	85
A-4c.	Ground screen and radials where field strengths were measured.	86
A-5.	Receiver and data collection system block diagram.	90
A-6.	Receiver and data collection van with an active antenna.	91
A-7.	Antenna pattern measurement system block diagram.	93
A-8.	Pattern measurements of an active antenna mounted on a van for 3 to 30 MHz.	95-101
A-9.	Pattern measurements of a passive antenna mounted on a van for 5 to 28 MHz.	102-103
B-1.	Receiver/antenna and rotation assembly.	105
B-2.	Overall wave-tilt measurement system.	106
B-3.	Receiver test stand.	107
B-4.	Photograph of receiver and digital multimeter.	108
B-5.	Photograph of wave-tilt system--front view with antenna oriented for minimum E-field measurement.	109
B-6.	Photograph of wave-tilt system--front view with antenna oriented for maximum E-field measurement.	110
B-7.	Photograph of wave-tilt system--side view.	111
B-8.	Photograph of receiver antenna and matching balun.	112

B-9.	Antenna resistance and reactance for a monopole above a ground plane [reprinted with permission from the Antenna Engineering Handbook, Jasik, H., Figures 3-3 and 3-4, McGraw-Hill Book Company (1961)].	114
B-10.	Receiver antenna matching balun [reprinted with permission from the Radio Amateur's Handbook, Figure 13-11C, ARRL (1969)].	116
B-11.	Receiver antenna and matching balun.	117
B-12.	Receiver block diagram [reprinted with permission from the Sony Corporation, Audio Group, Park Ridge, NJ (1982)].	118
B-13.	Receiver calibration curve for 28 MHz.	119
B-14.	Receiver calibration curve for 11.54 MHz.	120
B-15.	Receiver calibration curve for 7.5 MHz.	121
B-16.	Receiver calibration curve for 5.25 MHz.	122
B-17.	Photograph of transmitter antenna in open field to the south of the Department of Commerce Radio Building in Boulder, Colorado.	124
C-1.	Diagram of automated receiver for wave-tilt measurements.	128
C-2.	Cylindrical dipole receiver antenna mounted on gear assembly.	130
C-3.	Biconical dipole receiver antenna mounted on gear assembly.	131
C-4.	Antenna resistance and reactance for a conical monopole above a ground plane [reprinted with permission from the Antenna Engineering Handbook, Jasik, H., Figures 3-13, McGraw-Hill Book Company (1961)].	132
C-5.	Analog-to-Digital converter block diagram.	134
C-6.	Fiber-optic link block diagram.	136
D-1.	Block diagram of the pseudorandom noise transmitter.	138
D-2.	Block diagram of the pseudorandom noise receiver.	139

LIST OF TABLES

Table		Page
1	Ground Constants by the Wave-Tilt Method	53
2	Variation in Measured Median Path Loss vs. Frequency and Distance	70
3	Variation in Differences Between Measured Upper and Lower Decile Path Loss vs. Frequency and Distance	71
4	Range of Measured Ground Constant Values	72
5	Range of Ground Constant Values which Cause the Predictions to Bound the Measured Losses	76
A-1	Transmitter Antenna Gain Measurements	87-88
A-2	Receiver Antenna Gain as a Function of Frequency	94

MEASUREMENTS AND PREDICTIONS OF HF GROUND WAVE RADIO
PROPAGATION OVER IRREGULAR, INHOMOGENEOUS TERRAIN

J. E. Adams, J. C. Carroll, E. A. Costa, D. R. Ebaugh, Jr.,
J. R. Godwin, E. J. Haakinson, D. H. Layton, and D. Smith*

Measurements of radio propagation path loss were made over four paths in the 3 to 30 MHz band. The paths were of lengths up to 45 km in the Boulder, CO, area. They ranged from smooth to mountainous terrain, from open areas with few or no man-made structures to suburban areas with building heights up to three stories, and from open spaces with little vegetation to heavily forested regions. On one path, measurements were made with and without snow cover. The measurements were made in the daytime and because of the short paths, the primary mode of propagation was ground wave. Measurements of the ground constants at each of the four measurement frequencies were made at the transmitter site using the wave-tilt measurement technique.

One objective of gathering the HF propagation data was to compare the measurement results with ground wave propagation predictions made by a computer program that used the path profile, ground constants, and frequency as prediction parameters. The results of the predictions and the comparisons with the measured data are discussed.

Another objective of the measurement project was to describe the measurement technique and procedure in sufficient detail so that similar measurements could be made by others. The measurements were made with a fixed transmitter and mobile receiver and data collection system. Since measurements were made continuously while the receiver van was in motion, position location information was determined by recording the vehicle's speedometer shaft rotation. Antenna gain measurements were made and are presented for the transmitter antenna on a partial ground screen and for the receiver antenna mounted on a van.

Key words: HF ground wave; predictions and measurements; HF antenna with ground screen measurements; HF antenna on mobile measurements; propagation path loss; ground constants measurement; wave-tilt technique; irregular, inhomogeneous terrain

*The authors are with the Institute for Telecommunication Sciences, National Telecommunications and Information Administration, U.S. Department of Commerce, Boulder, CO 80303.

1. INTRODUCTION

1.1 Background and Objectives

High-frequency (HF) ground wave propagation is being considered as a method for reliable communications during periods of severe disturbances of the ionosphere, such as during nuclear warfare. In order to develop communication systems that use HF ground wave efficiently and effectively, system designers need an accurate method of predicting received signal strengths.

The Institute for Telecommunication Sciences (ITS) has developed a theoretical model for predicting HF ground wave propagation over irregular, inhomogeneous terrain with forests, urban areas, and snow cover (Hill, 1982). The model, named WAGSLAB, is a generalization of the ITS program WAGNER (Ott, 1971; Ott et al., 1979); WAGSLAB allows for the effect of lossy, anisotropic slabs over the irregular terrain. The slab parameters (height, length, and electrical constants) can be chosen to match those of the foliage, urban area, or snow cover that is on the terrain along the path. In addition, the ground constants can be specified as in the WAGNER program.

The objective has been to develop a measurement program that would adequately verify the model or provide the necessary information to make modifications to the model. Originally, the measurements were to be made over different conditions in the United States to demonstrate the model's ability to predict signal levels in a) flat terrain, forested areas, b) irregular terrain, forested areas, c) flat terrain, urban areas, etc. This report is limited to only the measurements and predictions of signal strengths for paths near Boulder, CO.

1.2 Approach for Measurements and Data Analysis

The approach used for the measurements and predictions program consisted of the following:

- a. Develop a propagation loss measurement system and procedure.

The original design called for a fixed, but transportable, transmitter along with a mobile receiver and data recording system. The transmitter

was to be controlled by a computer to transmit a sequenced series of cw transmissions in the 3-30 MHz band followed by a period of silence. The computer-controlled receiver and data collection system was to automatically tune to the correct frequency for the signal strengths and noise measurements, make a ground constants measurement, and record location and time data. This measurement system will be mentioned briefly in the report so that others may use the scheme, but this report discusses in detail the scaled-down measurement system we implemented and the measurements obtained.

These measurements used an available transmitter location near the Commerce Radio Building and a modified receiver van. The transmitter system consisted of a cw signal generator, a linear amplifier, and a monopole antenna over a ground screen that was elongated in the direction of one of the measurement paths. The receiver and data recording system consisted of an active and passive monopole antenna mounted atop a van, a spectrum analyzer for a receiver, and a computer with magnetic tape drive to control and record the received signal level data and position location data.

Since we are interested in knowing absolute received field strengths, the transmitter and the receiver systems were calibrated. Details of the propagation loss measurement system and its calibration are contained in Appendix A.

- b. Develop a ground and slab constants measurement system and procedure.

The requirements for the original electrical constants measurement system were that it be mobile and capable of making in situ measurements without disturbing the environment (e.g., drilling bore holes for core samples would not be acceptable). Several methods have been used by others with limited frequency range and questionable accuracy (IEEE, 1974). For the set of predictions used in this report, we have used the wave-tilt method of determining the electrical constants. Appendix B describes the technique and instrumentation for the measurements in detail. Appendix C describes an electrical constant measurement system that would automate the measurement process and increase the system's bandwidth.

- c. Select a measurement site and test frequencies.

The requirements for the single measurement site were that 1) it be accessible with enough clear area surrounding the transmitter for the installation of a wire-mesh ground screen, and 2) the paths away from the transmitter include a radial that is closely aligned with a road having little terrain irregularity and little foliage or urbanization. The latter requirement would allow us to compare the measurements and predictions against standard HF ground wave curves (CCIR, 1982a).

The test frequencies would have to be selected from those assigned to ITS and used on a noninterfering basis. Measurements would have to be made to ensure that local transmitters did not cause unacceptable interference to the desired signals.

- d. Record received signal levels and position data on selected paths.

After the installation of the ground screen at the transmitter site, field strength measurements at locations surrounding the transmitter were made at each test frequency for transmitter calibration. The receiver system was calibrated using an antenna range to measure the antenna patterns and using known field strengths to calibrate the receiver. After fix-tuning the transmitter and setting the power level, the receiver/data-recording van was driven along the selected paths while continuously recording data.

- e. Reduce the data and make comparisons with predictions.

The raw data was reduced to equivalent path transmission loss at each measurement point along the path. Statistics were computed for groups of closely spaced points to obtain median values; these values then were compared to the predicted losses using program WAGSLAB.

1.3 Scope

This report contains a description of the instrumentation used in making the HF ground wave propagation measurements and results of the measurements and predictions for one site with several measurement paths. As much as possible, we discuss effects and limitations of various components of the measurement system as they would relate to the efficiency of HF ground wave communications systems.

2. MEASUREMENT FREQUENCIES AND CONDITIONS

The test frequencies that were used for the measurements were among those already assigned to ITS by the Interdepartment Radio Advisory Committee in the 3 to 30 MHz range. Specifically, the assignments were 5.005-5.450 MHz, 7.300-8.815 MHz, 11.400-11.700 MHz, 11.975-12.330 MHz, and 27.540-28.000 MHz for 1000 watts on a noninterfering basis. The measurements for these tests were made during daylight hours to ensure that ground wave would dominate over sky wave for most of the measurements.

3. MEASUREMENT SITE AND PATHS

3.1 Selected Site

The site selected for the transmitter and transmitter antenna was an open field (located at 39 deg, 59 min, 42 sec N and 105 deg, 15 min, 34 sec W) on the site of the U.S. Department of Commerce Laboratories in Boulder, CO. The site is surrounded by one- and two-story homes with landscaping that includes several trees such as cottonwoods and evergreens on each lot. The land to the east is relatively flat, with suburban to rural environment and average to poor soil. The land to the north and south is more rolling, with the business district of Boulder to the north. The land to the west includes the foothills and the front range of the Rocky Mountains. The terrain becomes very rugged after only a few miles to the west of the site. Undeveloped areas to the east of the site usually are open pasture lands while those areas to the west are forested. Figures 1 and 2 show photographs of the transmitter site with the trailer and transmitter antenna.

3.2 Path Descriptions and Features

The heavy lines on the map shown in Figure 3 are the paths that were followed for the measurements. The terrain ruggedness is shown on the map with the terrain contours at 200 ft intervals.

East Path

The path that is straight east of the transmitter site (shown by star in Figure 3) is over relatively flat terrain with few man-made structures taller than two stories and with no forested areas. This was called the East Path, approximately 48 km (30 mi) in length from Boulder to Brighton, CO. It served as a control path against which we could compare the standard CCIR (1982a) HF

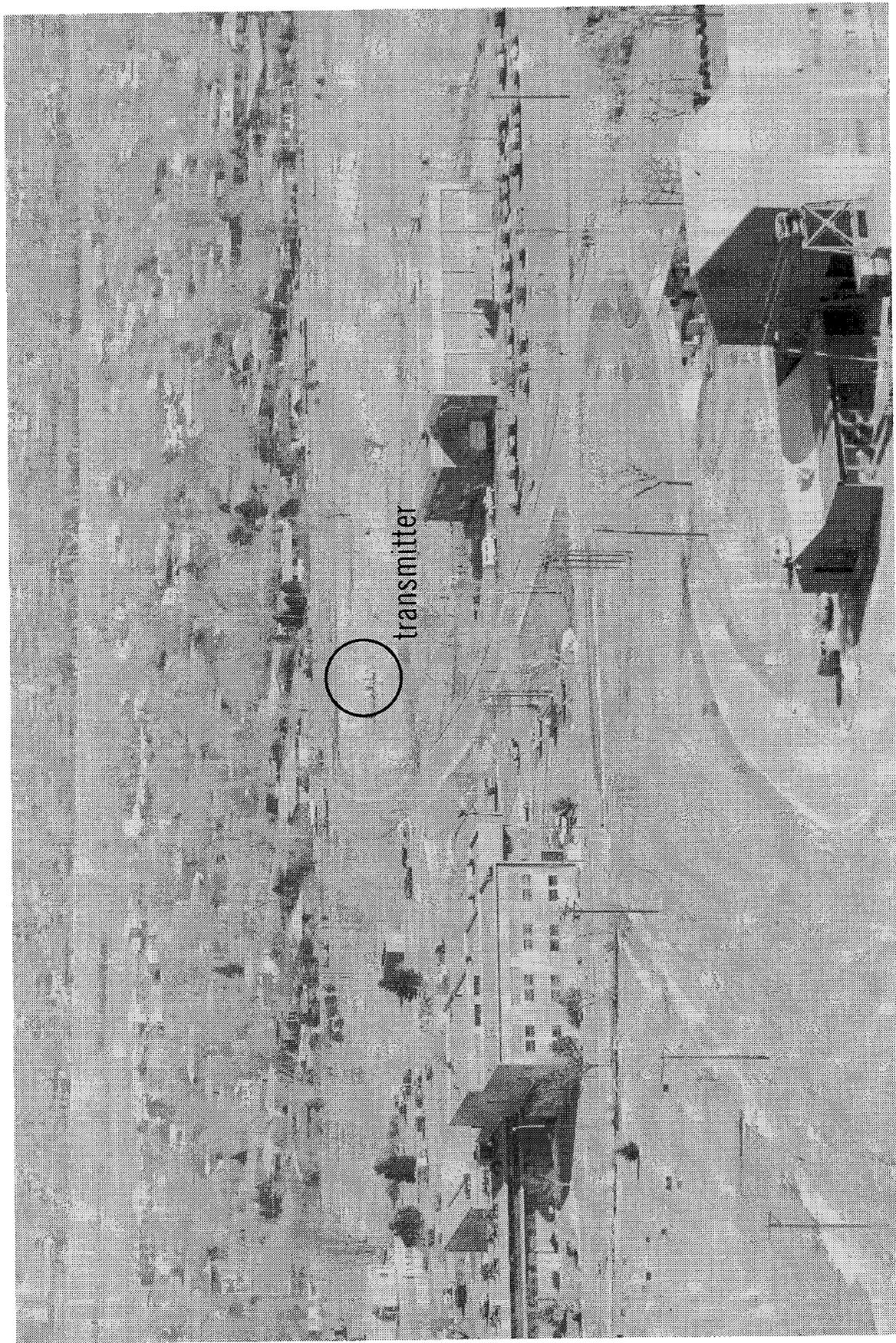


Figure 1. Transmitter site at Boulder, Colorado.

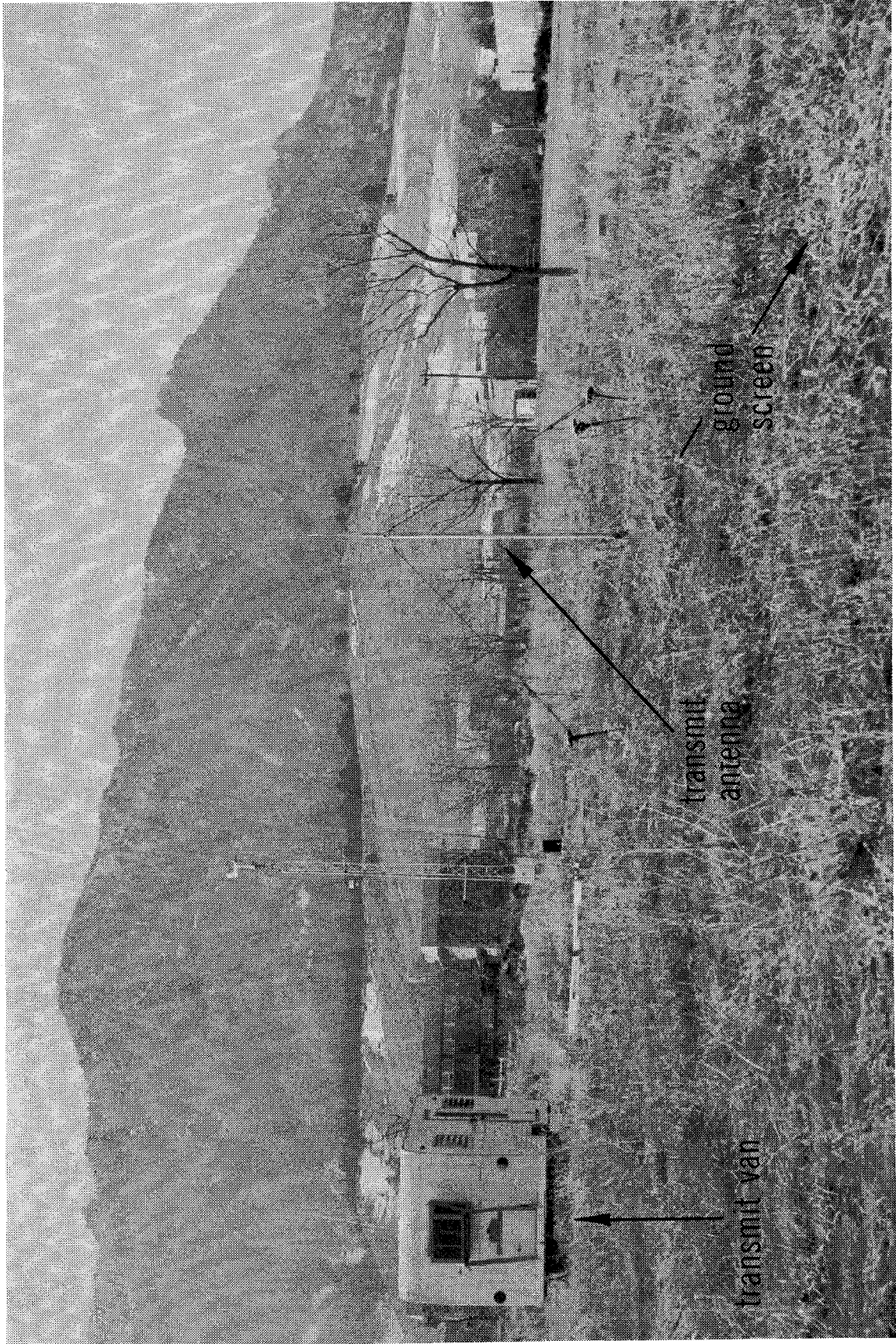


Figure 2. Transmitter van and antenna.

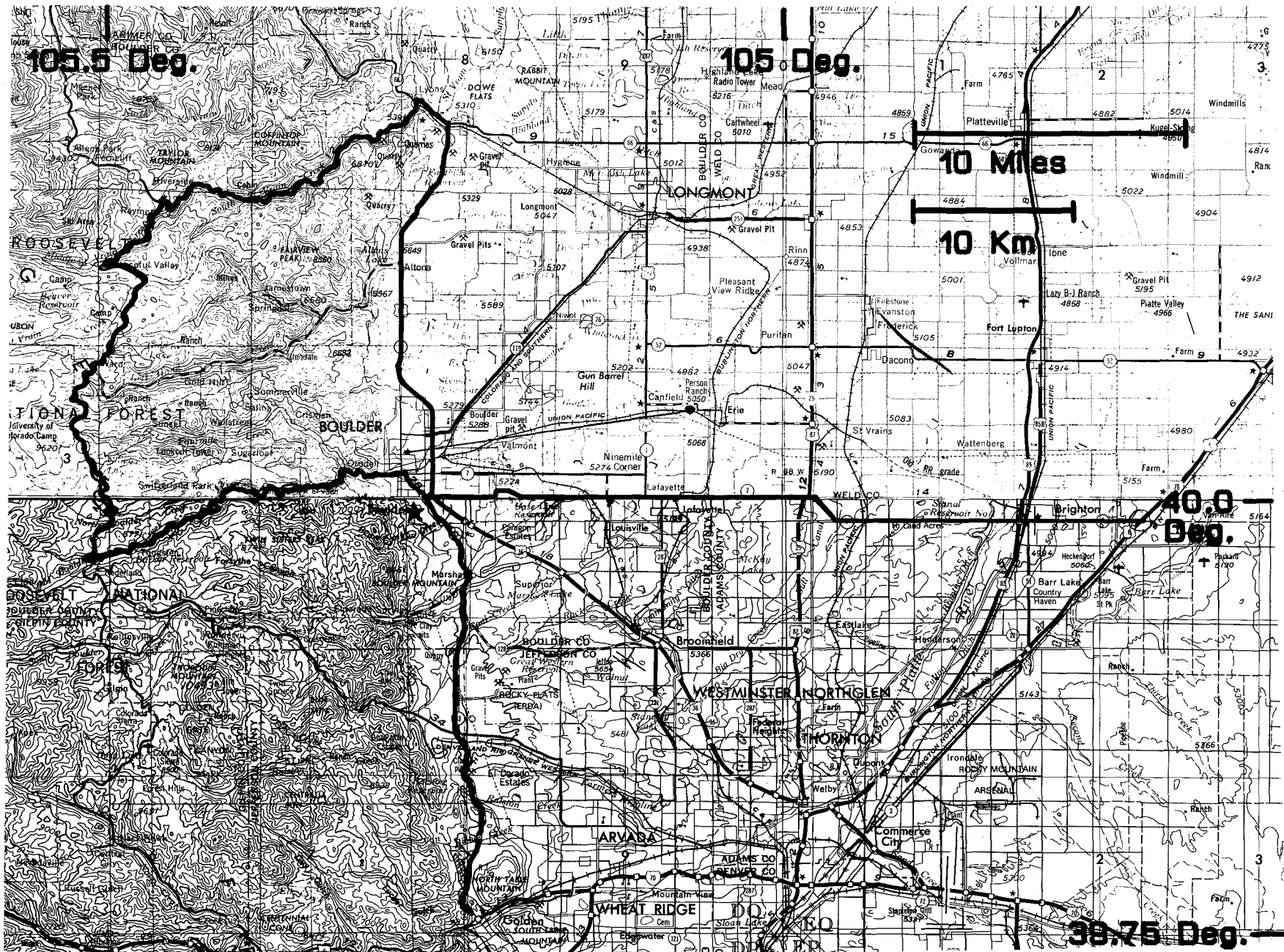


Figure 3. Topographic map showing transmitter site and measurement paths.

ground wave curves. Figure 4 shows the path from Boulder toward Brighton on the photograph.

Nineteen sets of measurements were made on this path: two on each of the four frequencies (while driving away from the transmitter and back towards the transmitter) with and without snow cover, and three noise runs (i.e., with no signal being transmitted) on 5.25, 11.5, and 28.0 MHz.

South Path

The South Path was over rolling terrain for approximately 24 km (15 mi) from Boulder to Golden, CO. Eight measurement sets were made on this path--two at each frequency, away from and back toward the transmitter.

North Path

The North Path was over relatively flat terrain from Boulder to Lyons, CO, for a distance of 20 km (12 mi). Four sets of measurements, one at each frequency, were made along this path.

Mountain Path

The path from Boulder to the west circling around to Lyons to the north was the mountain path. The loop is about 105 km (65 mi) in length and changes in elevation from 1525 to 3050 m (5000 to 10000 ft). Four sets of measurements were made on this path, one for each frequency.

Terrain Profiles

The terrain profiles were computed from digitized terrain data based on the U.S. Army 1 by 2 deg maps (National Geophysical Data Center, 1984). Figures 5 and 6 show the terrain profiles for the East, South, and North (Boulder to Lyons) paths.

4. TERRAIN AND OBSTACLE EFFECTS DISCUSSION

The wavelength at 5.25 MHz is approximately 57.1 m (187.5 ft) and at 28 MHz is about 10.7 m (35 ft). We would expect for this range of frequencies that natural objects, such as hills and forested areas, and man-made objects, such as buildings, would influence the received field from the transmitter by attenuating the direct path signal and by causing secondary signals which are reflections off buildings, hills, etc. We would expect to observe the direct

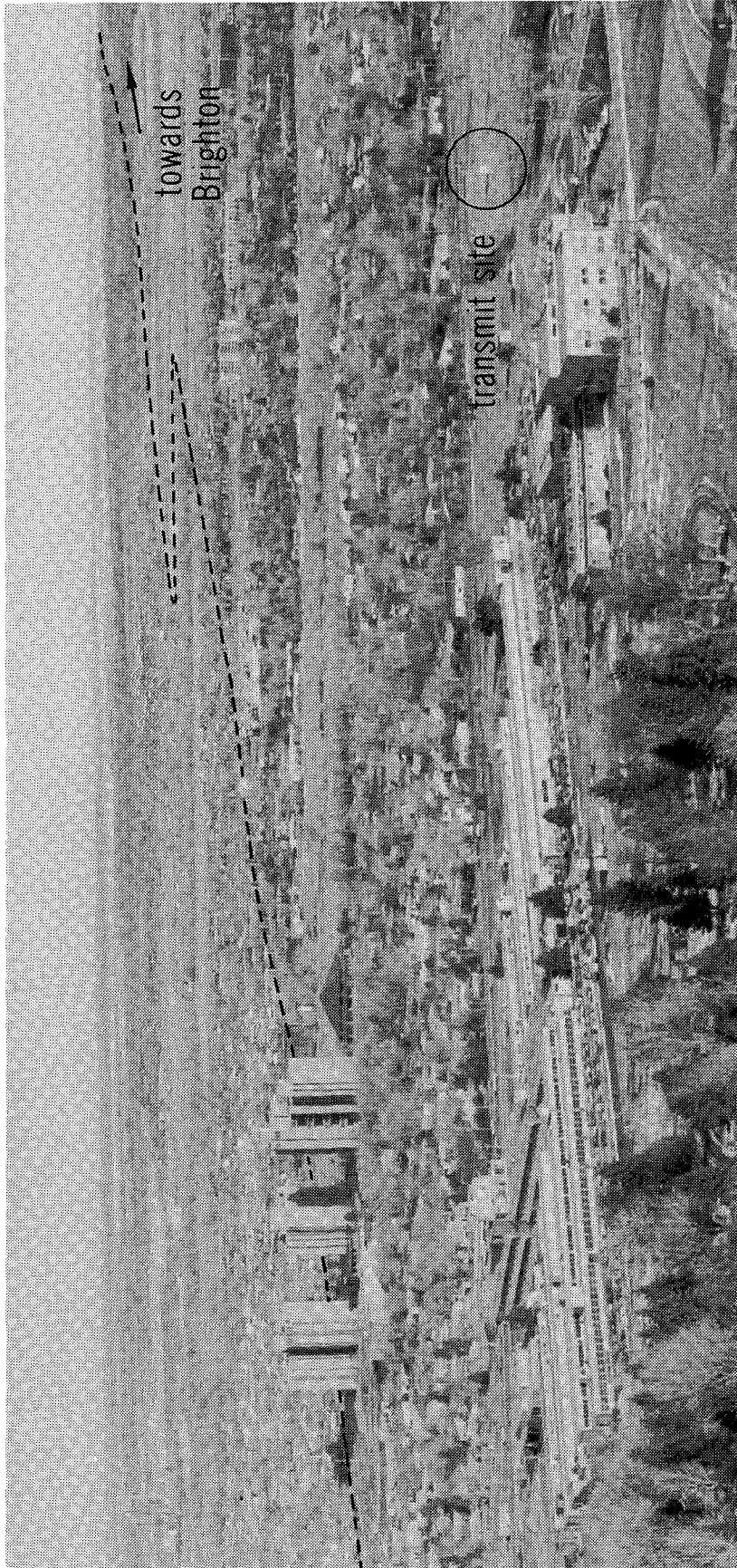


Figure 4. Photograph of a portion of the East Path.

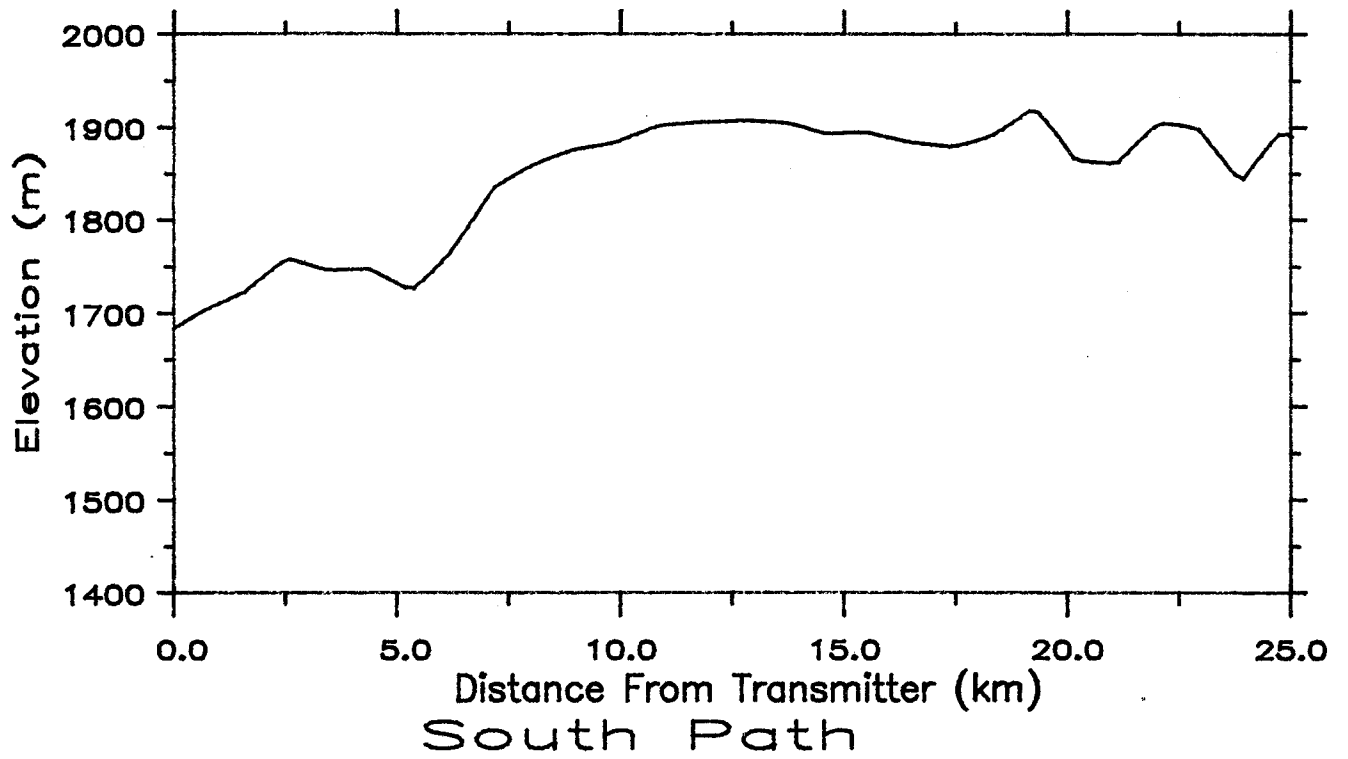
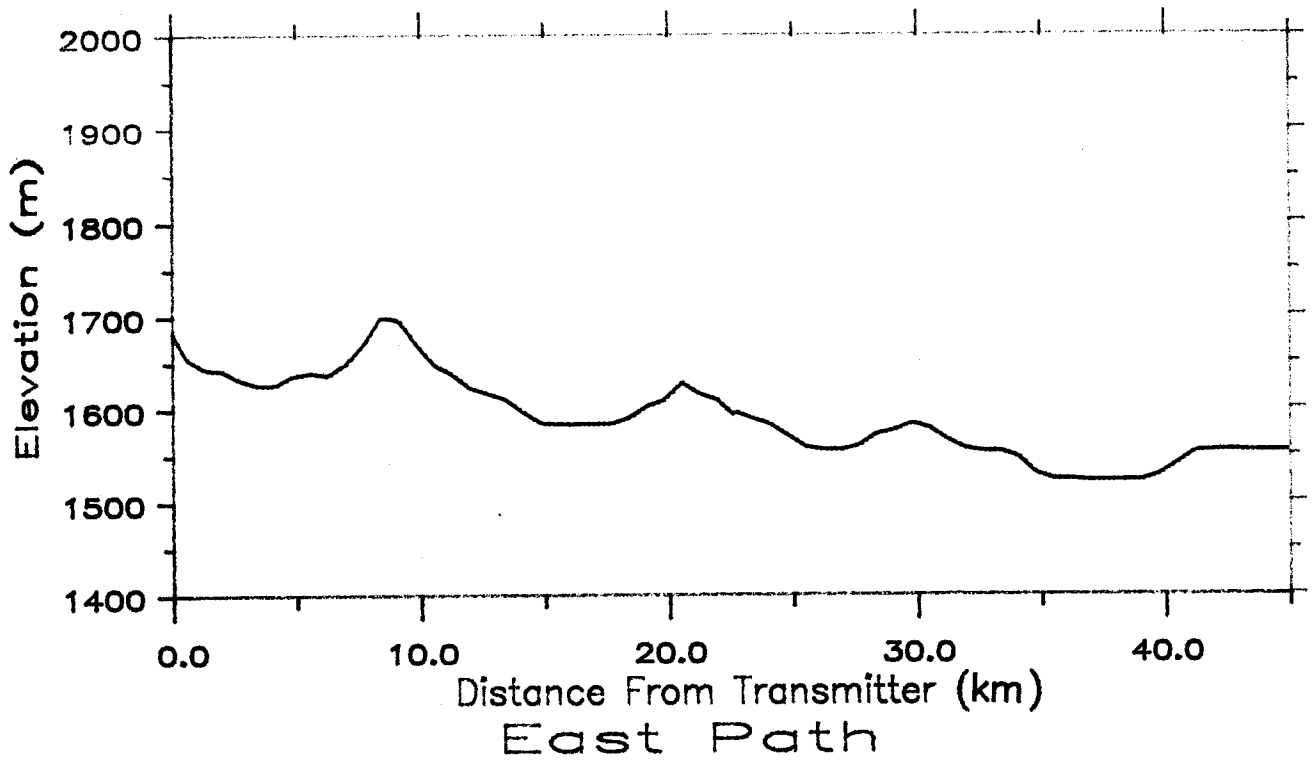


Figure 5. Terrain profiles from a digitized terrain data base for the East and South Paths.

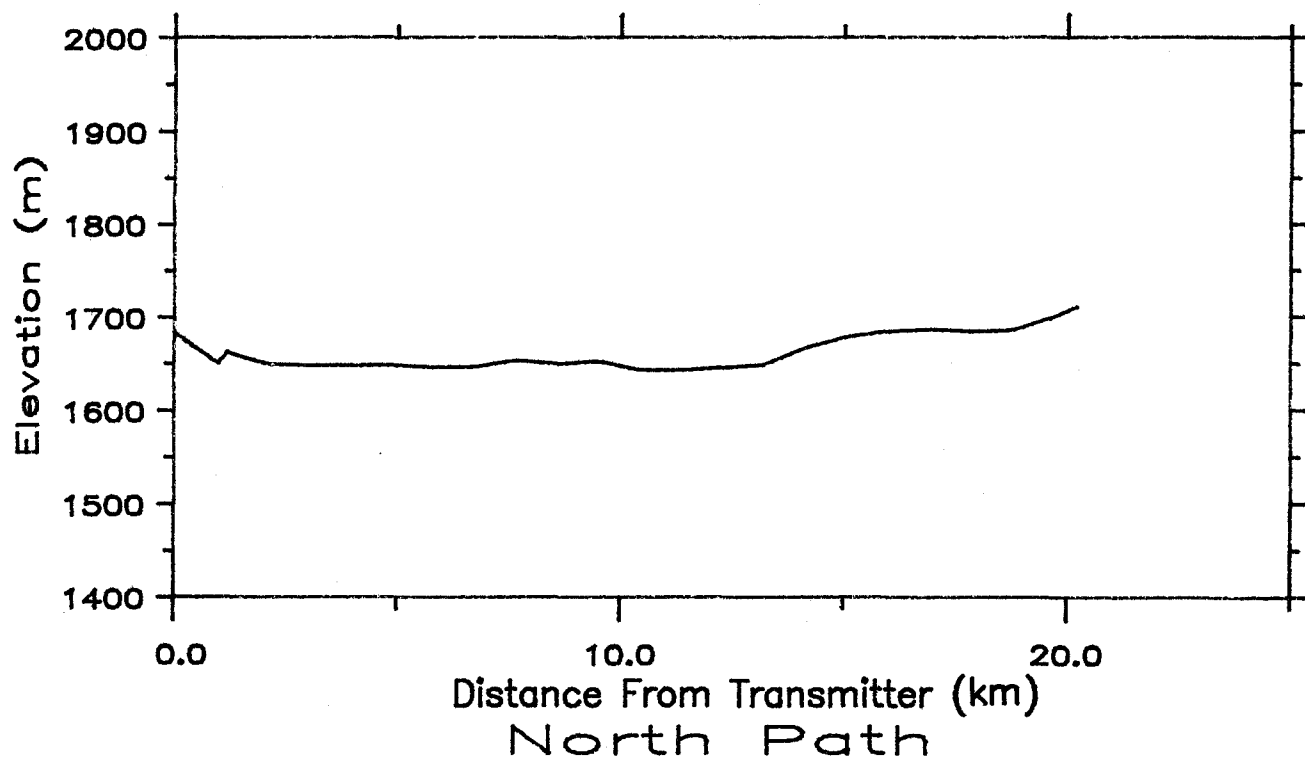


Figure 6. Terrain profile for the North Path.

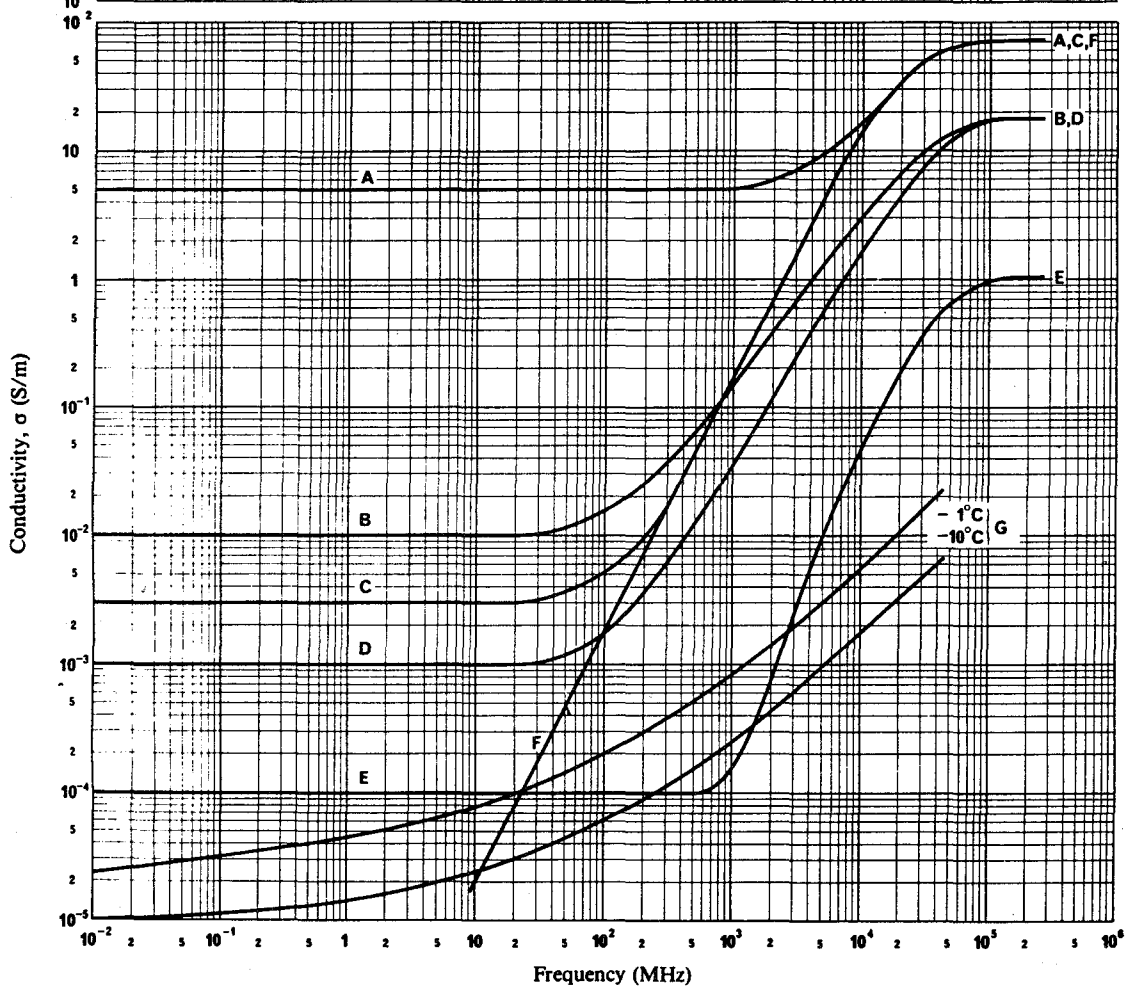
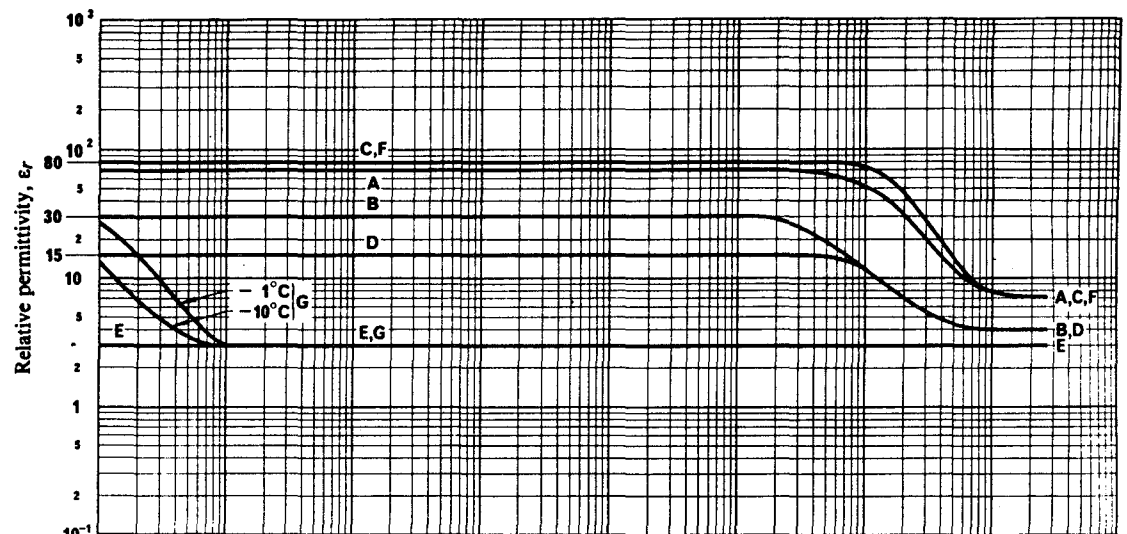
path signal as well as the reflected signals. This combination of direct and reflected signals results in measured values having Rayleigh or Rice-Nakagami distributions. As the prediction process only accounts for the two-dimensional terrain and slab features between the transmitter and receiver, the prediction estimates the direct signal without the addition of the multipath signals. Thus, in our comparison of the measured and predicted signals, the measured data are processed to provide the median value of the measured values within each distance increment.

Besides the terrain and slab profile, the prediction program requires information about the ground and slab electrical constants. The constants have been measured near the transmitter for four frequencies; however, there is no reliable calibration scheme to ensure that the values we have measured are accurate estimates of the true constants. The effect of the earth's crust or of the slab on the effective electrical constants actually depends on the depth of penetration of the radio signal into the earth or the slab. The depth to where the electric signal has fallen to $1/e$ of the incident signal is called the skin depth. Figures 7 and 8 show the effects of frequency on the ground constants and skin depth.

5. PROPAGATION MEASUREMENT RESULTS

5.1 Measurement Description

After calibrating the transmitter and receiver as described in Appendix A, the system was used to make propagation measurements along the paths described above. As the receiver/data collection van was driven along the path, the received signal power and the number of speedometer/odometer shaft revolutions were recorded. After the measurements were completed, the routes were digitized to provide coordinates along the path. When the data were reduced, calibration factors were computed to give the estimated distance traveled for each revolution of the speedometer shaft. This allowed us to determine the coordinate of each measurement point. Ideally, the calibration factors for each path would all be equal; the actual spread in values was less than 5 percent for the computed distance traveled per revolution of speedometer shaft. For some path segments, the calibration factor could not be computed (usually because of a tape drive malfunction); for these segments, an average of the other calibration factors from the same measurement set was used.



- A: sea water (average salinity), 20° C
- B: wet ground
- C: fresh water, 20° C
- D: medium dry ground
- E: very dry ground
- F: pure water, 20° C
- G: ice (fresh water)

Figure 7. Relative permittivity and conductivity as a function of frequency (CCIR, 1982a).

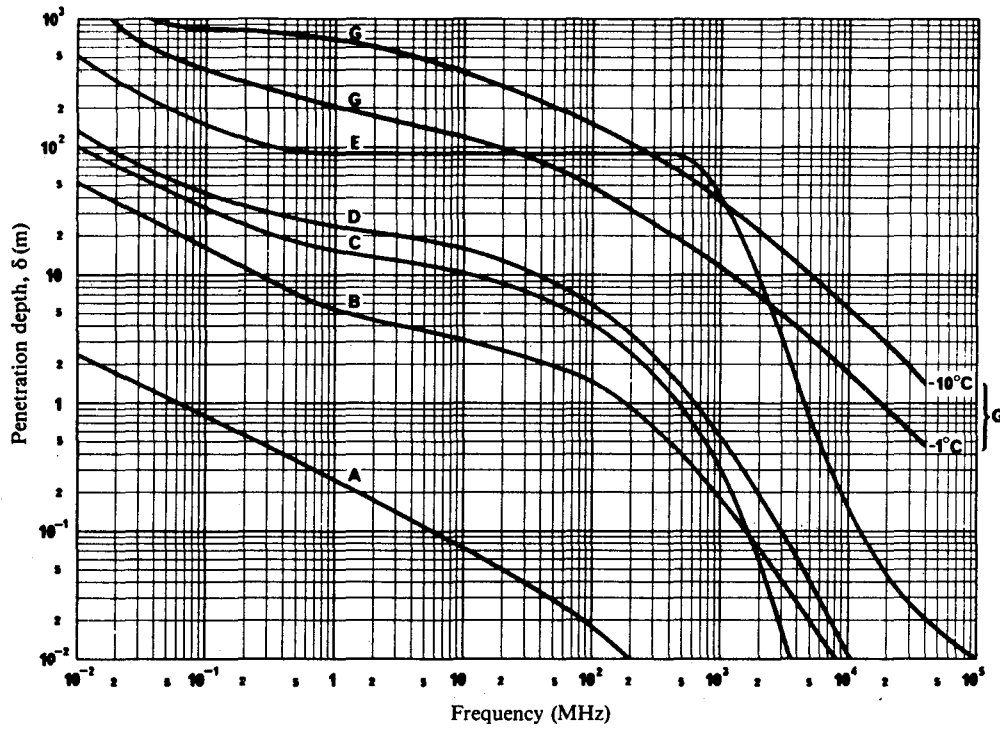


Figure 8. Skin depth as a function of frequency (CCIR, 1982a).

5.2 Raw Signal Level Measurements

Figures 9 and 10 show typical examples for each of the four frequencies of the raw signal levels in a 1 kHz bandwidth that were measured at the input to the spectrum analyzer in the receiver van. The received signal is the superposition of a number of signals that include the direct signal and other signals resulting from scattering, diffraction, and multipath. The effects of noise and unwanted signal interference also are included in these measurements.

The spectrum analyzer's noise level in a 1 kHz bandwidth was measured to be -110 dBm. Median external noise measurements are shown plotted in Figures 11 and 12. The noise measurements were made with the desired transmitter turned off. These measurements show that the measurement system's noise exceeded the measurable atmospheric and man-made noise.

5.3 Processed Measurements and Computed Path Loss Results

We divided each path into 0.16 km (0.1 mi) increments; within each increment we ordered all of the measured data so their statistics could be determined. Figures 13 through 24 show the median received signal level within each increment for the East and South paths. The upper plot for each frequency shows the data collected as the receiver was driven away from the transmitter; the lower plot shows the data collected as the receiver was driven back toward the transmitter. The measurements for Figures 17 through 20 were made with essentially no snow on the ground while those of Figures 21 through 24 were made after a snowstorm that left 0.15 to 0.3 m (0.5 to 1.0 ft) of snow cover.

To make comparisons of ground wave predictions with measurements, we need to remove the effects of equipment characteristics. The data were processed to remove the transmitter power, and the transmitter and receiver antenna gain patterns (as given in Appendix A). The result is the computed path loss and the plots are shown in Figures 25 through 40 for the East, South, North and Mountain paths. Note that the 11.5 MHz data along the Mountain Path in Figure 40 is relatively flat between 8 and 19 km. There was excessive attenuation in the receiver system that allowed the signal level to drop below system sensitivity. The problem was corrected later in the data collection as indicated by the data for distances from 19 to 26 km.

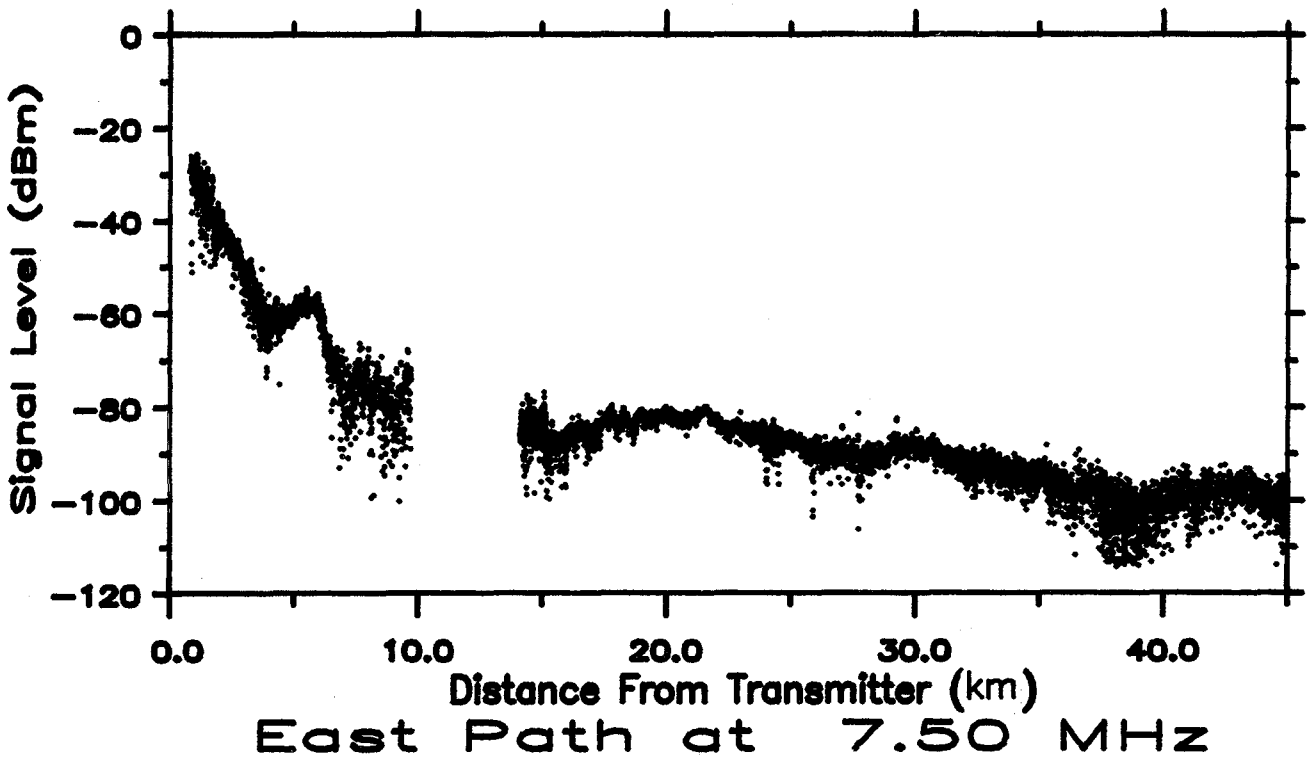
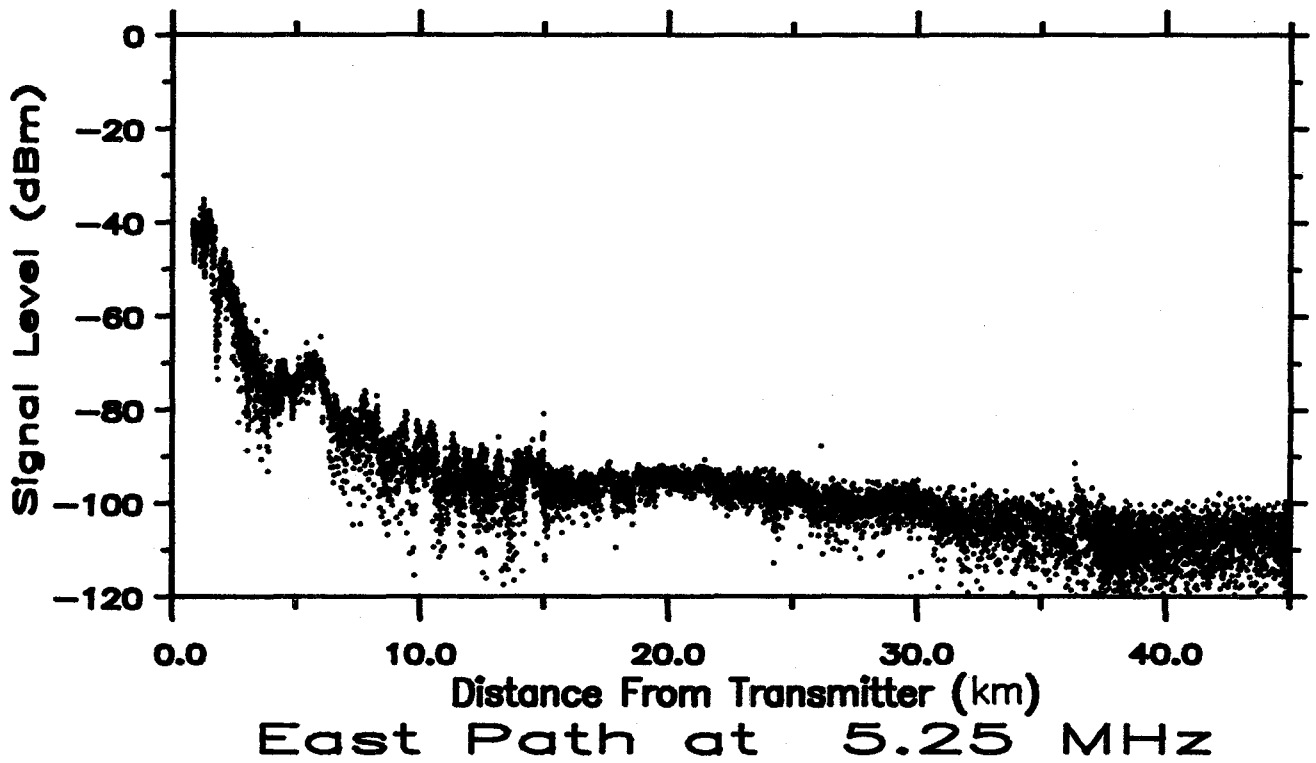


Figure 9. Scatter plots of measured signal levels along the East Path, 5.25 and 7.50 MHz.

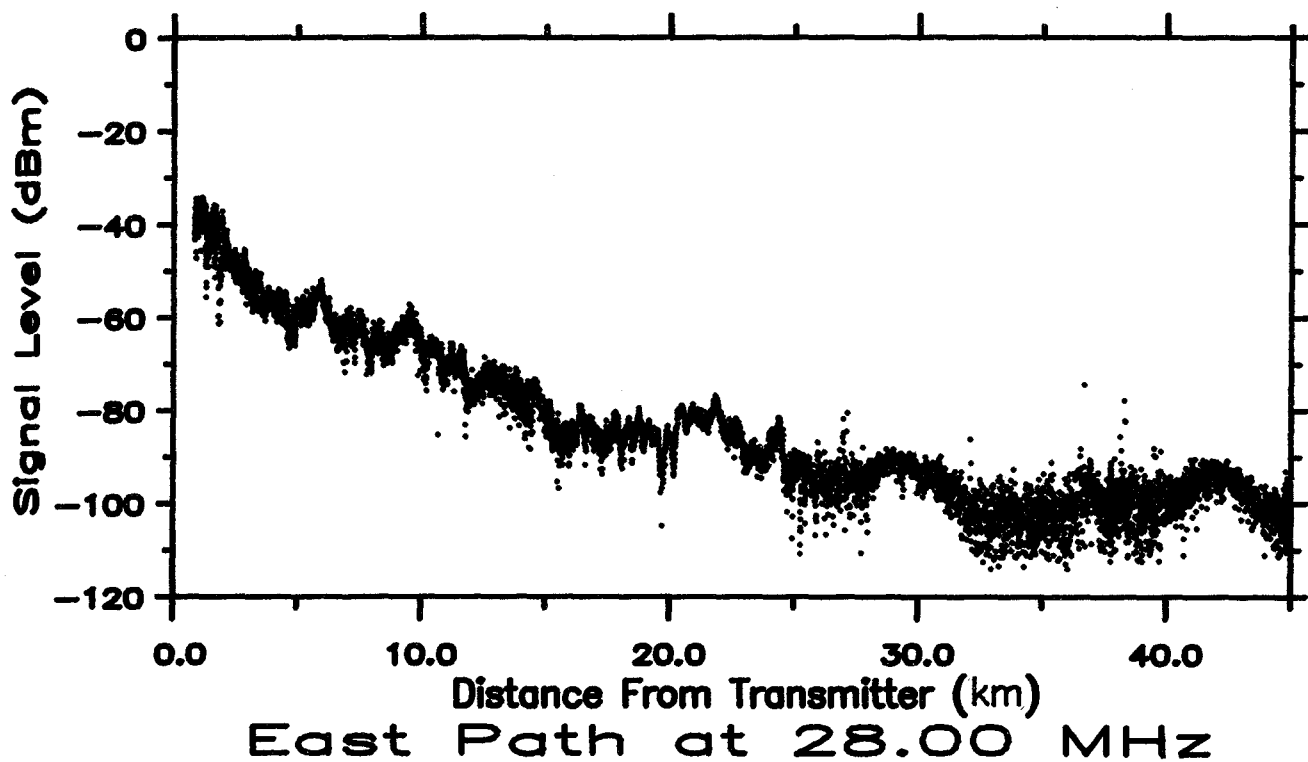
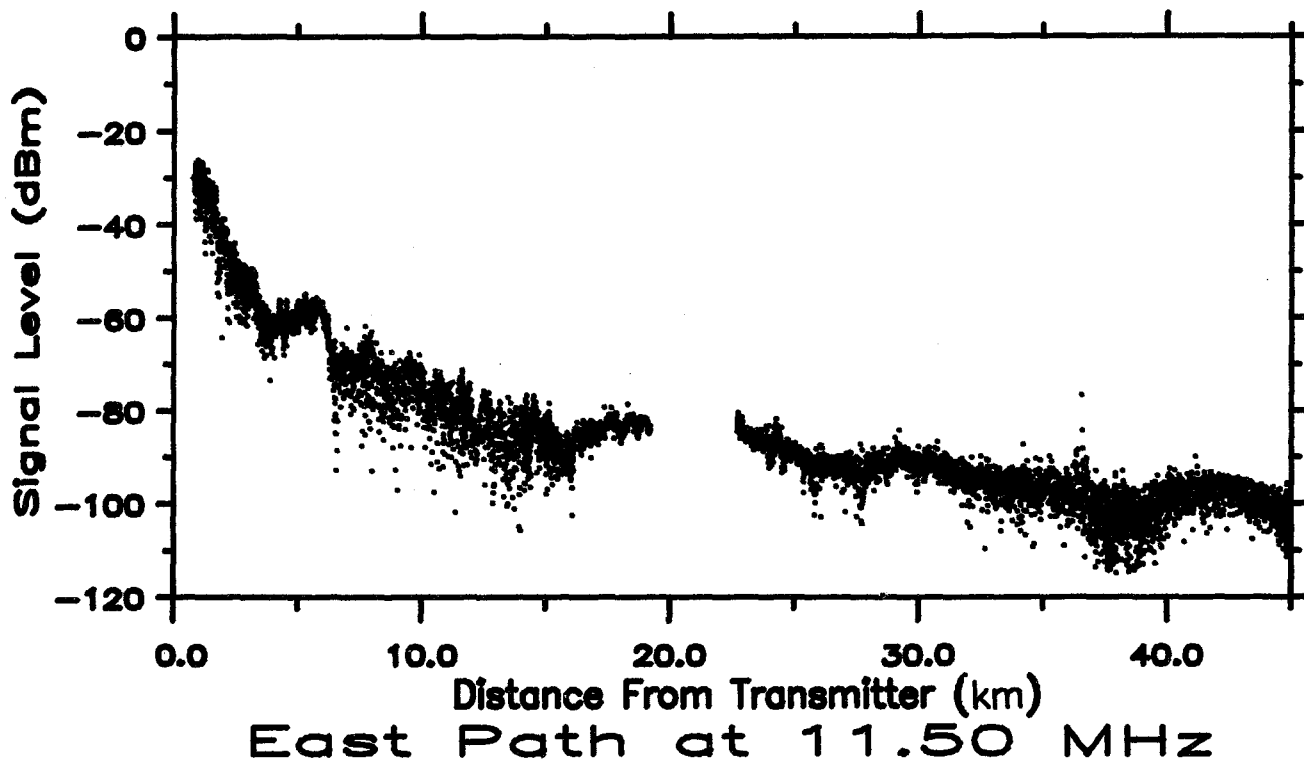


Figure 10. Scatter plots of measured signal levels along the East Path, 11.5 and 28.0 MHz.

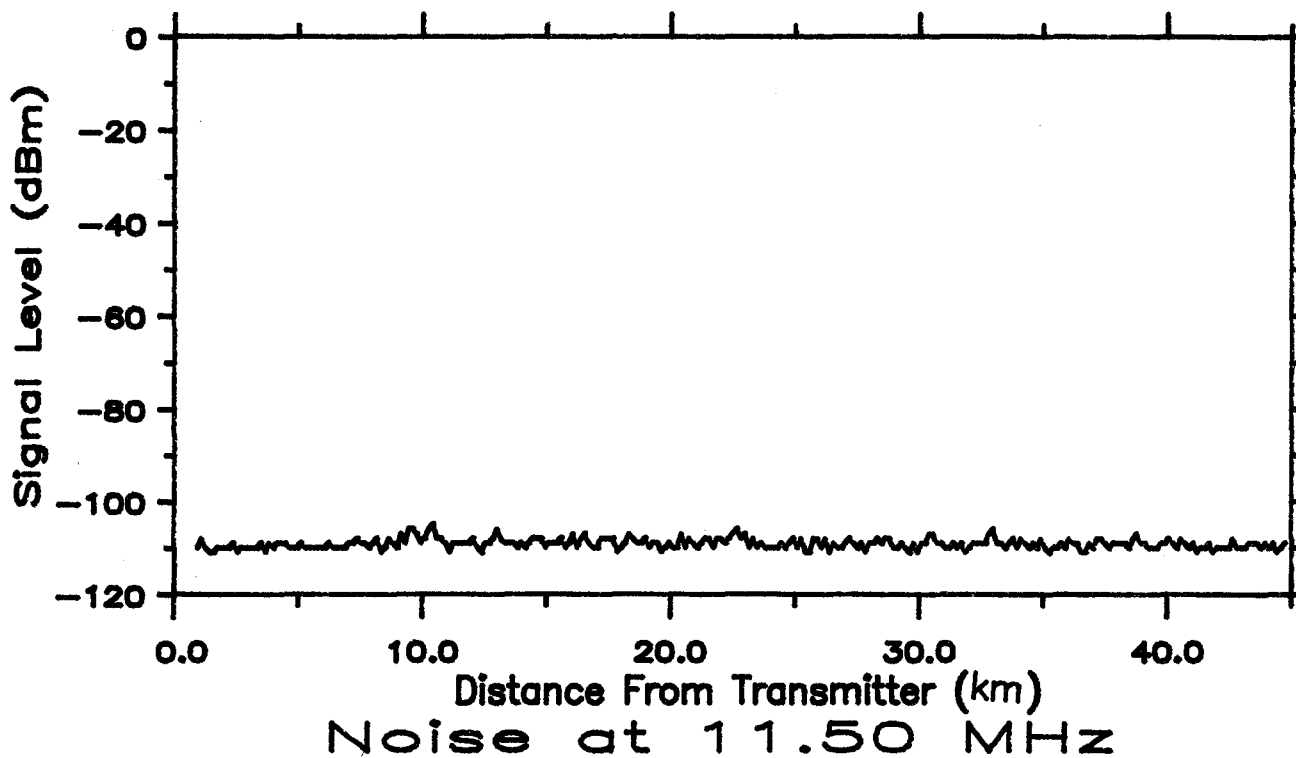
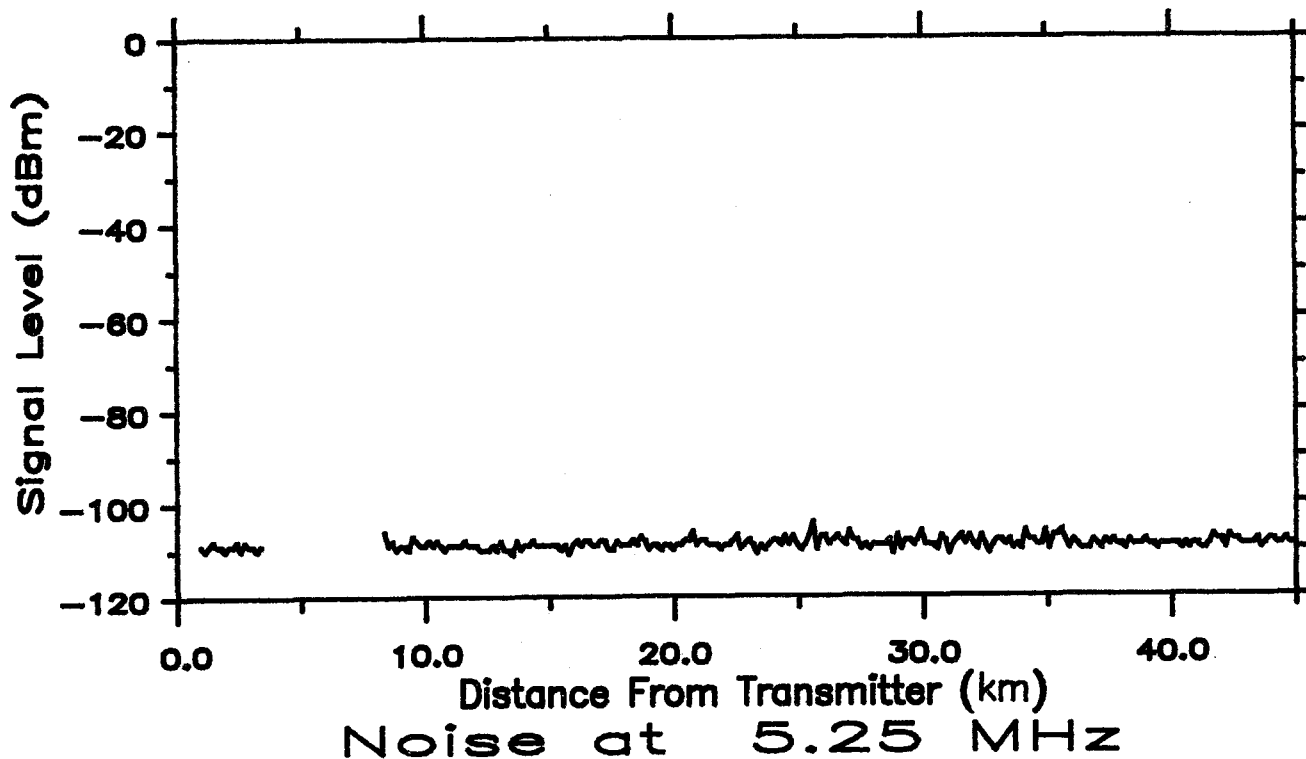


Figure 11. Plots of the median noise power at 5.25 and 11.5 MHz along the East Path measured at the input to the spectrum analyzer in a 1 kHz bandwidth with a system sensitivity of -110 dBm.

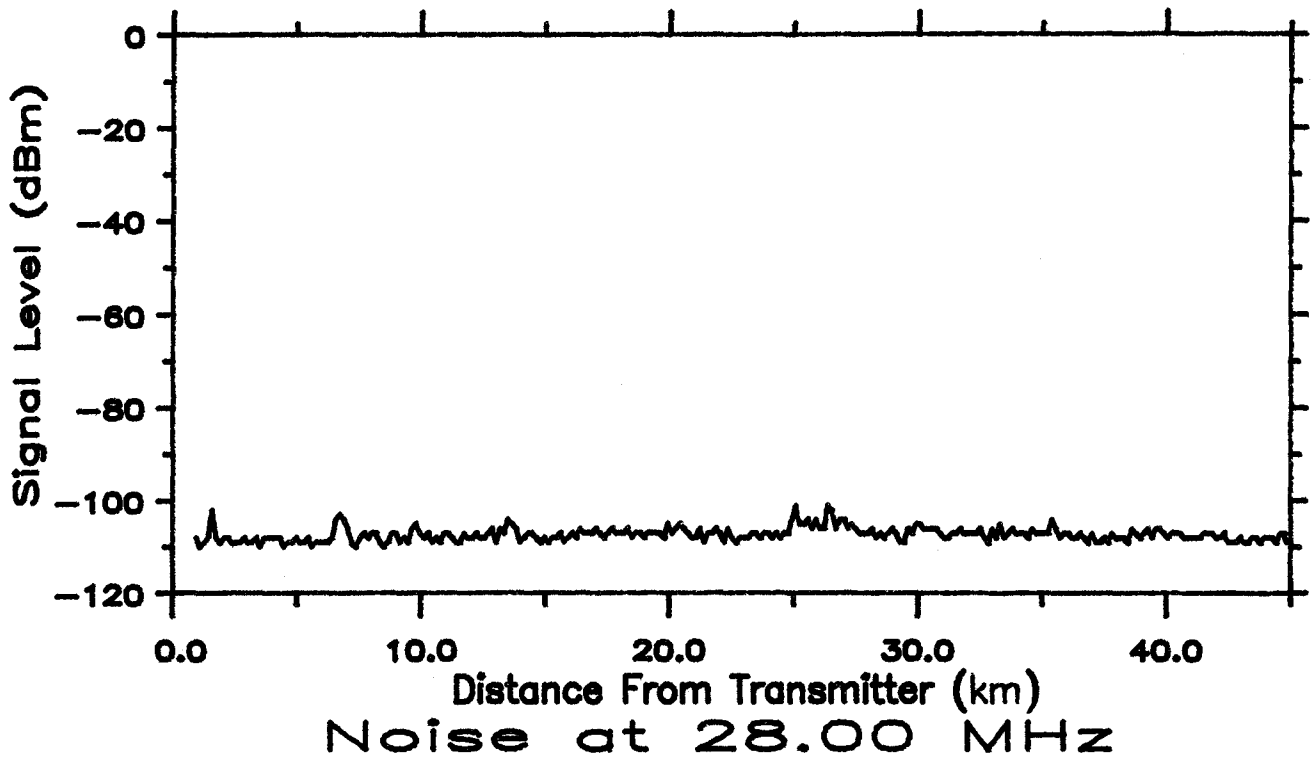


Figure 12. Plot of the median noise power at 28 MHz along the East Path measured at the input to the spectrum analyzer in a 1 kHz bandwidth with a system sensitivity of -110 dBm.

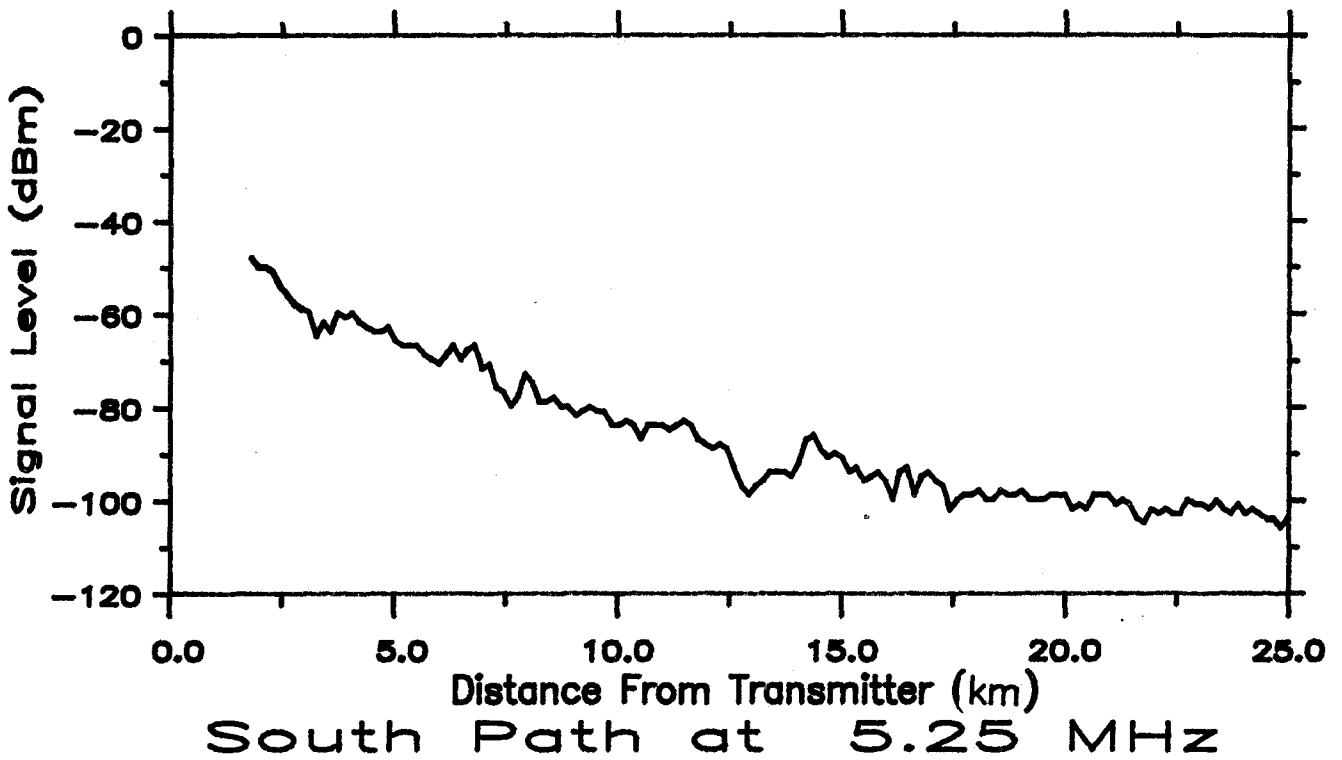
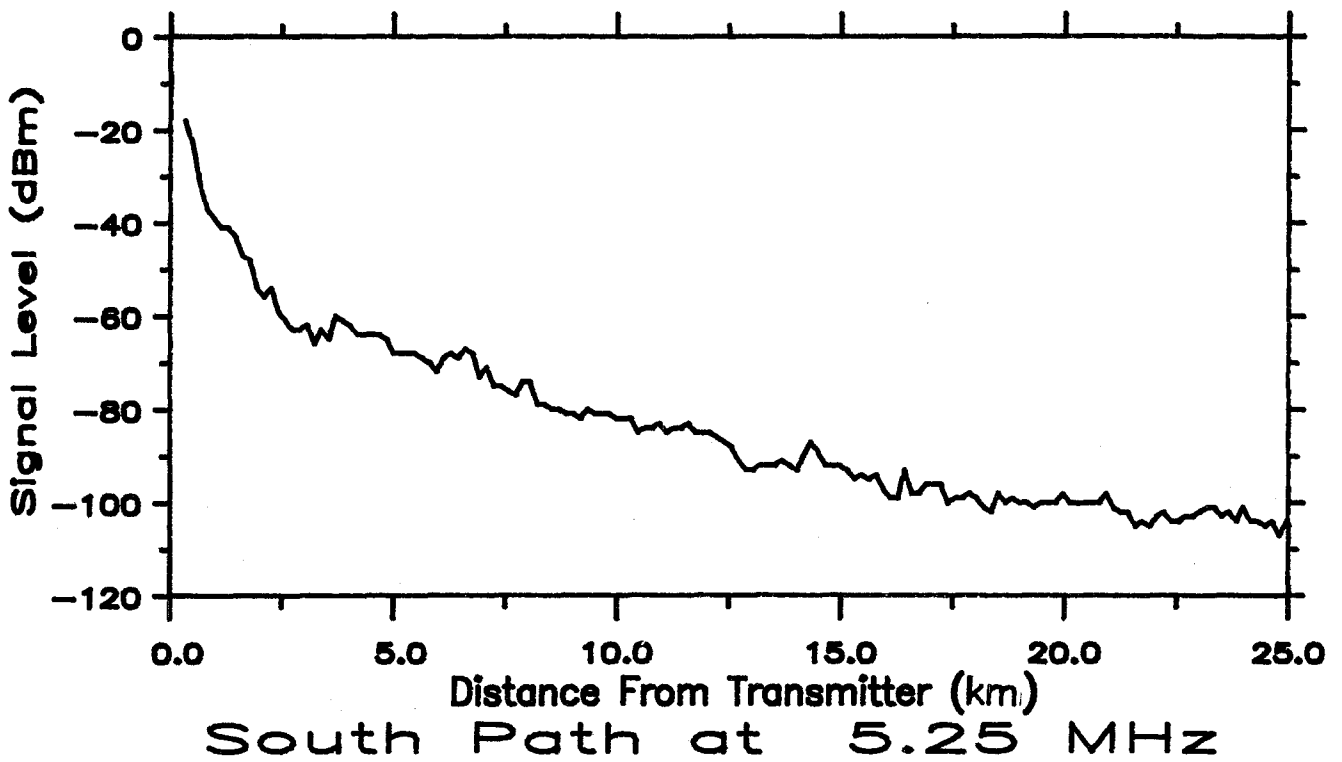


Figure 13. Plots of median received signal level measured along the South Path at 5.25 MHz.

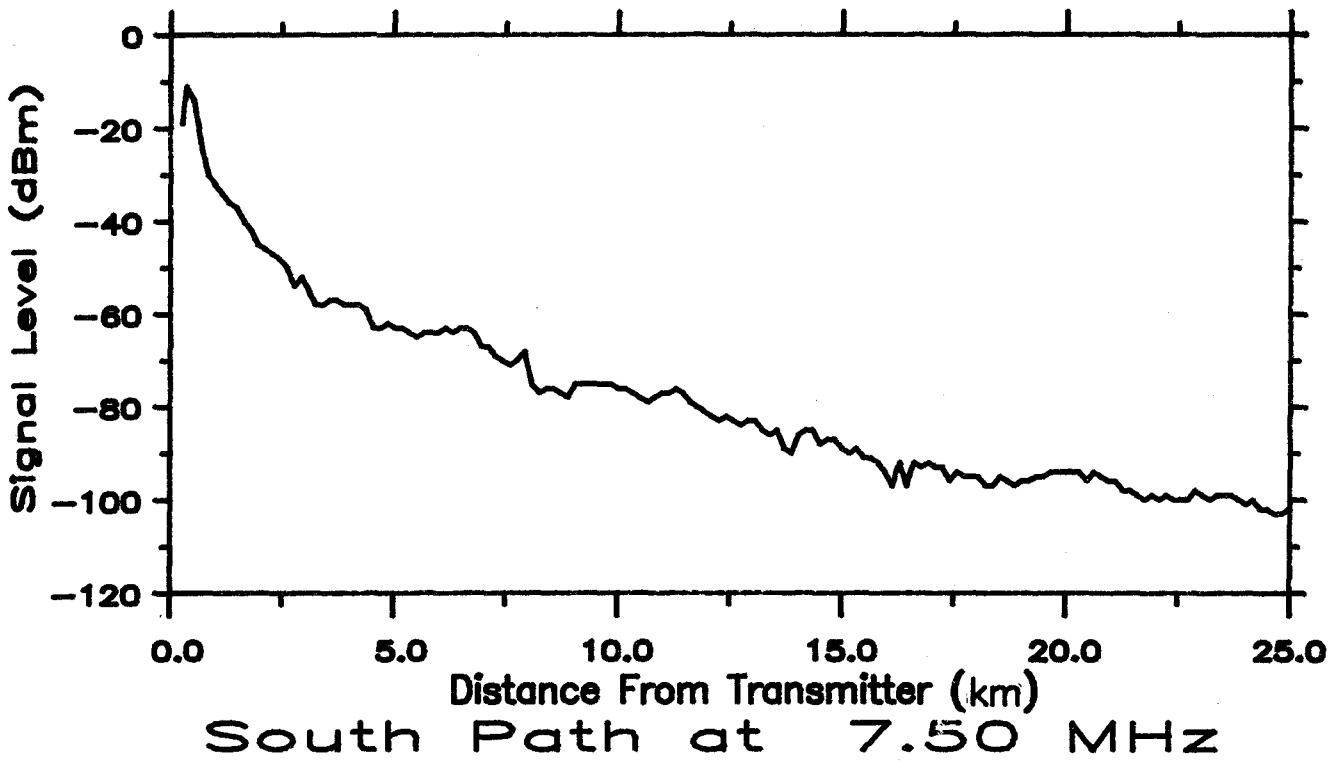
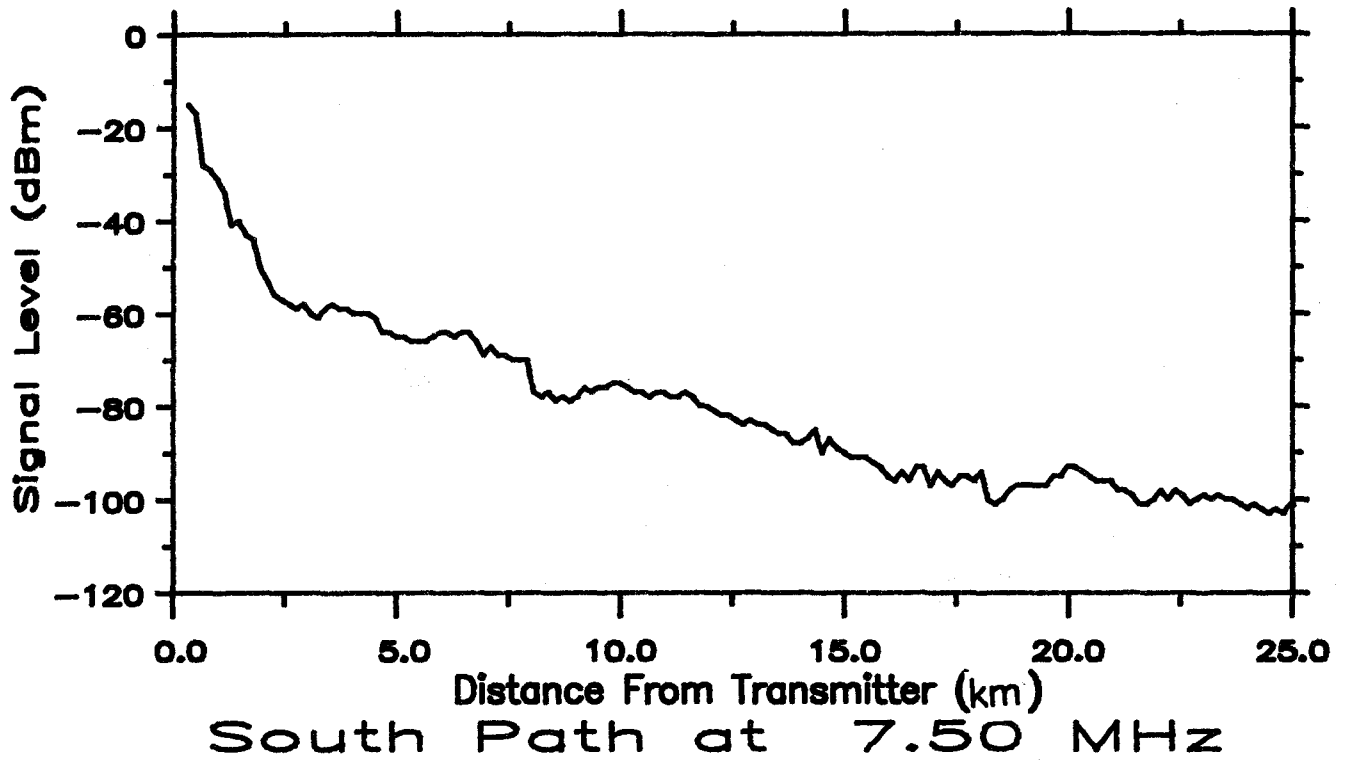


Figure 14. Plots of median received signal level measured along the South Path at 7.50 MHz.

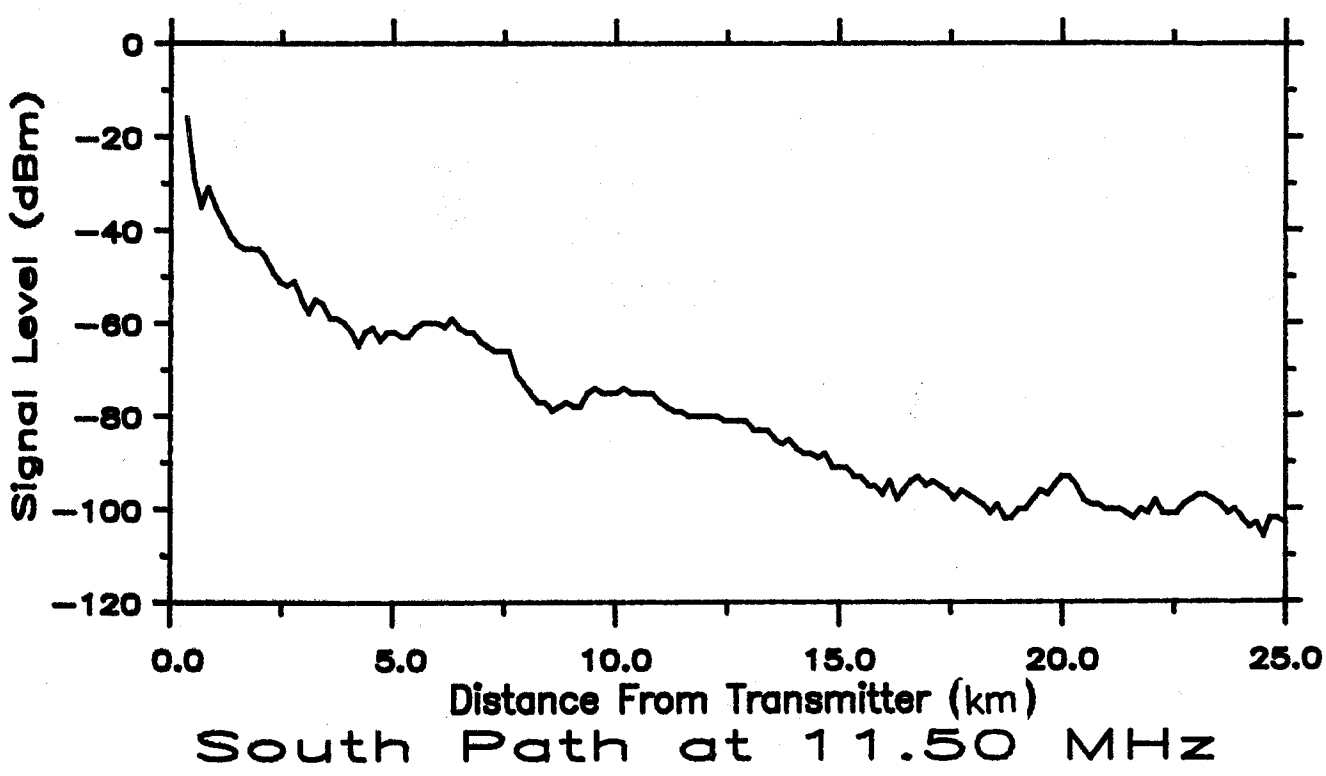
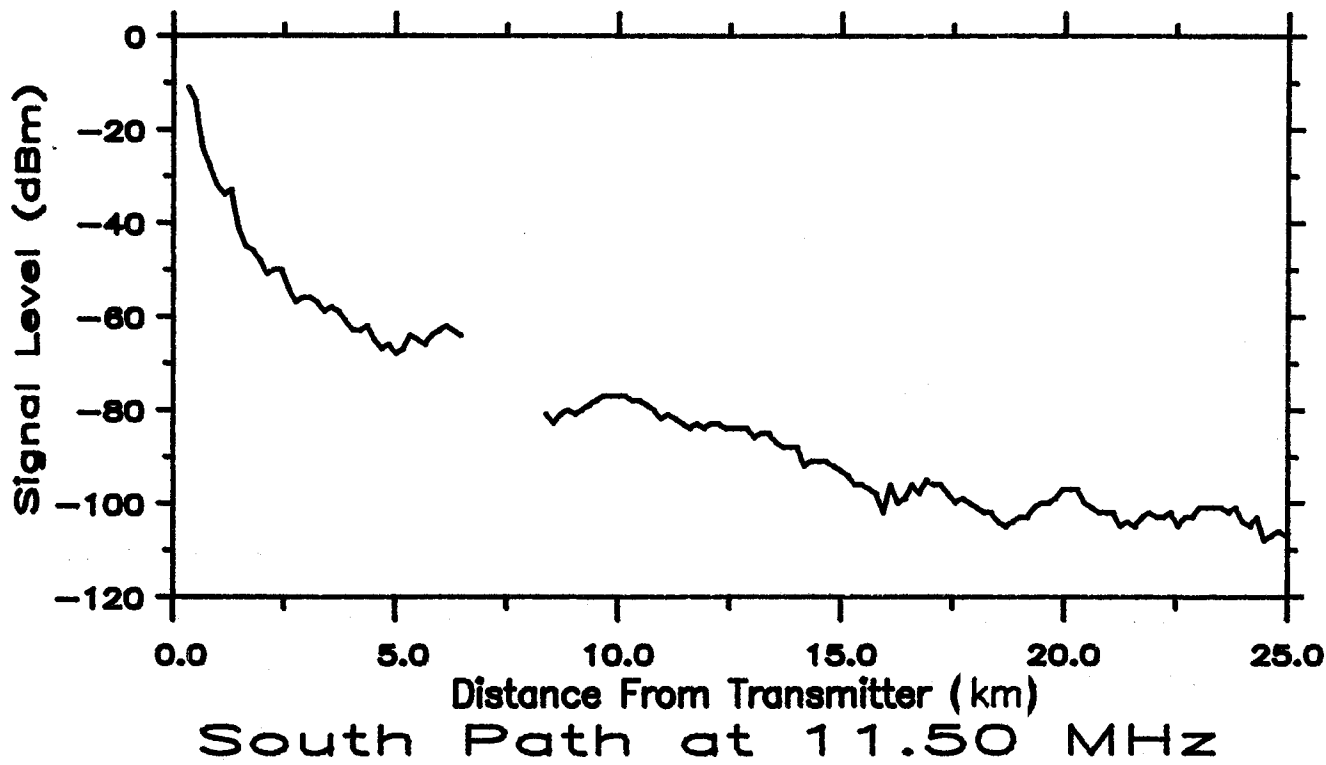


Figure 15. Plots of median received signal level measured along the South Path at 11.50 MHz.

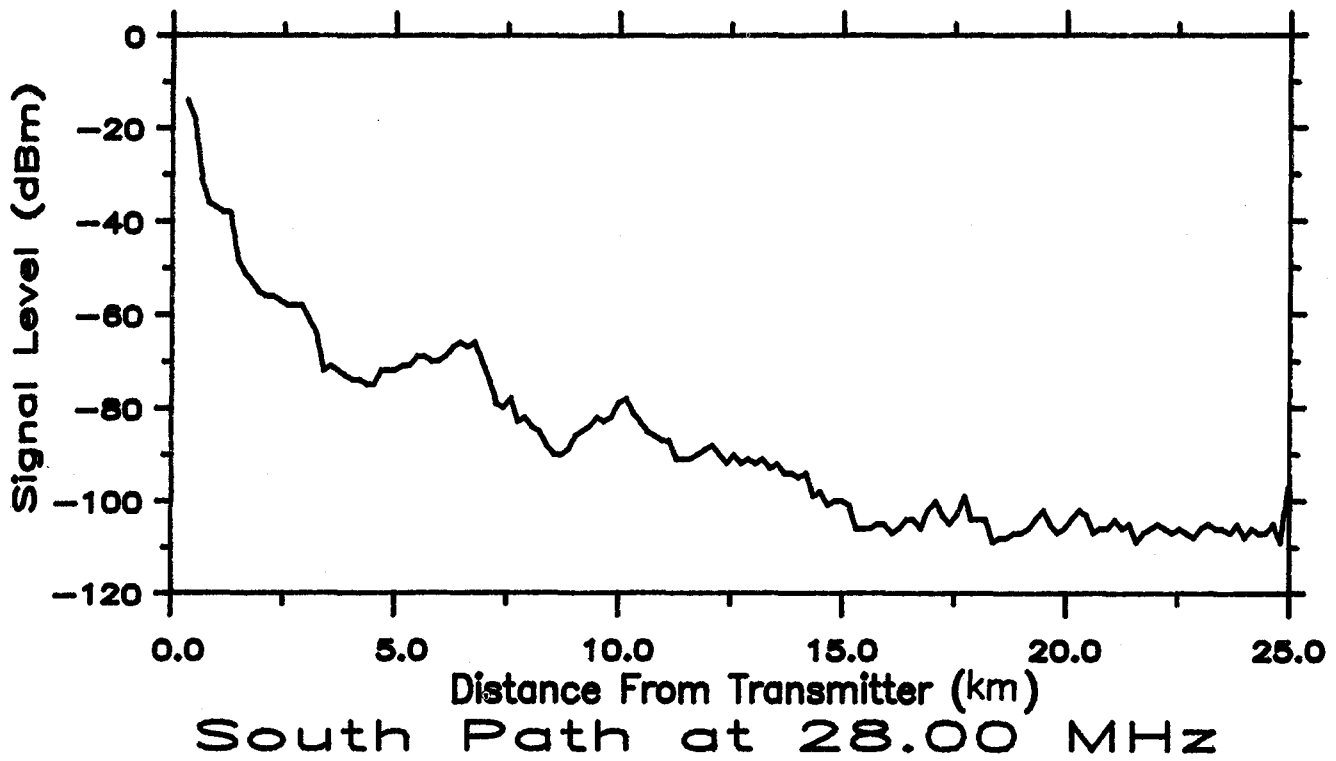
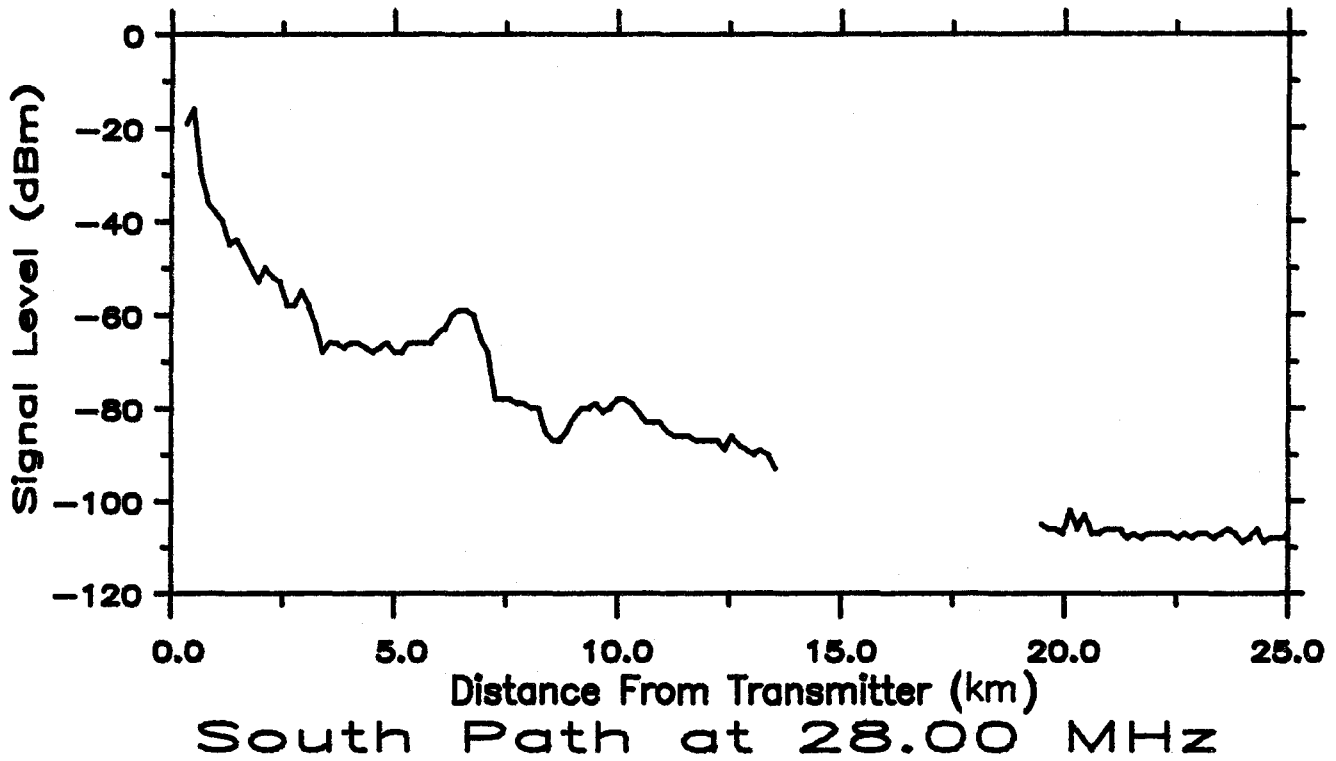


Figure 16. Plots of median received signal level measured along the South Path at 28.00 MHz.

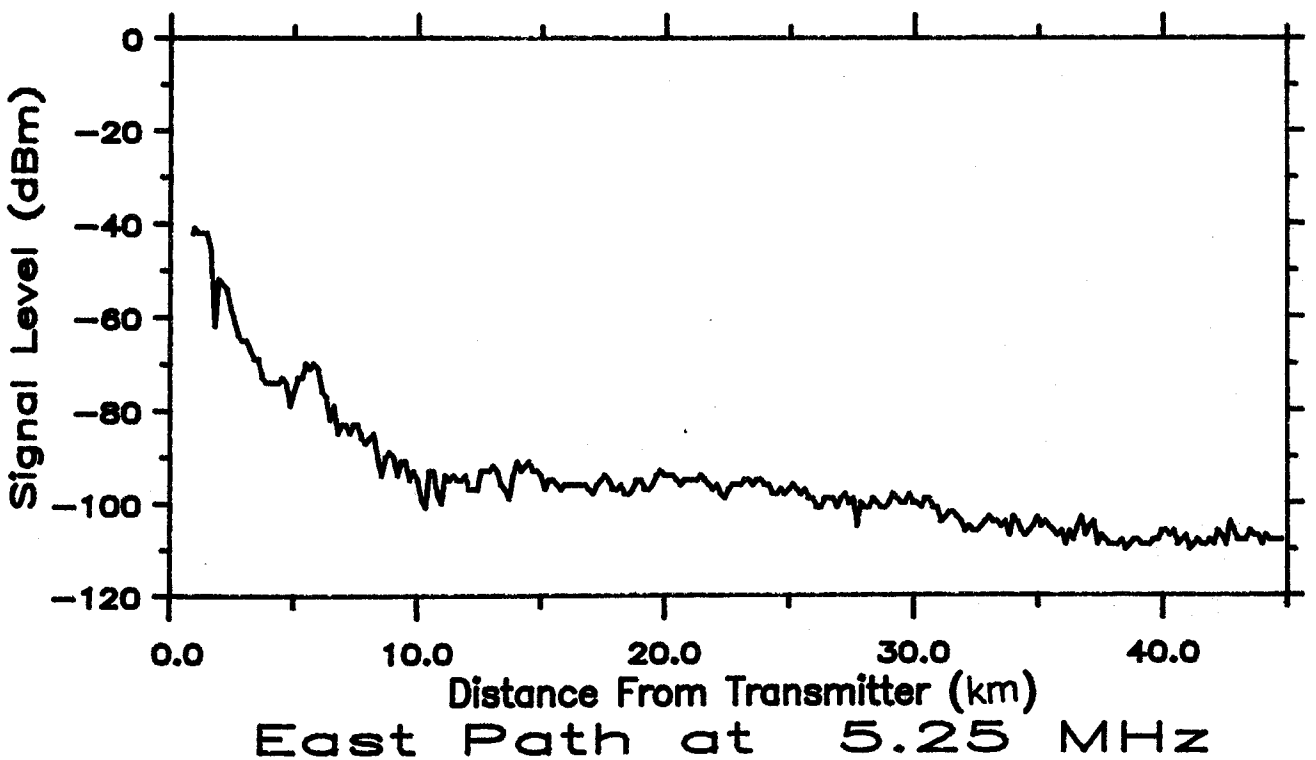
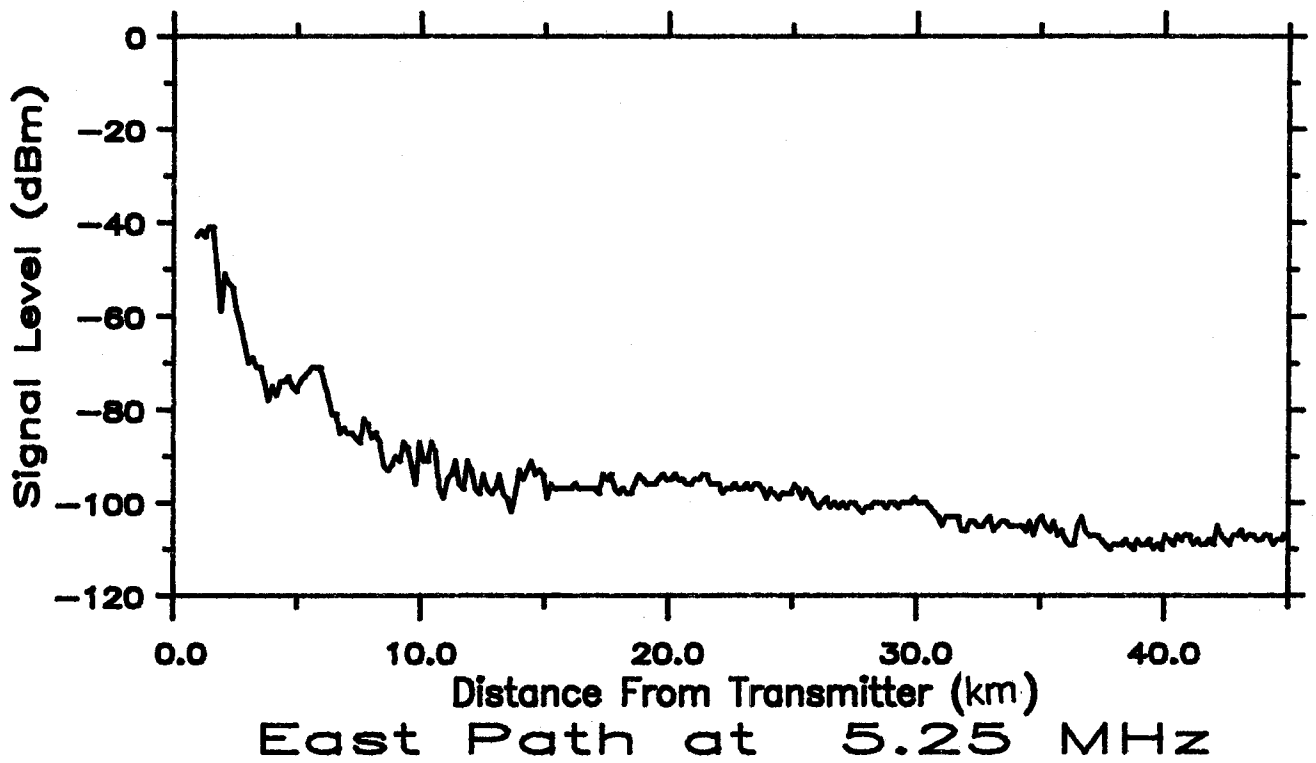


Figure 17. Plots of median received signal level measured along the East Path with no snow cover at 5.25 MHz.

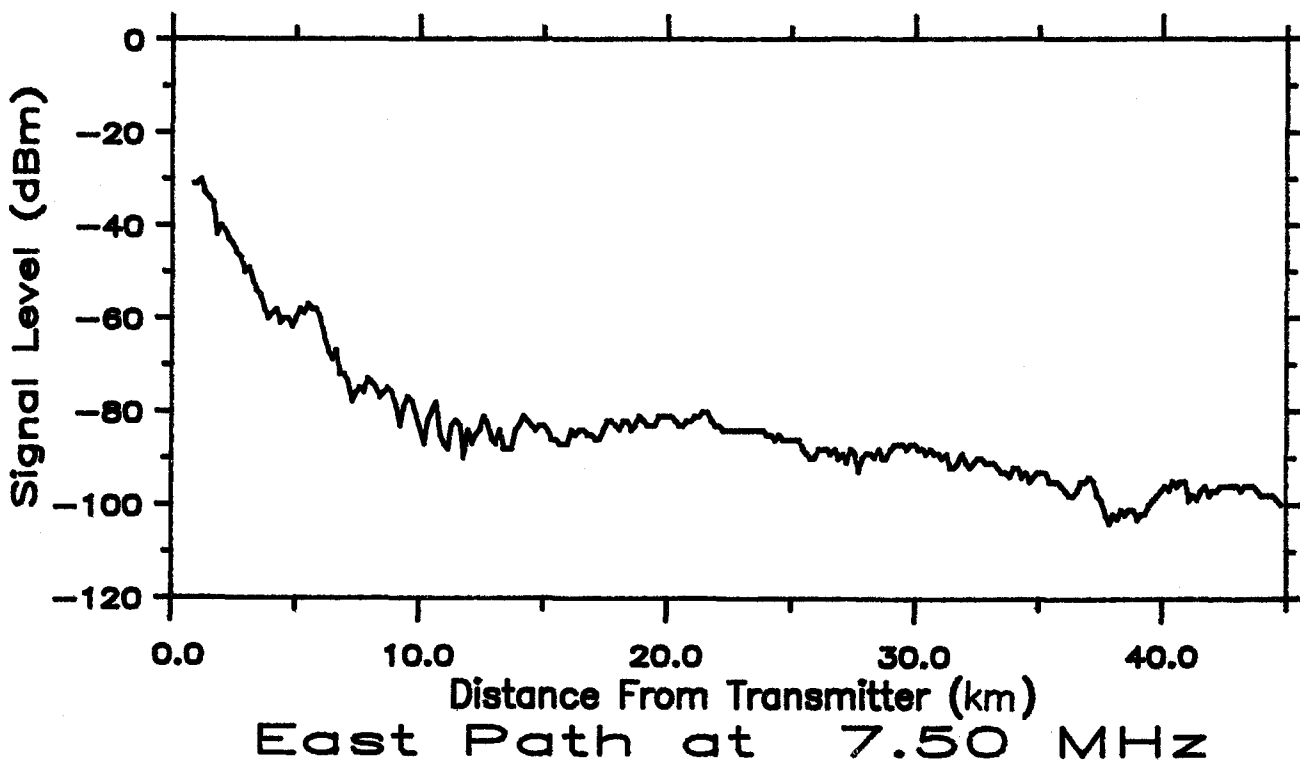
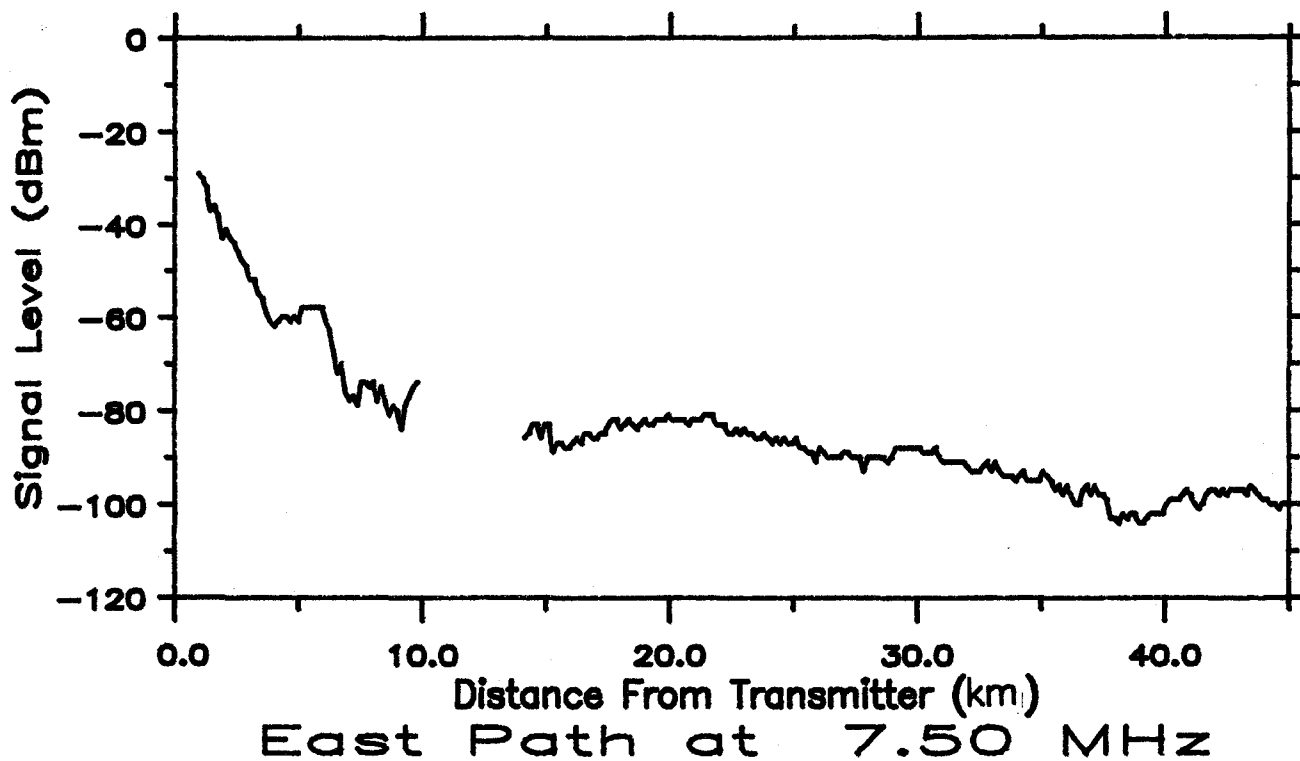


Figure 18. Plots of median received signal level measured along the East Path with no snow cover at 7.50 MHz.

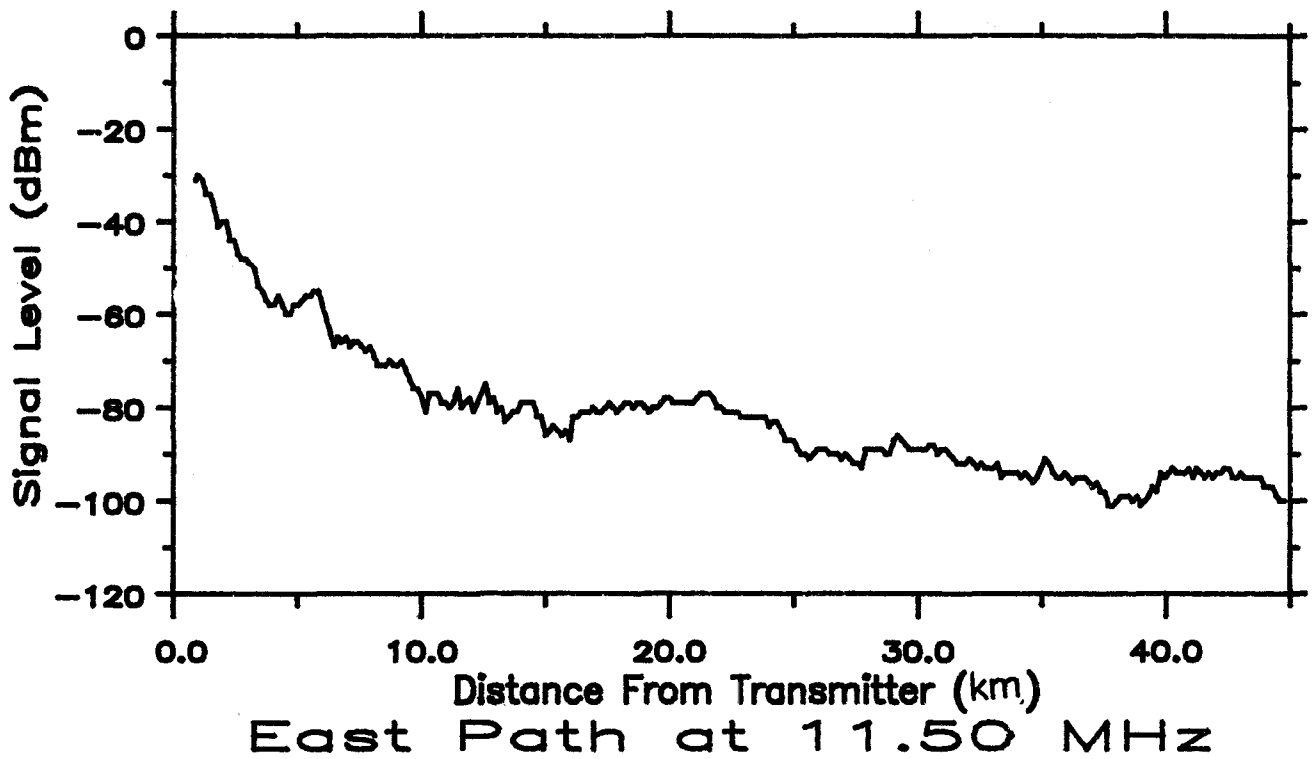
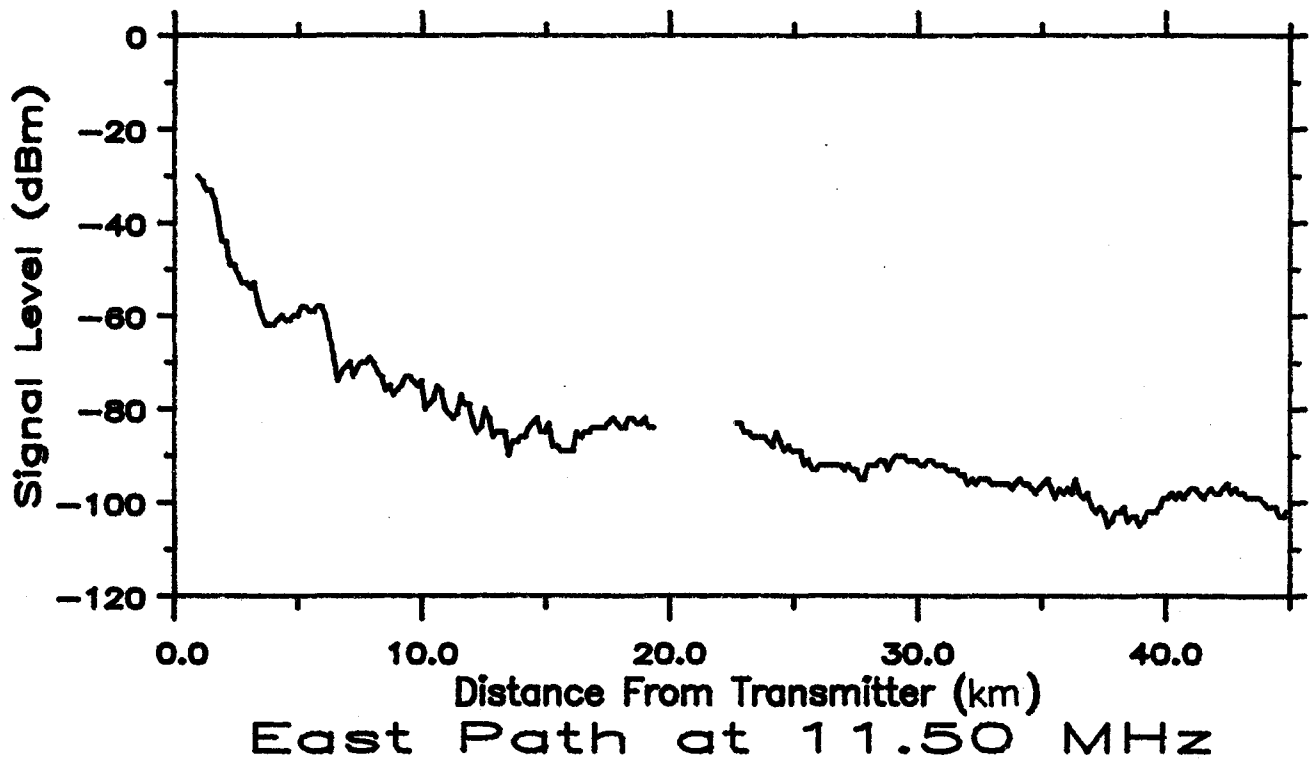


Figure 19. Plots of median received signal level measured along the East Path with no snow cover at 11.50 MHz.

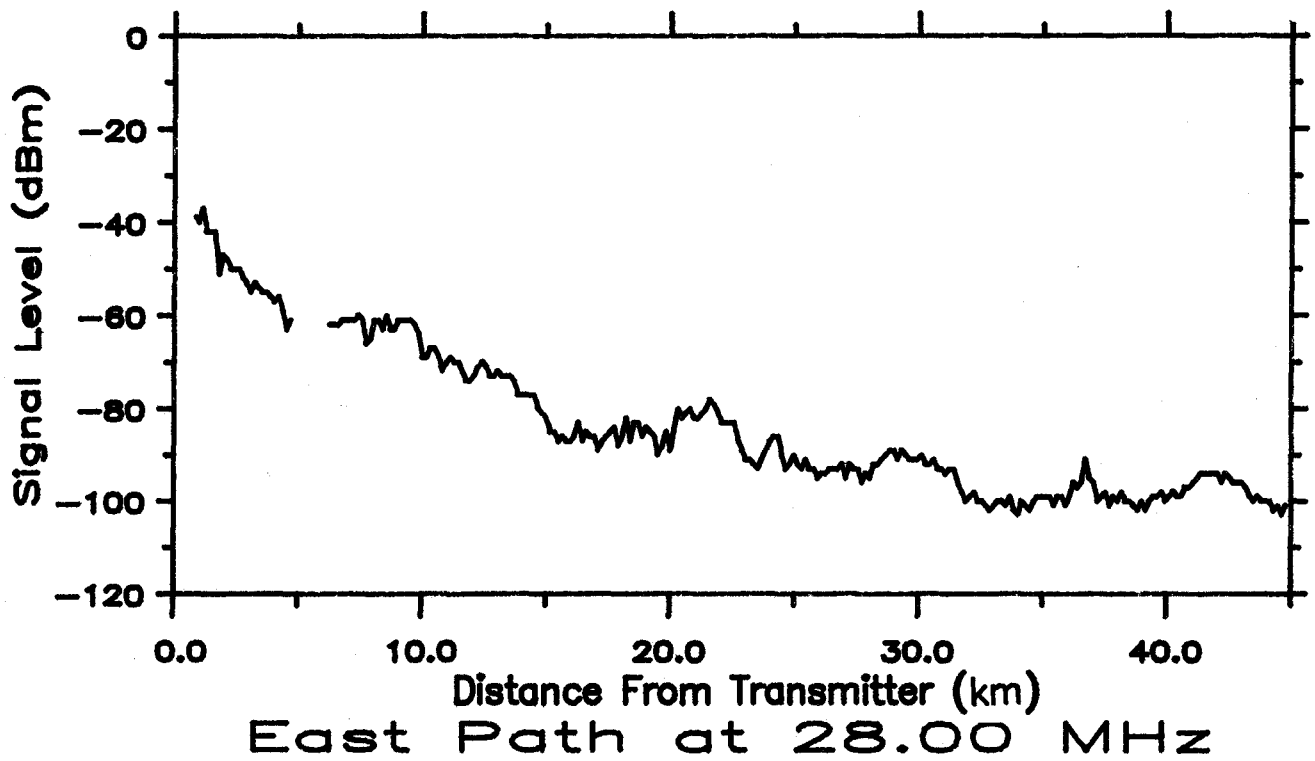
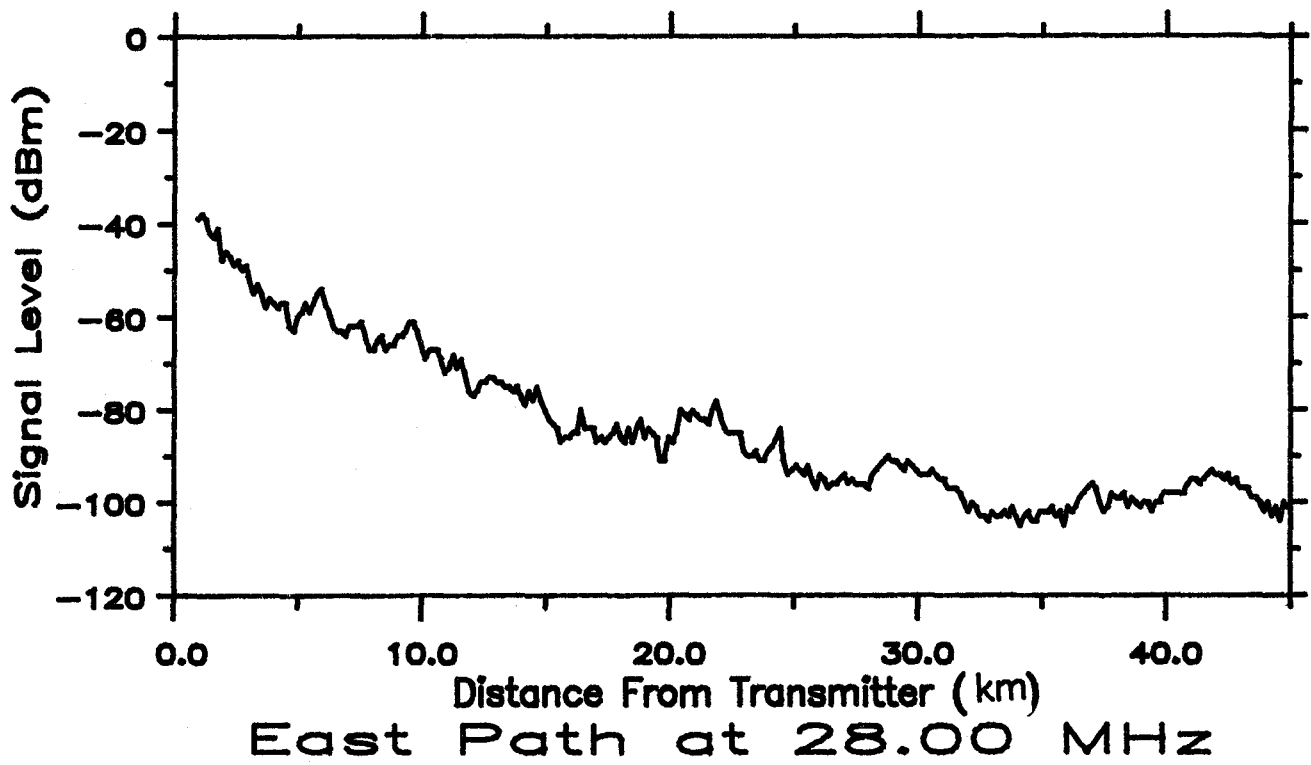


Figure 20. Plots of median received signal level measured along the East Path with no snow cover at 28.00 MHz.

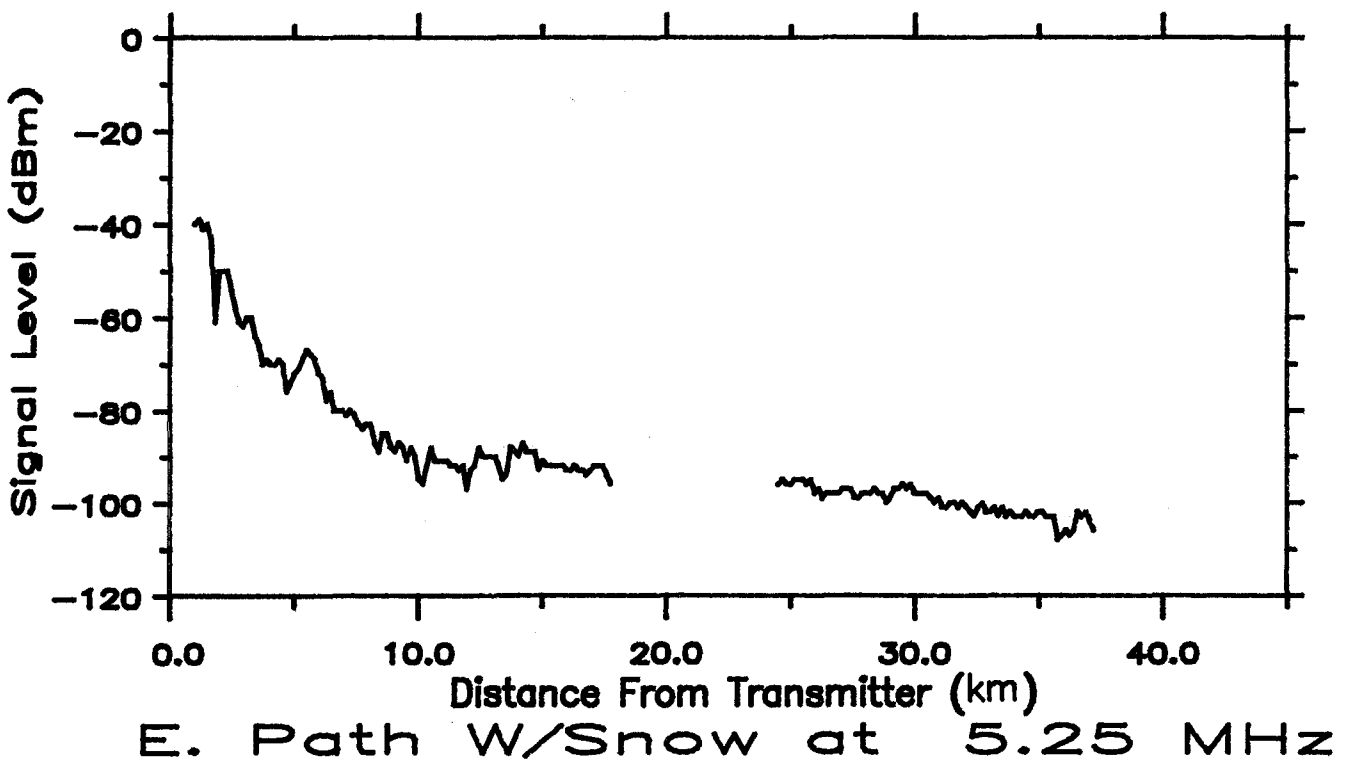
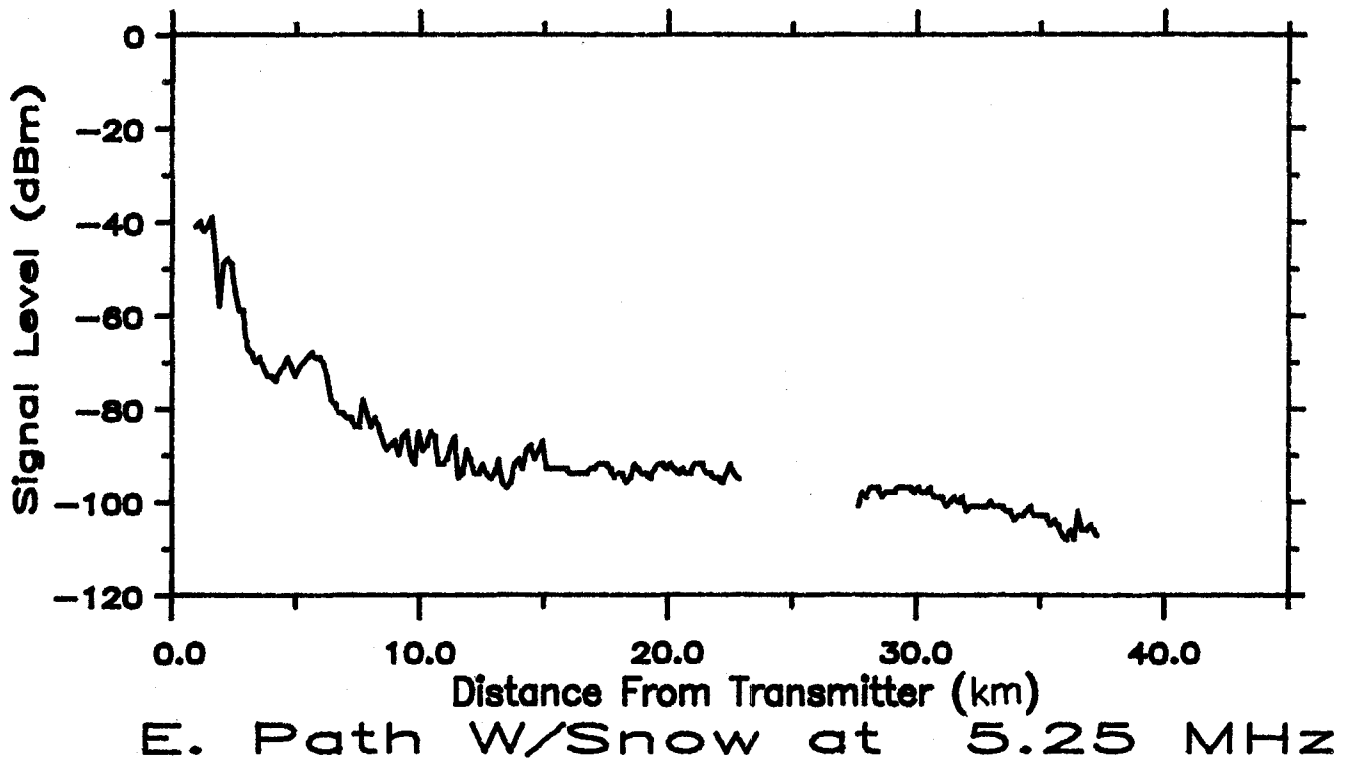
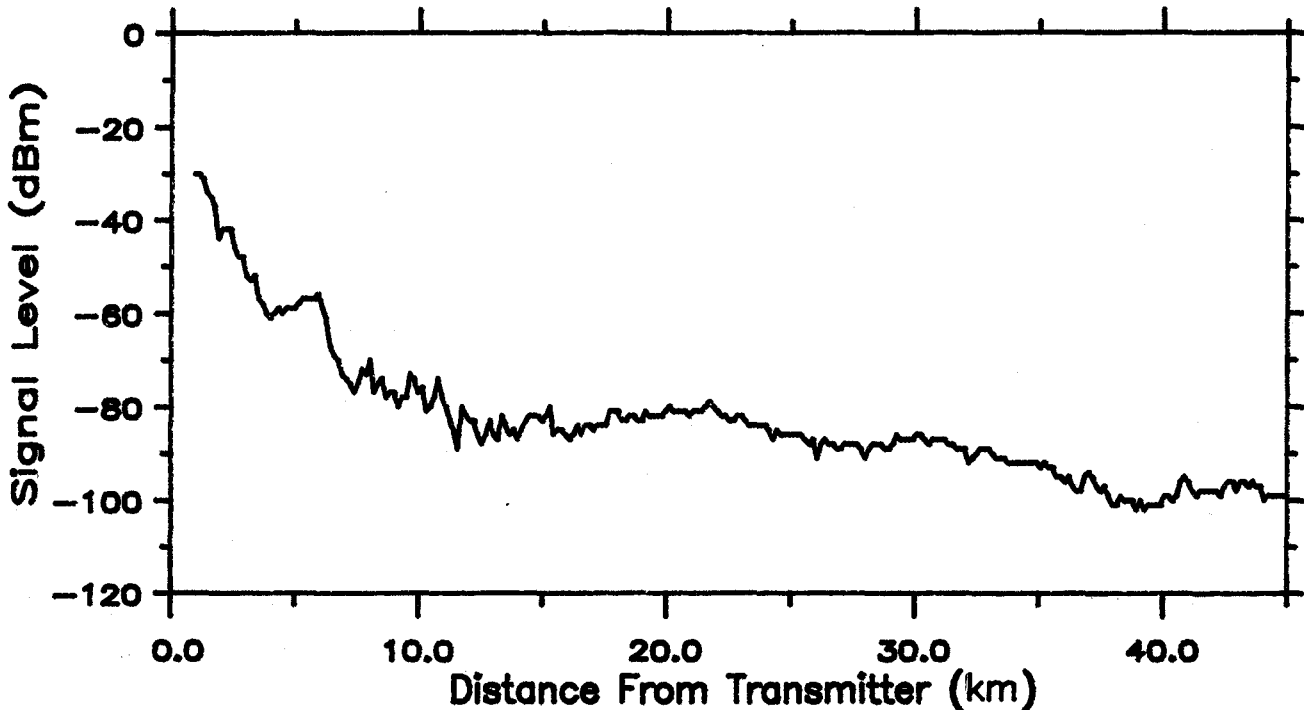
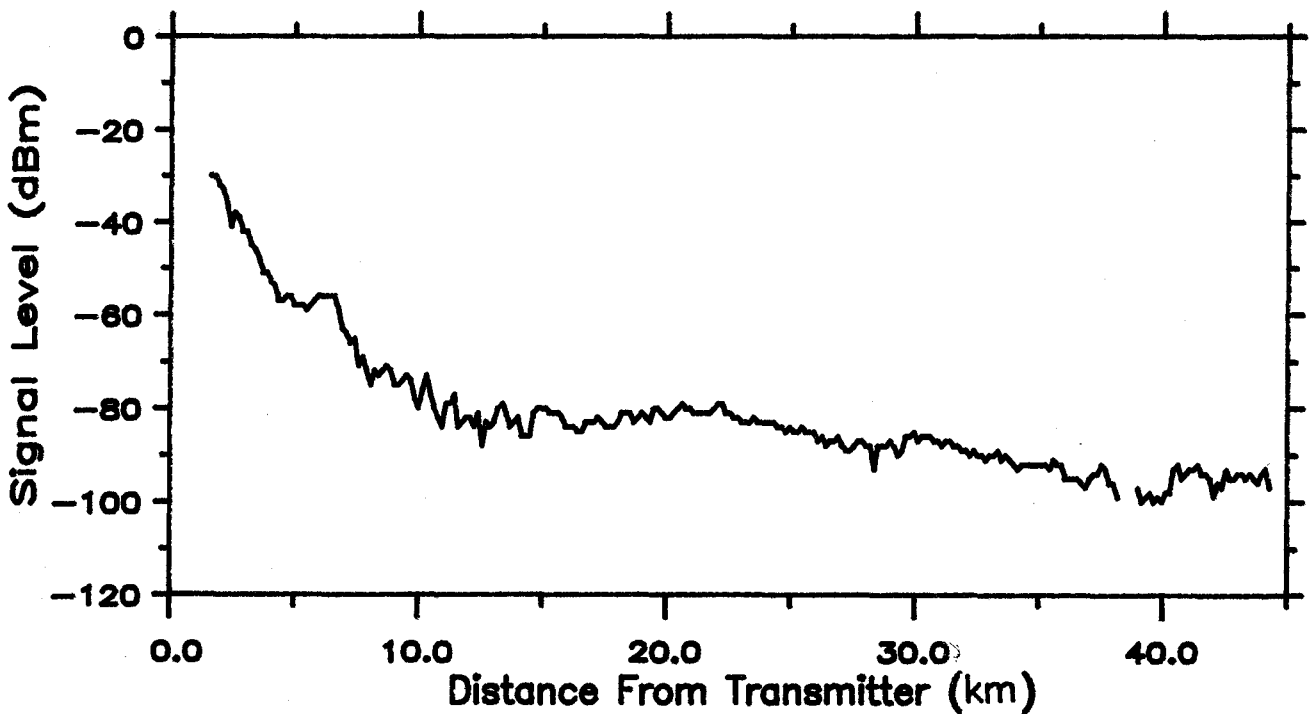


Figure 21. Plots of median received signal level measured along the East Path with snow cover at 5.25 MHz.

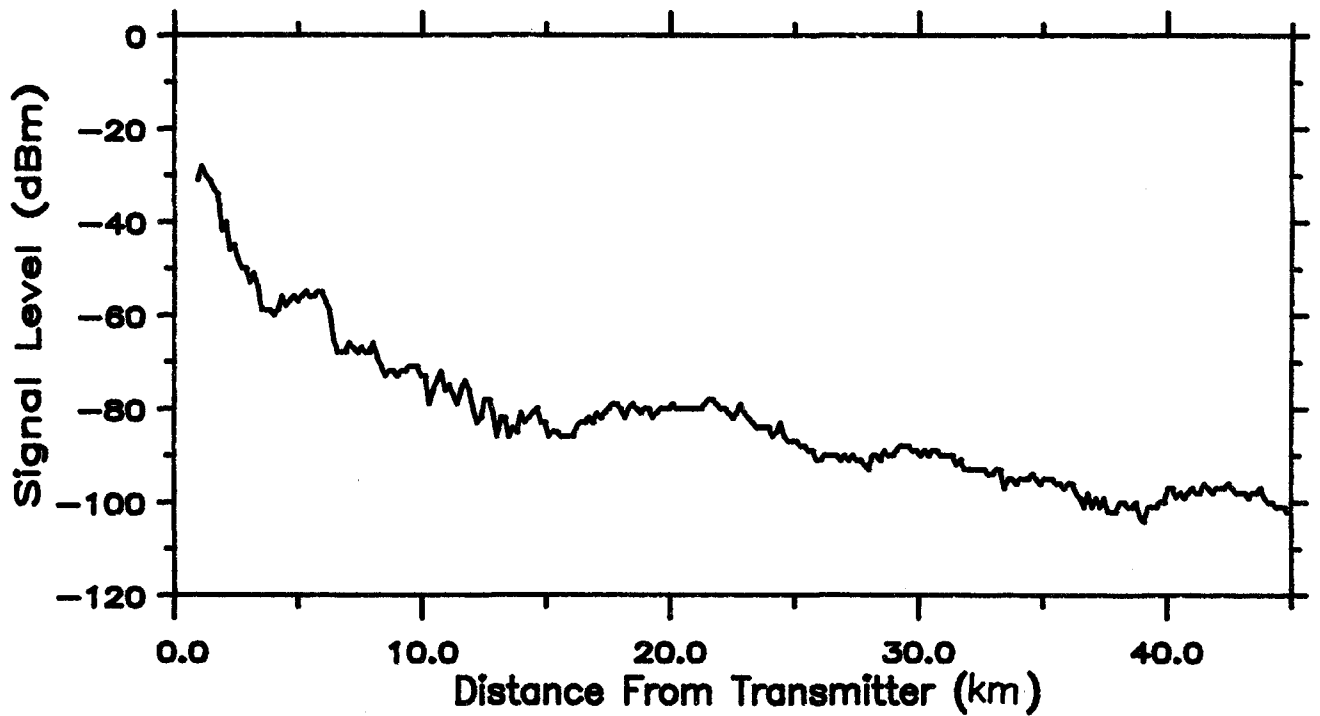


E. Path W/Snow at 7.50 MHz

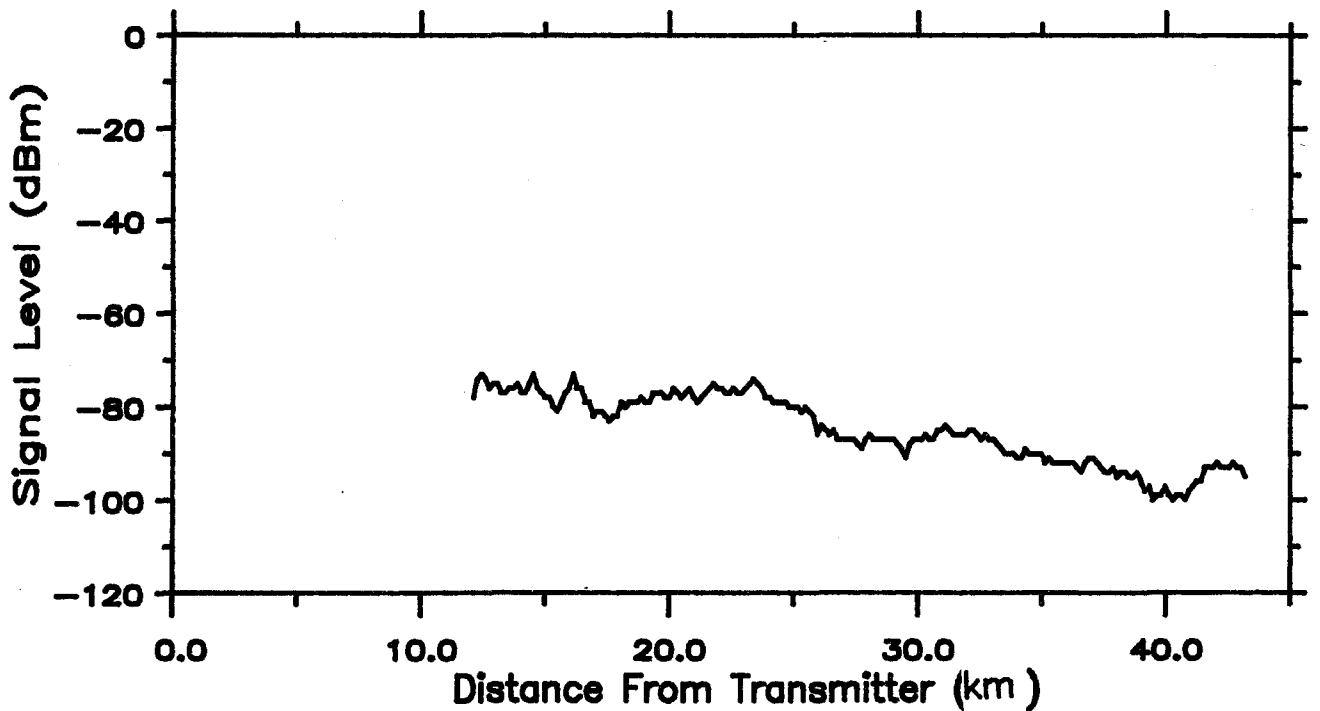


E. Path W/Snow at 7.50 MHz

Figure 22. Plots of median received signal level measured along the East Path with snow cover at 7.50 MHz.

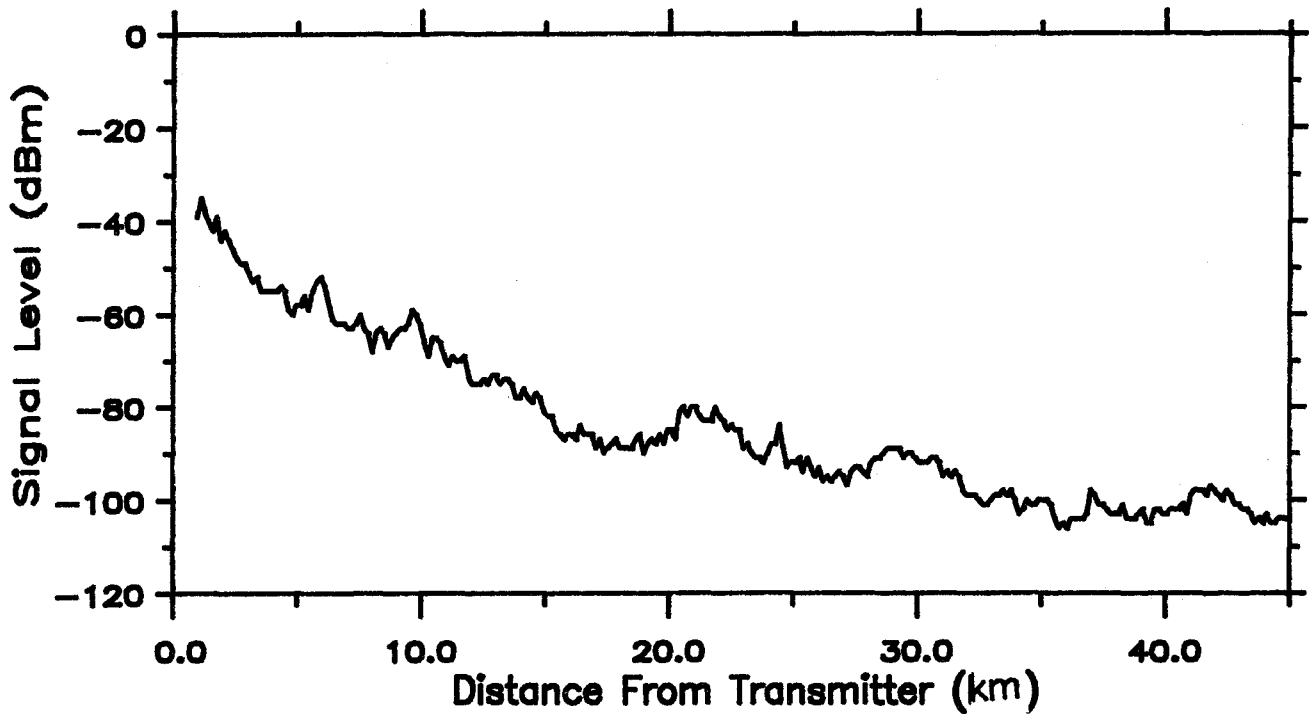


E. Path W/Snow at 11.50 MHz

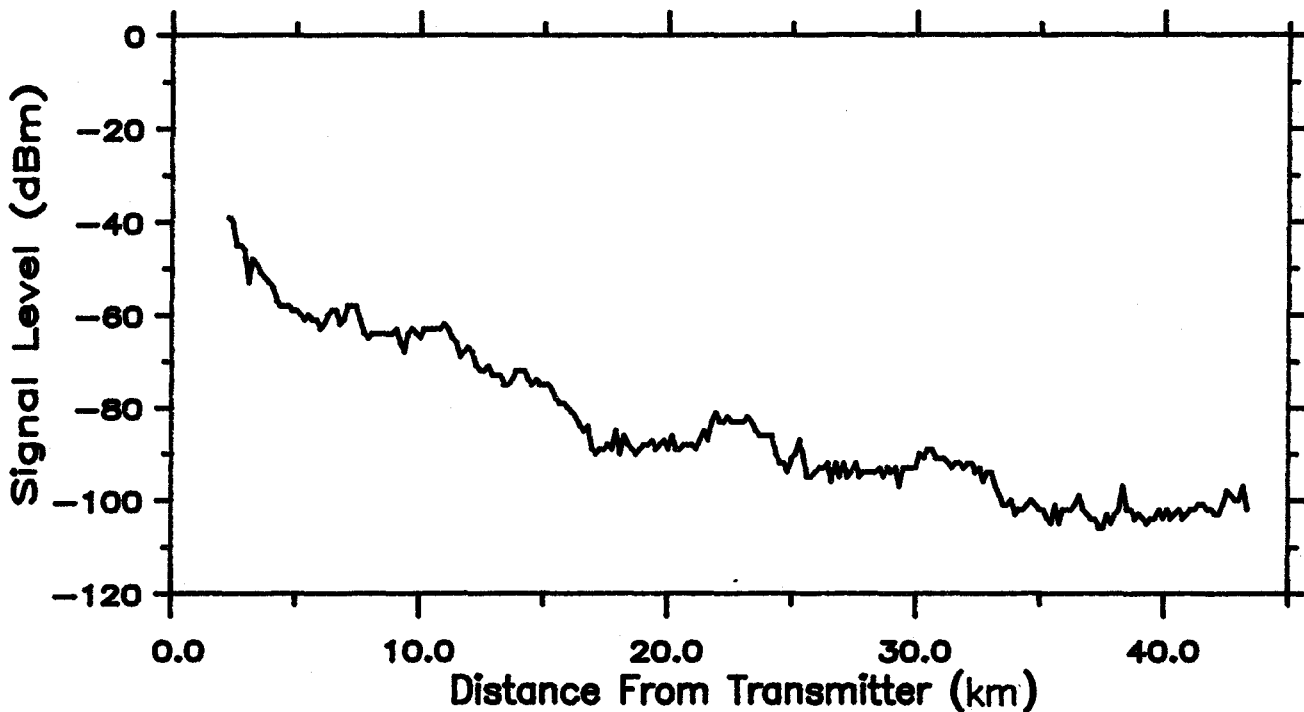


E. Path W/Snow at 11.50 MHz

Figure 23. Plots of median received signal level measured along the East Path with snow cover at 11.50 MHz.



E. Path W/Snow at 28.00 MHz



E. Path W/Snow at 28.00 MHz

Figure 24. Plots of median received signal level measured along the East Path with snow cover at 28.00 MHz.

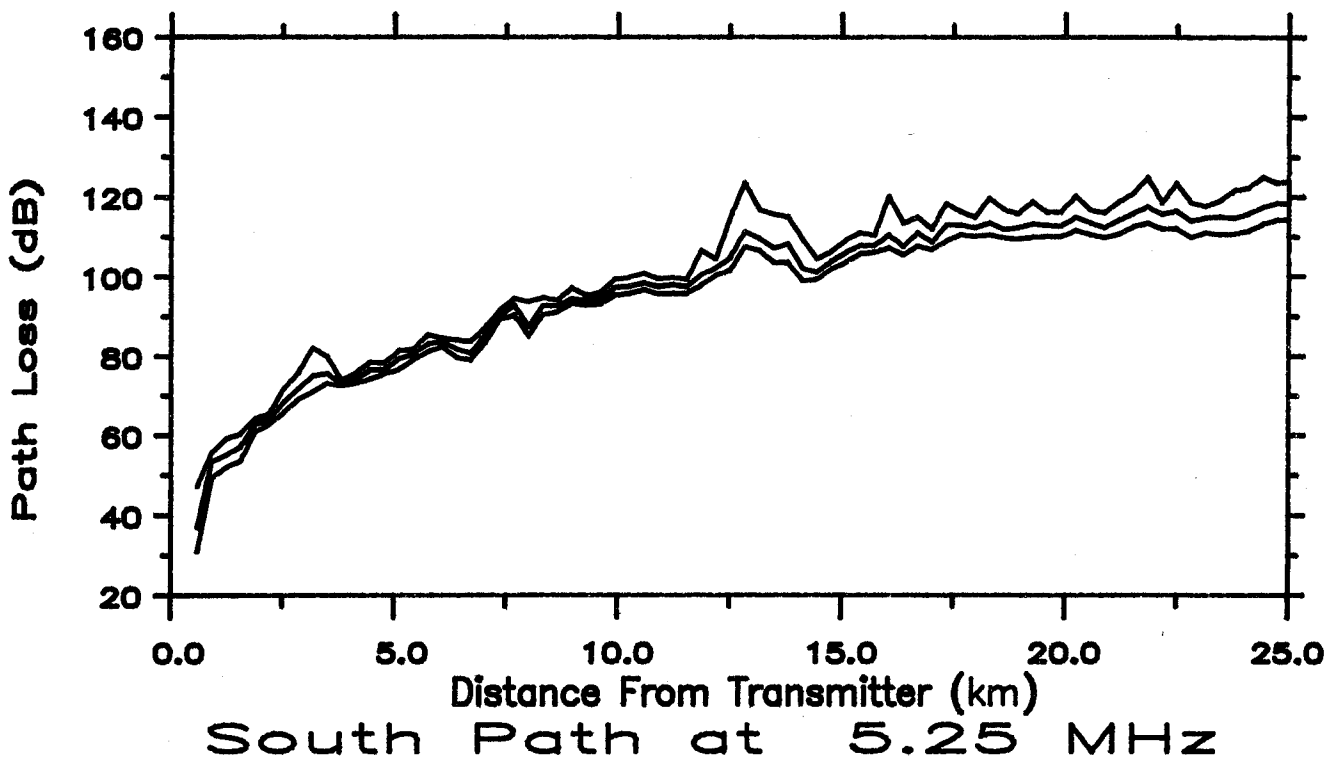
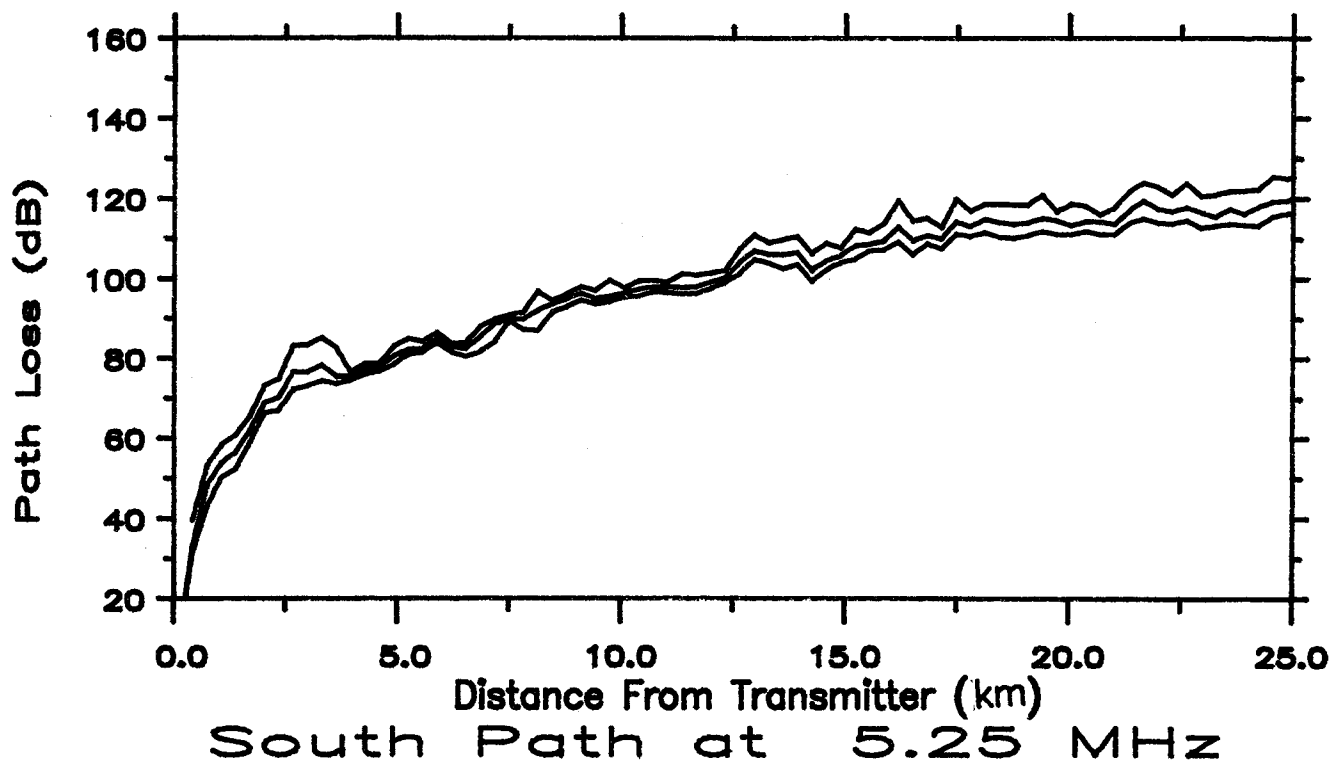


Figure 25. Plots of median, upper, and lower decile path loss measured along the South Path at 5.25 MHz.

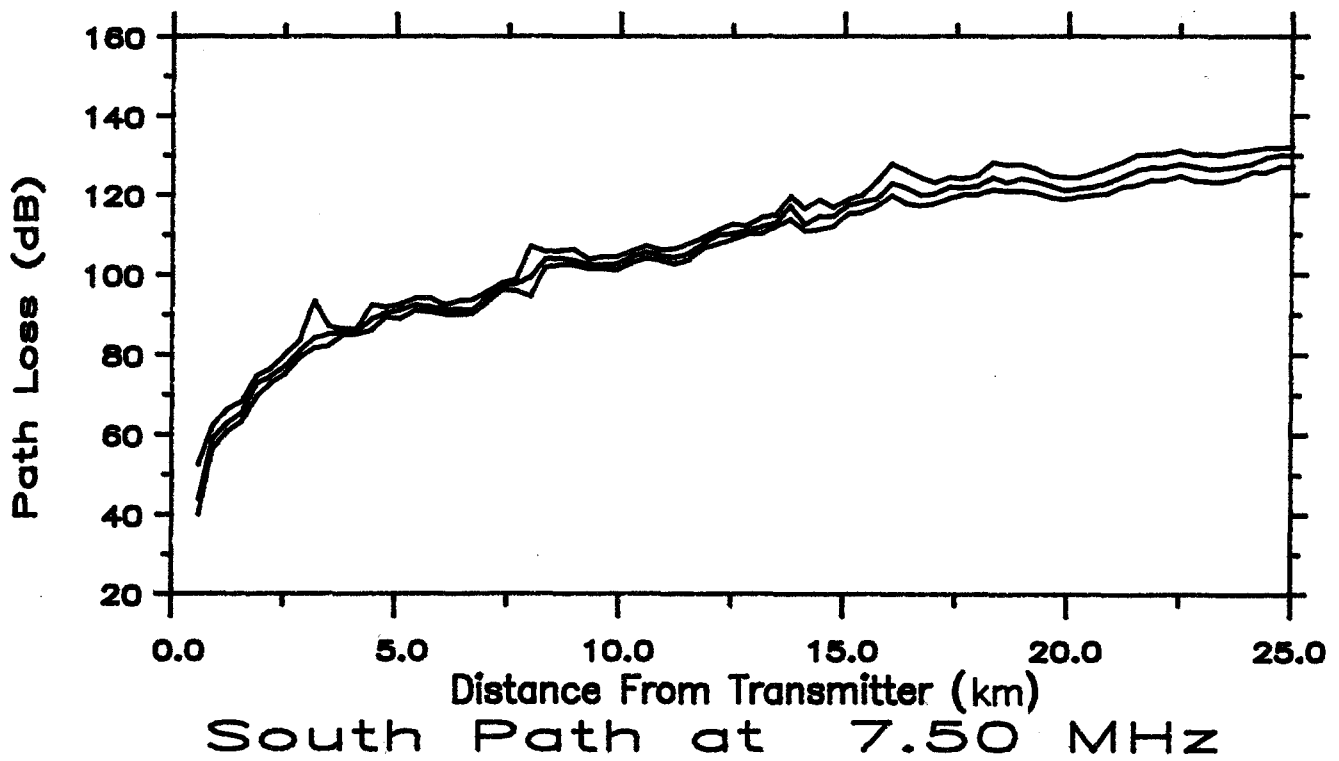
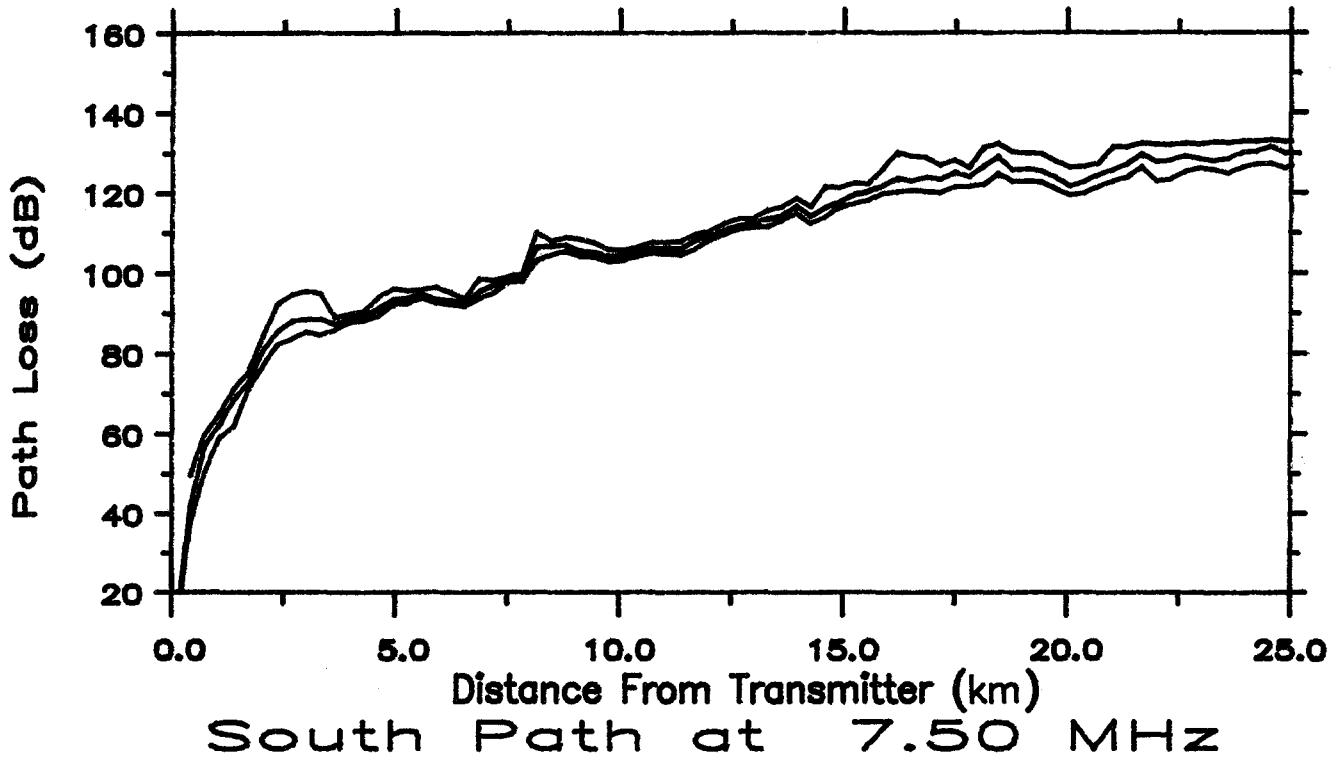


Figure 26. Plots of median, upper, and lower decile path loss measured along the South Path at 7.50 MHz.

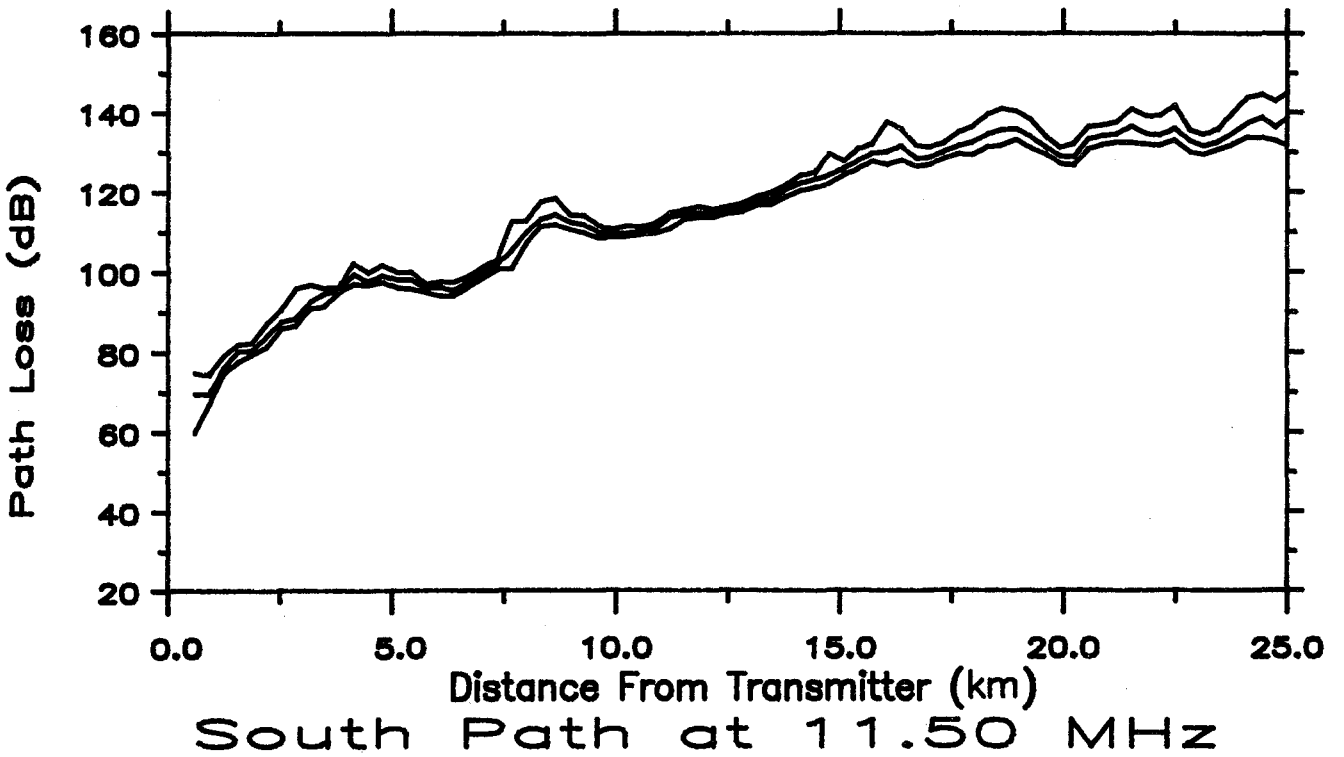
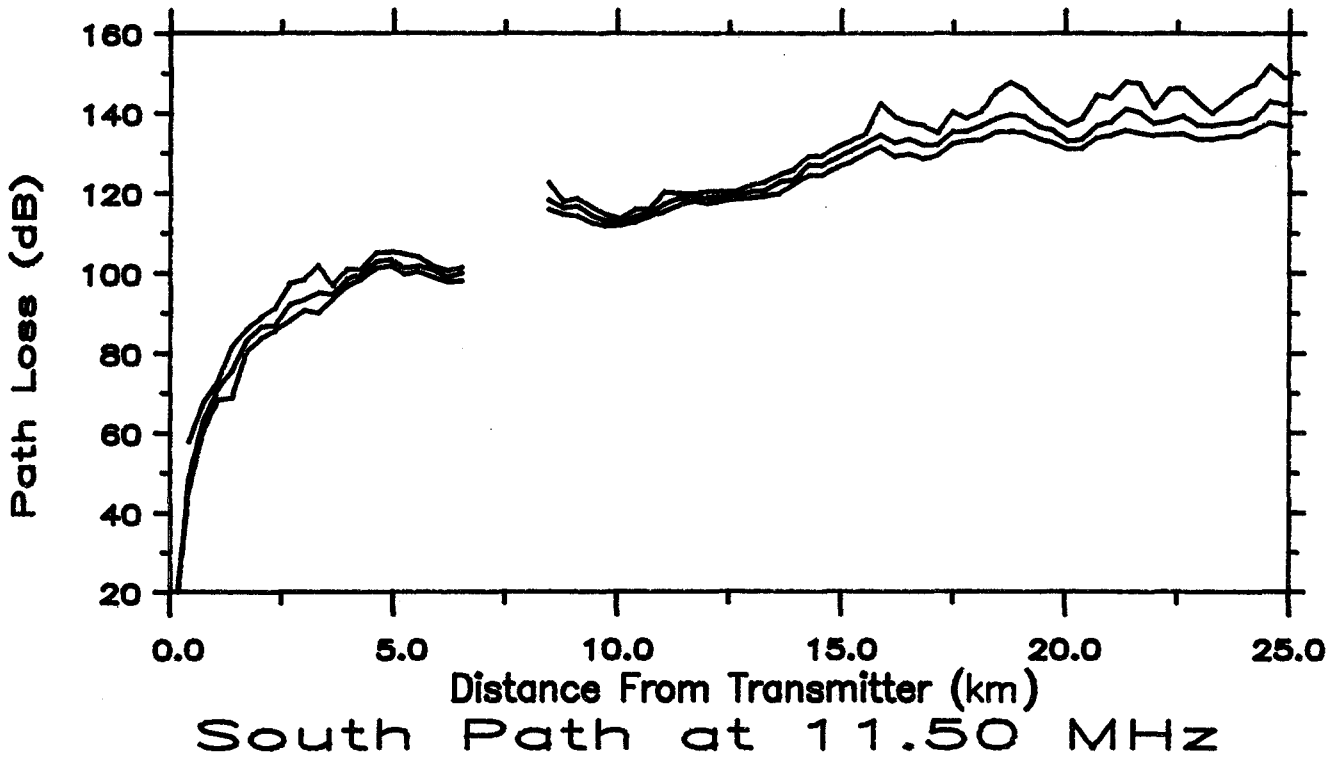


Figure 27. Plots of median, upper, and lower decile path loss measured along the South Path at 11.50 MHz.

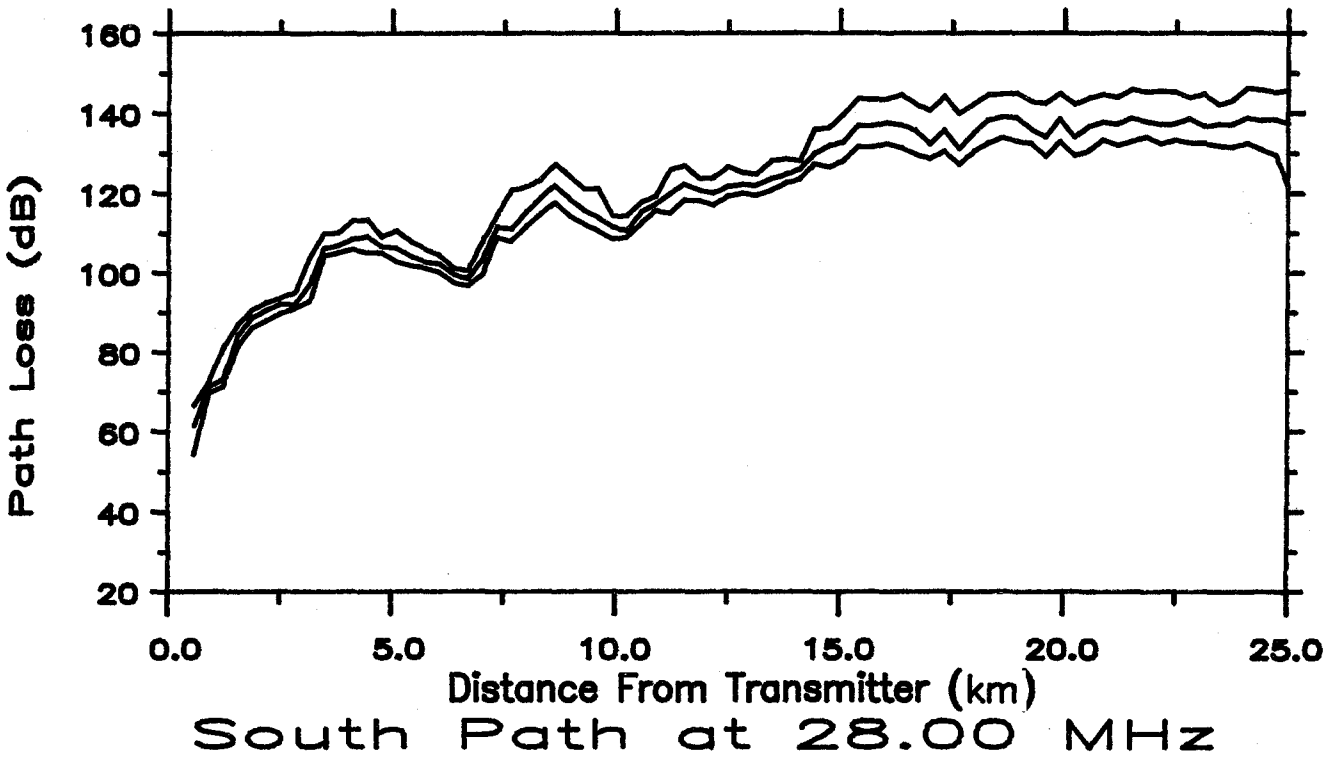
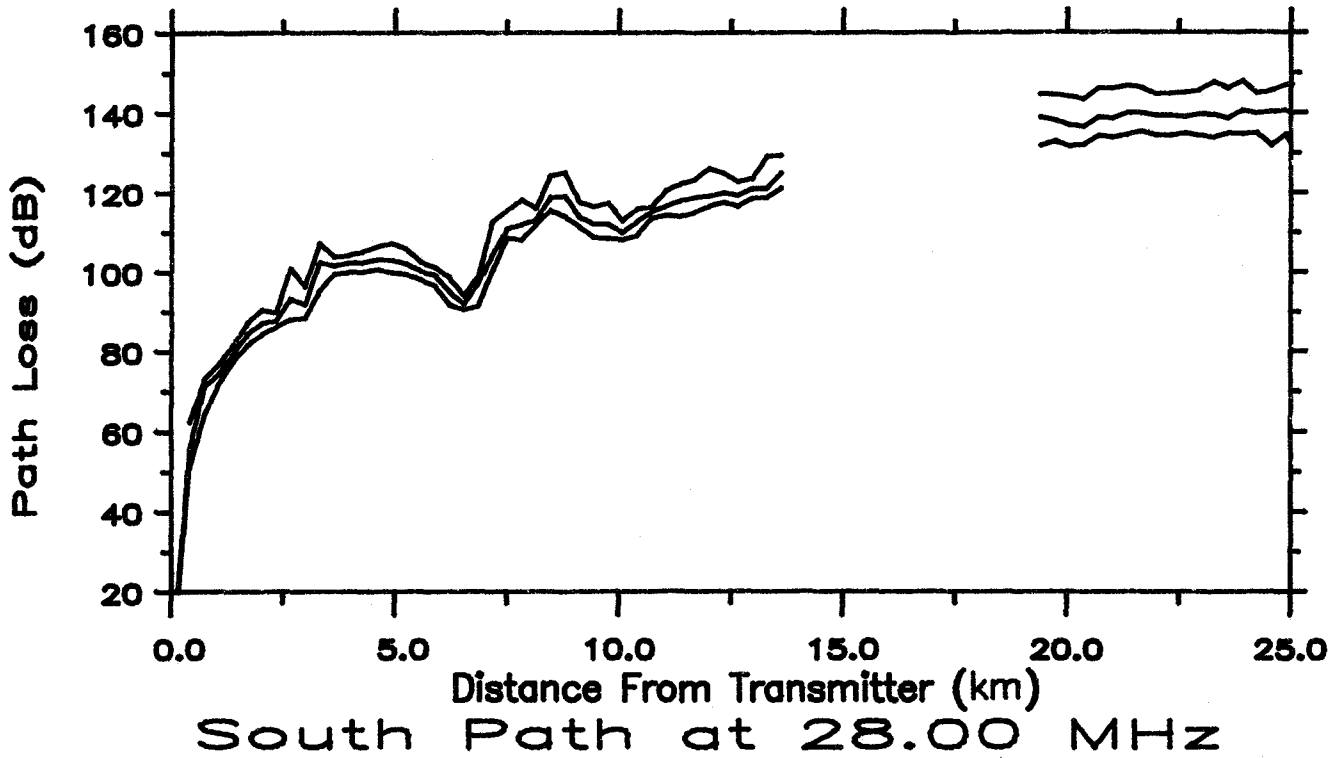


Figure 28. Plots of median, upper, and lower decile path loss measured along the South Path at 28.00 MHz.

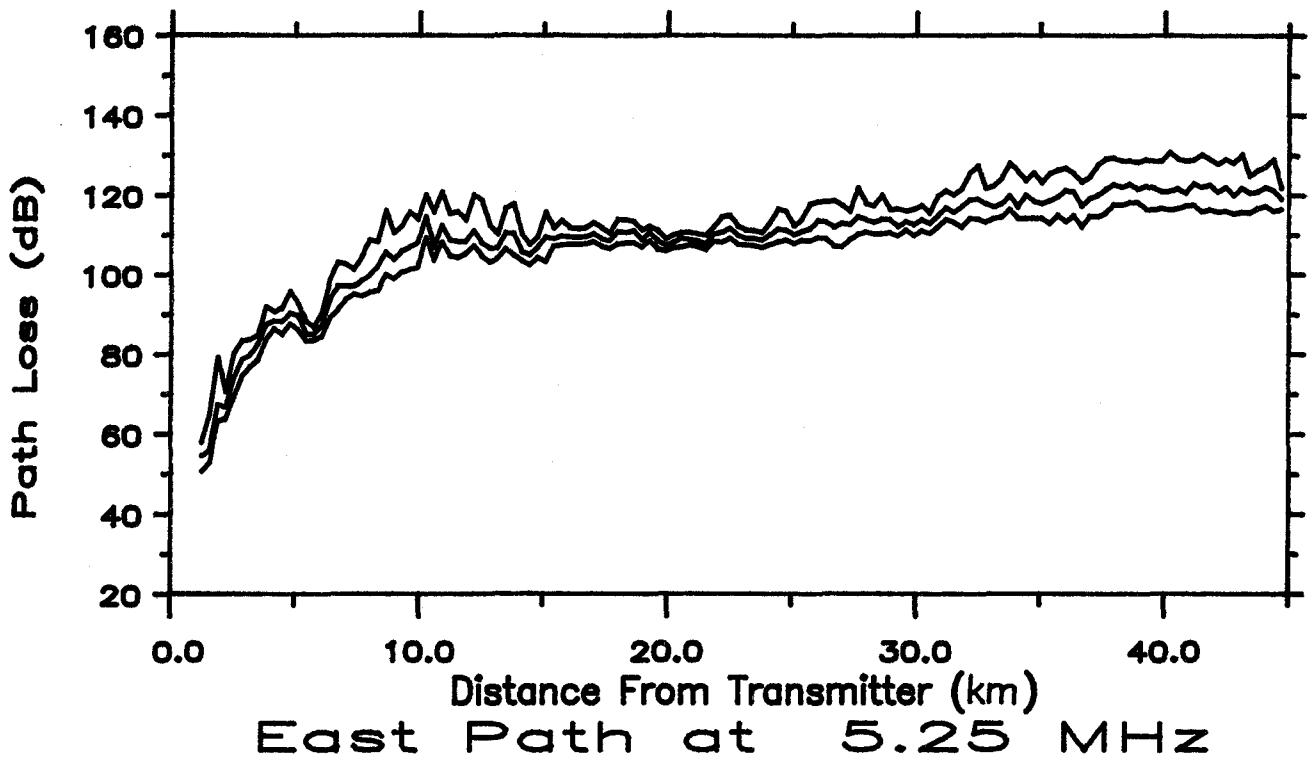
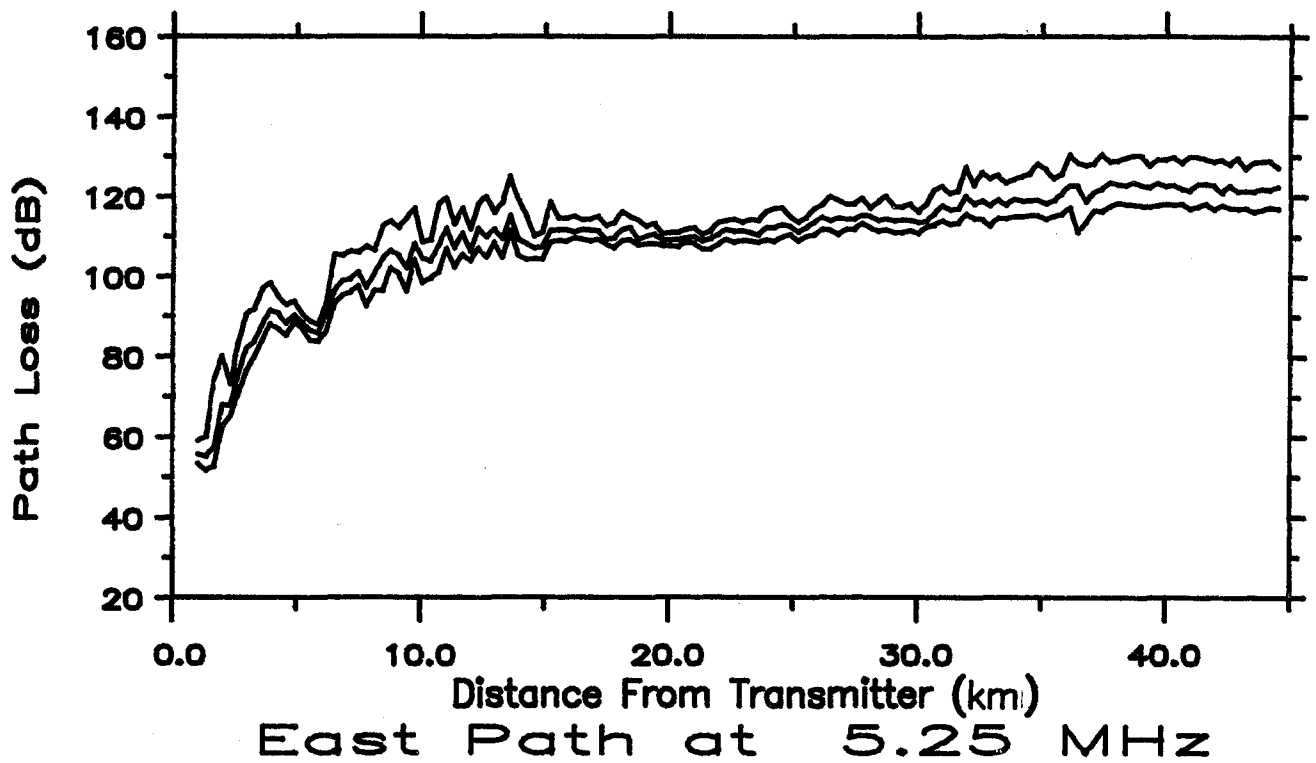


Figure 29. Plots of median, upper, and lower decile path loss measured along the East Path without snow cover at 5.25 MHz.

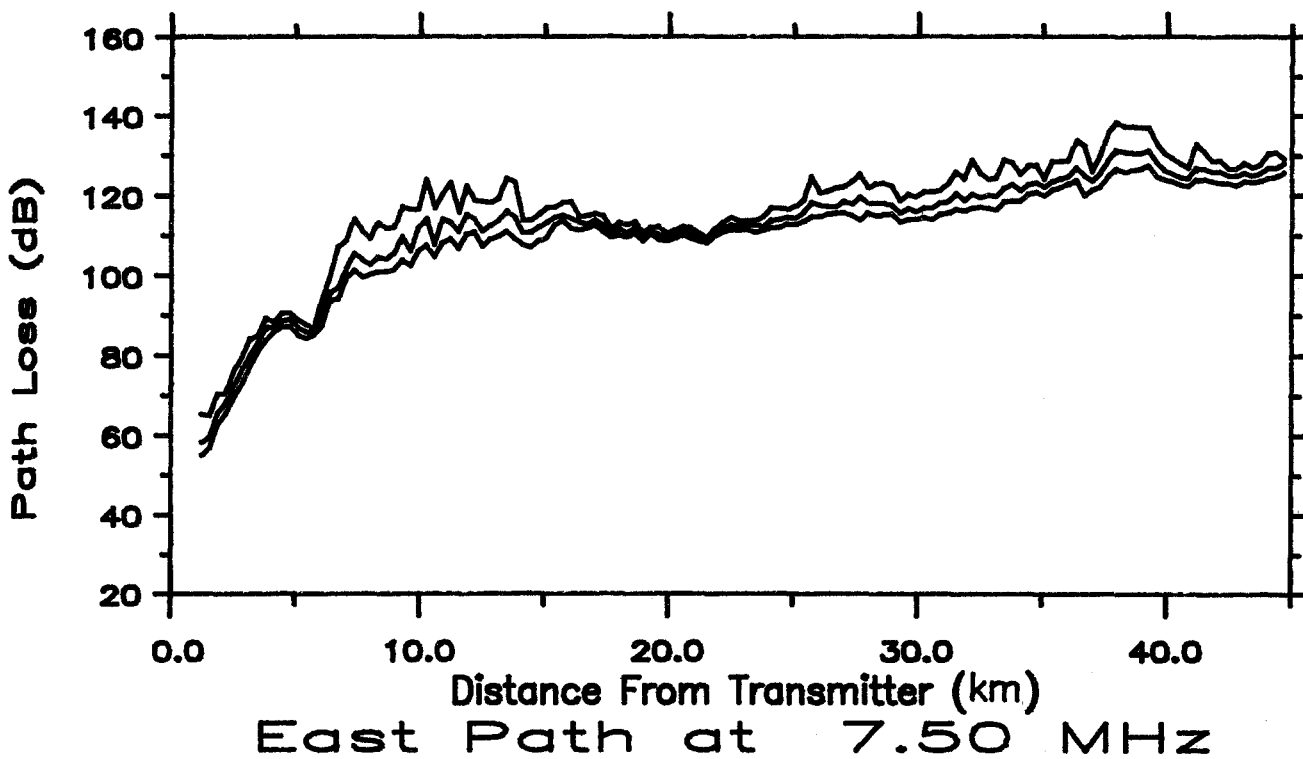
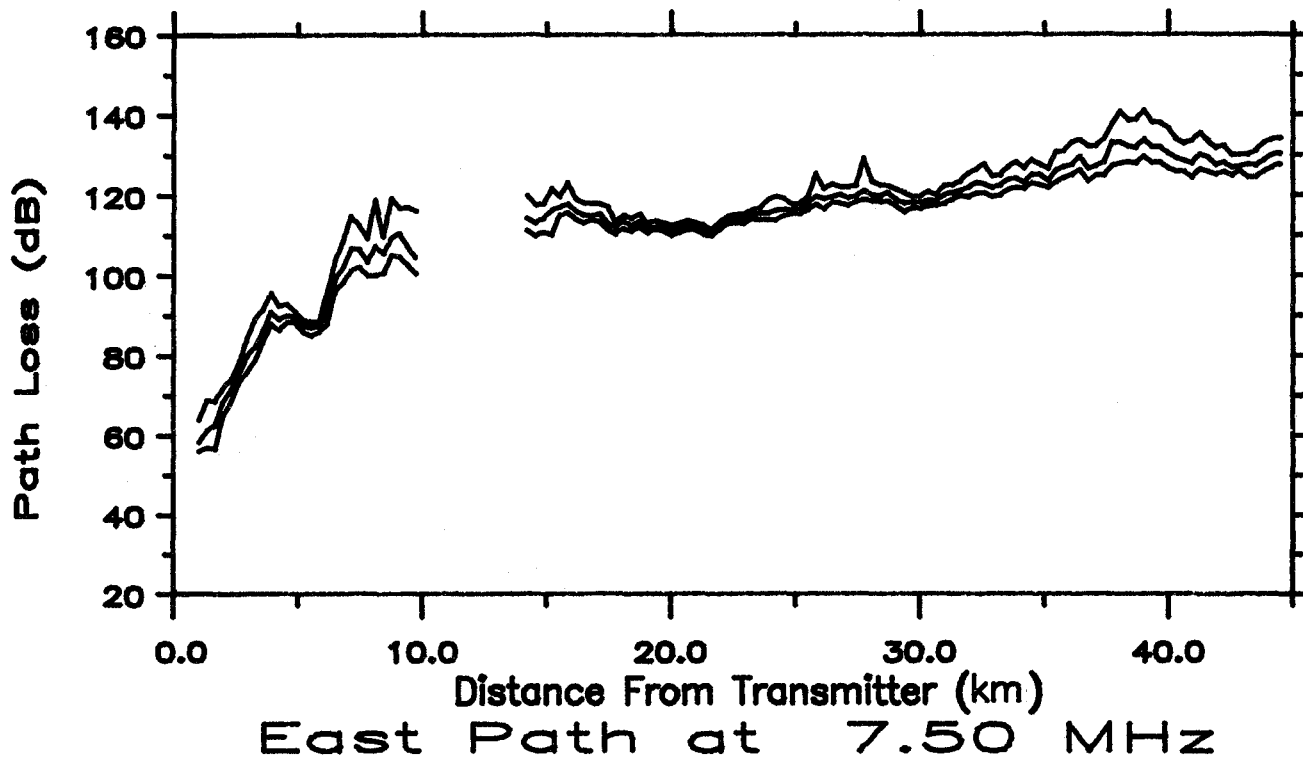


Figure 30. Plots of median, upper, and lower decile path loss measured along the East Path without snow cover at 7.50 MHz.

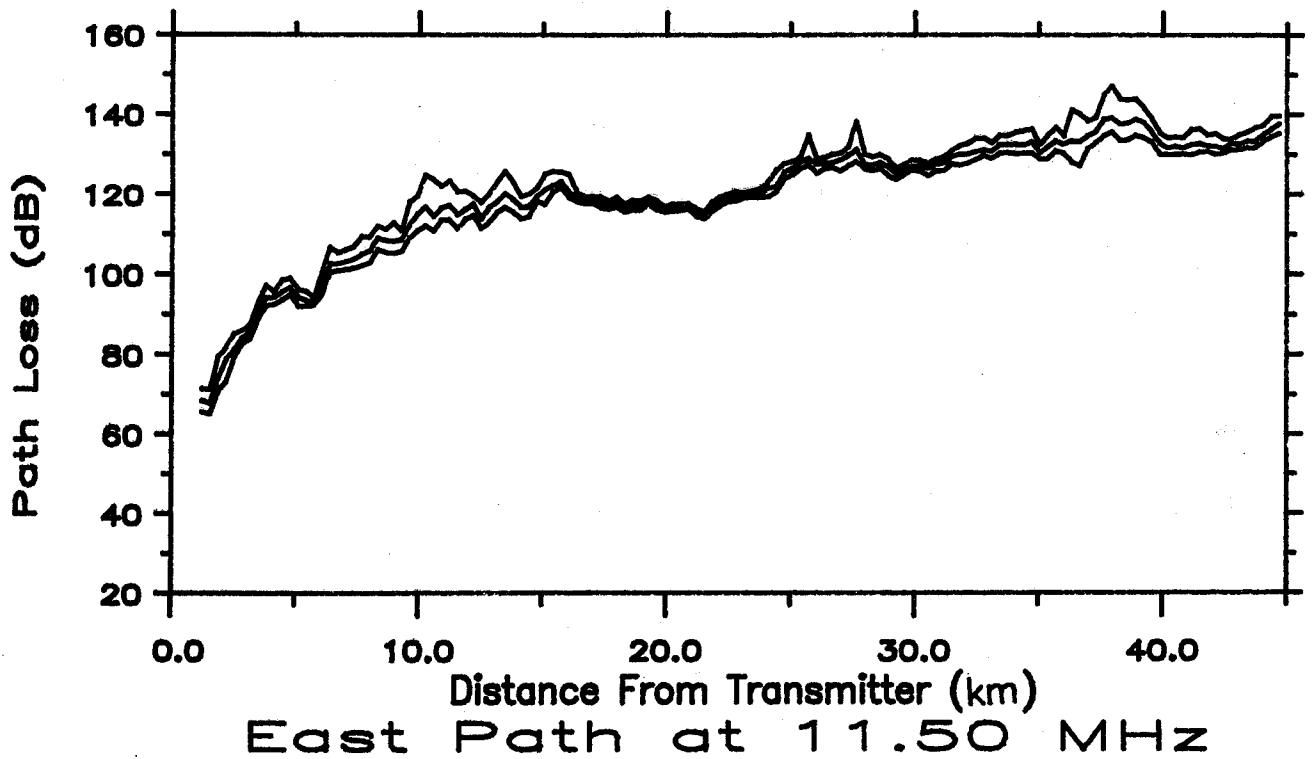
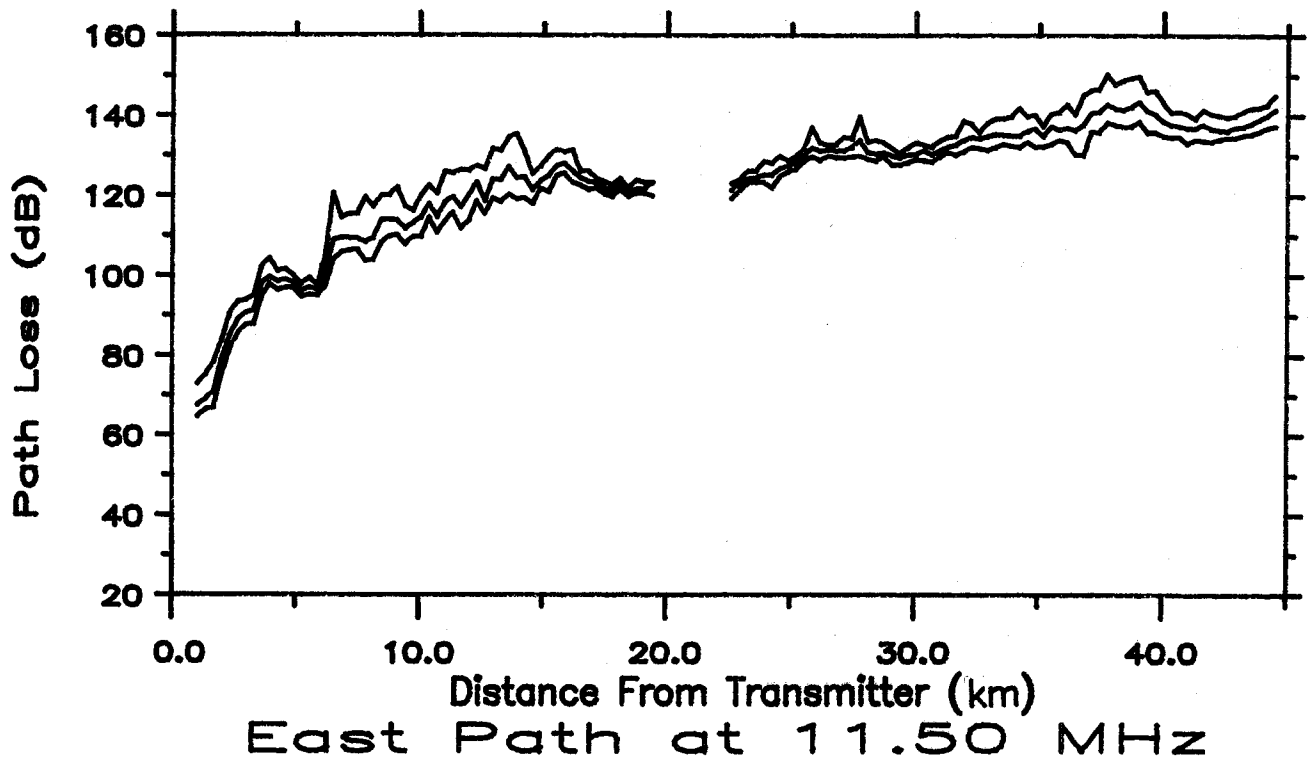


Figure 31. Plots of median, upper, and lower decile path loss measured along the East Path without snow cover at 11.50 MHz.

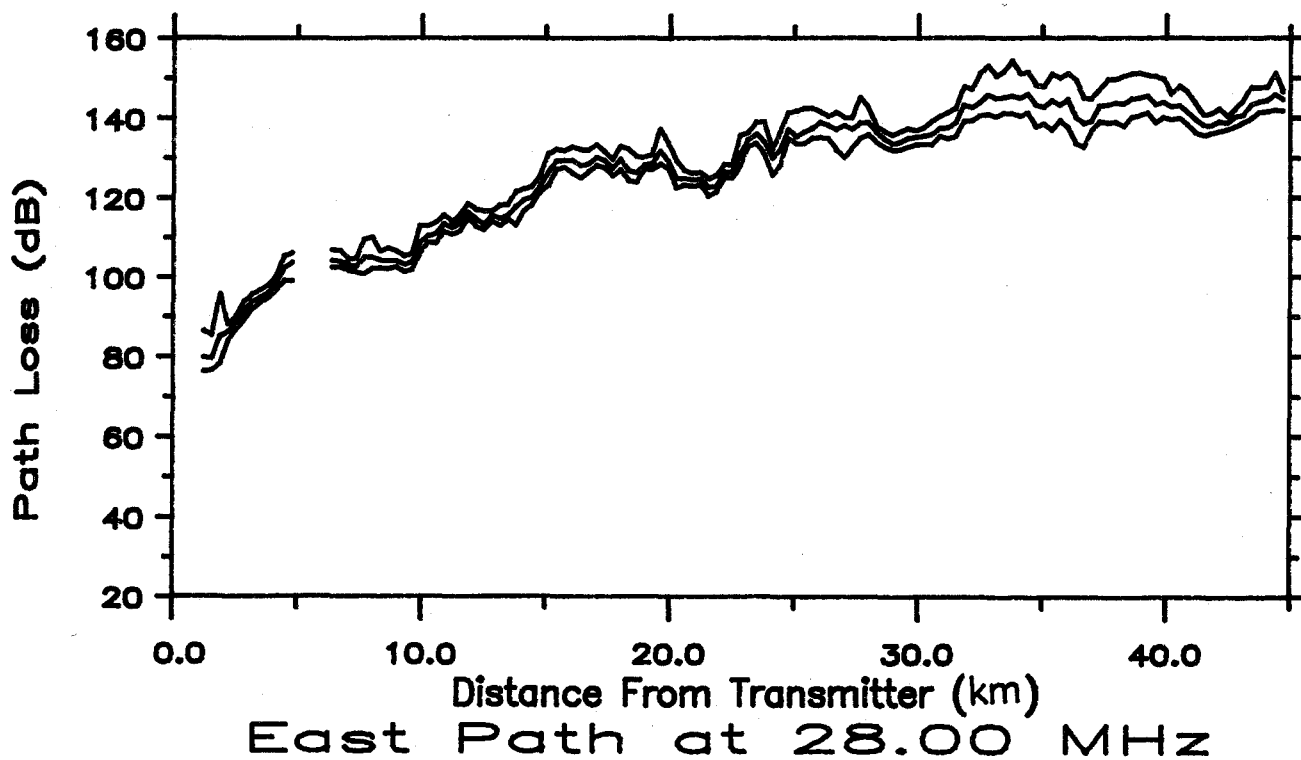
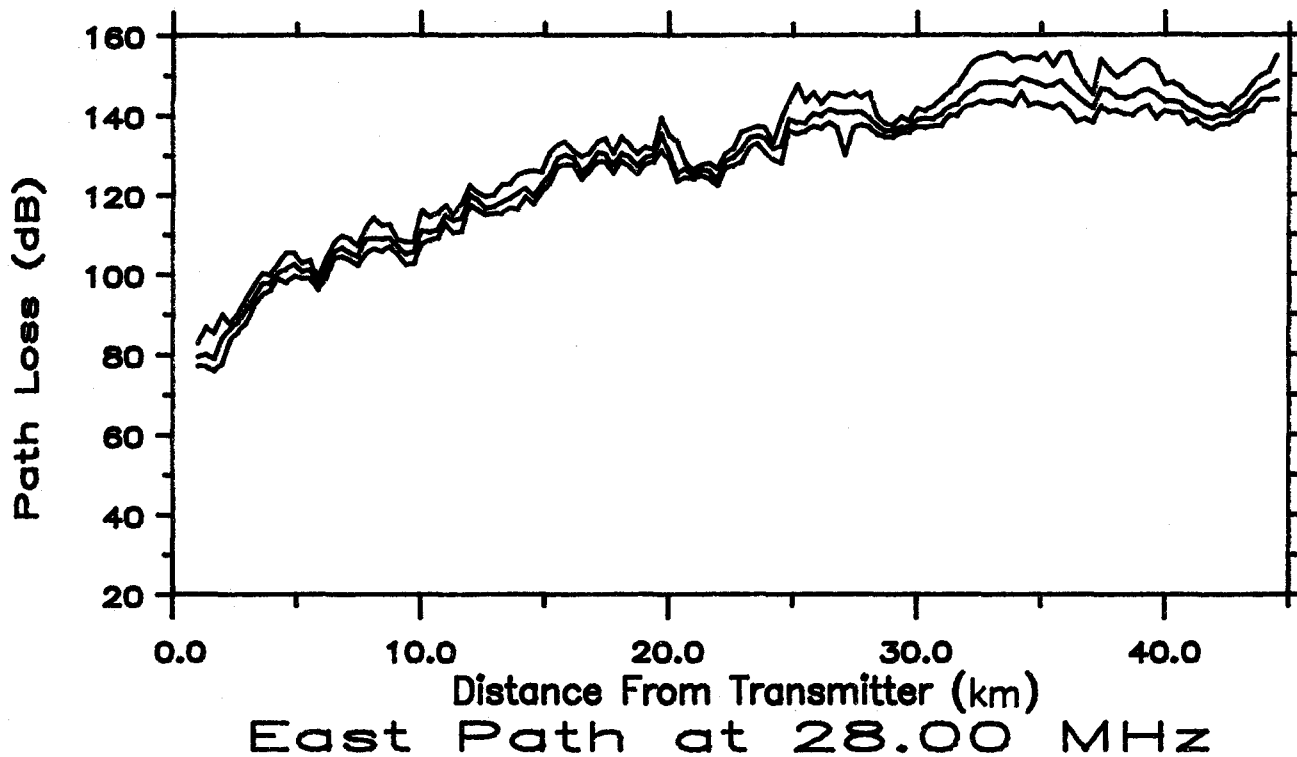
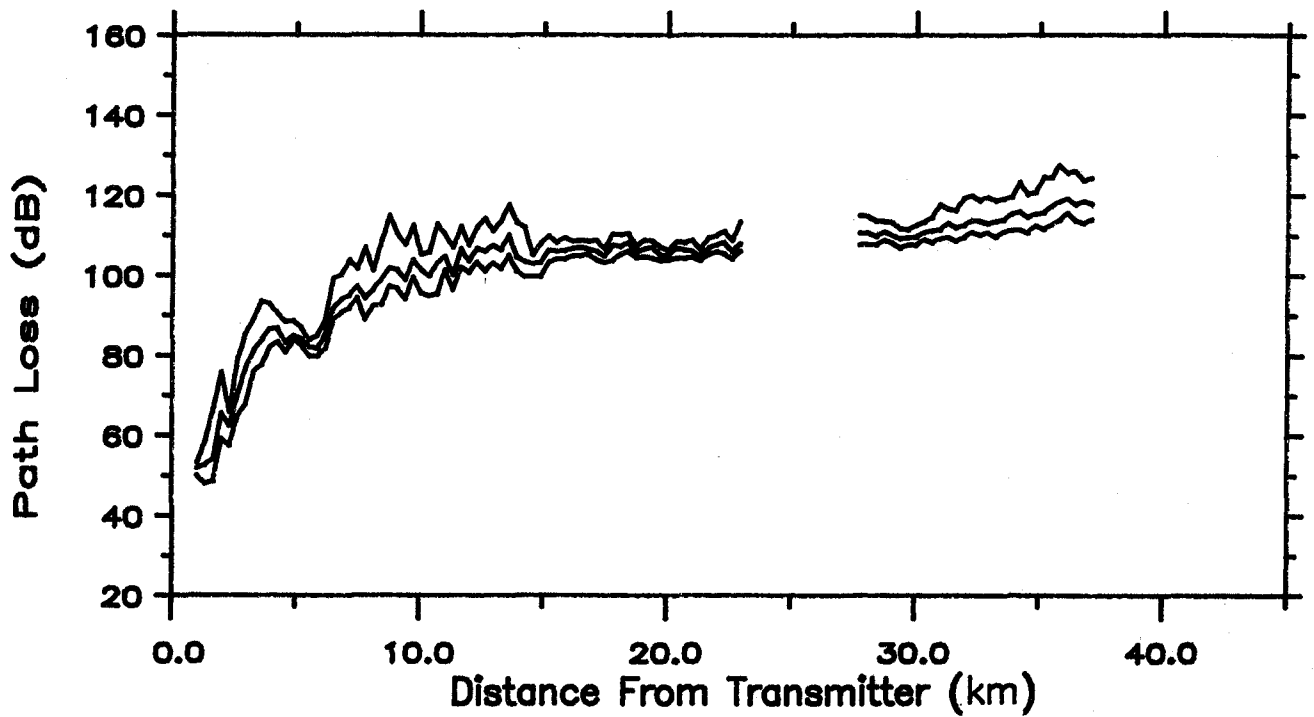
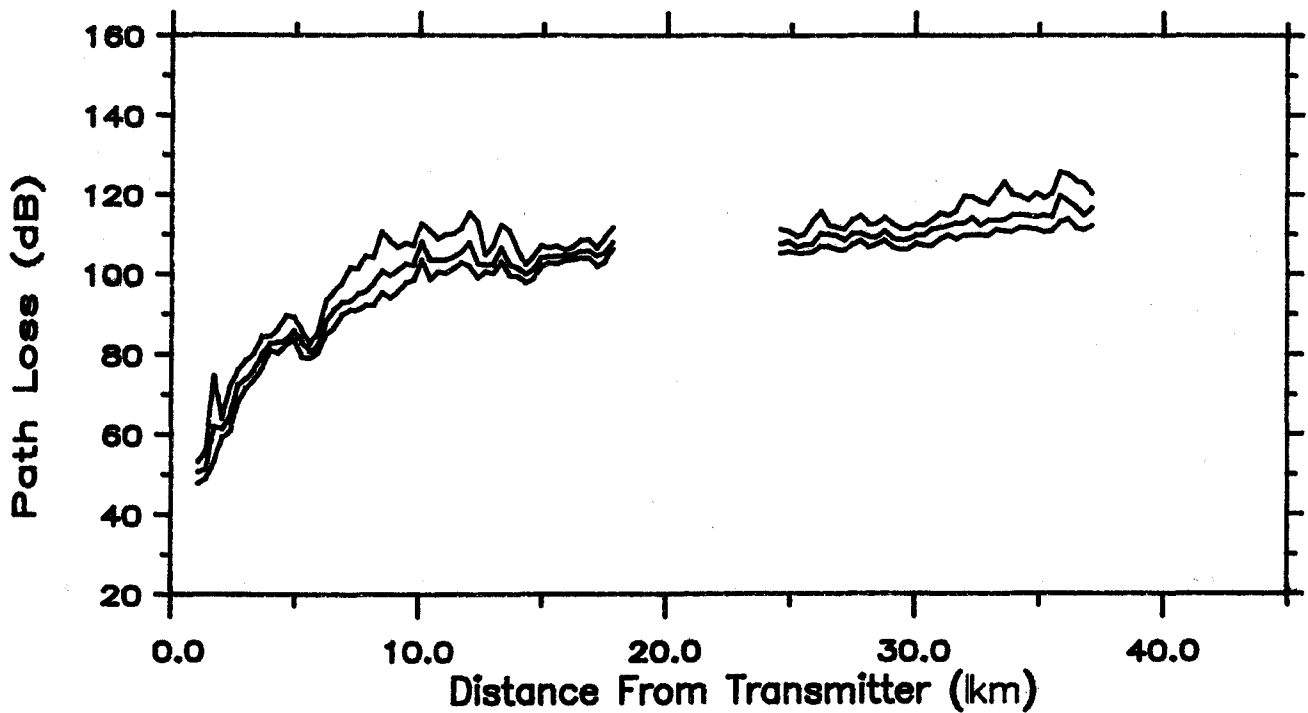


Figure 32. Plots of median, upper, and lower decile path loss measured along the East Path without snow cover at 28.00 MHz.



E. Path W/Snow at 5.25 MHz



E. Path W/Snow at 5.25 MHz

Figure 33. Plots of median, upper, and lower decile path loss measured along the East Path with snow cover at 5.25 MHz.

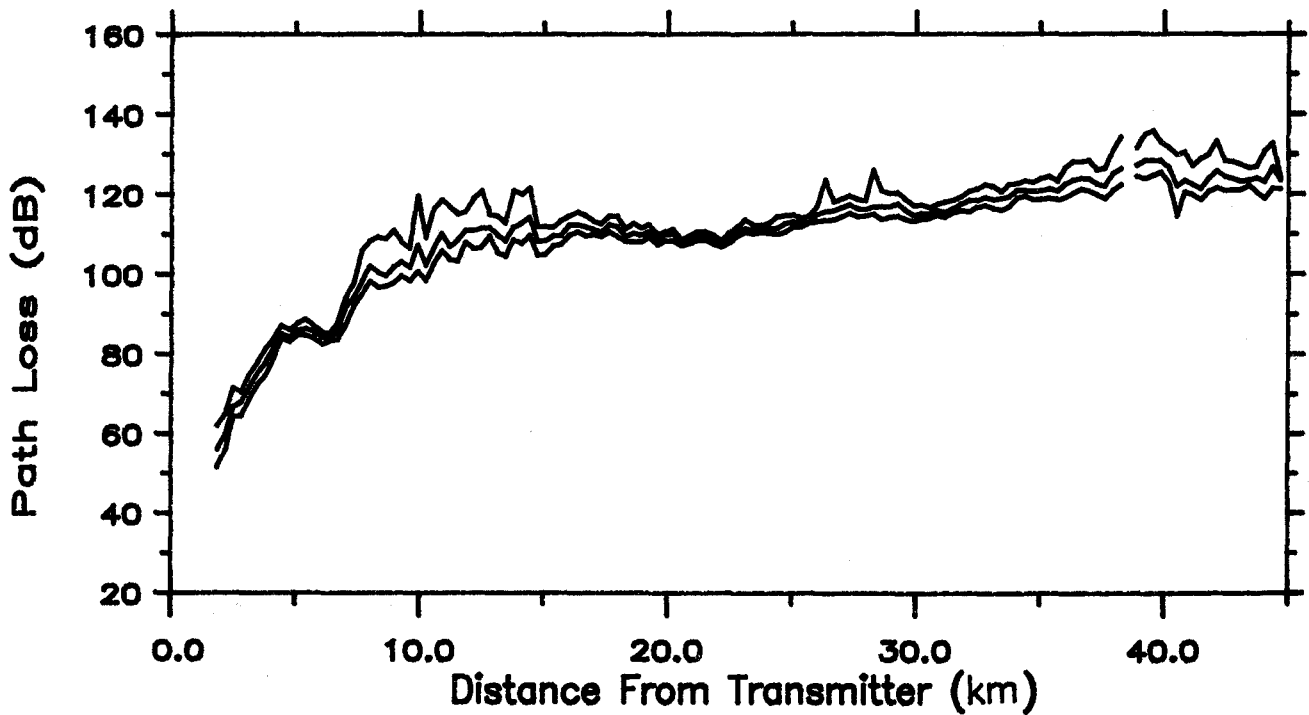
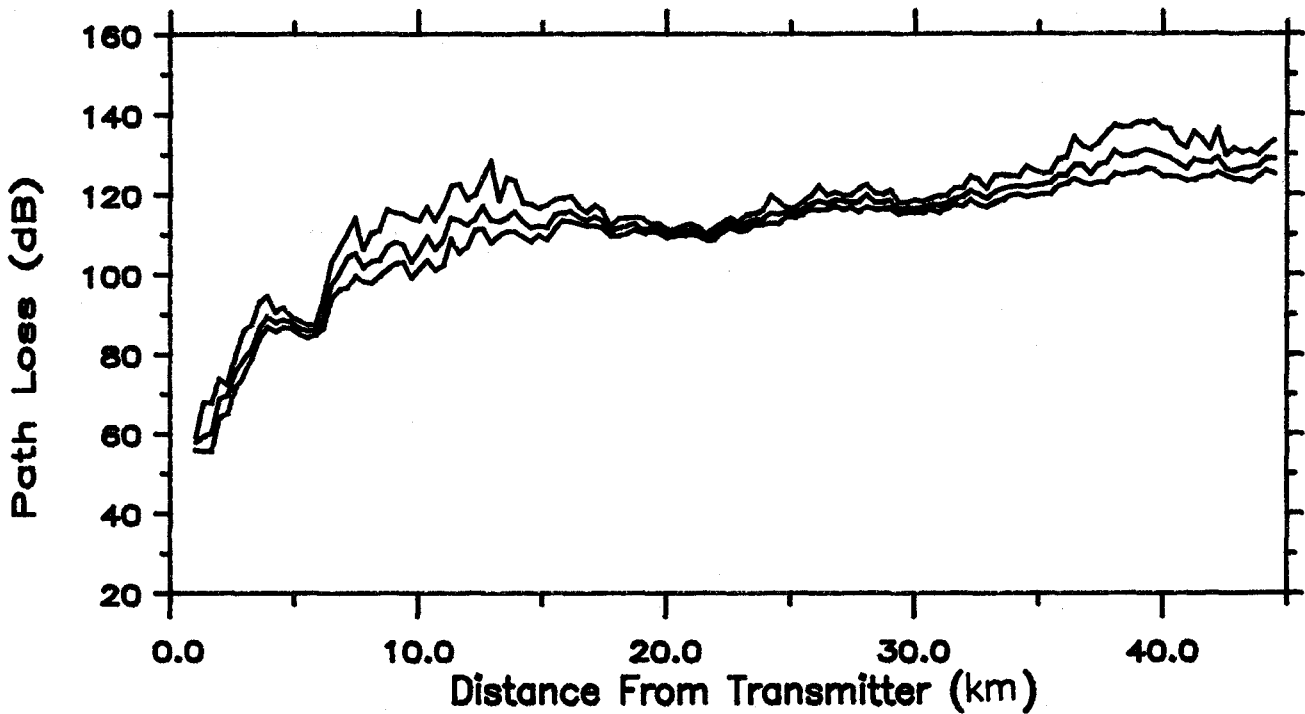


Figure 34. Plots of median, upper, and lower decile path loss measured along the East Path with snow cover at 7.50 MHz.

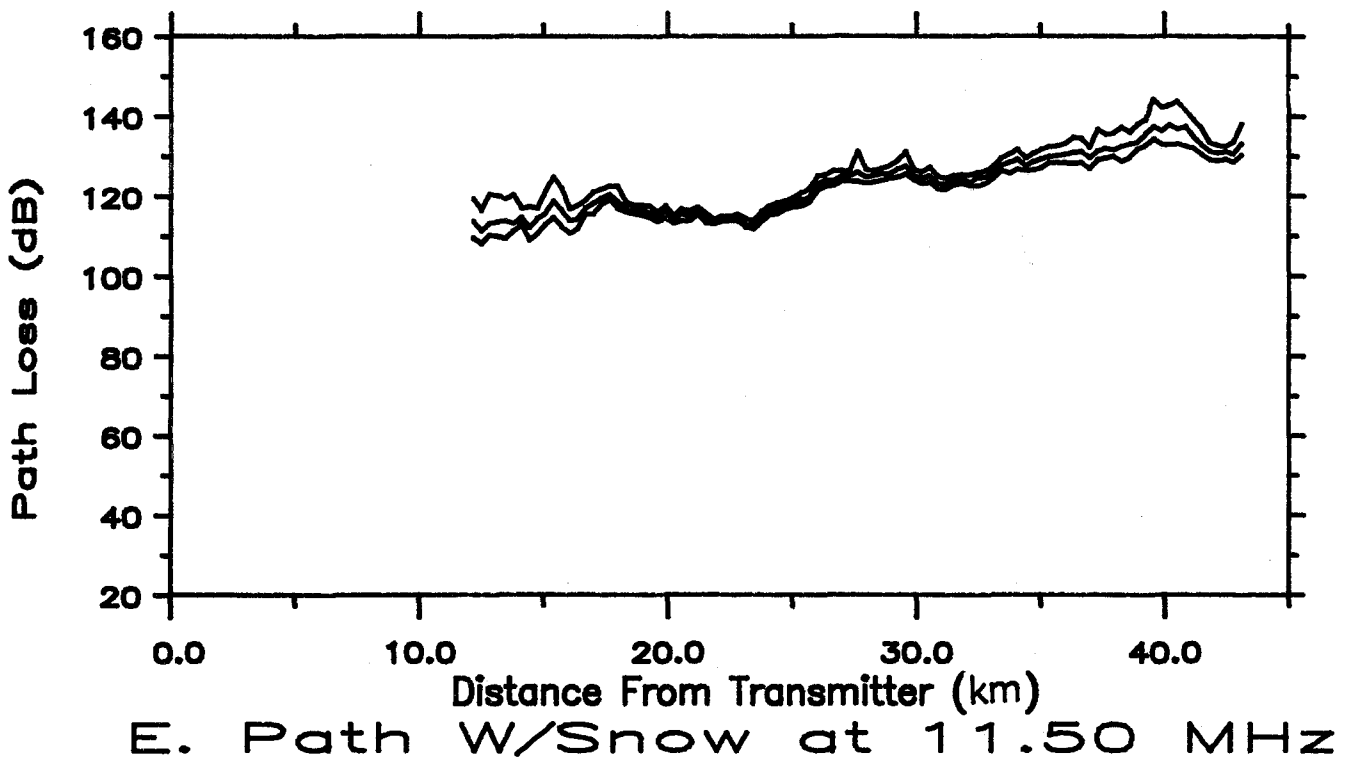
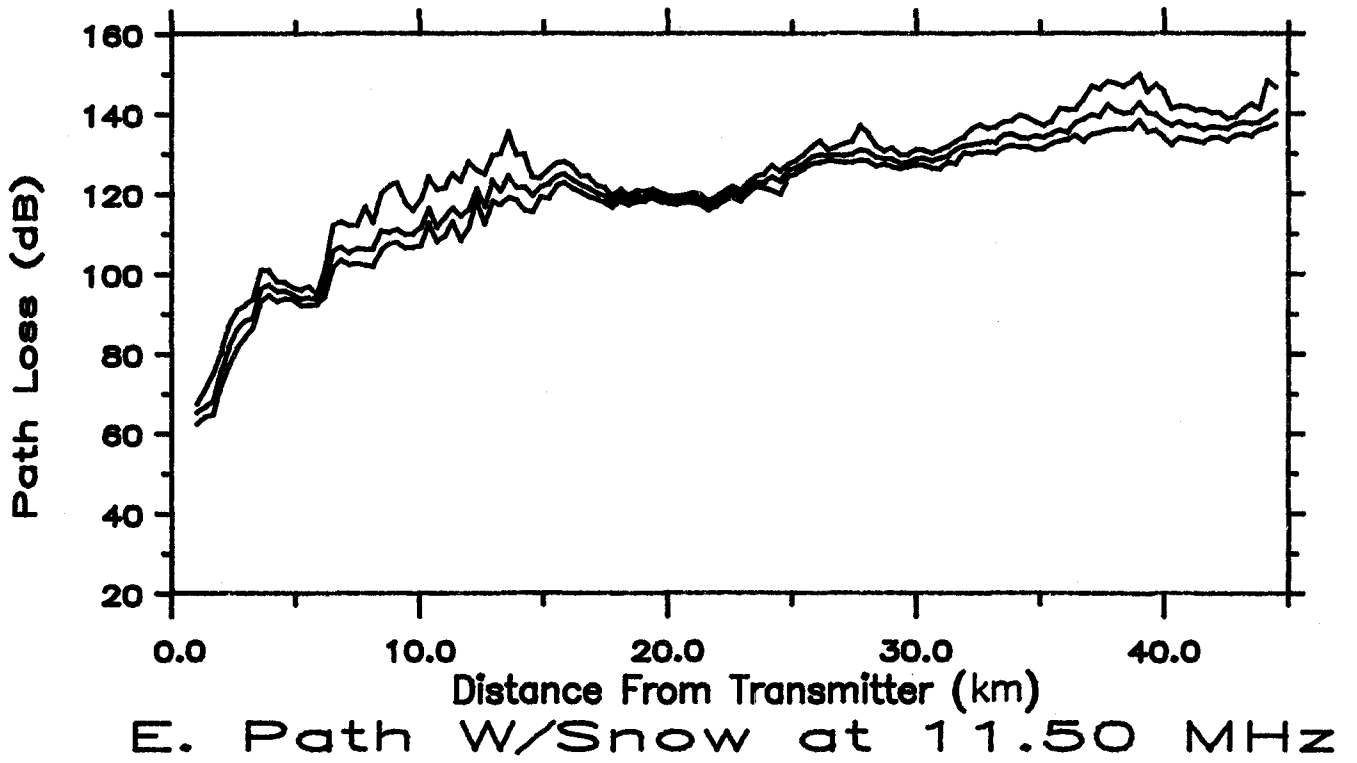
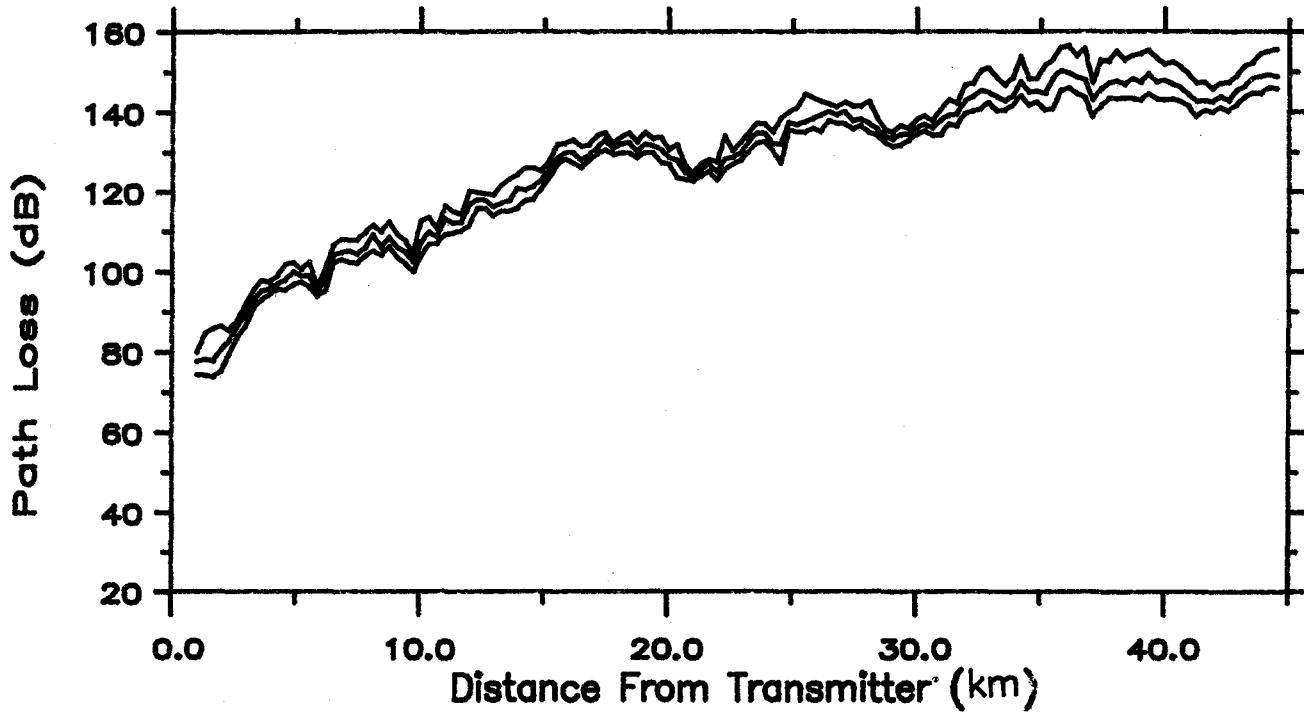
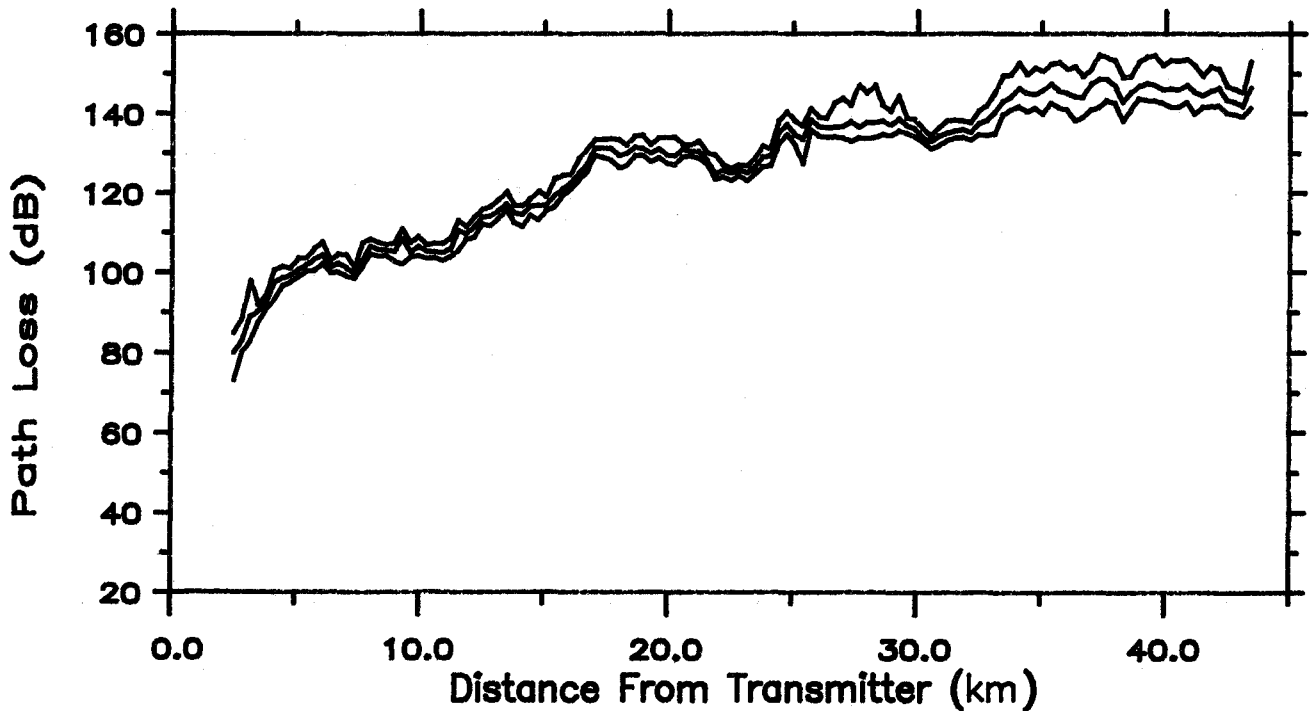


Figure 35. Plots of median, upper, and lower decile path loss measured along the East Path with snow cover at 11.50 MHz.



E. Path W/Snow at 28.00 MHz



E. Path W/Snow at 28.00 MHz

Figure 36. Plots of median, upper, and lower decile path loss measured along the East Path with snow cover at 28.00 MHz.

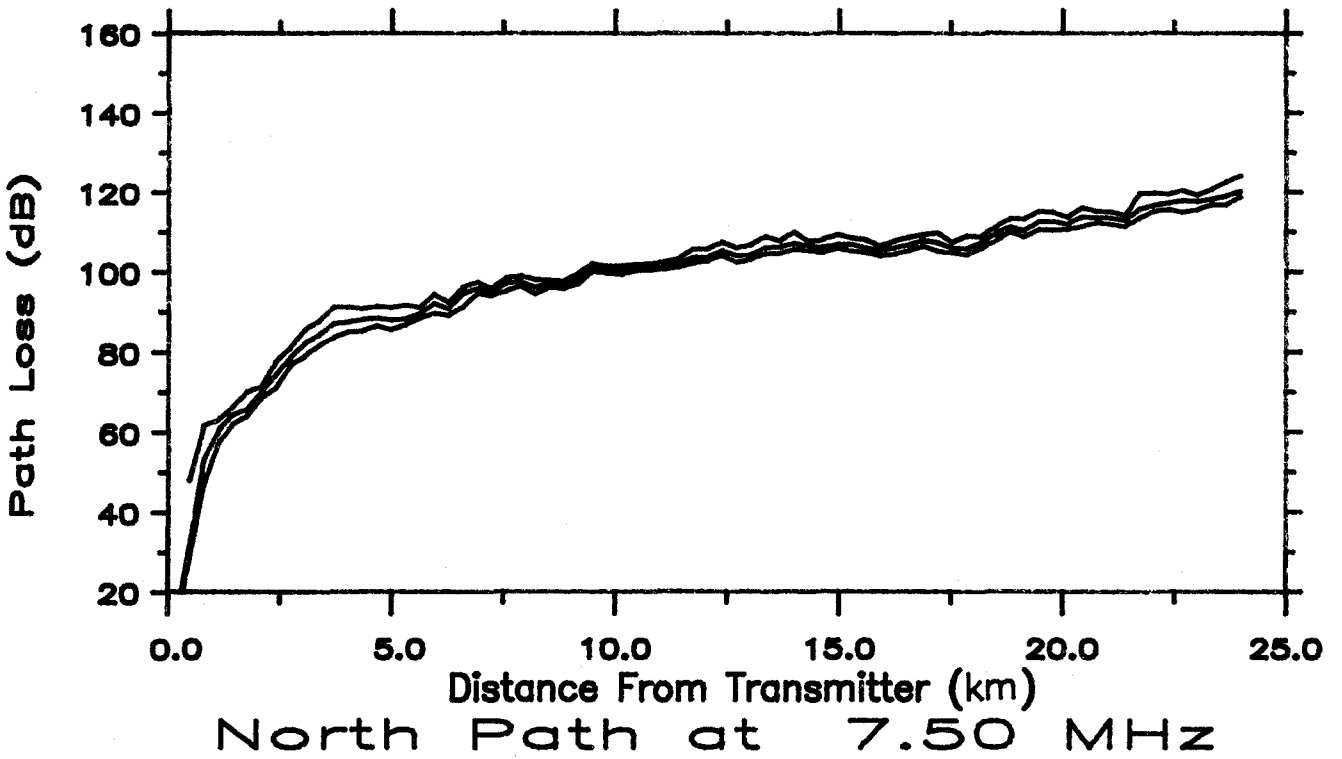
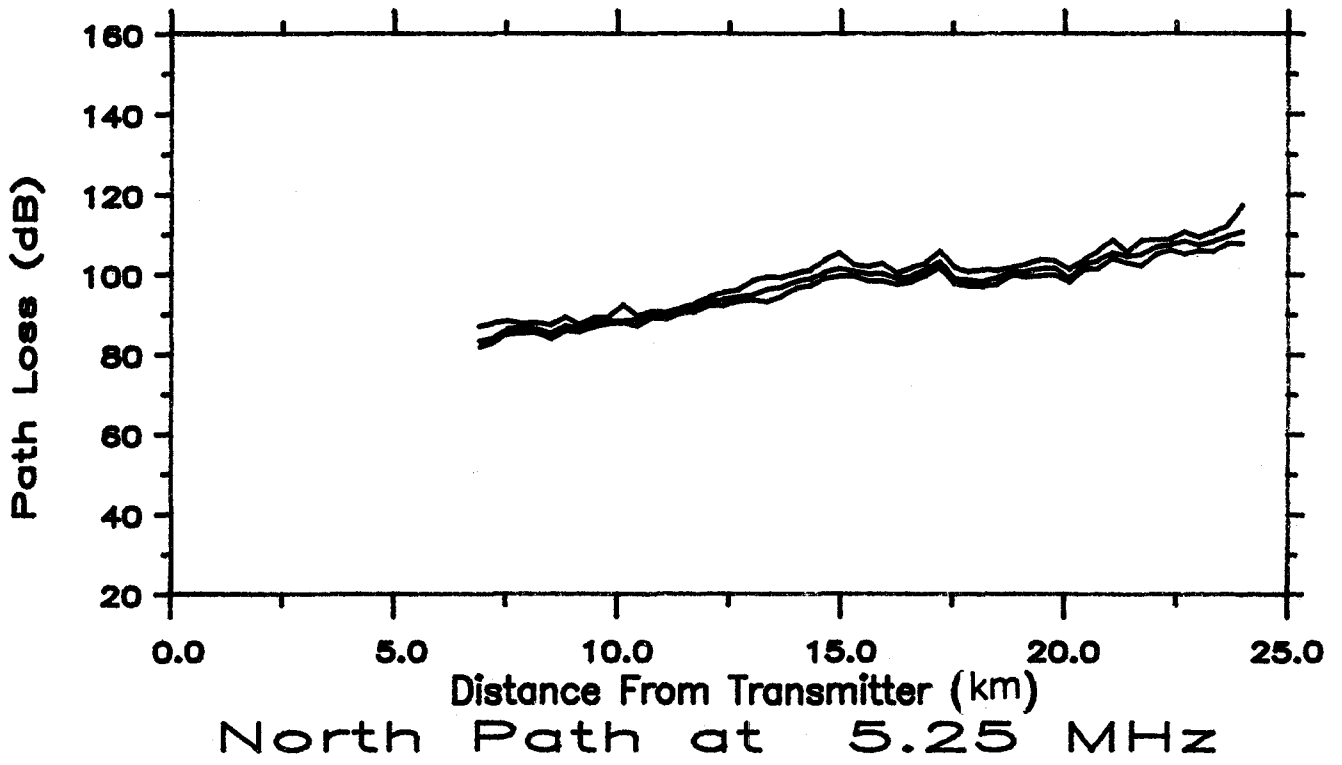


Figure 37. Plots of median, upper, and lower decile path loss measured along the North Path at 5.25 and 7.50 MHz.

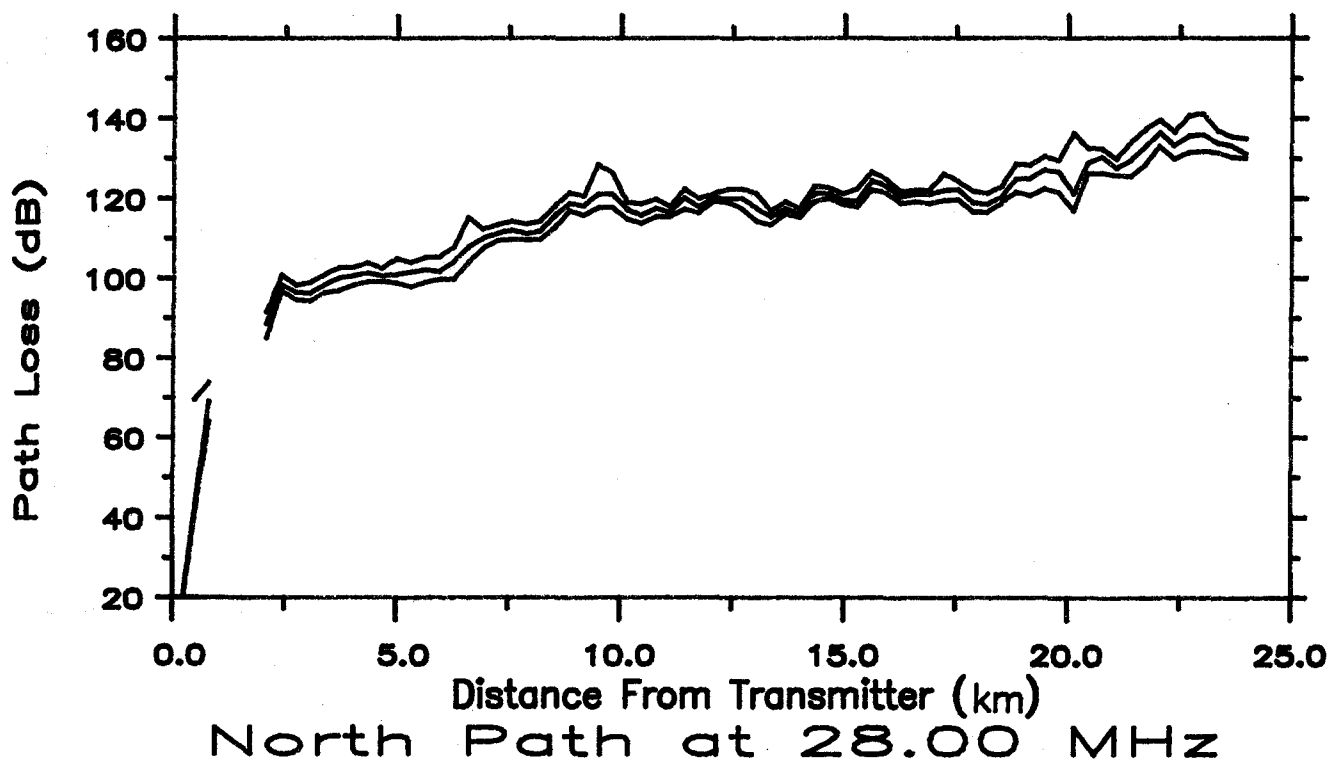
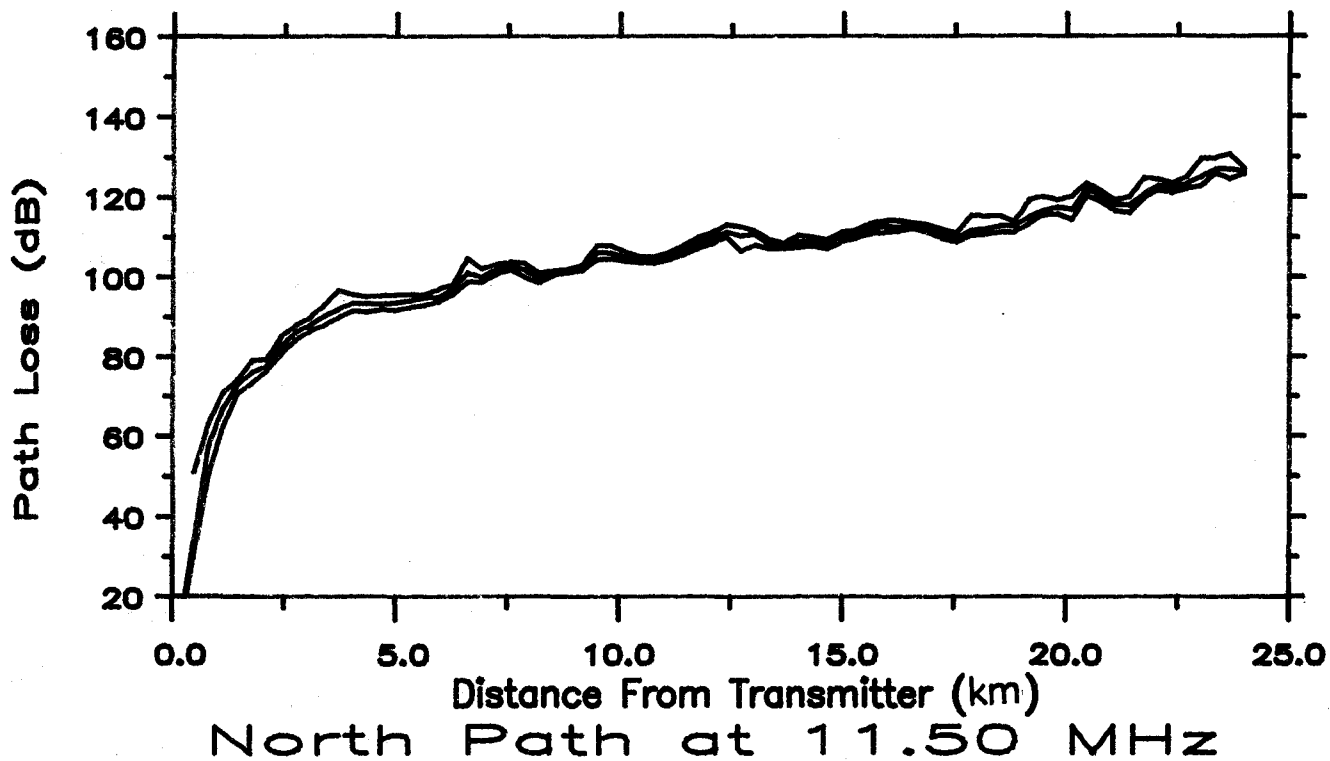


Figure 38. Plots of median, upper, and lower decile path loss measured along the North Path at 11.50 and 28.00 MHz.

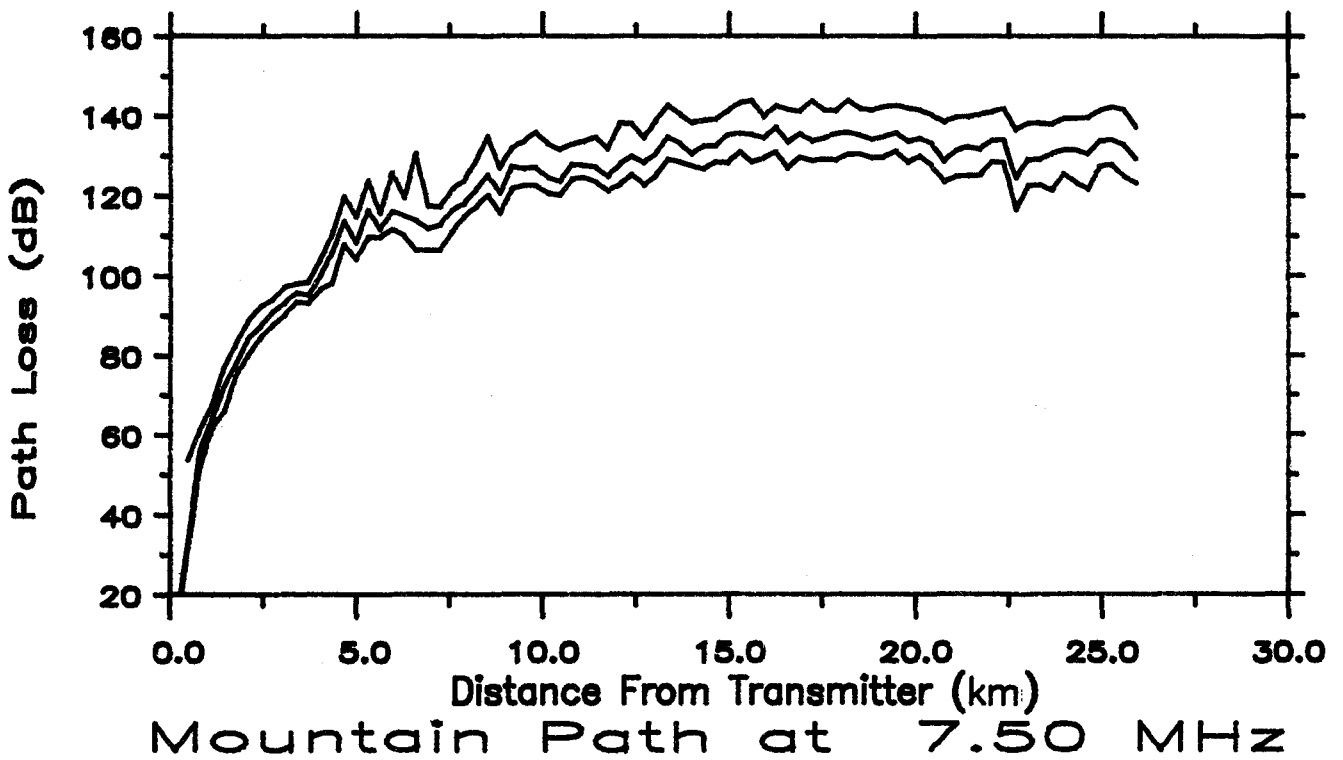
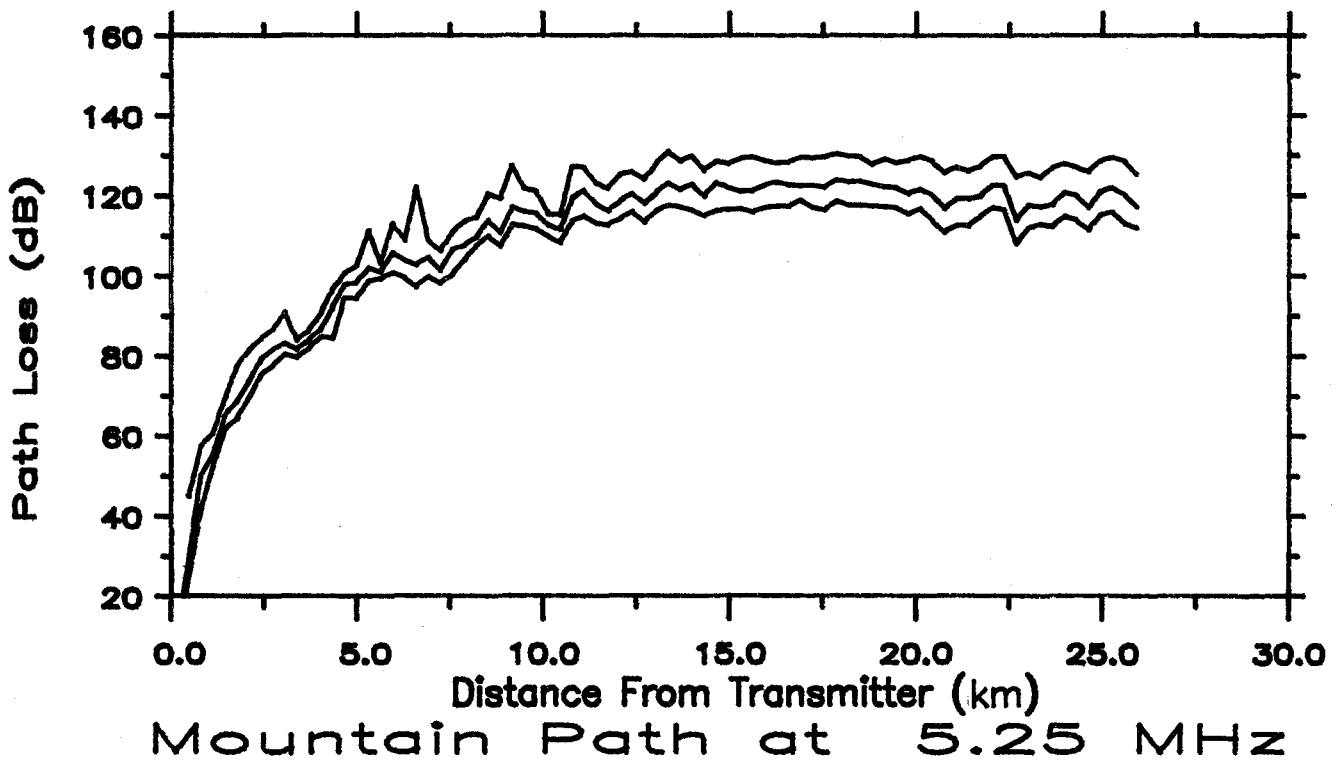


Figure 39. Plots of median, upper, and lower decile path loss measured along the Mountain Path at 5.25 and 7.50 MHz.

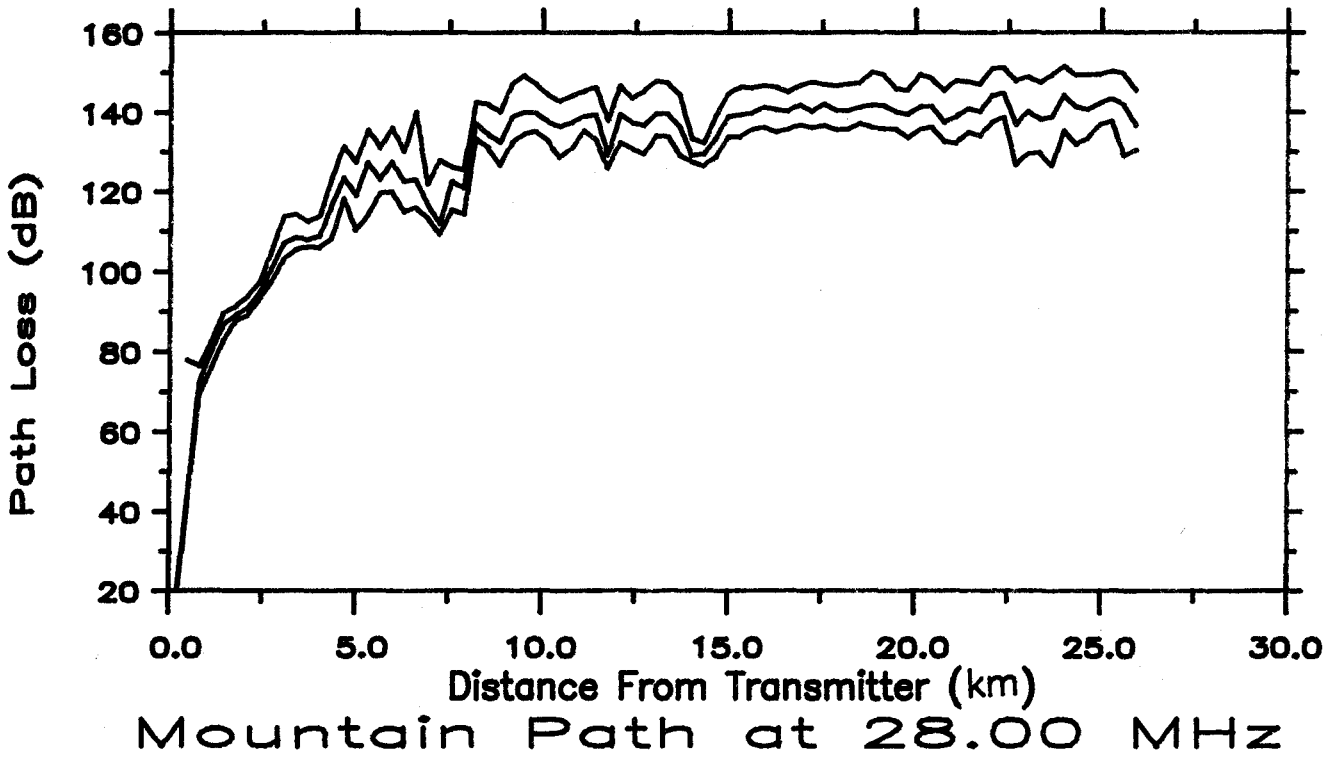
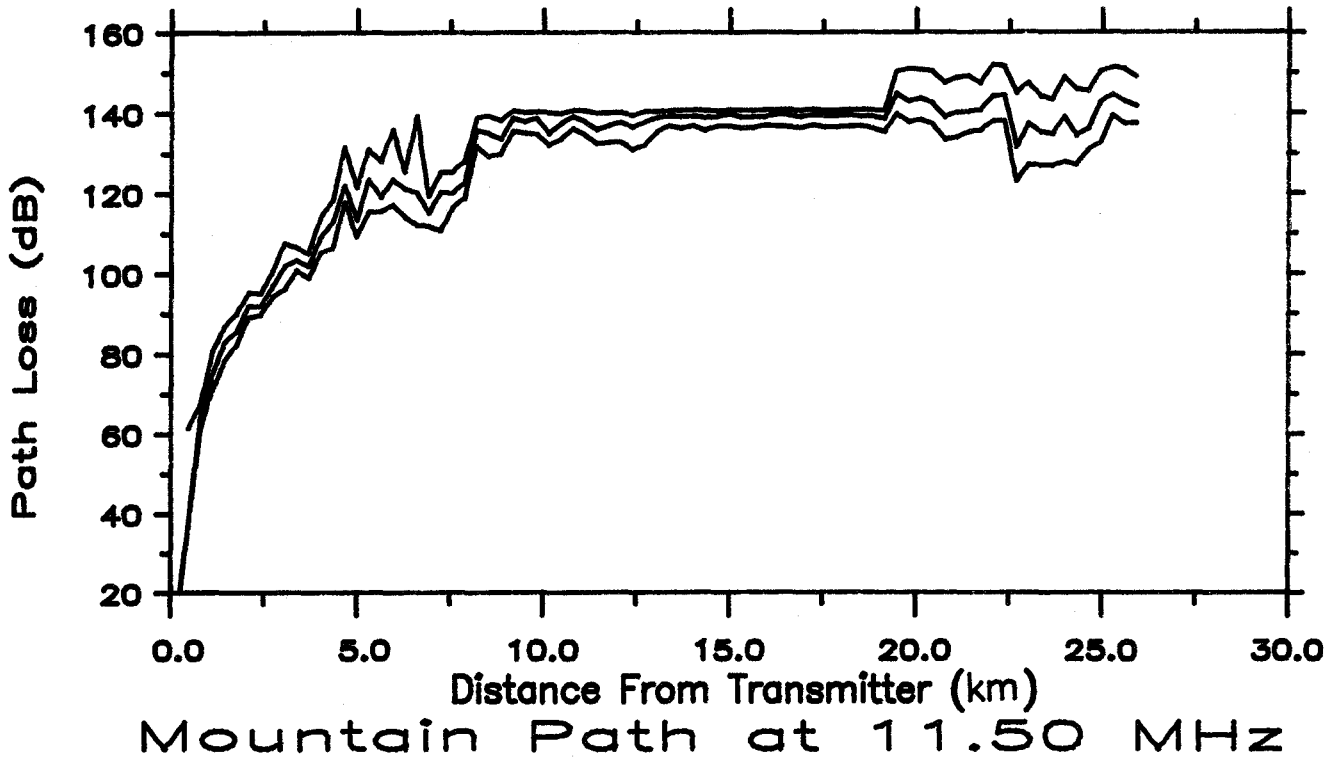


Figure 40. Plots of median, upper, and lower decile path loss measured along the Mountain Path at 11.50 and 28.00 MHz.

6. GROUND CONSTANT CALCULATIONS

6.1 Background

Two of the required parameters for the prediction program WAGSLAB are the terrain's ground constants, conductivity and permittivity. We selected the wave-tilt method for making the ground constants measurements. Details of the technique and the instrumentation are contained in Appendix B.

The underlying theory for the wave-tilt method is described in numerous reports (CCIR, 1982b; IEEE, 1974). An article by Eaton (1976) contains an informative description and development of the theory.

The relative permittivity, ϵ_r , is given by,

$$\epsilon_r = \frac{\left[\frac{1+r^2 \tan^2 \theta}{r^2 + \tan^2 \theta} \right] \left[\frac{[(1-r^2) \sin(2\theta)]^2 - 4r^2}{[(1-r^2) \sin(2\theta)]^2 + 4r^2} \right]}{\quad} \quad (1)$$

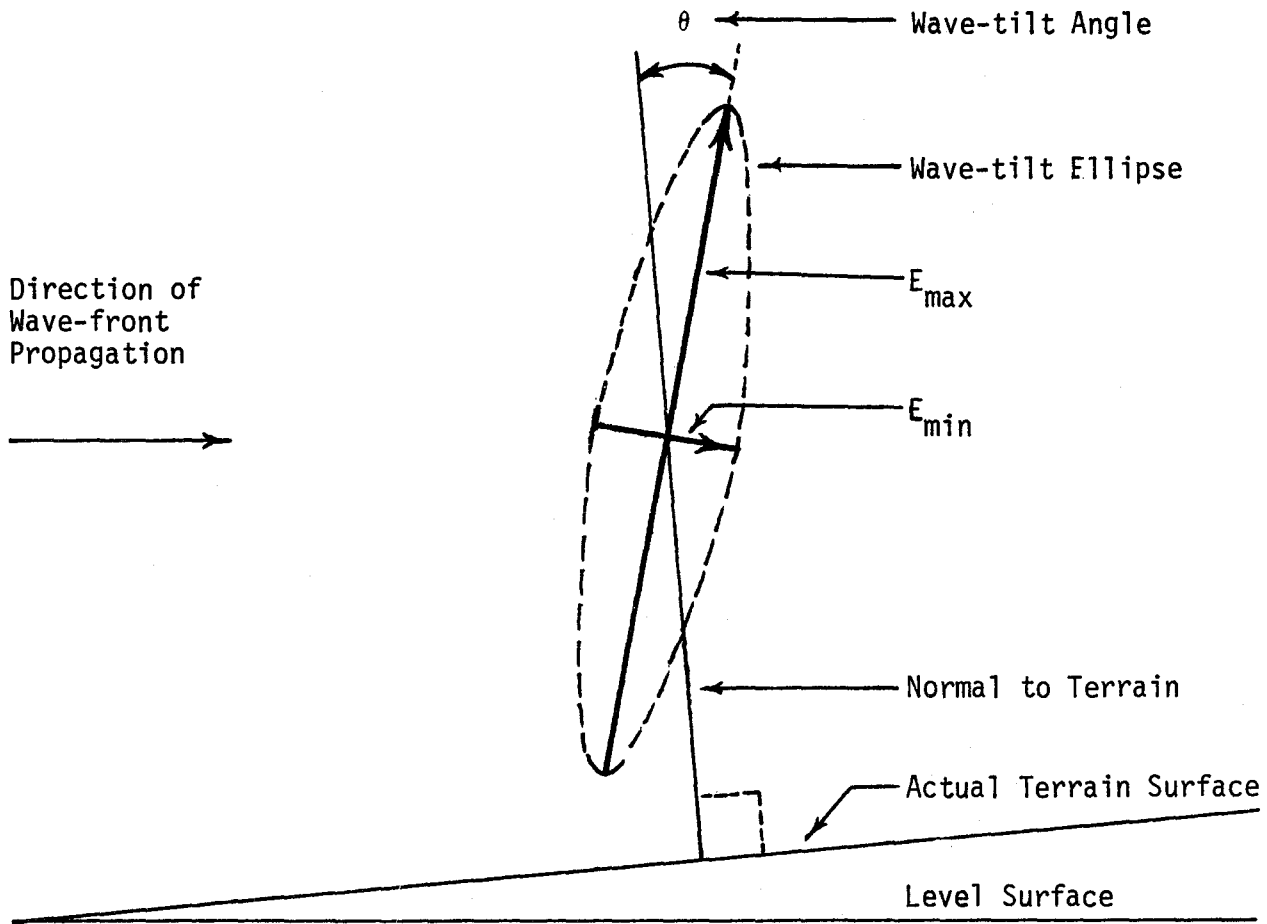
where θ is the tilt angle, and r is the minimum to maximum E-field component ratio (see Figure 41 for a sketch of the components). The effective conductivity over frequency, $\frac{\sigma}{f}$, is given by

$$\frac{\sigma}{f} = \frac{1}{18} \left[\frac{1+r^2 \tan^2 \theta}{r^2 + \tan^2 \theta} \right] \left[1 - \left(\frac{[(1-r^2) \sin(2\theta)]^2 - 4r^2}{[(1-r^2) \sin(2\theta)]^2 + 4r^2} \right)^2 \right]^{1/2} \quad (2)$$

where f is given in MHz, and σ in mS/m. By inserting measured values of r and θ , the relative permittivity and effective conductivity of the ground can then be determined.

6.2 Experimental Results

Six different closely-spaced receiver sites were used. Several of the sites chosen violated the measurement conditions mentioned in Appendix B, but



For a cw signal transmitted from a vertical electric monopole at the left, the ground constants ϵ_r and σ give rise to a component of E parallel to the earth. This component is much smaller than the perpendicular E component and leads it in phase. As a result, a time plot of the electric field vector endpoint traces out an ellipse. This elliptical polarization is shown above. The angle, θ , is known as the wave-tilt angle and the ratio of E_{min} to E_{max} is termed the wave-tilt ratio, r (Jordan et al., 1968).

Figure 41. Elliptical polarization of the electric vector at the surface of an earth that is not a perfect conductor.

were chosen intentionally to see what effects were detectable. Site 1 was located too close to the transmitter antenna and ground screen and near a large tree, Site 3 was only about 51 m (167 ft) from the transmitter; and Site 5 was near a thin line of trees. The reader should bear this in mind when looking at the test results. Test Sites 2, 4, and 6 best met the criteria under which the wave-tilt formulas, 1) and 2) above, have been deemed appropriate. A site map is shown in Figure 42.

The data measured as well as the ground constant results associated with the data are listed in Table 1 and plotted in Figures 43 through 46 as a function of r , θ , ϵ_r and σ . A sample calculation is given in Appendix B.

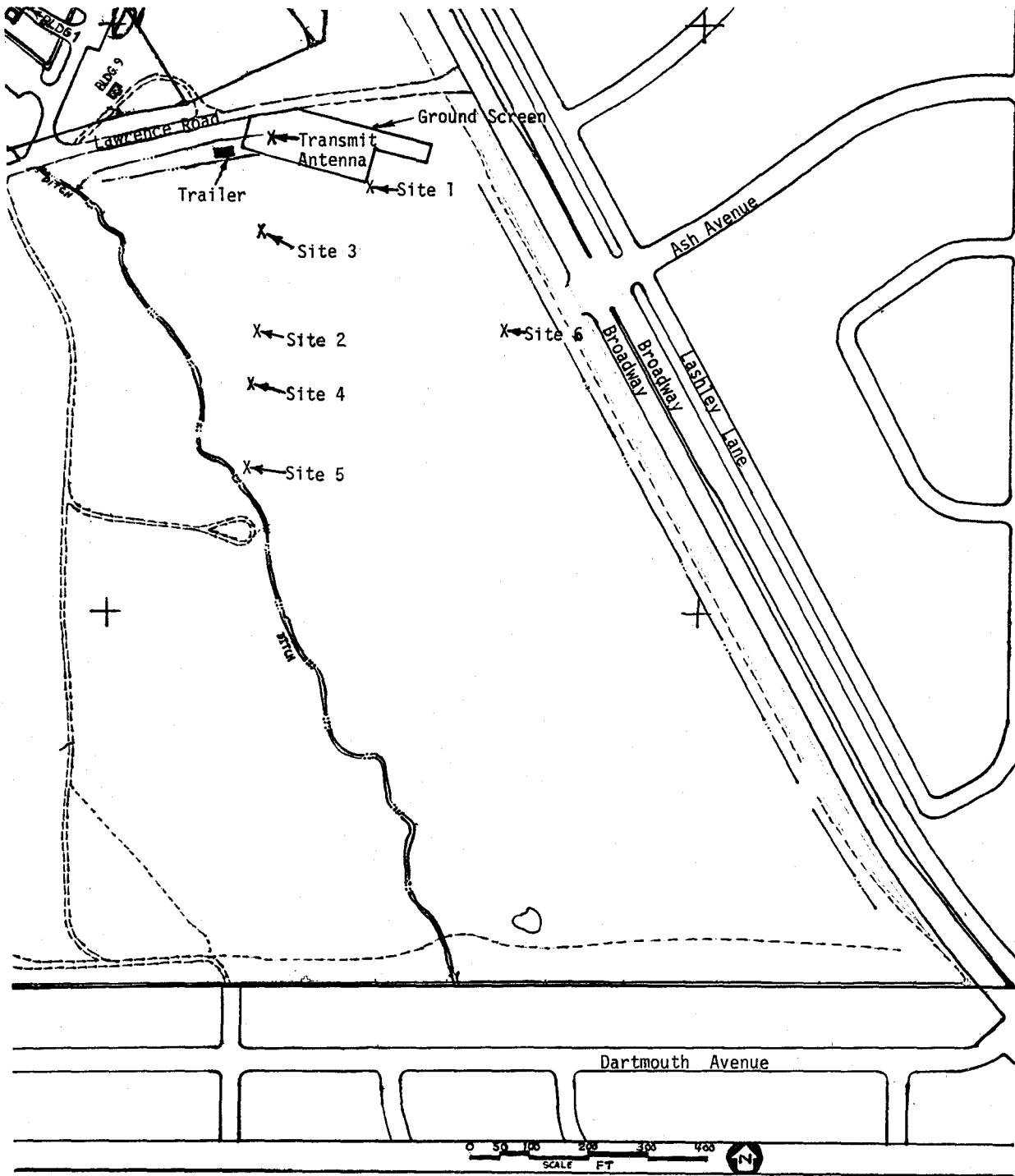
7. HF GROUND WAVE PREDICTIONS

7.1 Background

The computer program WAGSLAB (Hill, 1982) is used to numerically predict the electric field intensity of the propagating ground wave as a function of distance from the transmitting antenna. The algorithm is based upon an integral equation given by Ott (1971, 1979) in his model called WAGNER. The reader should consult the references for details on the WAGNER and WAGSLAB algorithms.

7.2 Inputs to the Model

In order to predict propagation loss over a given path, WAGSLAB requires a terrain profile of that path. The profile is provided as an array of values corresponding to terrain height as a function of distance from the transmitter. The dielectric constant and conductivity of the ground along the path must be specified. It is possible to divide the path into sections and assign separate electrical constants to each section. Any obstacles along the path (i.e., cities, buildings, forests, etc.) can be modeled as lossy, anisotropic, dielectric slabs sitting on top of the ground. WAGSLAB allows the user to specify the thickness and height of the slab as well as the horizontal and vertical conductivities and dielectric constants of the slab. Other parameters include antenna height for both the receiver and transmitter,



Transmitter located in an open field on the south grounds
of the Department of Commerce Radio Building in Boulder,
Colorado. Latitude: 39 deg, 59 min, 42 sec N
Longitude: 105 deg, 15 min, 34 sec W

Figure 42. Site map for wave-tilt measurements.

Table 1. Ground Constants by the Wave-Tilt Method

Site # and distance from XMTR m(ft)	Date	Freq f (MHz)	Ratio r	Tilt (deg)	Perm r	Cond (mS/m)	Comments:
1 55 (181)	12/30/83	28	0.0668	5.5	24.6	107.	3" Snow & F.G.
	01/03/84	28	0.0562	5.0	37.6	131.	2" Snow & F.G.
2 102 (335)	01/03/84	28	0.0668	15.5	10.7	9.3	2" Snow & F.G.
	01/03/84	28	0.0794	15.0	10.4	11.6	1.5" Snow & F.G.
	01/27/84	28	0.0649	16.0	10.3	8.4	No Snow & D.G.
	01/27/84	11.54	0.1155	11.0	8.6	11.3	No Snow & D.G.
	01/27/84	5.25	0.0917	6.0	6.	14.9	No Snow & D.G.
3 51 (166)	01/03/84	28	0.0355	10.	29.7	20.6	2" Snow & F.G.
	01/04/84	28	0.0422	9.5	29.3	25.4	1.5" Snow & F.G.
4 133 (435)	01/05/84	28	0.0084	9.5	35.4	5.7	1.5" Snow & F.G.
	01/05/84	28	0.0084	9.5	35.4	5.7	1" Snow & D.G.
	01/05/84	28	0.0087	9.5	35.4	5.9	1" Snow & D.G.
	01/05/84	28	0.0058	9.5	35.6	3.9	1" Snow & D.G.
5 172 (564)	01/05/84	28	0.0237	10.0	30.4	13.4	1.5" Snow & D.G.
	01/05/84	28	0.0237	10.0	30.4	13.4	Slush & D.G.
	01/09/84	28	0.0316	10.5	26.6	15.1	No Snow & D.G.
	01/09/84	28	0.0307	10.5	26.7	14.7	No Snow & D.G.
	01/10/84	28	0.0244	10.0	30.3	13.7	No Snow & F.G.
	01/11/84	28	0.0335	9.5	31.	20.5	0.5" Snow & F.G.
	01/11/84	5.25	0.0944	8.0	12.3	9.6	0.5" Snow & F.G.
	01/16/84	5.25	0.0708	8.0	23.4	9.6	3" Snow & F.G.
	01/16/84	7.5	0.0917	9.0	14.1	11.	3" Snow & F.G.
6 155 (510)	01/24/84	28	0.0244	15.0	13.5	4.2	0.5" Snow & F.G.
	01/24/84	11.54	0.0729	11.5	16.1	9.	0.5" Snow & F.G.
	01/24/84	5.25	0.0708	10.5	18.5	5.1	0.5" Snow & F.G.
	01/25/84	28	0.0156	15.5	12.9	2.5	0.5" Snow & D.G.
	01/25/84	11.54	0.0692	12.	15.8	7.9	0.5" Snow & D.G.
	01/25/84	7.5	0.0504	11.	21.4	5.2	0.5" Snow & D.G.
	01/27/84	28	0.0188	15.	13.7	3.2	No Snow & D.G.
	01/27/84	11.54	0.0729	11.	17.1	10.1	No Snow & D.G.
	01/27/84	7.5	0.0501	11.	21.5	5.2	No Snow & D.G.
	01/27/84	5.25	0.0917	10.	13.9	6.2	No Snow & D.G.

NOTES:

- 1) Site 1 was near the transmitter ground screen and a large tree.
- 2) Site 2 was unobstructed.
- 3) Site 3 was quite close to the transmitter.
- 4) Site 4 was unobstructed.
- 5) Site 5 was bordered by a thin line of trees.
- 6) Site 6 was unobstructed.
- 7) F.G. indicates frozen ground and D.G. indicates damp ground.

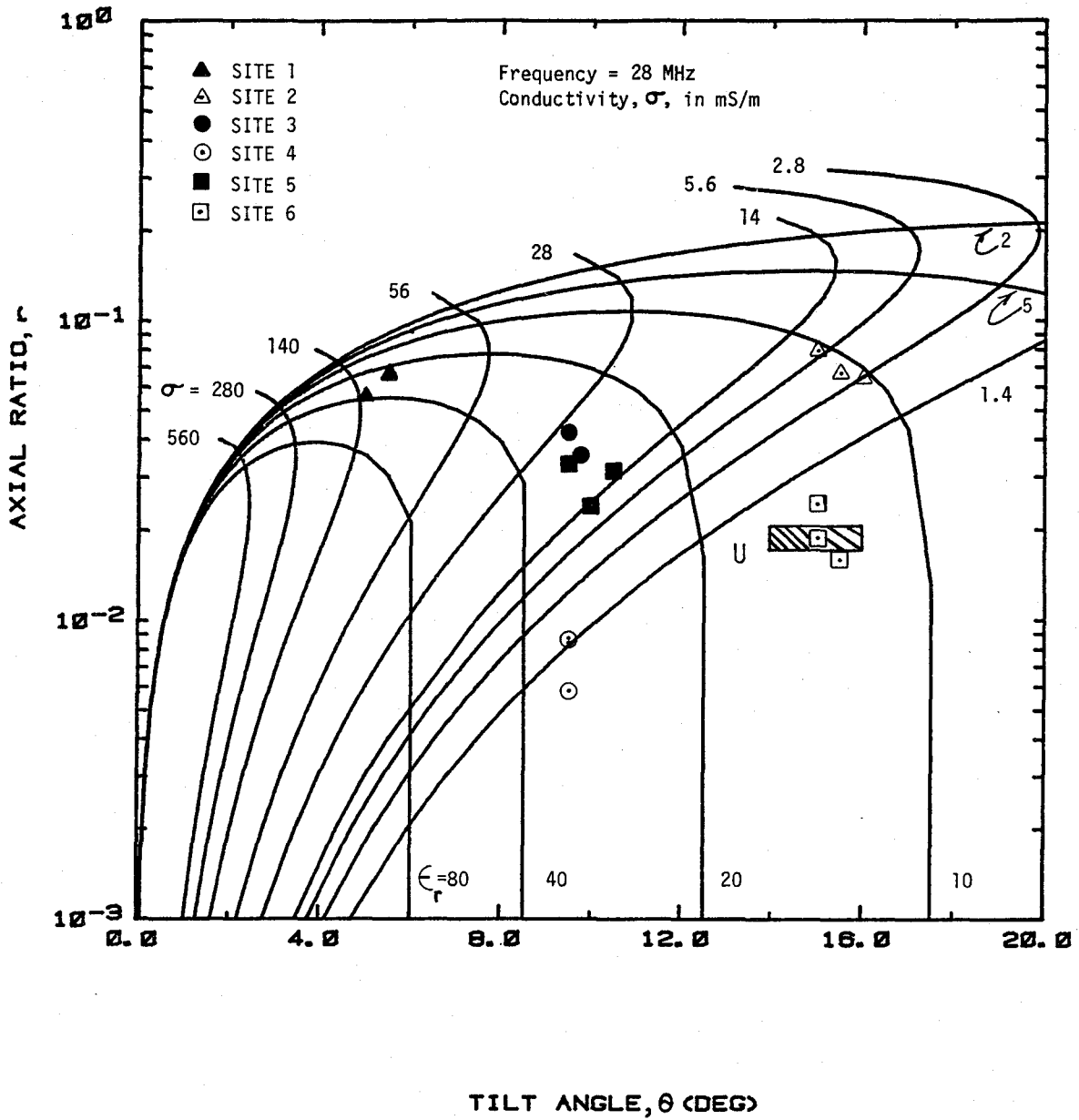


Figure 43. 28 MHz wave-tilt measurement results plotted on families of constant relative permittivity and conductivity curves.

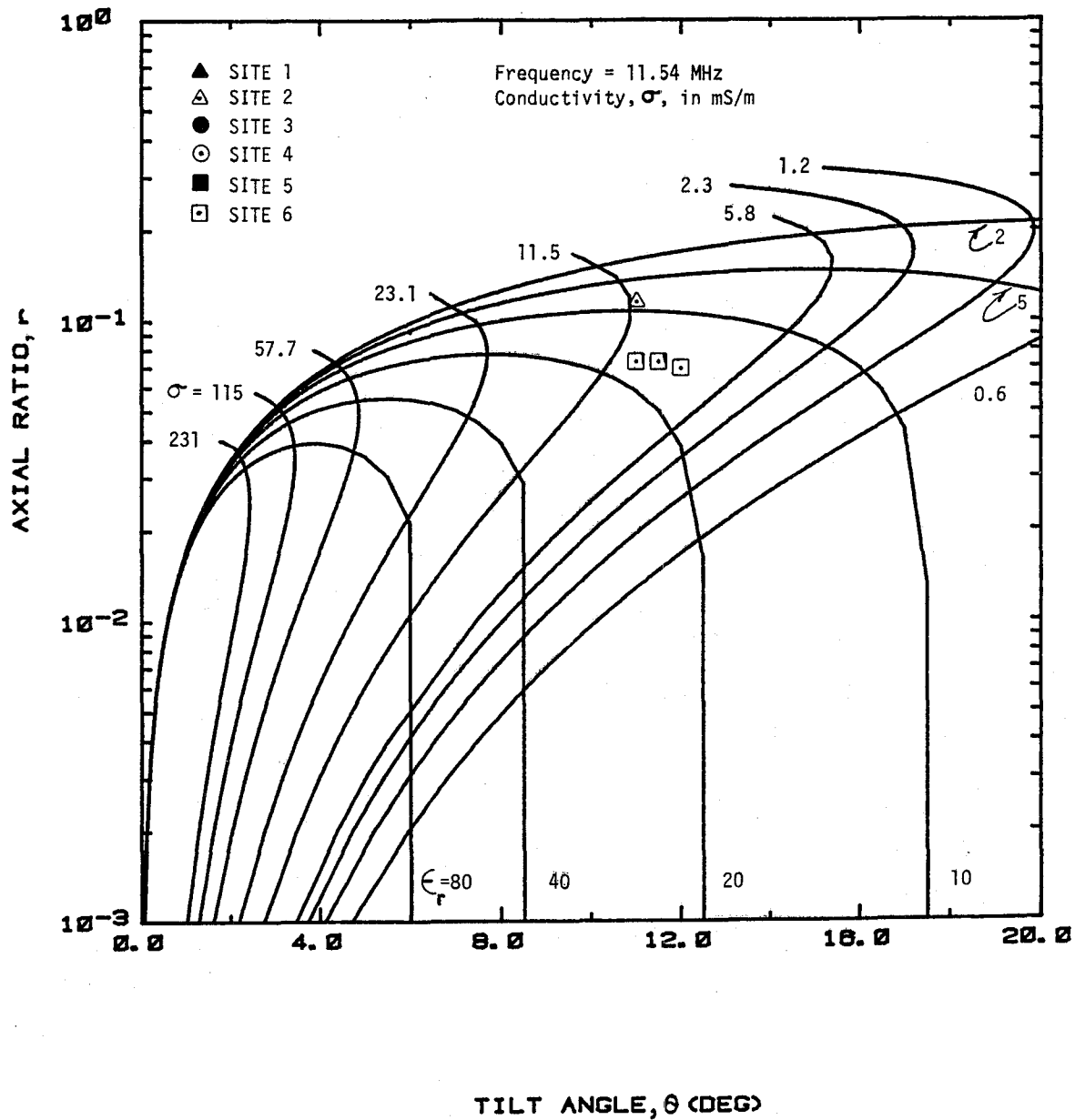


Figure 44. 11.54 MHz wave-tilt measurement results plotted on families of constant relative permittivity and conductivity curves.

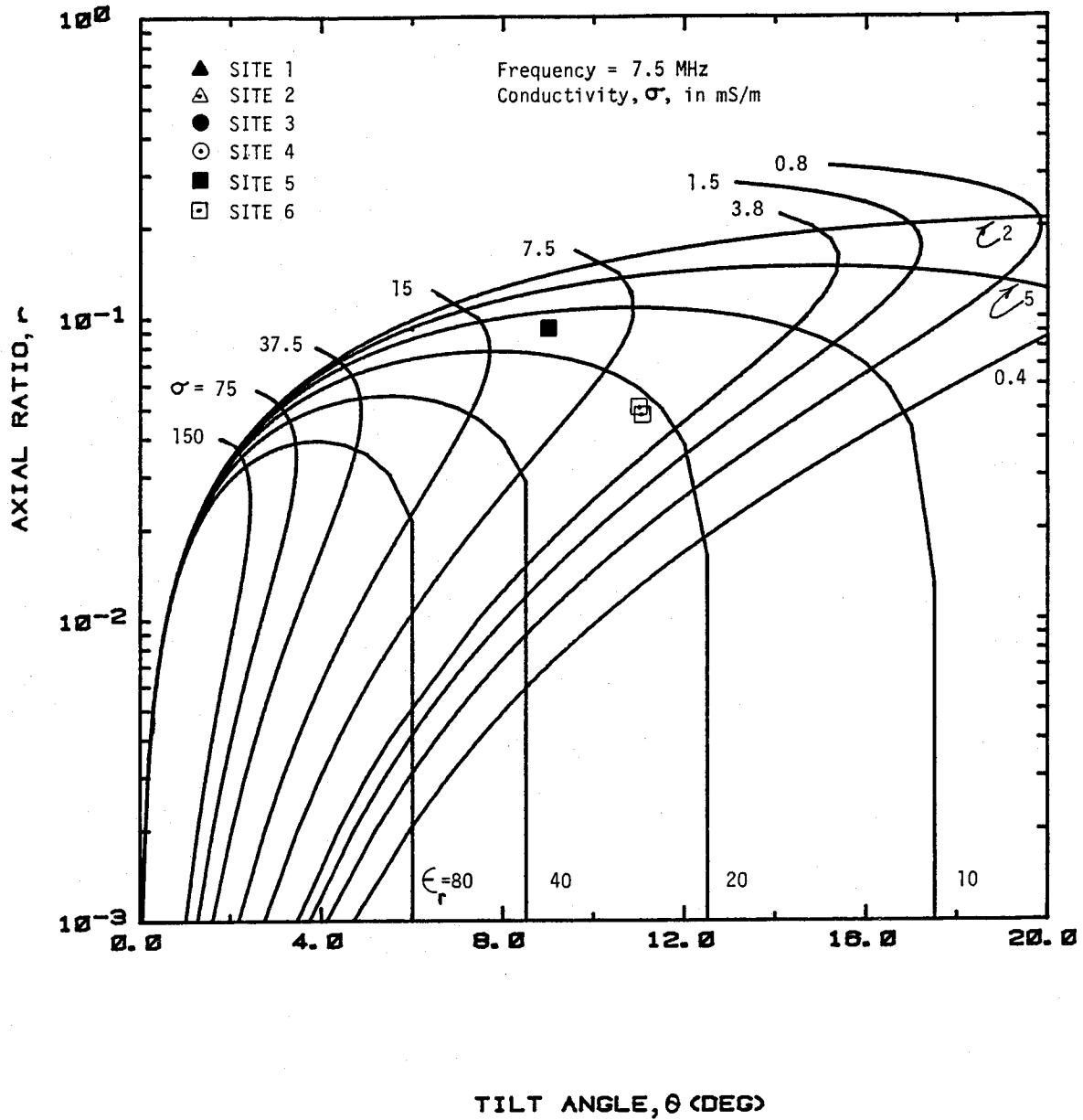


Figure 45. 7.5 MHz wave-tilt measurement results plotted on families of constant relative permittivity and conductivity curves.

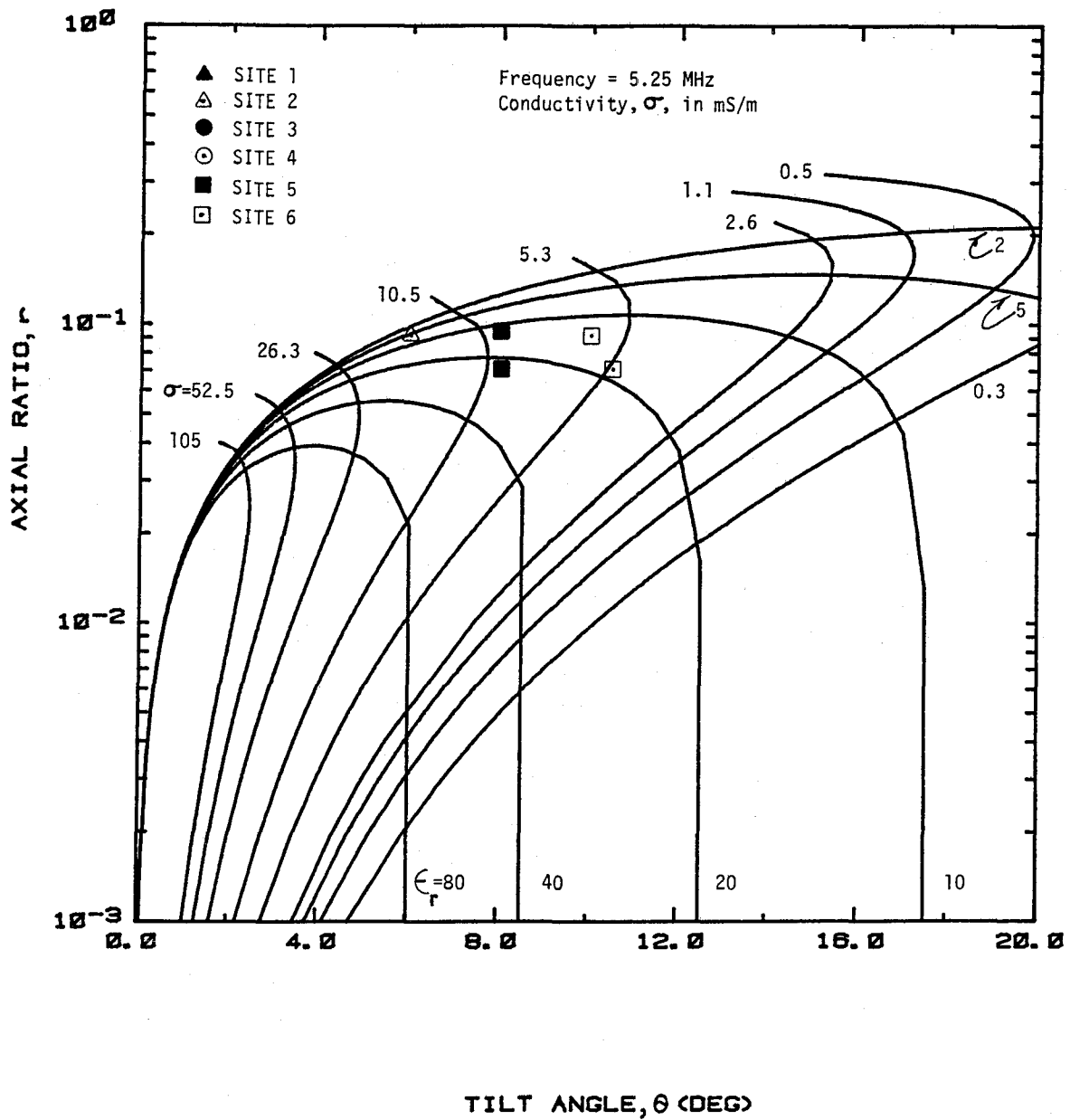


Figure 46. 5.25 MHz wave-tilt measurement results plotted on families of constant relative permittivity and conductivity curves.

frequency, and the points along the path at which the field intensity is to be evaluated.

7.3 Predictions

As an initial test of WAGSLAB, predictions were made for ground wave propagation over a smooth, curved earth. The predictions were then compared with published ground wave propagation curves (CCIR, 1982a).

WAGSLAB predictions were made for several paths, described earlier in the report, for which measured data were available. For the paths that run almost straight from the transmitter to some endpoint, predictions were made along a single radial drawn from the transmitter to the endpoint. This should be a good approximation when the terrain profiles along the actual path and the predicted path are similar. For the data collected in the mountains this is not the case. For each point at which data was measured, one radial was drawn from transmitter to that point and a prediction made along the radial to obtain a path loss prediction to the endpoint. Terrain profiles for the paths considered in this report were obtained from the ITS terrain data base of elevations on a grid spaced ever 30-sec over the United States taken from the Army Defense Mapping Agency's 1 deg by 2 deg maps. The resolution of the contours on these maps was 200 ft in mountainous regions. Therefore, it is possible that a major terrain feature may have been missed which would cause some inaccuracy in the predictions, especially for paths in the mountains where the terrain varies greatly over relatively short distances.

When using WAGSLAB, the user should be aware of some subtleties. The equation that the algorithm implements is of the form:

$$f(x) = W(x) + \int_0^x [f(y)g(x,y)dy] \text{ for distances from 0 to } x.$$

When calculating the field strength, $f(x)$, the algorithm starts at $x=0$ and continues out to the ending distance of the path. For the first five points $f(x)$ is calculated solely with the flat earth attenuation, $W(x)$, term; the integral does not contribute until the sixth iteration. This approximation, $f(x)=W(x)$, is valid for a flat earth, and for this reason care must be taken to assure that the terrain is flat from $x=0$ out to the fifth iteration point. If not, the first iterations for $f(x)$ will be incorrect; since later values of $f(x)$ are dependent on previous ones, the total prediction along the path will be unreliable.

Because calculation of the integral is recursive, it is important to have a spacing between calculation points sufficiently small to obtain a reliable approximation to the integral. At this time, there is no established criteria on which to make a confident decision on spacing size. It is known, however, that the spacing size is sensitive to such things as frequency and roughness of terrain. The higher the frequency and the rougher the terrain, then the smaller the spacing interval has to be for reliable results. For the predictions made for this report, the spacing size was chosen from previous experience and confirmed to be adequate by making some second predictions using a spacing of half the original value and verifying that the two cases agreed to within a suitable error margin. It should be noted that spacing size is a practical consideration with tradeoffs involved; smaller spacing is obtained at the expense of increased computer run time.

Figures 47 through 50 show the predictions along the East Path for several sets of ground constants. The irregular-shaped curve shown in each plot is a repeat of the measured median loss as given in Section 5 for each corresponding path. The dashed curve (one long dash followed by three short dashes) represents the prediction made by an HF ground wave smooth earth model (Stewart et al., 1983) with the ground constants provided the smooth earth prediction to indicate the difference between it and those predictions made by WAGNER. The other solid line curves on each plot are the WAGNER predictions. The top curve is Curve 1 and has the ground constants characteristics given in the legend. The second curve from the top is Curve 2, etc. Several sets of ground constants were used for each path in an attempt to bracket or bound the measured losses.

At the lower measurement frequencies (5.25, 7.5, and 11.5 MHz), the conductivity parameter had more influence on the prediction than did relative permittivity. At 28 MHz, the relative permittivity parameter was more dominant (compare Figures 49 and 50 at 28 MHz). Similar plots and results are shown in Figures 51 through 53 for the South Path and Figures 54 and 55 for the North Path. No predictions were made for the Mountain Path.

8. ANALYSIS OF MEASURED AND PREDICTED PROPAGATION LOSSES

This section reviews the propagation loss measurements and predictions. We will state some observations that are apparent to us and provide some insight when appropriate.

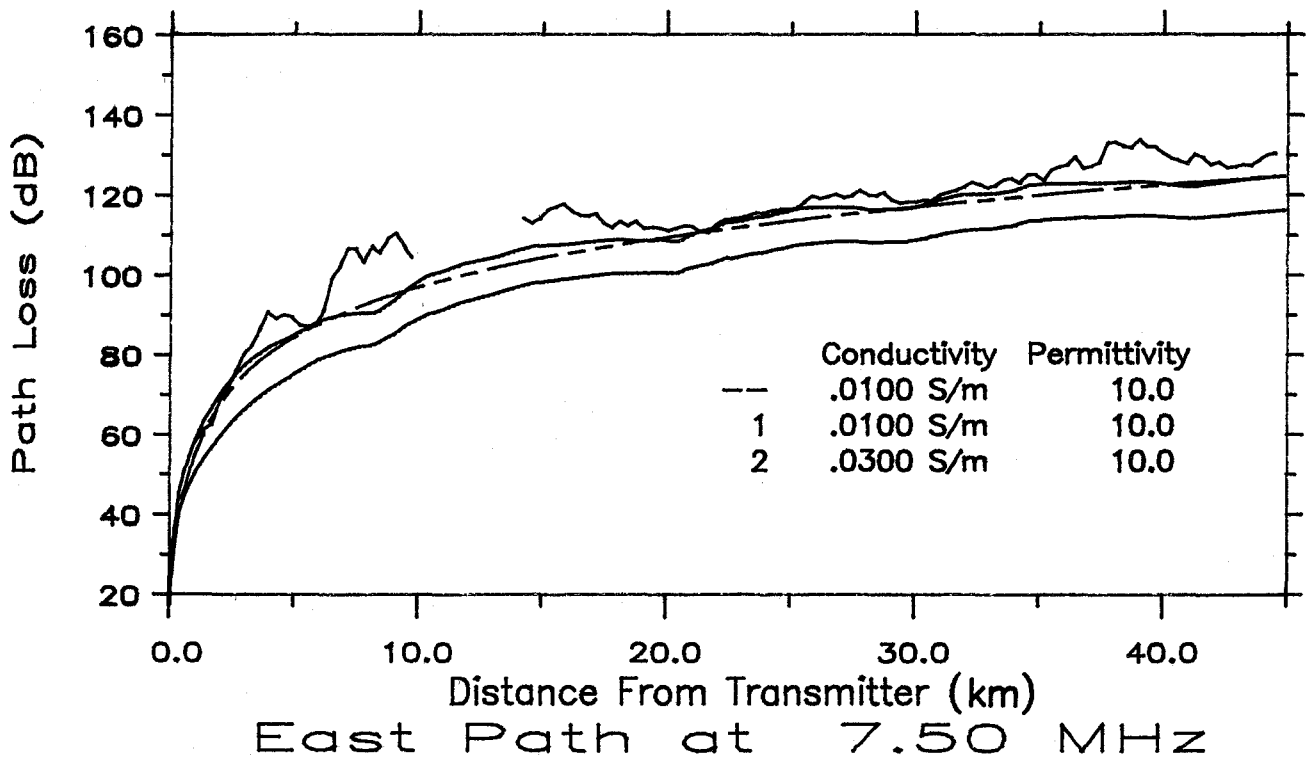
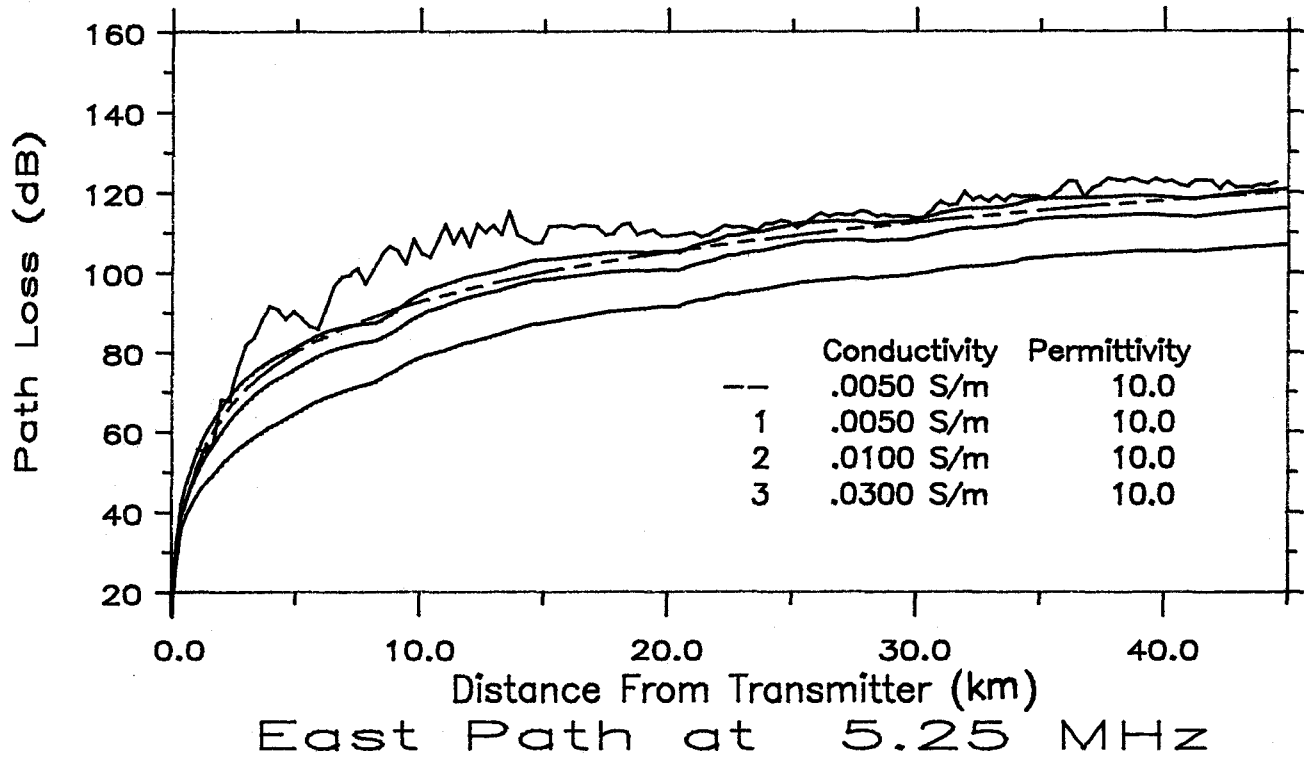


Figure 47. Predicted and measured median loss for the East Path at 5.25 and 7.5 MHz.

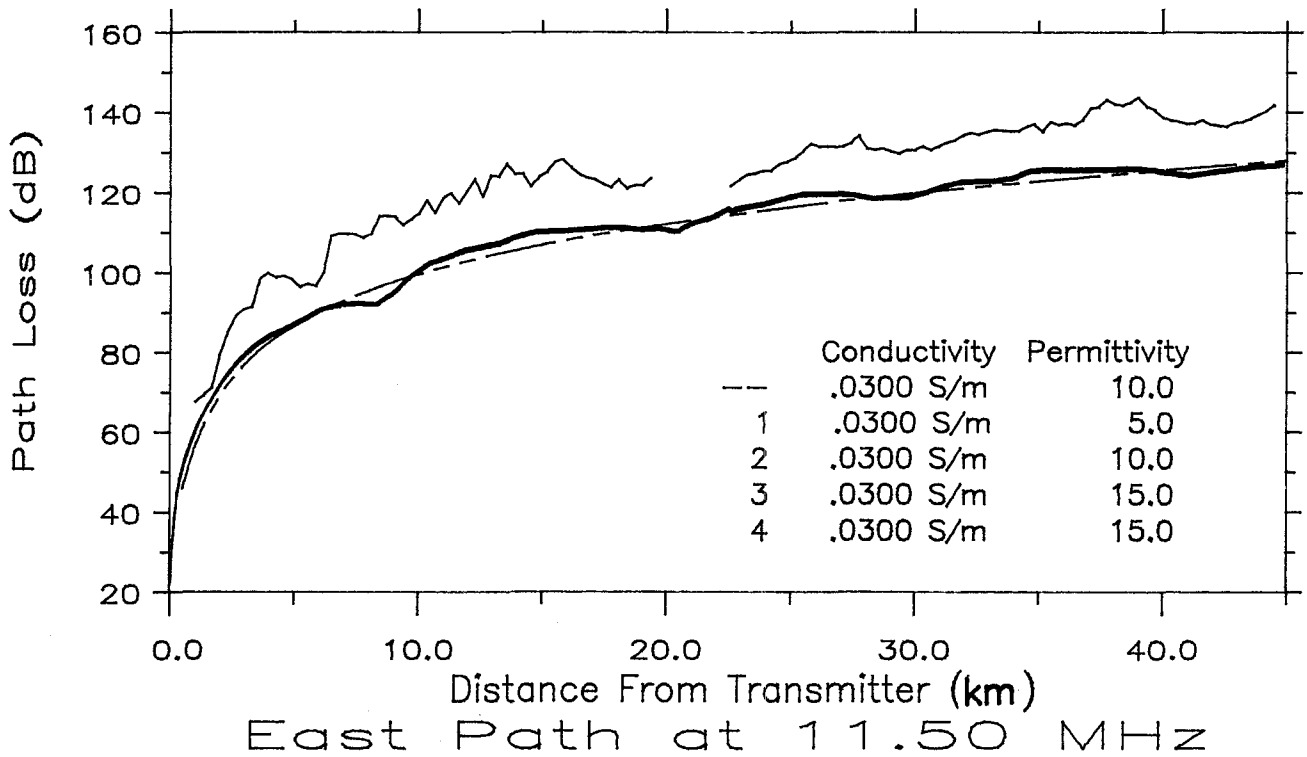
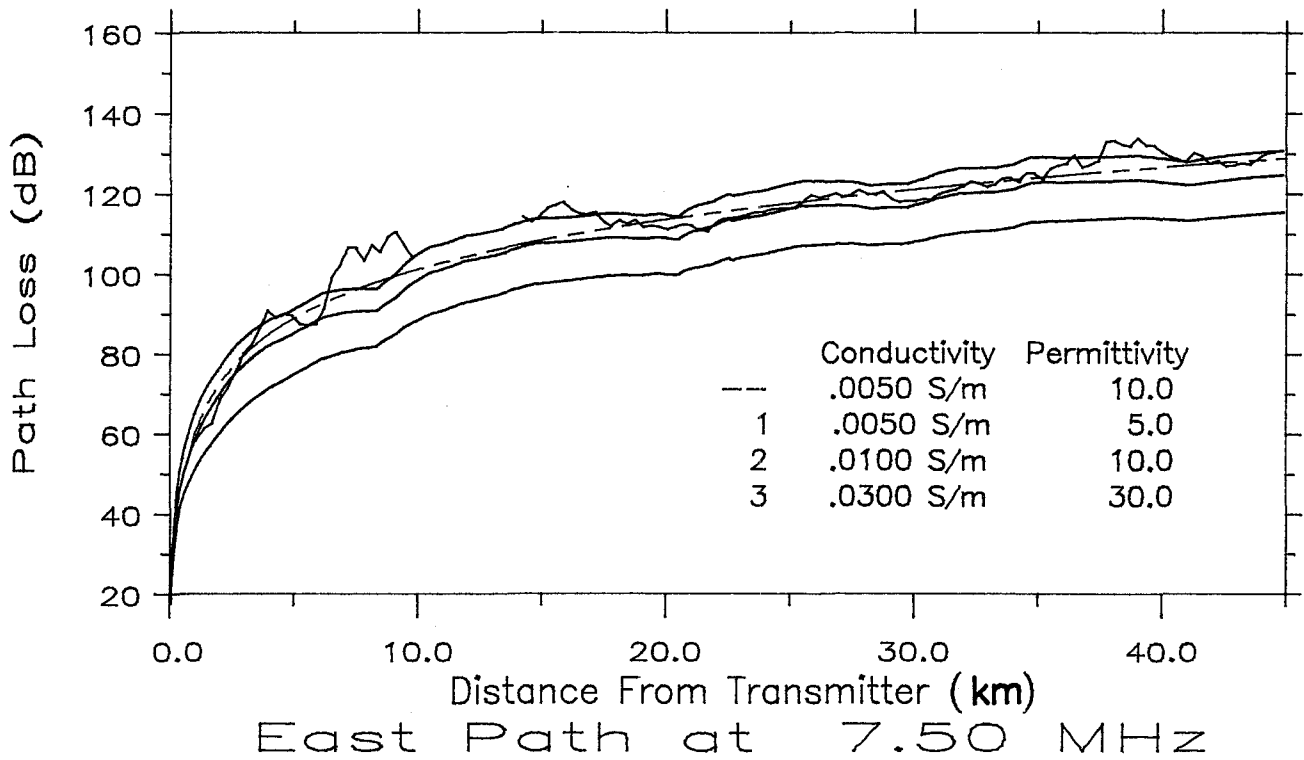


Figure 48. Predicted and measured median loss for the East Path at 7.5 and 11.5 MHz.

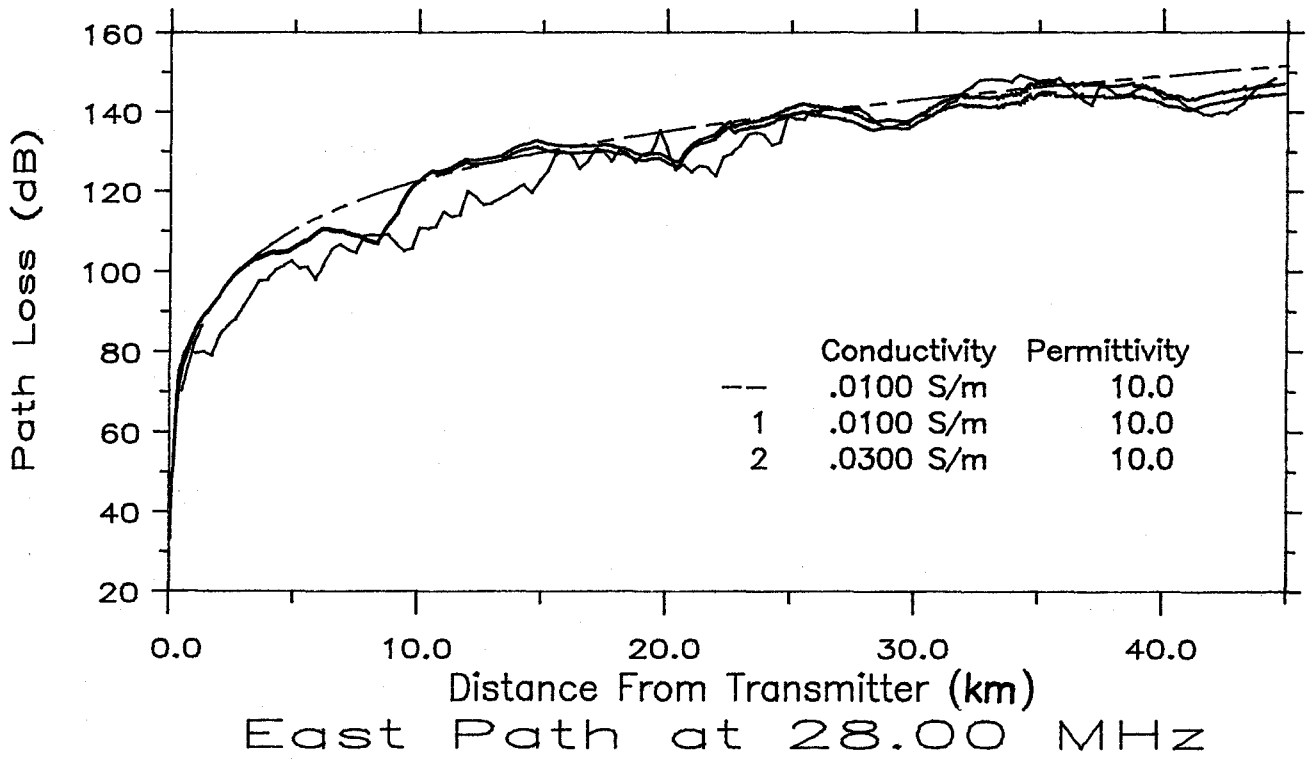
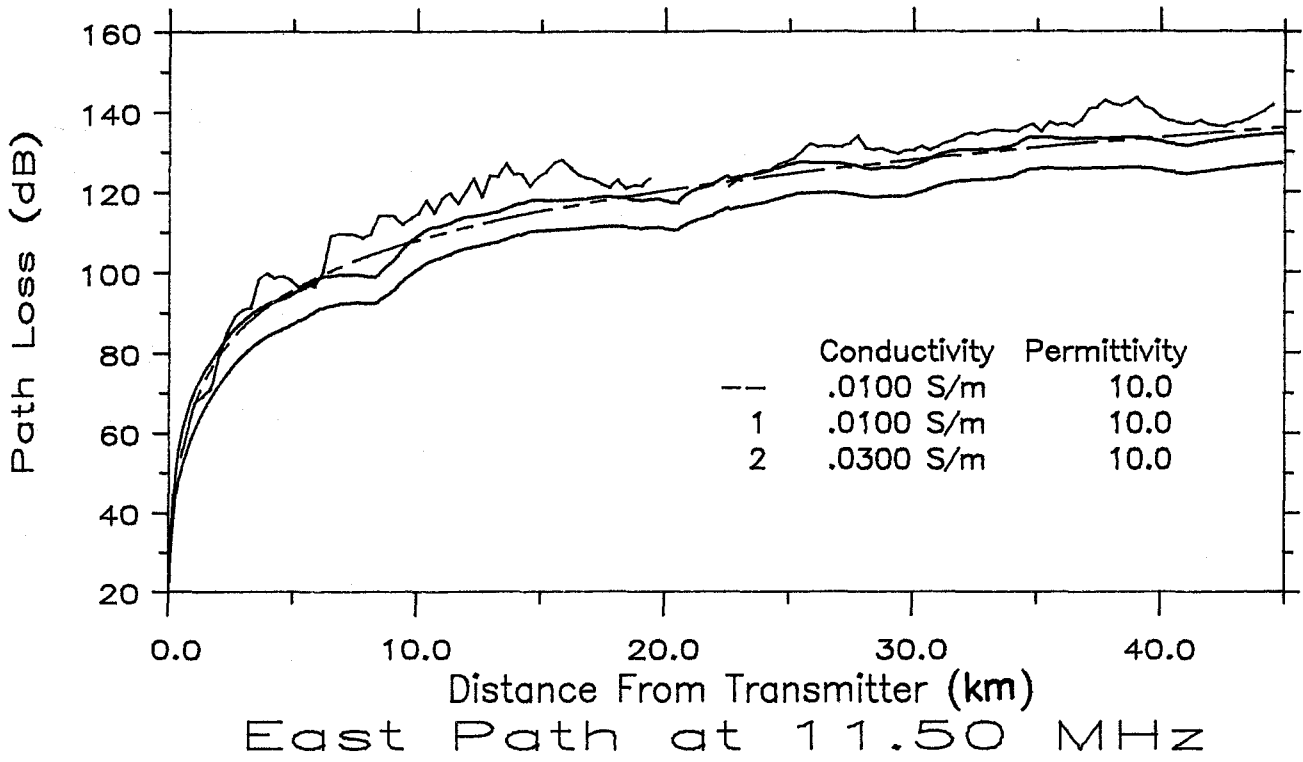


Figure 49. Predicted and measured median loss for the East Path at 11.5 and 28 MHz.

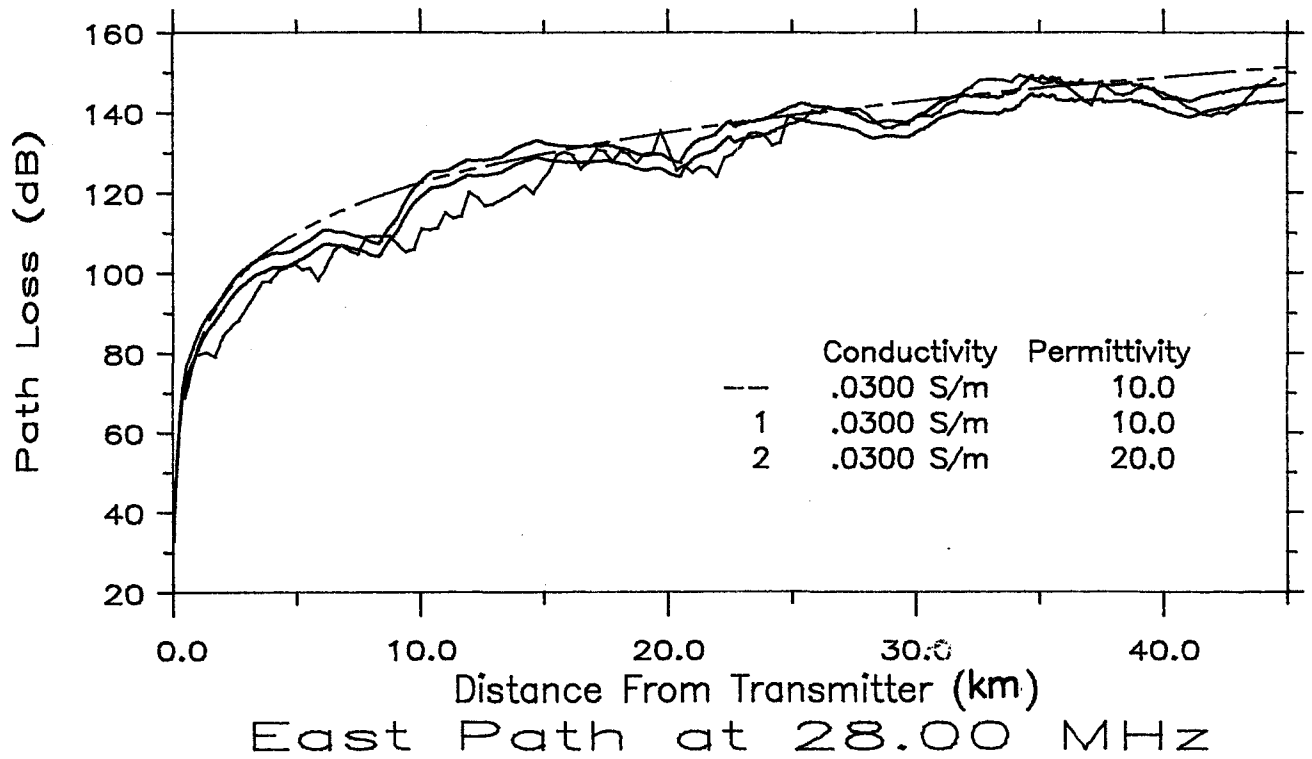


Figure 50. Predicted and measured median loss for the East Path at 28 MHz.

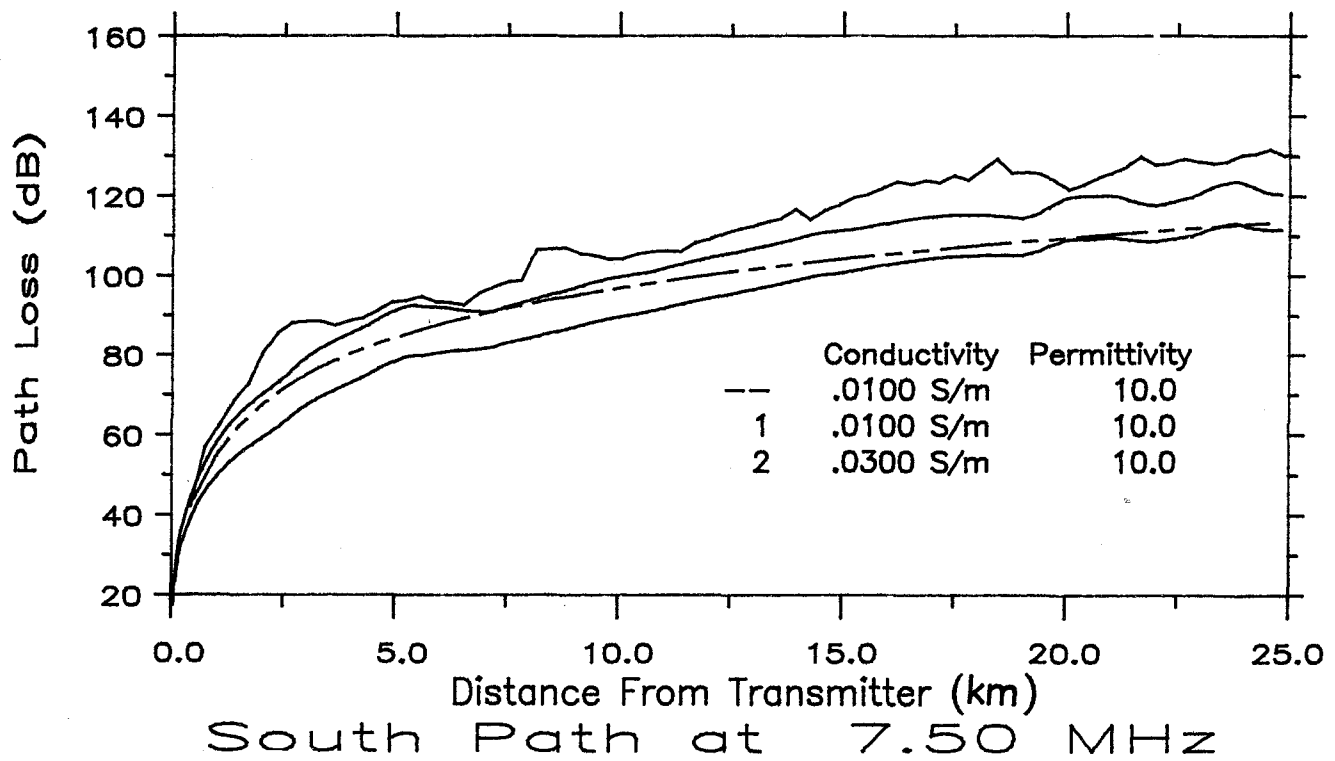
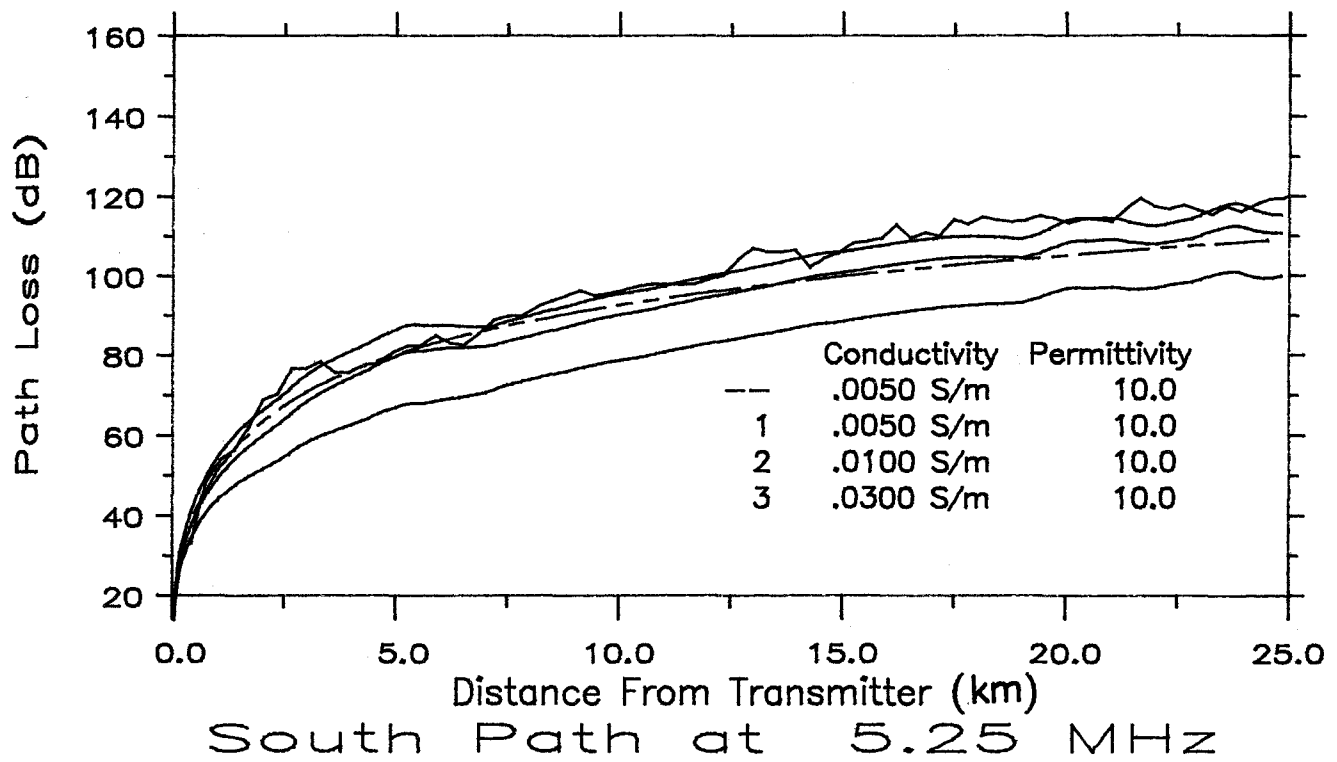


Figure 51. Predicted and measured median loss for the South Path at 5.25 and 7.5 MHz.

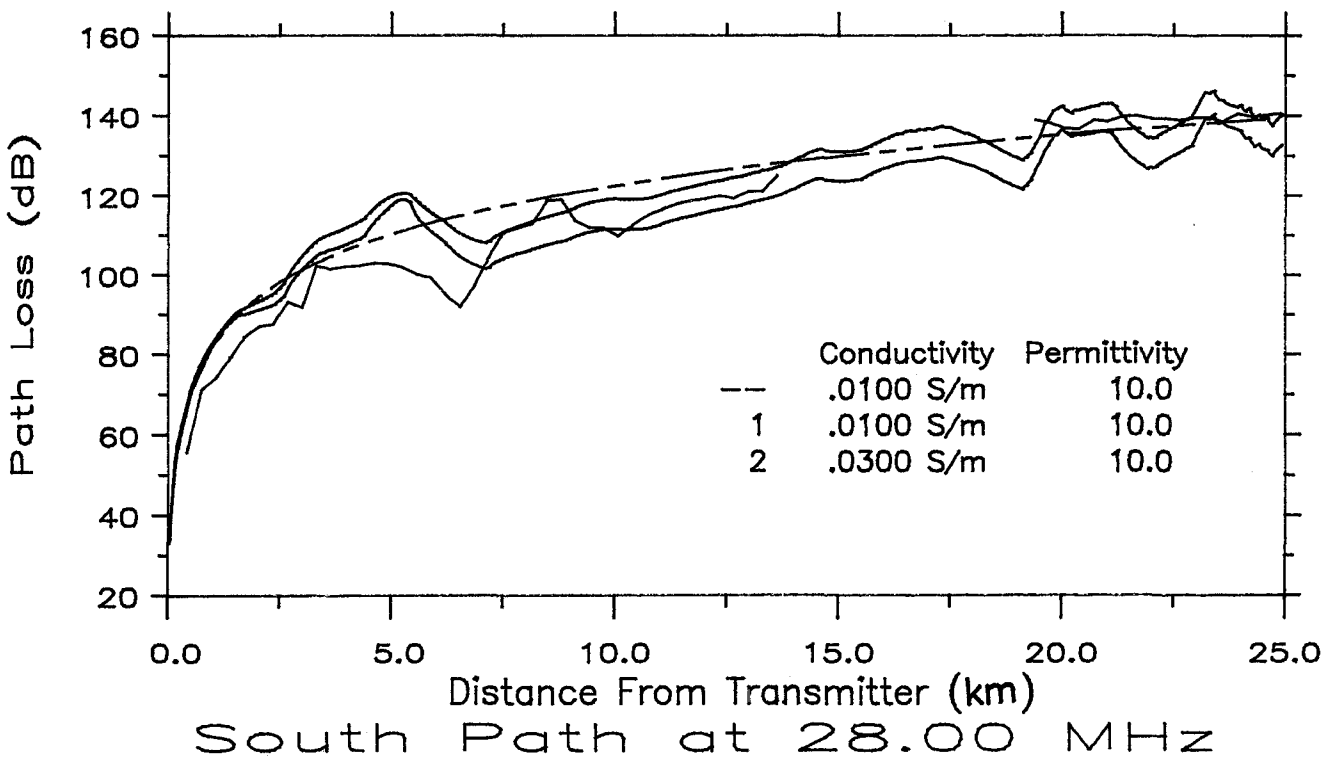
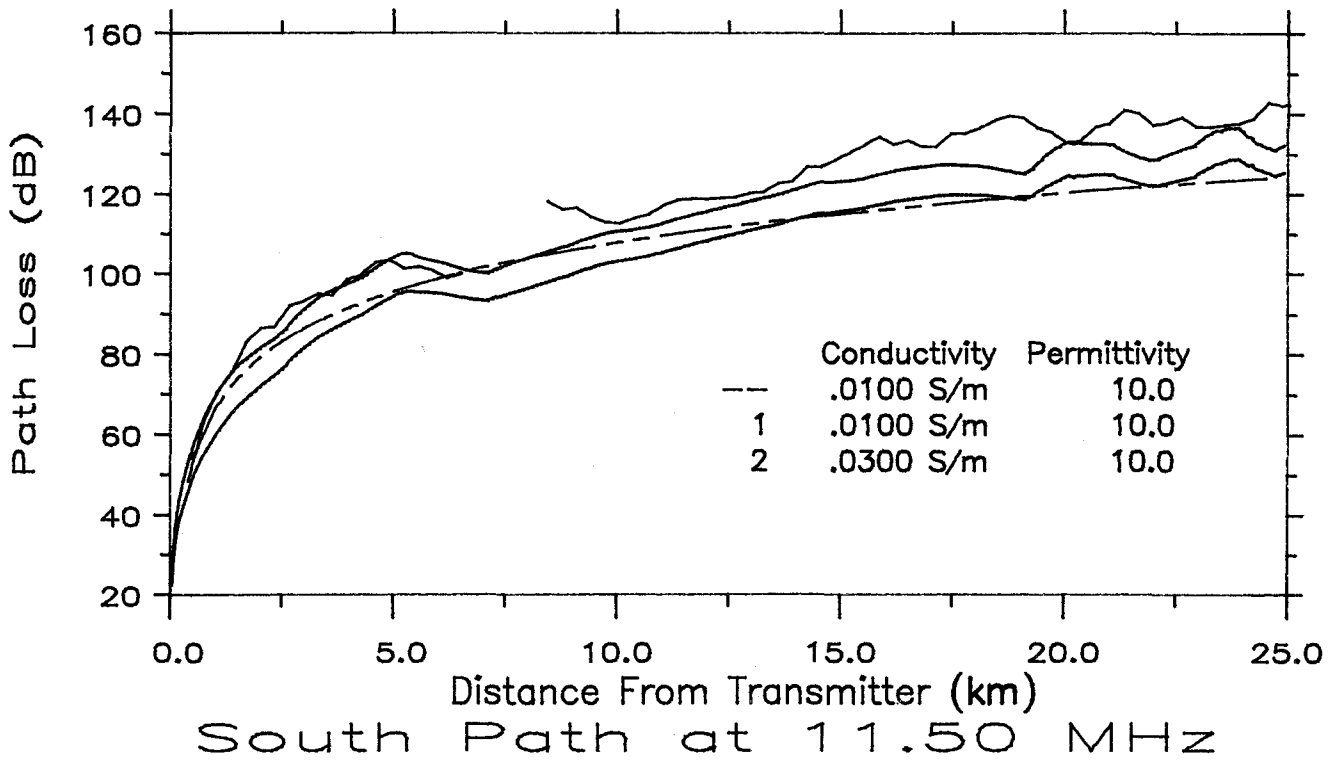


Figure 52. Predicted and measured median loss for the South Path at 11.5 and 28 MHz.

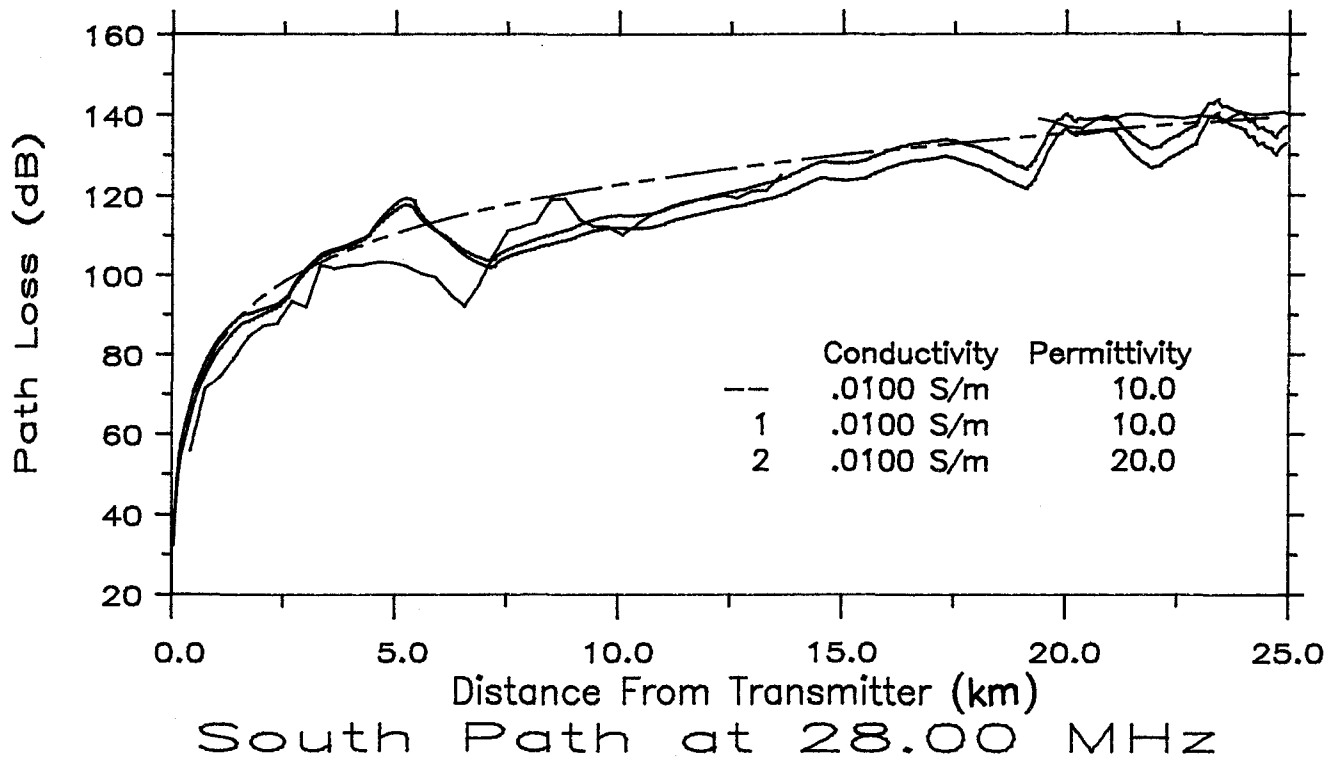


Figure 53. Predicted and measured median loss for the South Path at 28 MHz.

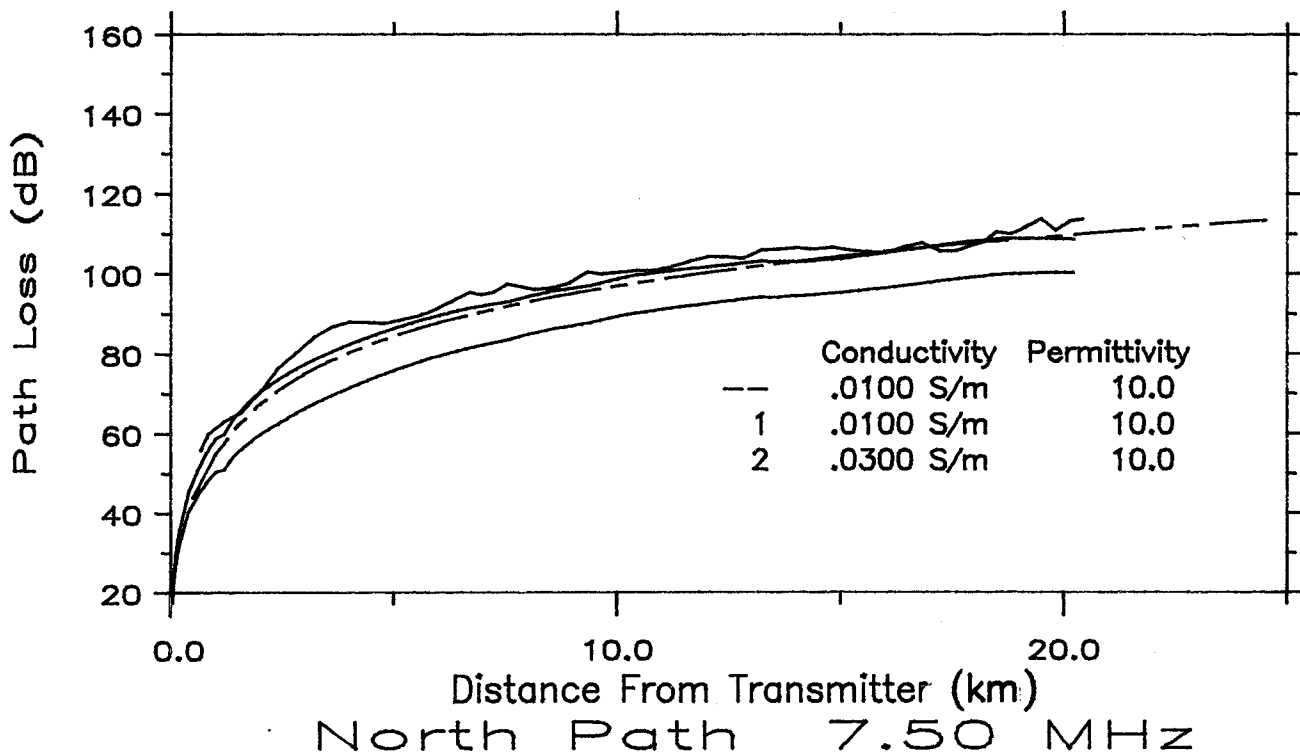
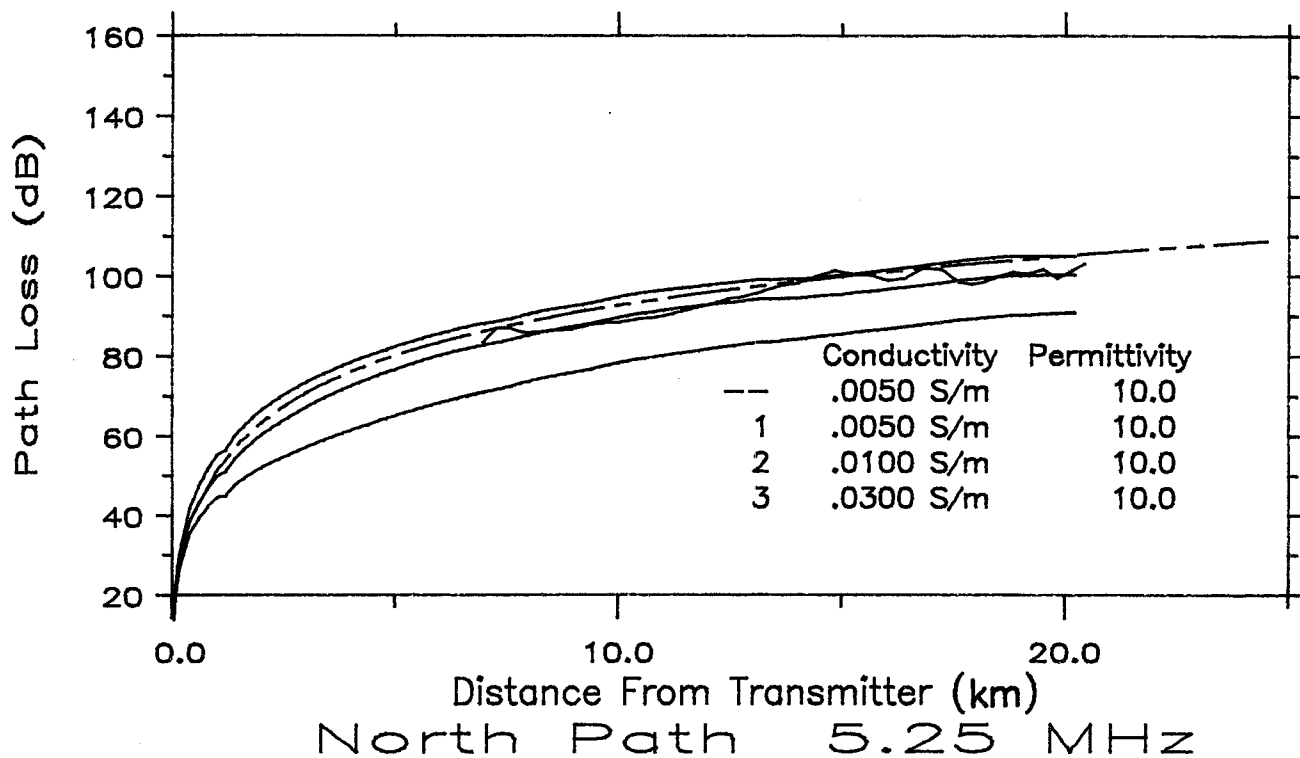


Figure 54. Predicted and measured median loss for the North Path at 5.25 and 7.5 MHz.

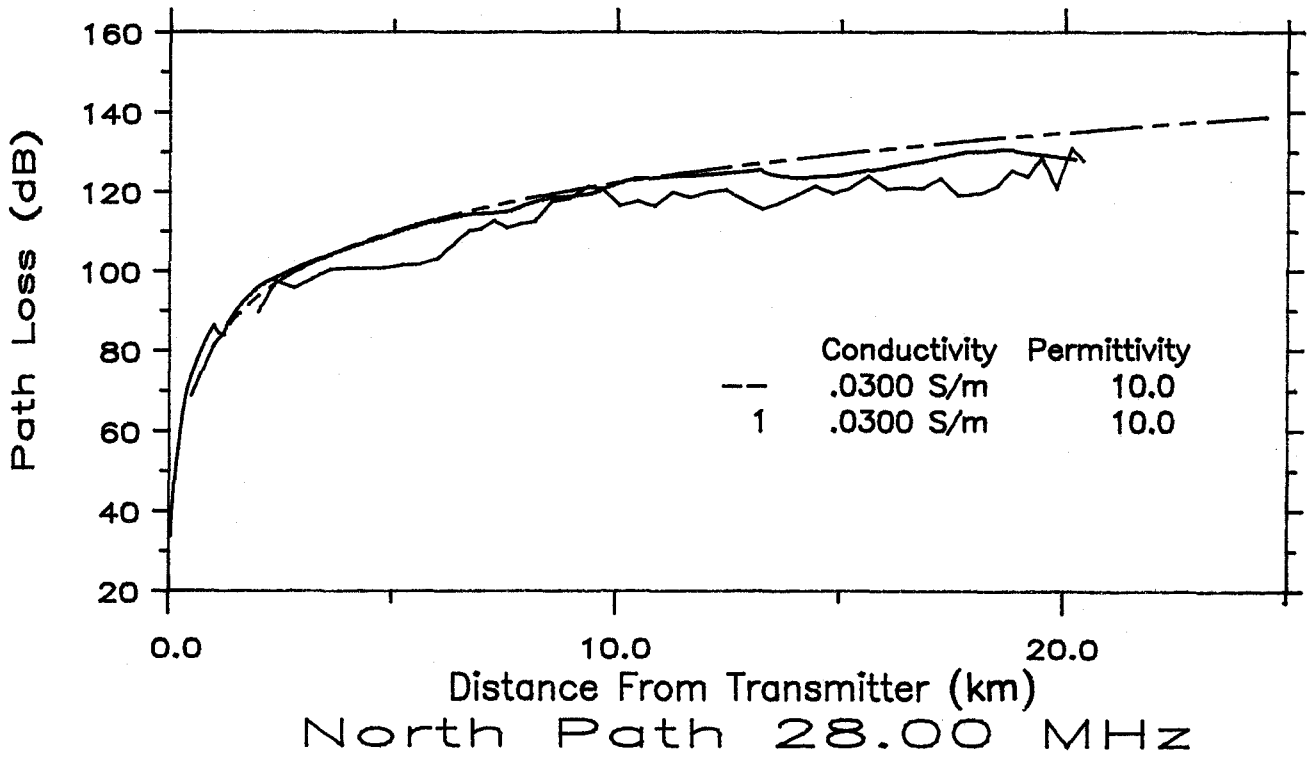
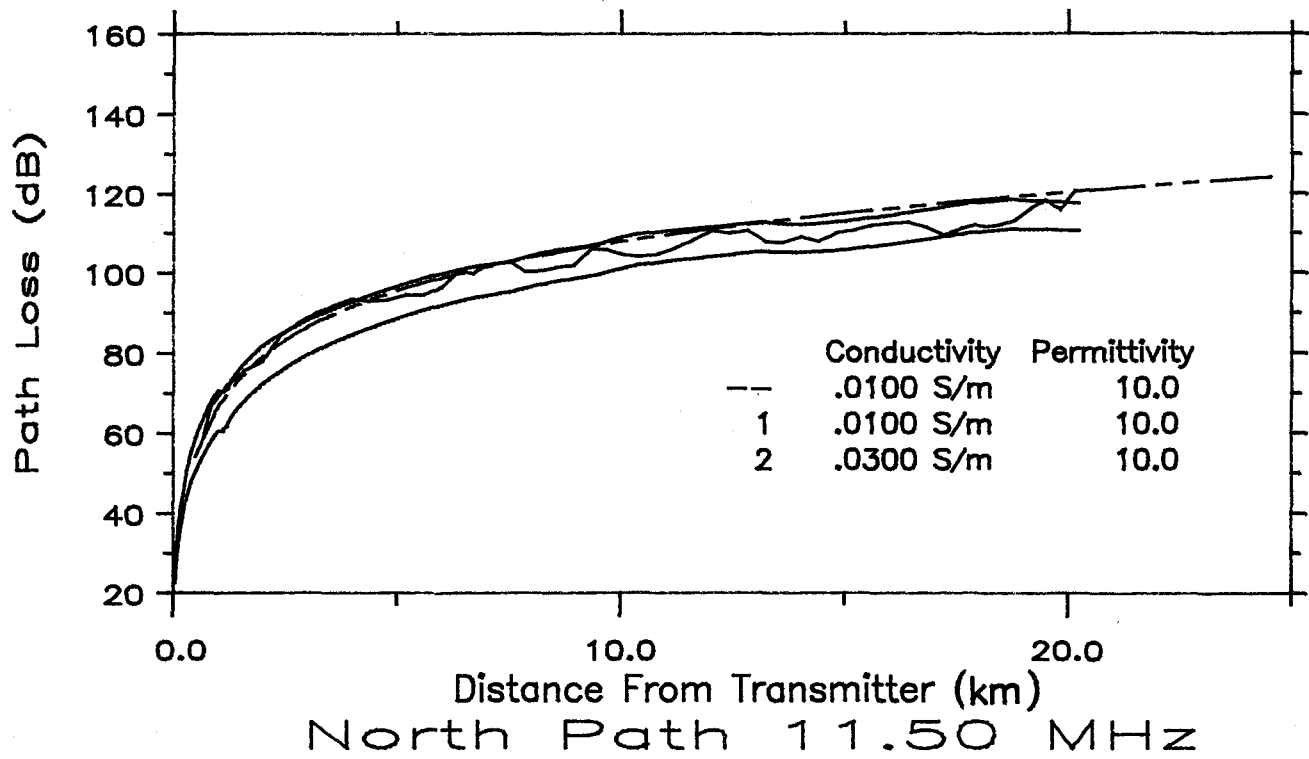


Figure 55. Predicted and measured median loss for the North Path at 11.5 and 28 MHz.

8.1 Measured Propagation Losses

In Section 4, we stated that HF groundwave signals would be affected by obstacles that are approximately one wavelength or larger. Now we can show how much the propagation loss varies for different paths at the same distance from the transmitter. In Table 2, we have estimated the median path loss from the measured data at distances from the transmitter of 5 to 40 km in 5 km steps. Note that the North Path, which was the flattest and smoothest, had the least path loss at each distance increment. The Mountain Path, the most rugged path, had the most path loss at nearly every increment. For most cases, as the distance from the transmitter increased, the path loss increased as well. Also, as the frequency increased, the path loss increased. These are two results one would expect. An interesting result occurs with the Mountain Path data. Note for distances of 15 to 25 km from the transmitter, the path loss stays relatively constant for each frequency. A round, smooth earth prediction for the same distance change would have estimated 10 dB more loss at 25 km than at 15 km.

The snow cover had no appreciable effect on the propagation loss except at 5.25 MHz. For this case, the losses were 5 dB less with snow cover compared with data measured at the same distances without snow cover. It is suspected, but not proven, that this was caused by a change in effective radiated power (ERP) and not by propagation effects.

Table 2 shows the median loss for each path grouped for a single frequency and distance increment. The upper left-hand group, for example, shows a median loss of 100 dB for the Mountain Path and 80 dB for the South Path; the difference between the maximum and minimum medians for this group is 20 dB. The differences for the other groups at 5.25 MHz are 24, 20, 18, and 12 dB. Thus, the differences stay fairly constant from 5 km out to 25 km. The same results are observed for the other three frequencies. Typically we could say that the difference between the largest and smallest median propagation loss for different paths is 20 dB regardless of distance from the transmitter or frequency.

In Table 3 we have listed what we estimate to be the difference between the upper and lower decile propagation losses for each path at each frequency for distances of 5 km to 40 km from the transmitter. Here again, we note that the North Path shows the least difference between the upper and lower decile losses and the Mountain Path shows the largest difference at most distances. We note that there is no appreciable change in the differences as the

frequency is increased from 5.25 to 28.0 MHz; nor is there any appreciable change as the distance from the transmitter is increased.

Table 2. Variation in Measured Median Path Loss vs. Frequency and Distance

Freq (MHz)	Path	Median path loss for given distance							
		5 km (dB)	10 km (dB)	15 km (dB)	20 km (dB)	25 km (dB)	30 km (dB)	35 km (dB)	40 km (dB)
5.25	East	90	105	110	110	112	115	120	123
	E. snow	85	100	105	105	108	110	115	
	South	80	96	108	115	120			
	North		88	100	102				
	Mount'n	100	112	120	120	120			
7.5	East	90	105	115	112	117	119	125	130
	E. snow	88	105	112	112	115	117	123	131
	South	93	105	120	122	130			
	North	88	101	108	114				
	Mount'n	102	125	135	133	133			
11.5	East	98	115	125	120	128	130	136	139
	E. snow	93	111	122	119	127	128	135	138
	South	103	113	130	134	143			
	North	93	105	111	118				
	Mount'n	120			144	144			
28.0	East	100	110	124	131	138	140	148	145
	E. snow	100	107	125	129	138	135	145	148
	South	103	110	133	138	140			
	North	100	118	120	127				
	Mount'n	120	138	139	140	142			

Table 3. Variation in Differences Between Measured Upper and Lower Decile Path Loss vs. Frequency and Distance

Freq (MHz)	Path	Difference between upper and lower decile path loss for given distance							
		5 km (dB)	10 km (dB)	15 km (dB)	20 km (dB)	25 km (dB)	30 km (dB)	35 km (dB)	40 km (dB)
5.25									
	East	5	10	8	4	5	5	12	11
	E. snow	5	10	8	3	5	6	12	
	South	6	6	5	8	9			
	North		4	6	3				
	Mount'n	8	11	13	13	13			
7.5									
	East	3	15	8	3	3	3	5	10
	E. snow	4	12	8	3	3	3	6	12
	South	4	3	5	8	7			
	North	5	2	4	3				
	Mount'n	6	13	13	12	14			
11.5									
	East	3	9	8	2	3	5	7	8
	E. snow	3	12	7	2	3	5	7	11
	South	5	2	5	6	12			
	North	5	3	2	6				
	Mount'n	15			12	17			
28.0									
	East	5	8	7	6	8	5	13	7
	E. snow	5	8	4	4	6	4	11	9
	South	8	6	11	12	13			
	North	7	5	3	13				
	Mount'n	18	12	11	13	12			

The effects of sky wave signals on the measurements were not determined directly for these data. One technique for observing sky wave is to find a measurement site that is clear of moving reflectors, such as other vehicles, that would add multipath components. Then by observing the received signal at the stationary site, the ground wave component would be relatively constant in signal strength while the sky wave component would be time-varying. The ripple amplitude would tell us the amount of sky wave present. As the site is moved further in distance from the transmitter, the sky wave component would be more significant compared with the ground wave.

The effects of multipath on the received signal were measured by moving the data collection vehicle at a reduced but constant speed and taking recordings. Sky wave is not believed to contribute to these measurements because the receiver van was less than 20 km from the transmitter. Figure 56 through 58 show the measured signal level over a short distance at 7.5 and 11.5 MHz. The signal variation due to the multipath can be as large as 20 dB over a distance of less than 50 m. The signal level peaks (and nulls) are spaced approximately every 20 m or one-half wavelength at 7.5 MHz. This is the characteristic of multipath fading. Because the fading has nearly a sine wave shape, we would suppose that there is one dominant signal and one weaker signal (rather than many weaker signals of similar amplitude and uniformly distributed phase) received at the data collection van. Many weaker signals would give rise to a Rayleigh-distributed received signal and we do not appear to have that situation.

8.2 Measured Ground Constants

One problem encountered with a ground constants measurement technique such as the wave-tilt method is that there is no location with known ground constant characteristics over which we can calibrate the system. Thus, we took the wave tilt measurements, reduced the data to equivalent ground constants, and used the values in the predictions without any knowledge of the accuracy of the wave-tilt technique. Table 4 gives the range of ground constant values as determined from the measurements.

Table 4. Range of Measured Ground Constant Values

Frequency (MHz)	Conductivity (S/m)	Relative Permittivity
5.25	.005 - .015	5 - 25
7.5	.005 - .015	10 - 25
11.5	.01 - .015	5 - 20
28.0	.005 - .015	10 - 30

In Table 5 we provide the range of ground constants that cause the predictions to straddle the measured propagation losses.

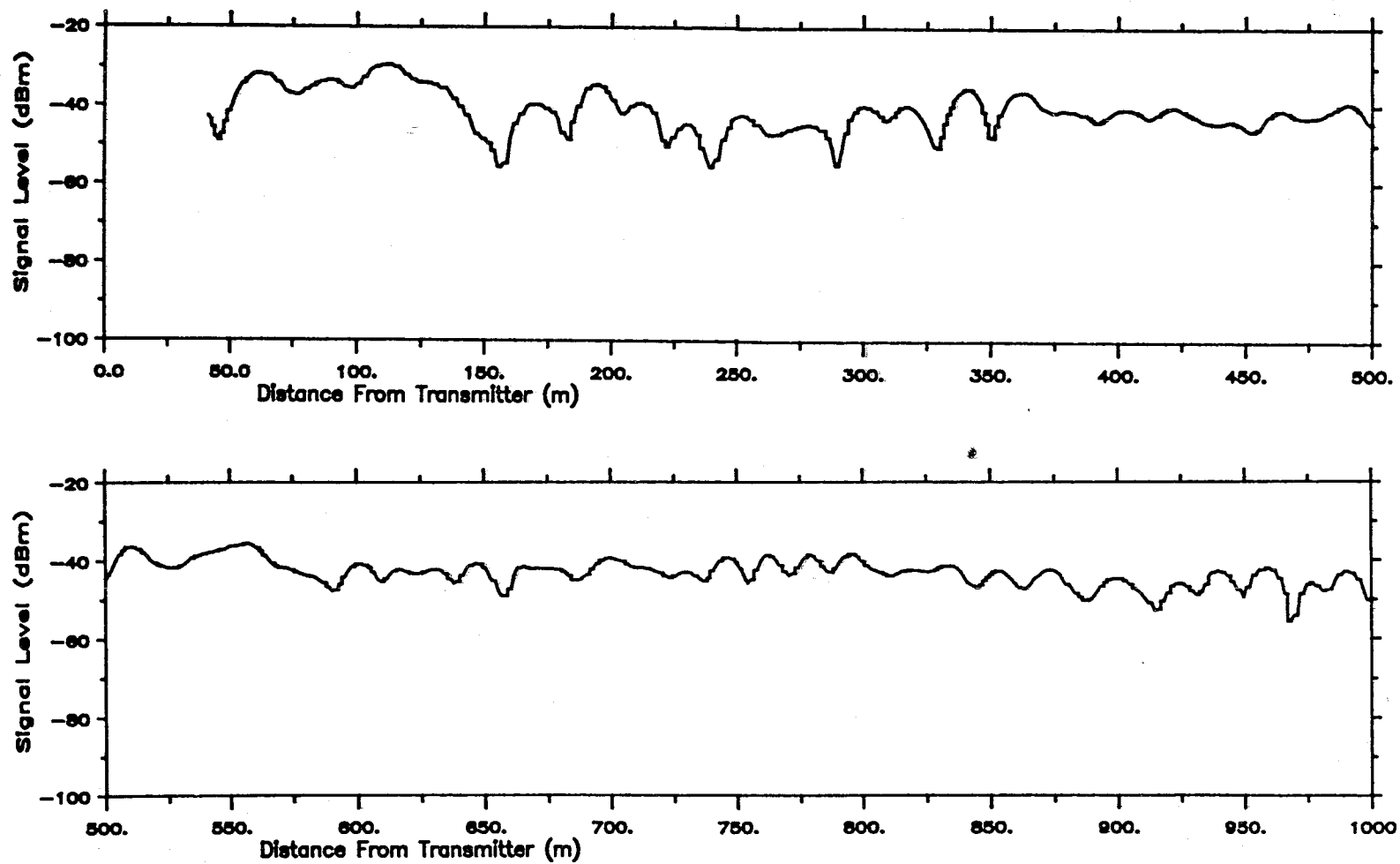


Figure 56. Signal level variation over a short distance 1.1 to 2.1 km from the transmitter at 7.5 MHz.

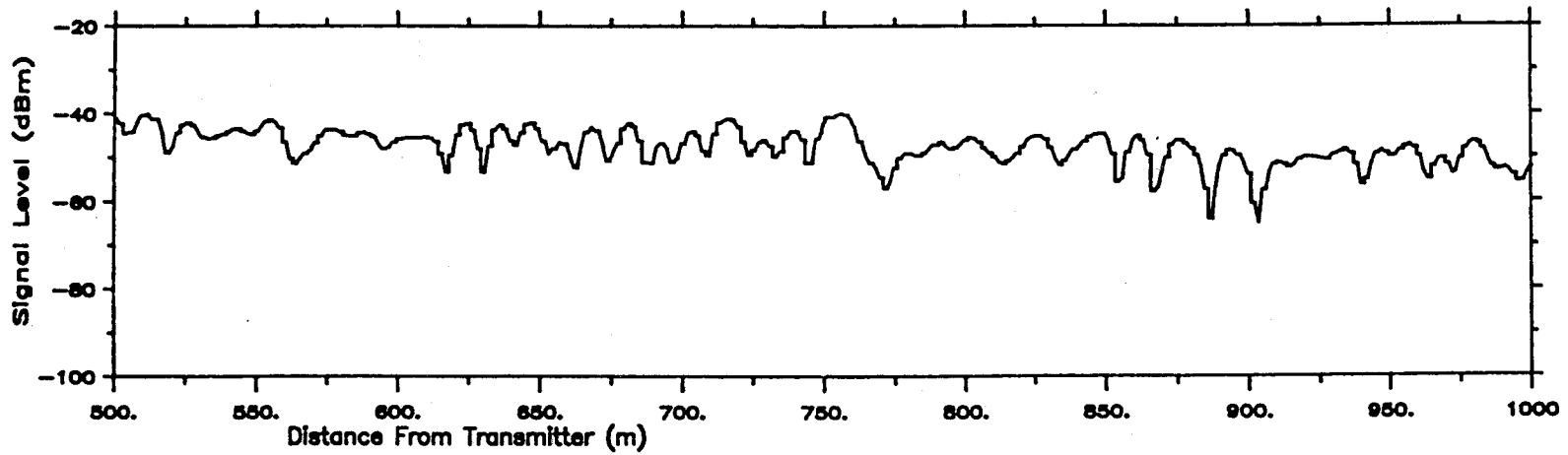
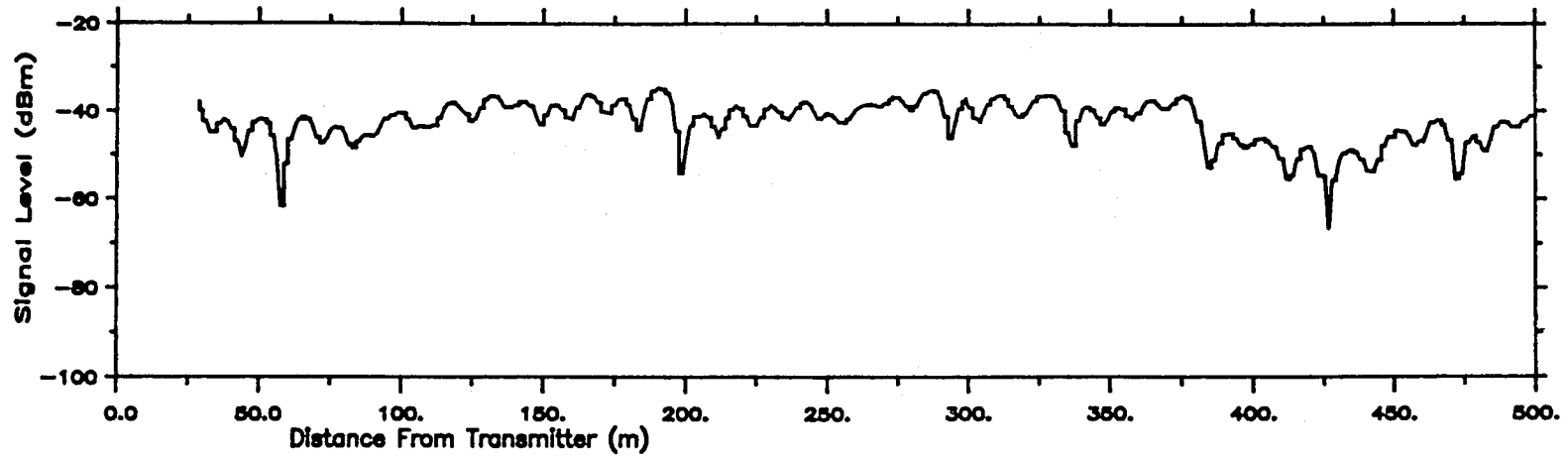


Figure 57. Signal level variation over a short distance 1.0 to 2.0 km from the transmitter at 11.5 MHz.

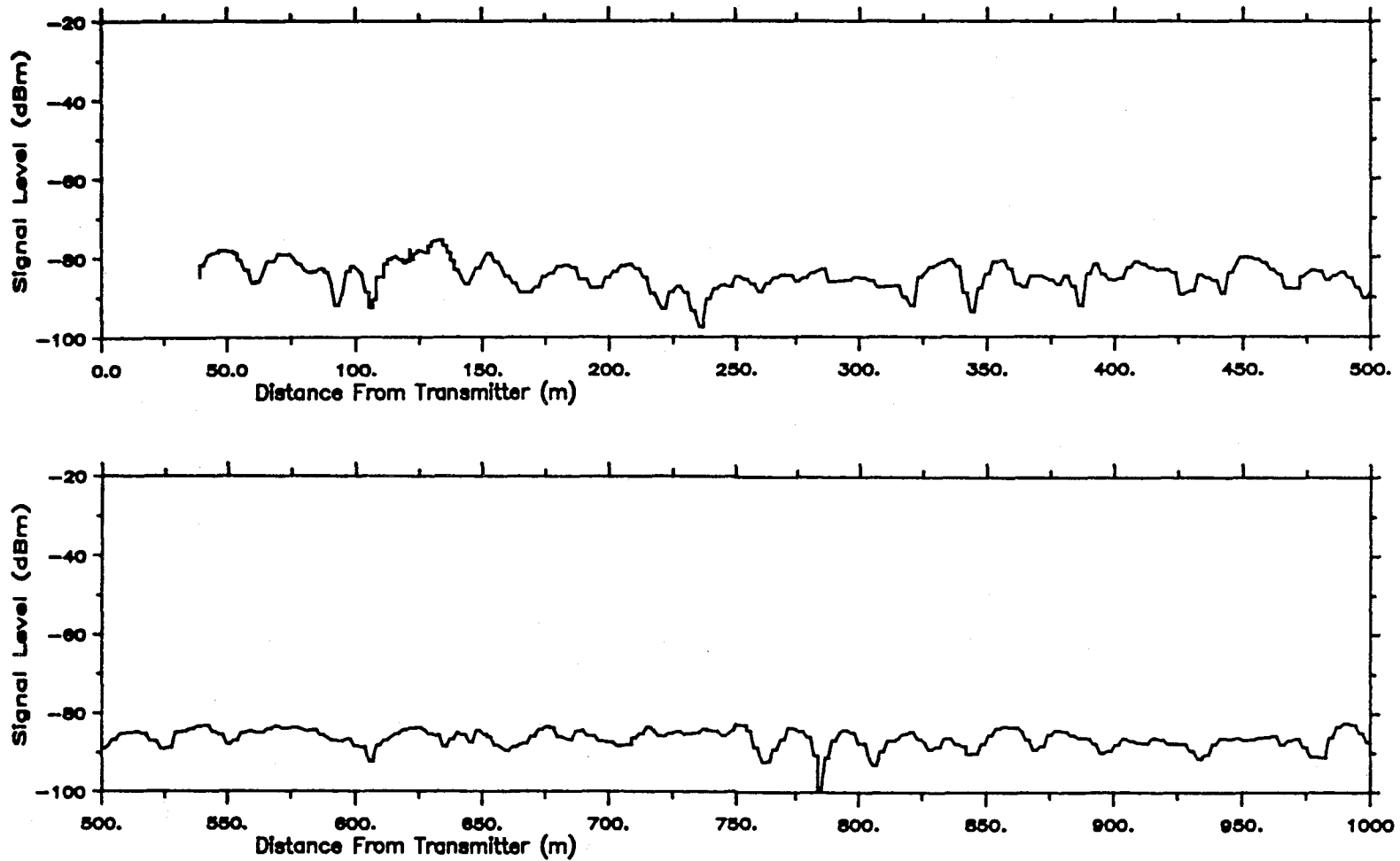


Figure 58. Signal level variation over a short distance 15.3 to 16.3 km from the transmitter at 7.5 MHz.

Table 5. Range of Ground Constant Values which Cause the Predictions to Bound the Measured Losses

Frequency (MHz)	Conductivity (S/m)	Relative Permittivity
5.25	.001 - .01	10
7.5	.001 - .01	20
11.5	.05 - .03	10
28.0	.01 - .03	10 - 30

Thus, the wave-tilt method gave us ground constants that appear to be less than a factor of 5 in error compared to those constants that cause the predictions to best fit the measurements.

8.3 Predicted Propagation Losses

The North Path was the smoothest path and had the least variation between the smooth earth prediction, the WAGNER predictions, and the measured median of path loss as shown in Figures 54 and 55. With increasing frequency, the effects of the terrain (and other scatterers) become more noticeable on both the WAGNER prediction and the measured median loss. Compared with the WAGNER prediction, the smooth earth prediction would be adequate for this path.

The East Path, as shown in Figures 47 through 50, is the next smoothest path. Given the same ground constants, there is very little difference between the smooth earth prediction and the WAGNER prediction at 5.25, 7.5, and 11.5 MHz. However, at 28 MHz, there can be as much as 15 dB between the two predictions due to terrain (see Figures 49 and 50 at 8, 21, 30, and 42 km).

The measured median along the East Path was fairly well predicted at 5.25, 7.5 and 11.5 MHz for distances greater than 20 km from the transmitter. For distances less than 20 km, the differences between the median and the predictions were as large as 20 dB, with the median showing more loss than was predicted for the terrain. At 28 MHz, WAGNER proved to be fairly good by predicting the loss valleys and peaks almost exactly as measured (see Figure 50).

The South Path was the most irregular of the three paths considered in these comparisons. At 5.25 MHz, the difference between WAGNER and the smooth earth prediction was as much as 10 dB; at 7.5 MHz, it was as much as 15 dB; at

11.5 MHz, as much as 20 dB; and at 28 MHz, as much as 15 dB. Depending on the distance from the transmitter and the terrain conditions, the smooth earth usually predicted too little loss but in some cases predicted too much loss.

Given the right ground constants, the WAGNER prediction shows good agreement with the measured median at 5.25 MHz in Figure 51. In the same figure, the WAGNER prediction may have shown better agreement if conductivity had been set to 0.005 S/m. Finally in Figure 52, the WAGNER prediction shows little agreement, except for slope, with the measured median at 11.5 and 28 MHz. For these two cases, the differences are as large as 15 dB at 11.5 MHz and 25 dB at 28 MHz.

9. CONCLUSIONS

A system was developed for making HF ground wave measurements over irregular terrain. The transmitter was fixed with a ground screen over a portion of the foreground. The receiver was mobile with equipment for recording the received signal level and the vehicle's odometer shaft rotation (for position information).

Path loss measurements were made over four paths having terrain roughness ranging from smooth terrain to mountainous terrain in the Boulder, CO, area. The measurements were made at 5.25, 7.5, 11.5, and 28 MHz for distances up to 45 km from the transmitter.

A ground constants measurement system was developed using the wave-tilt technique. The system was used to make measurements in the field near the transmitter site. The measured ground constants were used in the prediction model. Based on the comparisons between the measured losses and the predicted path losses, the wave-tilt technique and equipment proved to be a very good ground constants measurement tool.

Transmitter antenna patterns for the four measurement frequencies are given in the report. The ground screen had little noticeable affect at 5.25 and 7.5 MHz but was quite evident at 11.5 and 28 MHz, providing about 3 dB above an isotropic antenna at 11.5 MHz and about 6 dBi at 28 MHz.

Antenna patterns for an active and a passive antenna mounted on top of a van for frequencies from 3 to 30 MHz are given in the report.

The measurements show that snow cover (with a depth of 0.3 m) had no appreciable effect on the propagation losses, except at 5.25 MHz where the losses appear to be 5 dB less when snow cover is present. (The latter may be due to an instrumentation error.)

The signal variation due to multipath was measured to be as large as 20 dB over a distance of less than 50 m. In the area the multipath signal was measured, there appeared to be one predominant signal and one weaker signal. The result was a sinusoidal ripple rather than the Rayleigh-distributed signal level associated with many weaker signals of similar amplitude and uniformly-distributed phase.

Each measurement path was divided into 0.16 km (0.1 mi) increments; within each increment, the median, the upper decile, and the lower decile of the measured path loss was determined. Plots of the median and the upper and lower deciles of measured path loss are given in the report for each path and each frequency. If the terrain roughness is ignored the differences between the largest median and smallest median loss is about 20 dB regardless of frequency and distance from the transmitter.

The difference between the upper decile and the lower decile path loss was typically 13 dB for the mountainous terrain and 6 dB for the smooth terrain paths.

Ground wave predictions for three of the paths were made using a smooth earth model and the WAGNER program. There was little difference between the smooth earth model and WAGNER predictions for the smooth terrain paths but for the irregular terrain paths, the differences were as large as 10 dB at 5.25 MHz, 15 dB at 7.5 MHz, 20 dB at 11.5 MHz, and 15 dB at 28 MHz. The smooth earth model predicted too little loss compared to WAGNER's predictions in most cases; sometimes, however, the smooth earth model predicted more loss than the WAGNER prediction. This happens, for example, when the terrain features indicate a line-of-sight condition for the WAGNER model and the smooth earth model is in the "beyond the horizon" region.

The WAGNER predictions proved to be a good estimator of the path loss for some of the measurement conditions but not for others. It appears to give good predictions when the terrain is fairly smooth or when the terrain obstacles are well defined, such as long ridges perpendicular to the propagation path. When the terrain is very irregular, such as in the mountaineous regions, the WAGNER estimates can differ considerably from the measured path loss. The reasons probably are evident. WAGNER only considers the terrain along the radial from the transmitter to the receiver site. Any signals that arrive at the receiver along different routes other than the direct path are not accounted for by WAGNER.

10. REFERENCES

- CCIR (1982a), Ground wave propagation curves for frequencies between 10 kHz and 30 MHz, Recommendation 368-4, Propagation in Non-Ionized Media, Vol. V., CCIR XVth Plenary Assembly, Geneva.
- CCIR (1982b), Electrical characteristics of the surface of the earth, Recommendation 527-1, Propagation in Non-Ionized Media, Vol. V, CCIR XVth Plenary Assembly, Geneva.
- Eaton, J. L. (1976), The wave-tilt method of measuring electrical ground constants in the L.F. and M.F. bands, BBC Research Department Technical Report BBC-RD-1976/15, June.
- Hill, D. A. (1982), HF ground wave propagation over forested and built-up terrain, NTIA Report 82-114, November (NTIS Access. No. PB 83-194175).
- IEEE (1974), IEEE guide for radio methods of measuring earth conductivity, IEEE Trans. Ant. Prop. AP-22, No. 2, pp. 373-400.
- Jordan, E. C., and K. G. Balmain (1968), Electromagnetic Waves and Radiating Systems (Second Edition (Prentice Hall Book Co., Inc., Englewood Cliffs, NJ), Section 16.05.
- National Geophysical Data Center (1984), Elevation data for North America, Inventory No. TGP-0050, Department of Commerce, NOAA, Boulder, CO 80303.
- Ott, R. H. (1971), A new method for predicting HF ground wave attenuation over inhomogeneous, irregular terrain, U.S. Dept. of Commerce, Office of Telecommunications, TRER 7, January (NTIS Accession No. AD721179).
- Ott, R. H., L. E. Vogler, and G. A. Hufford (1979), Ground wave propagation over irregular, inhomogeneous terrain: comparison of calculations and measurements, NTIA Report 79-20, May (NTIS Accession No. PB 298668/AS).
- Stewart, F. G., L. A. Berry, C. M. Rush, and V. Agy (1983), An air-to-ground HF propagation prediction model for fast multicircuit computation, NTIA Report 83-131, August (NTIS Access. No. PB 84-145861).

APPENDIX A: THE PROPAGATION MEASUREMENT SYSTEM AND PROCEDURE

A.1 Introduction

A measurement system was instrumented to transmit a cw HF signal from a fixed site and to automatically collect and record the received signal power as measured at the input to a mobile receiver. A van-type truck housing the receiver system was driven along and across radials that originate from the transmitter site. Along with the measured received power, the number of revolutions of the speedometer shaft also was recorded. The number of revolutions was converted to van position information for each measurement data point at data analysis time. Figure A-1 is a block diagram of the ground wave measurement system. The following sections describe the measurement system in more detail.

A.2 Transmitter System

Although the transmitter used for the propagation measurements was operated from a fixed site, it could be housed in a van and made portable so field strengths could be measured along different kinds of paths. Figure A-2 is a block diagram of the system.

Transmitter Exciter Unit

The transmitter exciter unit was a programmable rf synthesizer that provides frequency generation, determination of transmitter output power level, and the modulation of the power amplifier.

Selection of the transmitter output frequency was made by direct keyboard entry on the synthesizer. The cw frequency accuracy and the long term stability at any output frequency was determined by the synthesizer's internal 10 MHz reference oscillator, which has an accuracy and stability of 3 parts in 10^9 per 24 hours.

The level of transmitter output power was controlled directly by manual adjustment of the output power level of the synthesizer.

Transmitter Power Amplifier

The power amplifier was a broadband linear amplifier with a nominal output power rating of 300 W. The amplifier has a flat frequency response throughout the HF band with a gain of 55 dB \pm 1 dB. Less than 0.8 mW of input

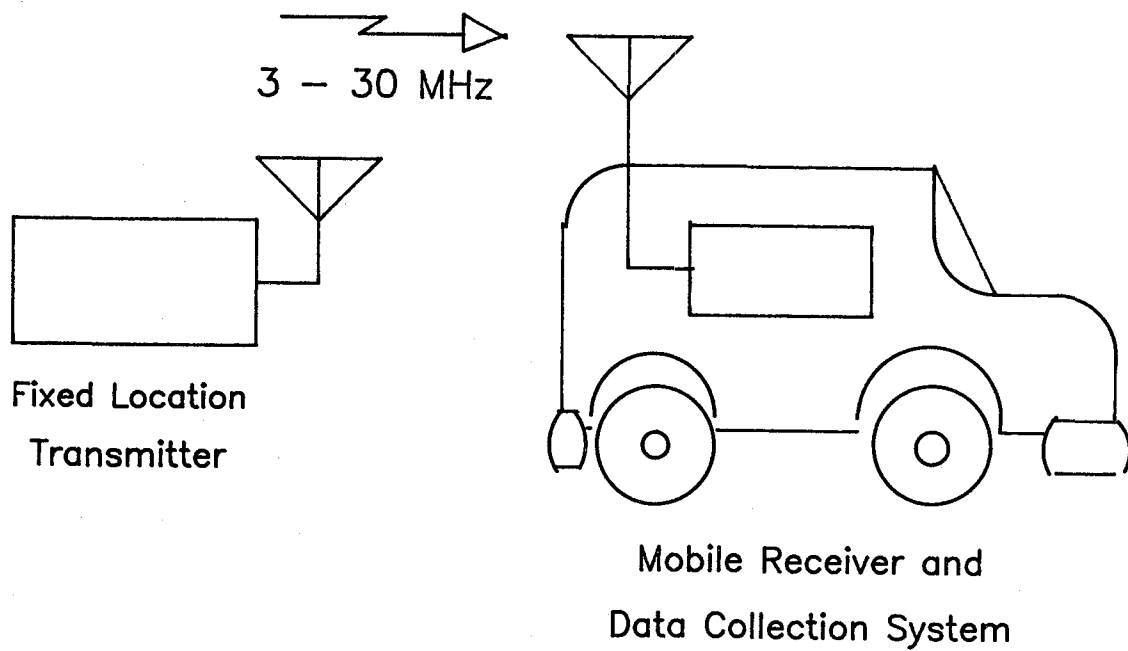


Figure A-1. Ground wave measurement system block diagram.

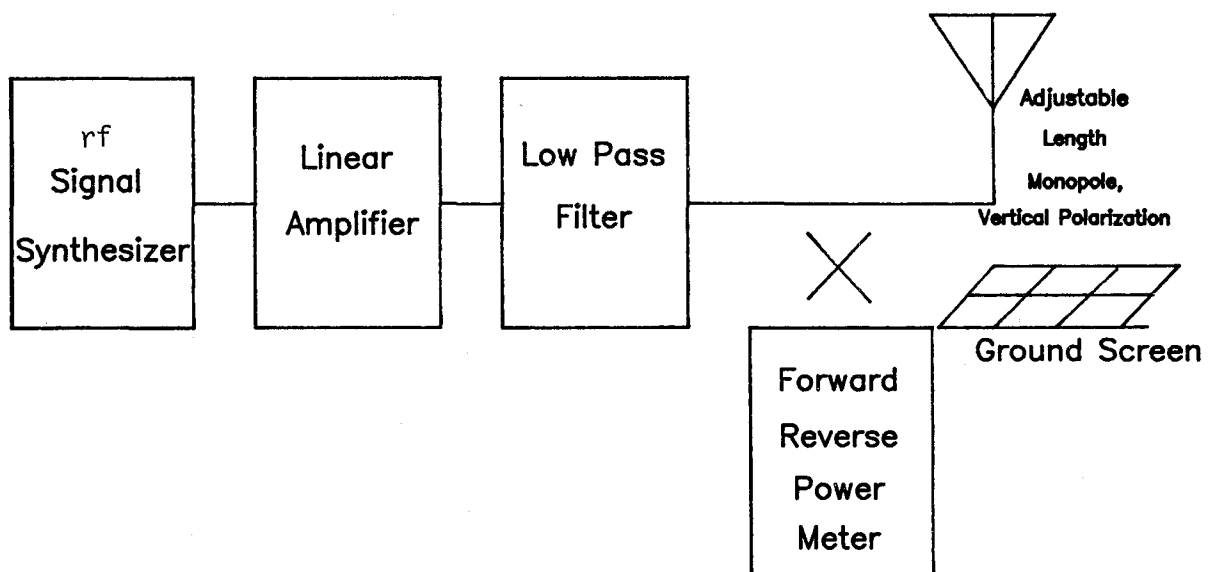


Figure A-2. Transmitter system block diagram.

power was required for an output of 250 W. At 250 W, the second harmonic was more than 35 dB below the output at the fundamental frequency, and the third harmonic was more than 25 dB below the fundamental. Typical third order intermodulation intercept point was +64 dBm.

A low pass filter was connected between the power amplifier and the antenna to provide an additional 80 dB attenuation above 30 MHz. For an output of 250 W, the power amplifier requires a single phase input power of approximately 2000 W.

Transmitter Antenna

Although a quarter-wavelength vertical monopole antenna based on a ground screen was used for initial radiation pattern measurements, a broadband antenna would be essential when the transmitter frequency agility is fully utilized. Figure A-3 shows the transmitter antenna. Several rolls of wire fence were stretched out beneath the antenna and used as the ground screen. The rolls of fence were overlapped and bonded together to reduce electrical resistance. Figure A-4a is a map of the transmitter site showing the location of the antenna, its ground screen, the transmitter van, nearby streets, and buildings. The location of power lines is shown on the map in Figure A-4b.

The transmitter antenna pattern was determined by measuring the field strength at known distances along radials away from the antenna (see Figure A4c). The transmitter antenna gain, as a function of angle ϕ measured from true north, is:

$$G_t(\phi) \text{ [dBi]} = E \text{ [dB V/m]} - P_t \text{ [dBm]} + 20\log(R \text{ [ft]}) - 115.$$

Table A-1 gives the antenna gain for each of the four frequencies. In each case the transmitter power was set to 40 dBm, the antenna was adjusted in length to provide the least reflected power back to the transmitter, and the field strength measurements were made on top of the receive van.

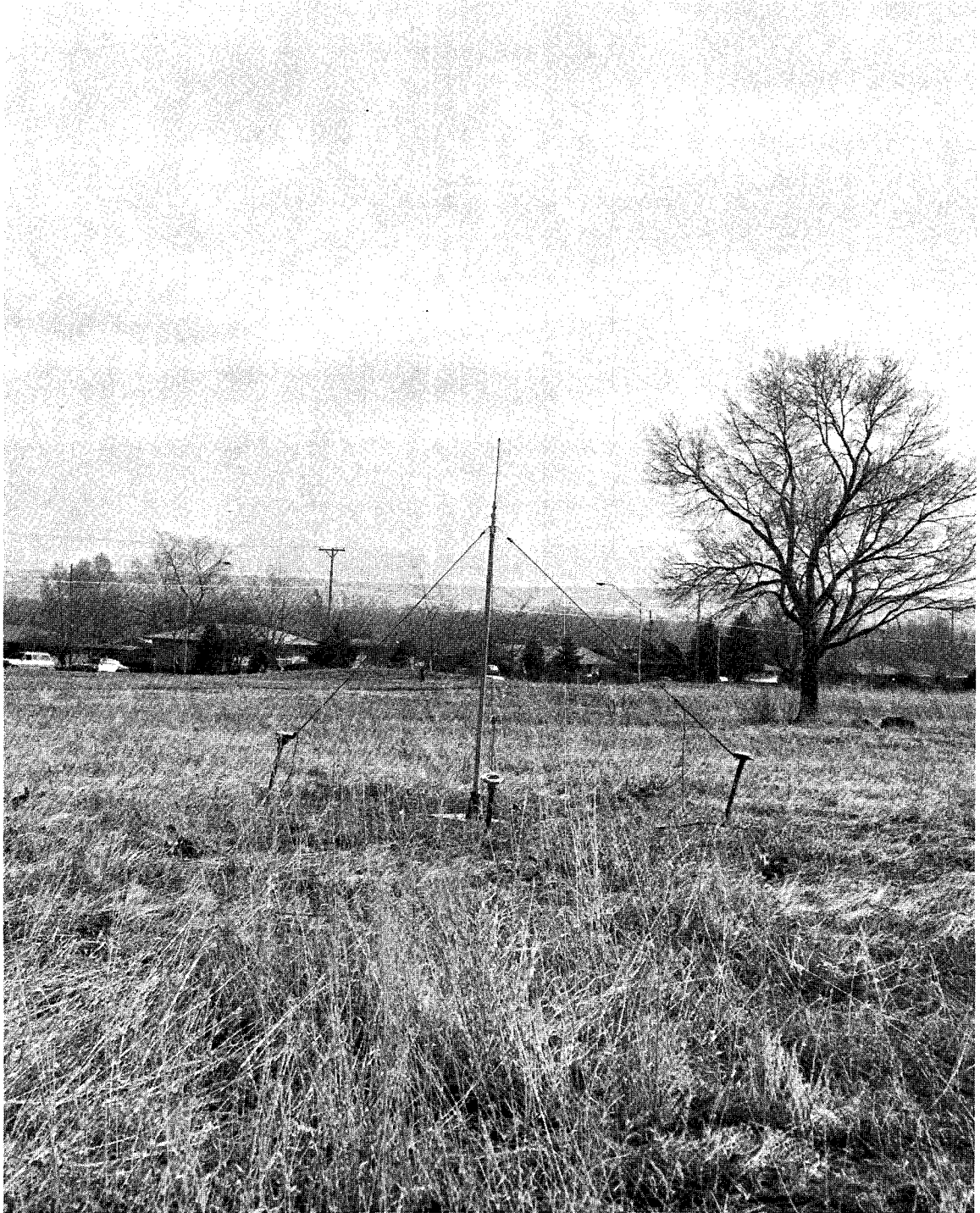


Figure A-3. Adjustable length vertical monopole transmitter antenna with ground screen.

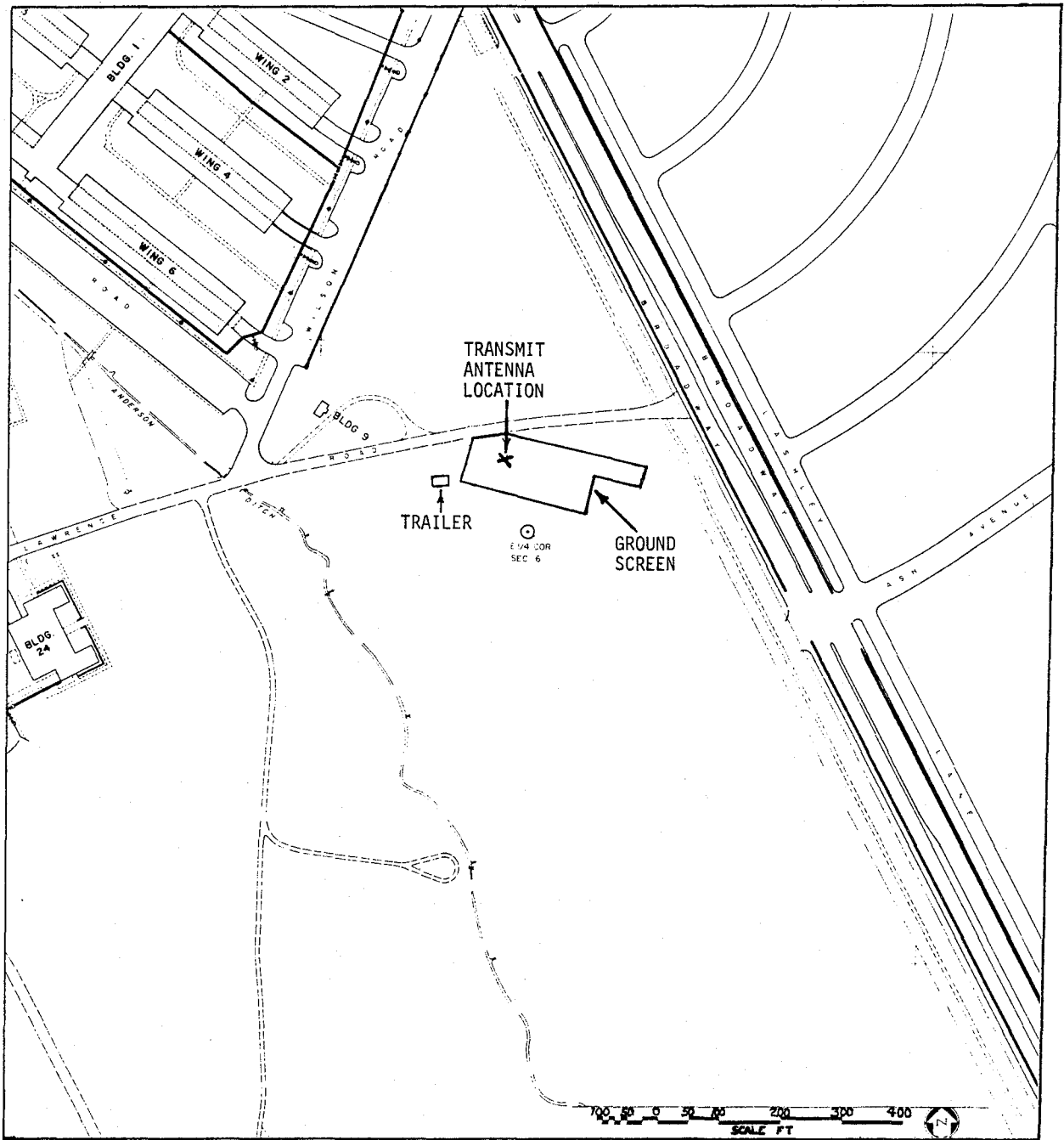


Figure A-4a. Transmitter site map. Location of antenna, ground screen, roads, and buildings.

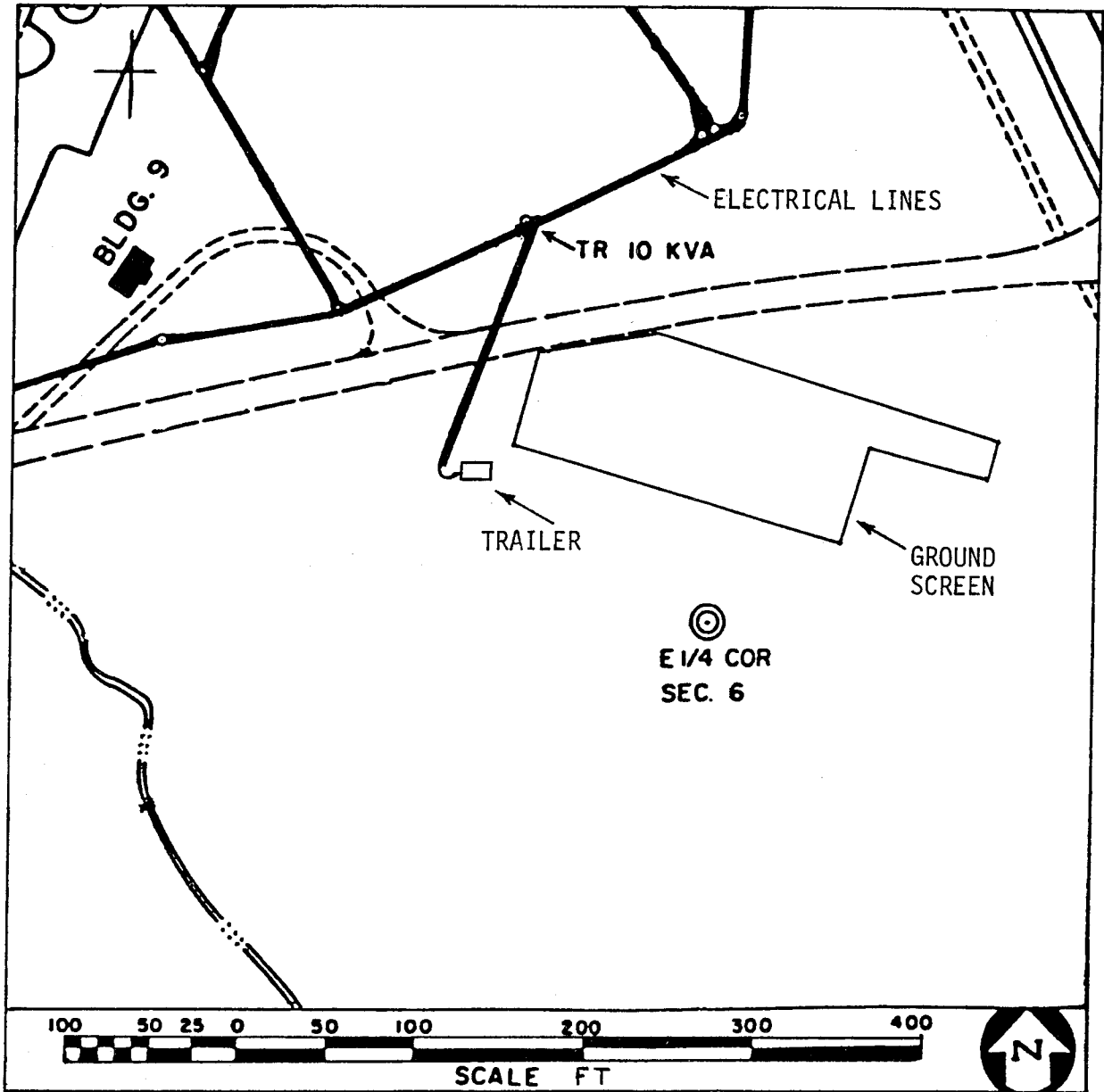


Figure A-4b. Location of electrical lines.

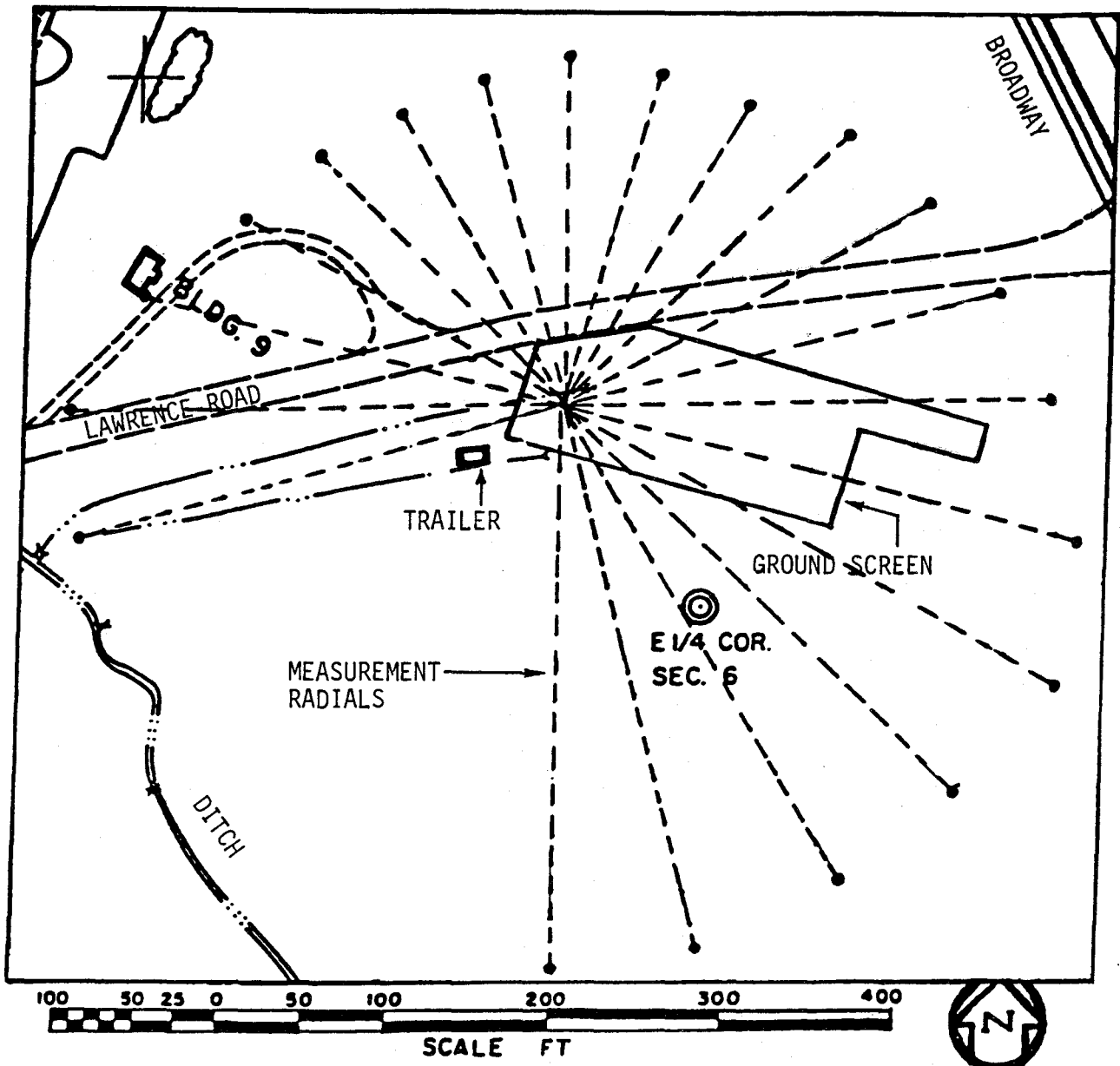


Figure A-4c. Ground screen and radials where field strengths were measured.

Table A-1. Transmitter Antenna Gain Measurements

Angle from true north (deg E of N)	Radial distance (ft)	Field strength (dB V/m)	Spectrum analyzer signal strength (dBm)	Antenna gain (dBi)
5.25 MHz				
0	205		-22.1	-2.9
15	205		-23.4	-4.2
30	205		-23.5	-4.3
45	233		-23.3	-3.0
60	243		-23.7	-3.1
75	261		-23.6	-2.3
90	283		-25.1	-3.2
105	314	100.5	-27.7	-4.9
120	339	100.5	-28.8	-5.3
135	326	100.5	-26.2	-3.0
150	328	101.0	-27.0	-3.8
165	336	101.0	-26.5	-3.1
180	336	101.0	-26.8	-3.4
255	287		-25.1	-3.0
270	302		-26.2	-3.7
285	257		-25.1	-4.0
300	226		-22.9	-2.9
315	213		-23.6	-4.1
330	202		-23.8	-4.8
345	201		-22.2	-3.2
7.5 MHz				
0	205		-10.7	2.9
15	205		-10.4	3.2
30	205		-14.3	-0.7
45	233		-12.5	2.3
60	243		-11.9	3.2
75	261		-12.9	2.8
90	283		-12.6	3.8
115	314	108.5	-14.5	2.8
120	339	106.5	-15.7	2.3
135	326	107.25	-15.0	3.0
150	328	107.0	-14.7	3.0
165	336	107.5	-15.5	2.4
180	336	107.0	-15.3	2.6
255	287		-13.2	3.4
270	302		-14.2	2.8
285	257		-15.5	0.1
300	226		-12.4	2.1
315	213		-12.0	2.0
330	202		-10.9	2.6
345	201		-10.9	2.5

Table A-1. Transmitter Antenna Gain Measurements (Continued)

11.5 MHz

0	205		- 8.7	1.5
15	205		- 6.6	3.6
30	205		-11.4	-1.2
45	233		- 9.7	1.6
60	243		-10.1	1.6
75	261		- 9.5	2.8
90	283		- 9.0	4.0
105	314	108.0	-10.4	3.5
120	339	107.5	-11.1	3.5
135	326	107.0	-12.3	2.0
150	328	106.0	-12.8	1.5
165	336	106.0	-13.2	1.3
180	336	104.5	-15.0	-0.5
255	287		-11.5	1.7
270	302		-12.3	1.3
285	257		-12.6	-0.4
300	226		- 8.7	2.4
315	213		- 8.4	2.2
330	202		- 8.2	1.9
345	201		- 9.2	0.9

28 MHz

0	205		-12.4	-1.9
15	205		- 8.5	2.0
30	205		-13.5	-1.9
45	233		-13.0	-1.0
60	243		-10.0	2.0
75	261		- 9.5	3.1
90	283		- 6.8	6.5
105	314	108.5	- 7.5	6.7
120	339	105.5	-14.1	0.8
135	326	102.0	-17.0	-2.4
150	328	101.5	-18.1	-3.5
165	336	99.5	-21.0	-6.2
180	336	99.0	-21.9	-7.1
255	287		-12.1	1.4
270	302		-13.2	0.7
285	257		-11.7	0.8
300	226		-10.7	0.6
315	213		- 8.7	2.2
330	202		- 9.8	0.6
345	201		-12.1	-1.7

The point to note about the antenna gain data is that the ground screen, which lies toward the east under the antenna, is most effective at the higher frequencies, particularly at 28 MHz. At azimuths of 75 to 90 deg east of north, the 28 MHz pattern gain is 6 dB above an isotropic antenna and at

11.5 MHz, the gain is about 3 dBi. At 5.25 and 7.5 MHz, the ground screen has no apparent effect on the gain.

A.3 Receiver System

Initially, the data input to the model will result from similar measurements at four different frequencies. Currently, these four frequencies are selected from these bands: 5.005-5.450 MHz, 7.300-8.815 MHz; 11.400-11.700 MHz; 11.975-12.330 MHz; and 27.540-28.000 MHz. To reduce the overall time and effort required to make these measurements, it is essential that both the receiver and transmitter have some degree of frequency agility.

Figure A-5 is a block diagram of the receiver system.

Receiver Antenna

Primarily to satisfy the requirement of frequency agility and to simplify the receiver system calibration, the receiver antenna is a monopole usable from extremely low frequencies (ELF) to the very high frequencies (VHF). The overall frequency response of this antenna and its active network at the output terminal is uniform across the HF band. While the voltage gain of this network is less than one, the power gain is about 23 dB at 1 MHz. Above 100 kHz, the noise generated by the network is comparable to that generated by a 50 ohm resistor at room temperature. The signal output voltage from the network terminated in 50 ohms is related to the antenna incident signal strength by a measured antenna factor of 13 dB.

The antenna, pictured along with the measurements van in Figure A-6, is a vertical monopole about 2 m long mounted near the midpoint of the receiver van roof, with the metal roof used as the antenna ground plane. Because the network input impedance is very large, (comparable to the reactive component of the antenna input impedance), the antenna current is small and ground losses are not significant.

The active whip's technical characteristics were:

Effective height: Approximately 0.3 meter over entire frequency range
Sensitivity: Better than 0.05 V/m above 300 kHz (0 dB S/N and 1 kHz bandwidth)
Input impedance: 50 ohms
Voltage mismatch: Less than 2:1, referenced to 50 ohms

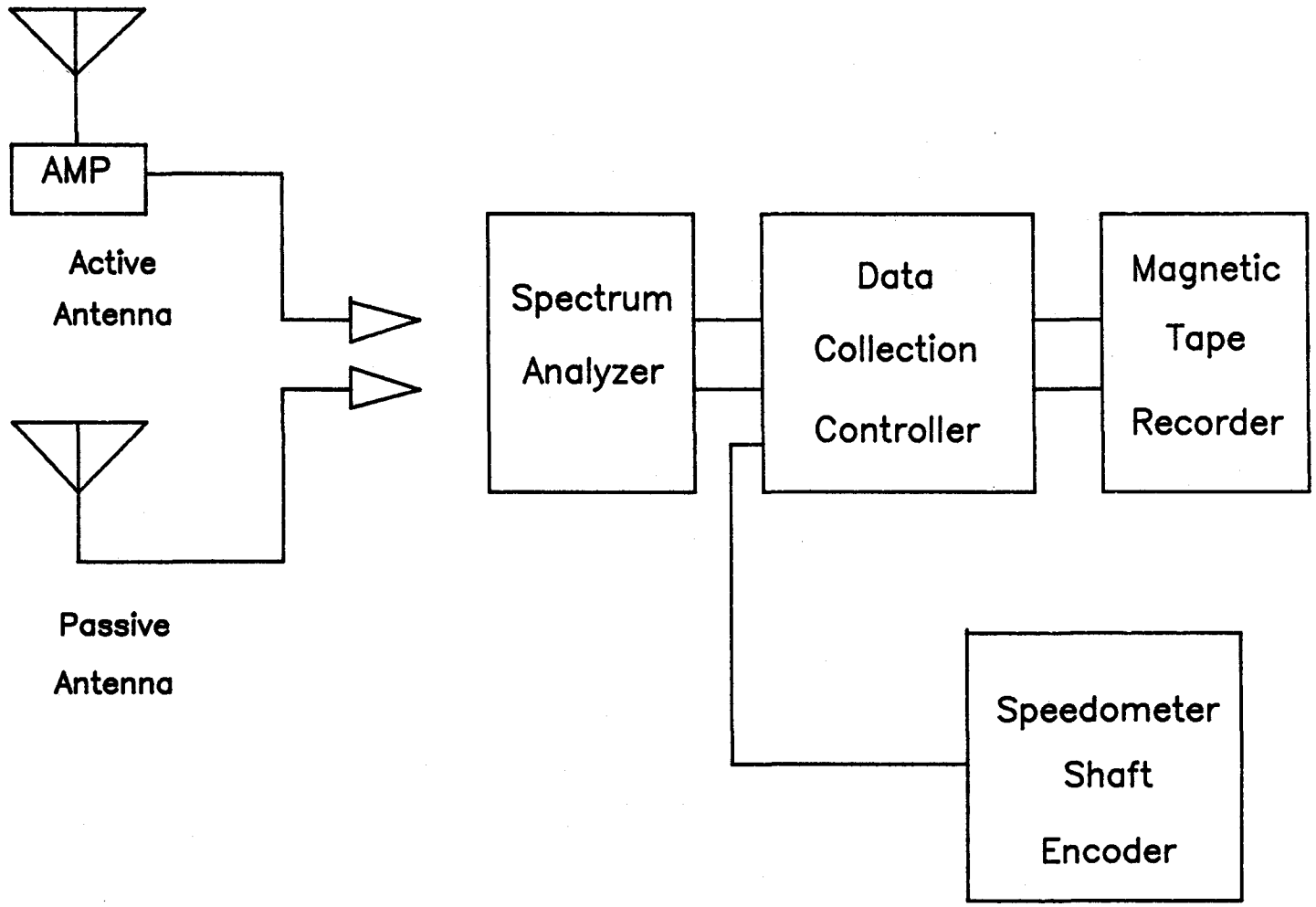


Figure A-5. Receiver and data collection system block diagram.

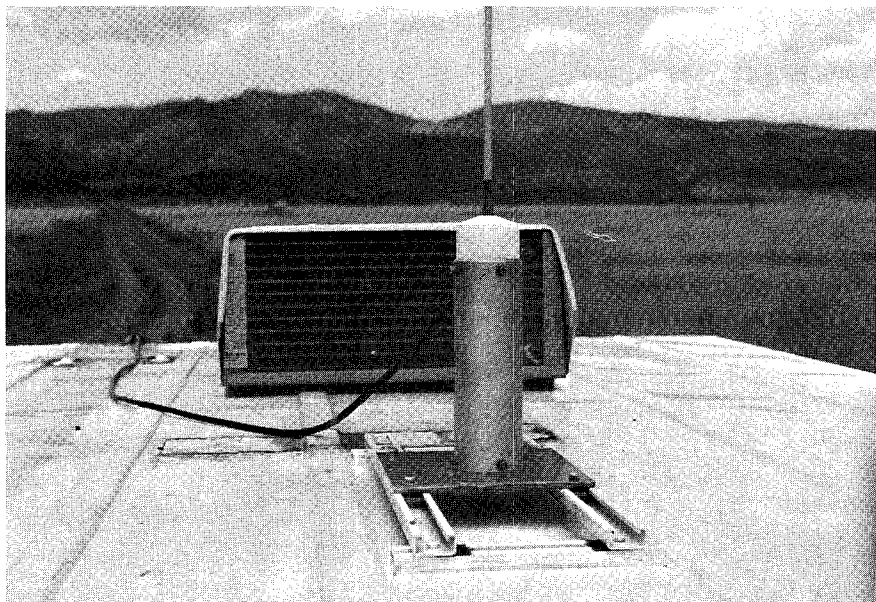


Figure A-6. Receiver and data collection van with an active antenna.

Antenna factor: 13 dB (Volts/meter relative to volts output across 50 ohms)
Overload: Approximately 2 V/m signal results in 1 dB compression in gain

Harmonics: 1 V/m signal generates the following harmonic components:
(1) second harmonic--more than 34 dB below fundamental
(2) third harmonic--more than 60 dB below fundamental

Description of Antenna Pattern Measurements

Antenna pattern measurements were made with the antenna mounted on the receiver van roof. The measurements were made at the Institute's Table Mountain facility located just north of Boulder, Colorado. This site is equipped with a powered turntable with direct digital readout of azimuth that allows automatic data collection by use of the computer controlled system shown in Figure A-7. The site also includes a signal source located approximately 0.4 km (1/4 mi) from the turntable. The majority of the measurements were made using the antenna described above. A small amount of data were taken using a 4.9 m (16 ft) passive whip antenna also.

The procedure used to collect the data was as follows:

1. The van was parked on the turntable as nearly centered as possible after which the turntable was rotated so the front of the van pointed at the signal source. The turntable azimuth encoder was then adjusted to read 0 deg. Because of the gearing of the encoder, azimuth readings increase in the counter-clockwise direction (looking down on the turntable) so that at 90 deg azimuth the passenger's side of the van is facing the signal source.
2. The turntable and the signal source were turned on and the spectrum analyzer tuned to the signal source frequency. The chosen frequencies were first checked with the spectrum analyzer to ensure no interfering signals were present. At the lower frequencies, especially, it was difficult to find frequencies free of other signals and noise.
3. At this point the computer was given control of the spectrum analyzer and recorded the amplitude and azimuth readings for periods of 5 to 45 min depending on the amount of noise observed on the spectrum analyzer display.

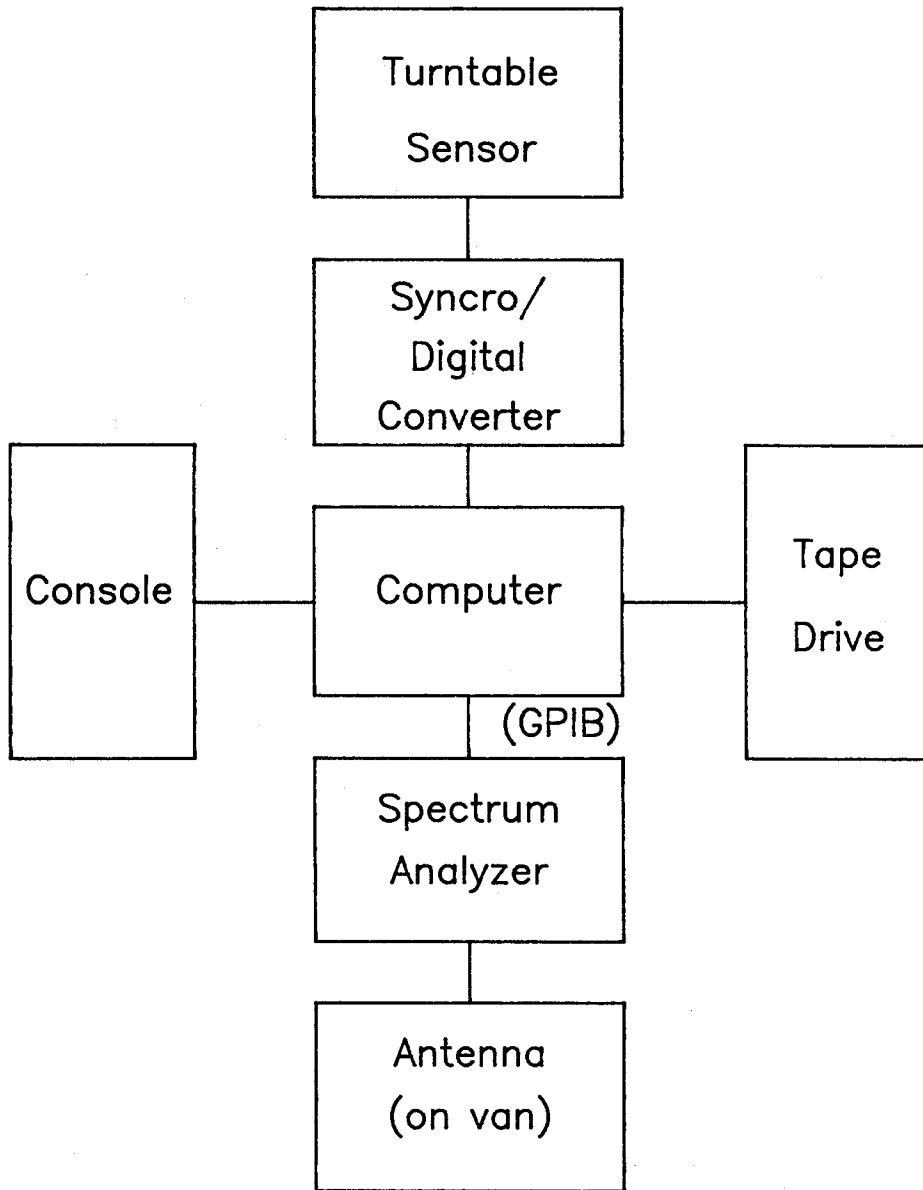


Figure A-7. Antenna pattern measurement system block diagram.

4. After data were taken from 3 to 30 MHz at frequency increments of approximately 2 MHz, the data tape was returned to the ITS lab for processing on a laboratory computer. The data were averaged and plotted (see Figures A-8 for the active antenna measurements and A-9 for the passive antenna pattern plots).

Receiver Antenna Gain

The passive receiver antenna gain was determined from the measured field strength on top of the receiver van and the measured signal power at the spectrum analyzer input. The field strength and signal power measurements given in Section A.2 were made with the driver's side of the receive van facing the transmitter antenna. The following equation relates the receive antenna gain to the measured field strength and signal power with a 50 ohm receiver input impedance:

$$E \text{ [dB}_{\mu}\text{V/m]} = P_r \text{ [dBm]} - G_r(f) \text{ [dBi]} - G_r(\theta) \text{ [dB]} \\ + 20\log(f[\text{MHz}]) \text{ [dB]} + 77.2$$

where

θ = azimuth relative to the front of the receiver van
to the transmitter site
= 270 deg (for these measurements)

$G_r(\theta)$ = receiver antenna gain as a function of θ ; see Figure A-9.

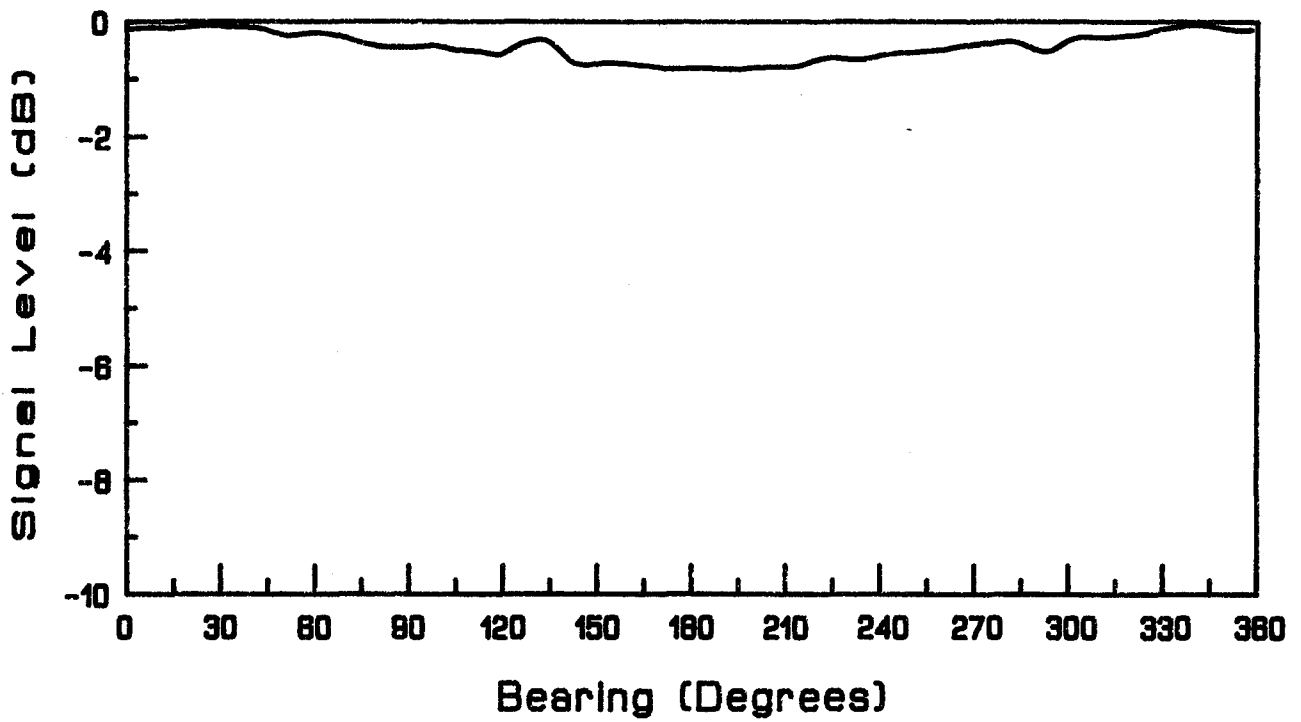
Table A-2 gives the measured receiver antenna gain.

Table A-2. Receiver Antenna Gain as a Function of Frequency

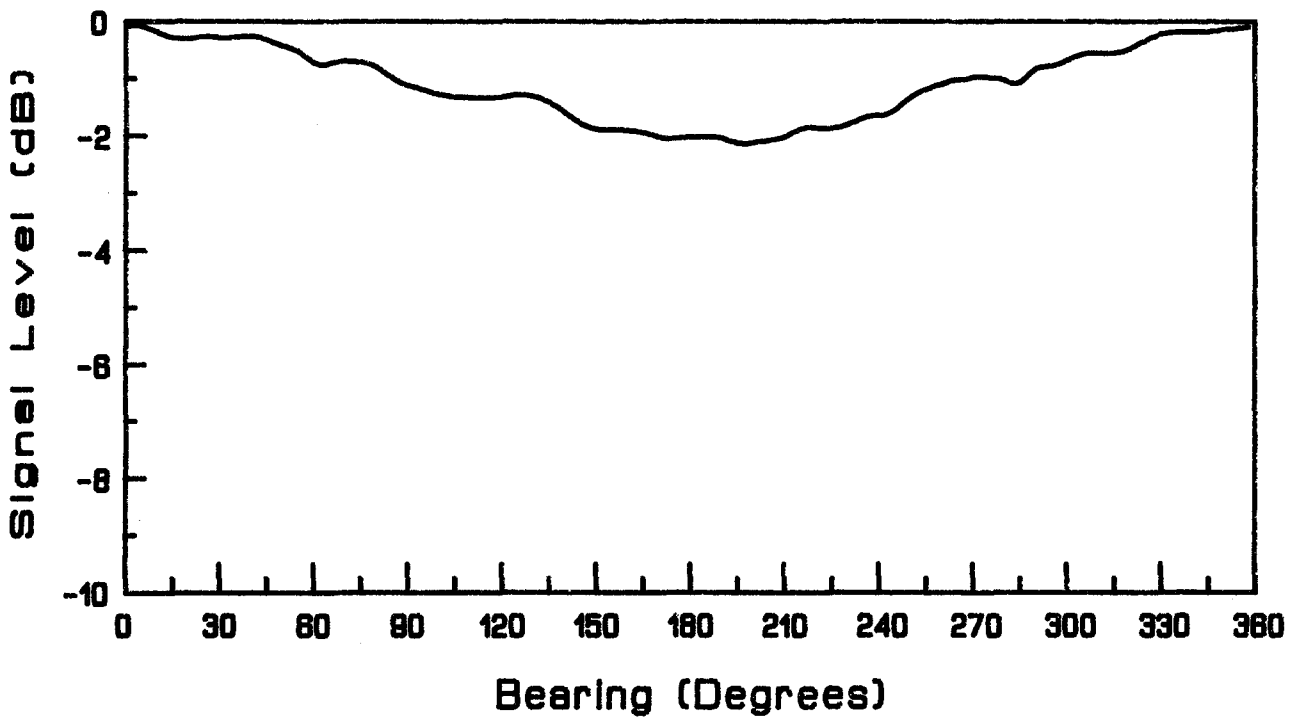
Frequency (MHz)	Antenna Gain (dBi)
5.25	-36
7.5	-28
11.5	-21
28.0	-13

Receiver Instrumentation

Initial measurements along typical paths indicated the active antenna was affected by power lines and external noise. Thus, the passive antenna was used exclusively for the propagation measurements. The passive monopole antenna fed into a spectrum analyzer that was configured as the basic component of the receiver. The analyzer provided: frequency selectivity to

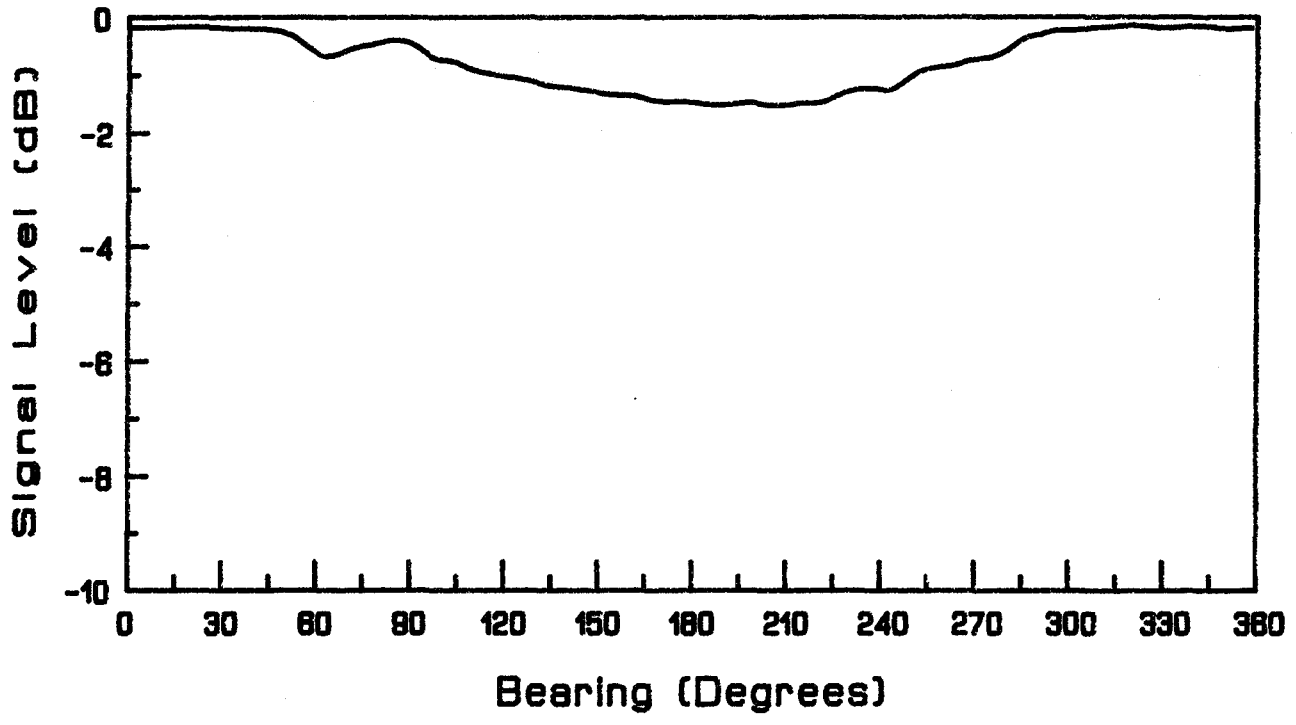


Active Whip Antenna Pattern At 5.25 MHz

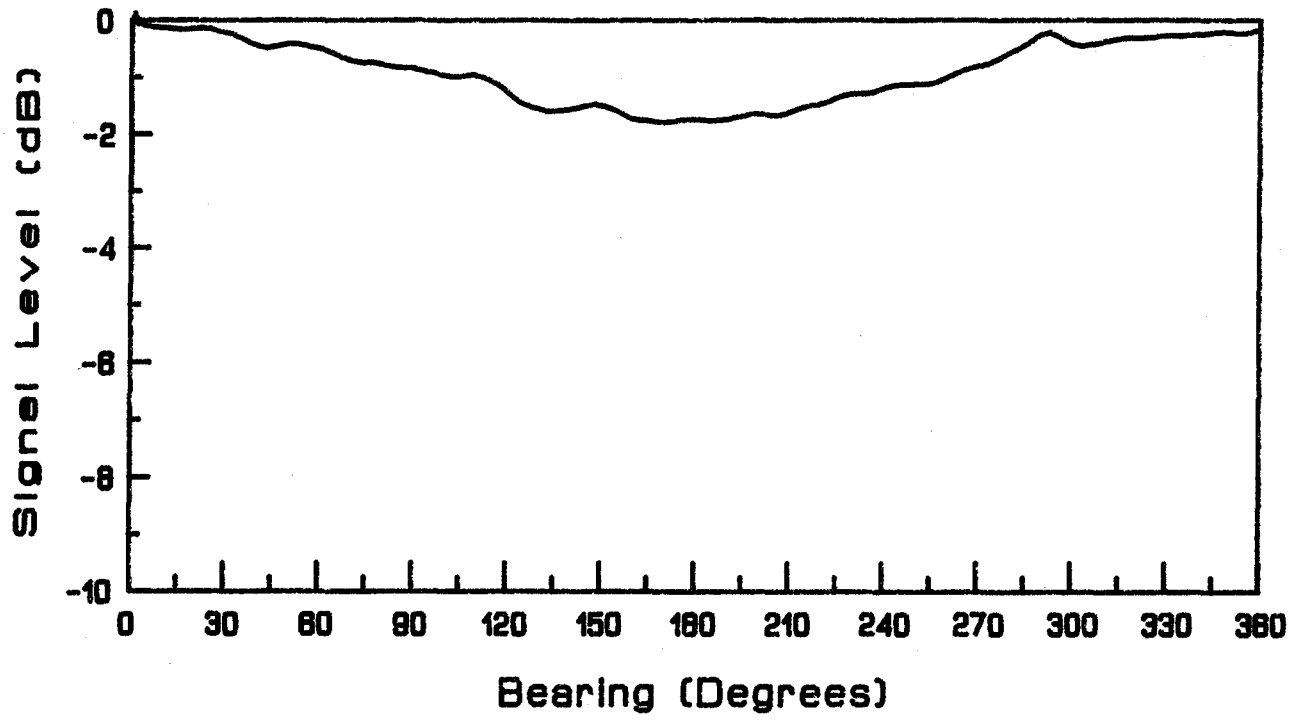


Active Whip Antenna Pattern At 7.50 MHz

Figure A-8. Pattern measurements of an active antenna mounted on a van for 3 to 30 MHz.

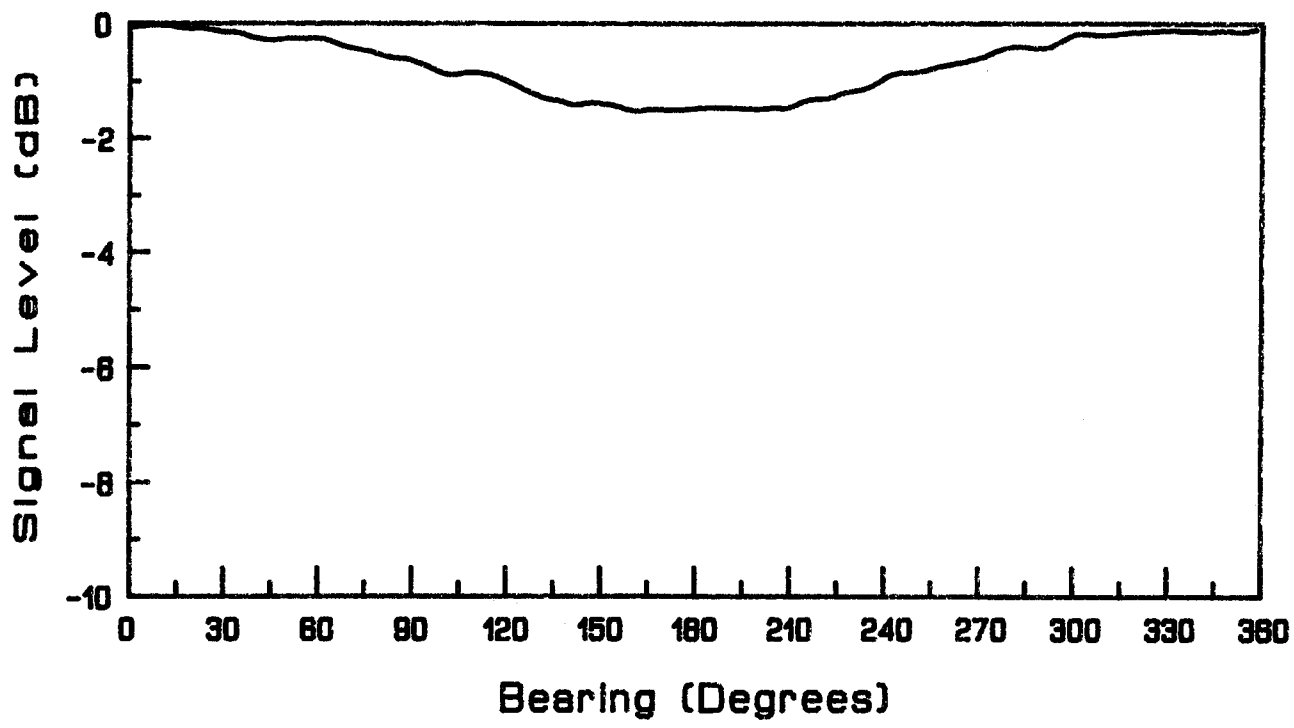


Active Whip Antenna Pattern At 8.95 MHz

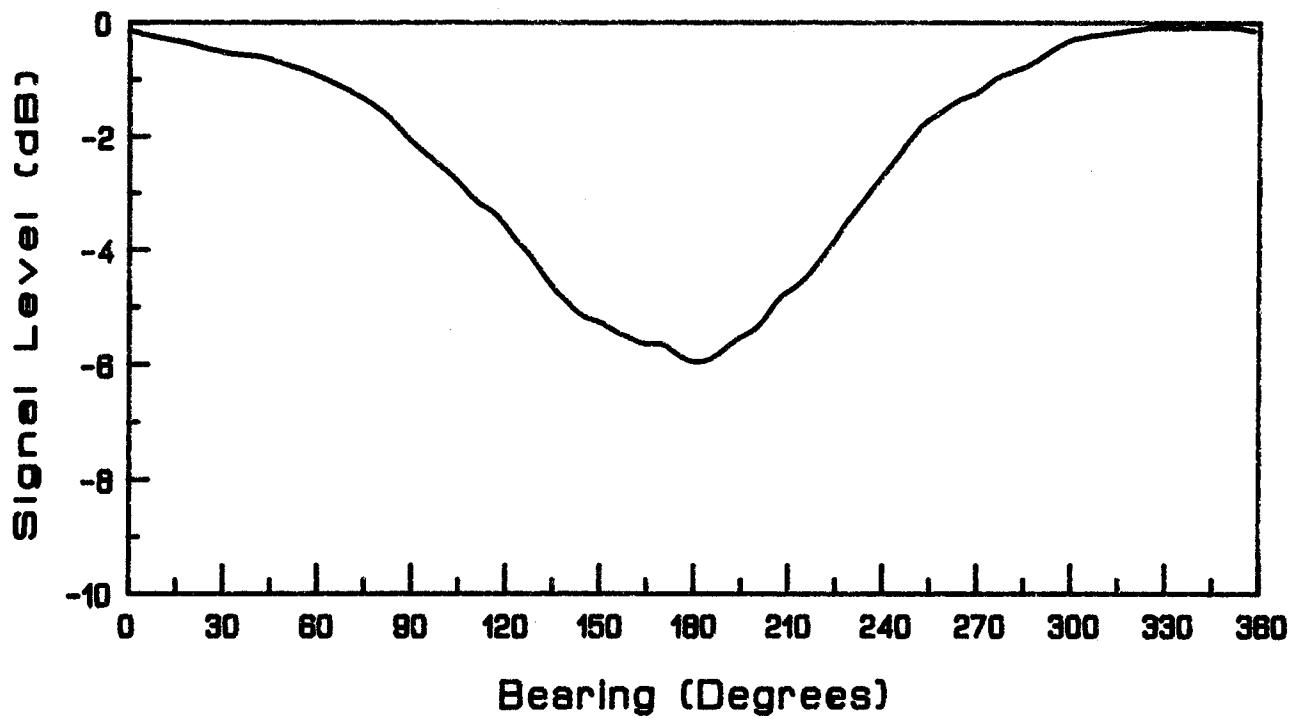


Active Whip Antenna Pattern At 11.80 MHz

Figure A-8 (Cont.)

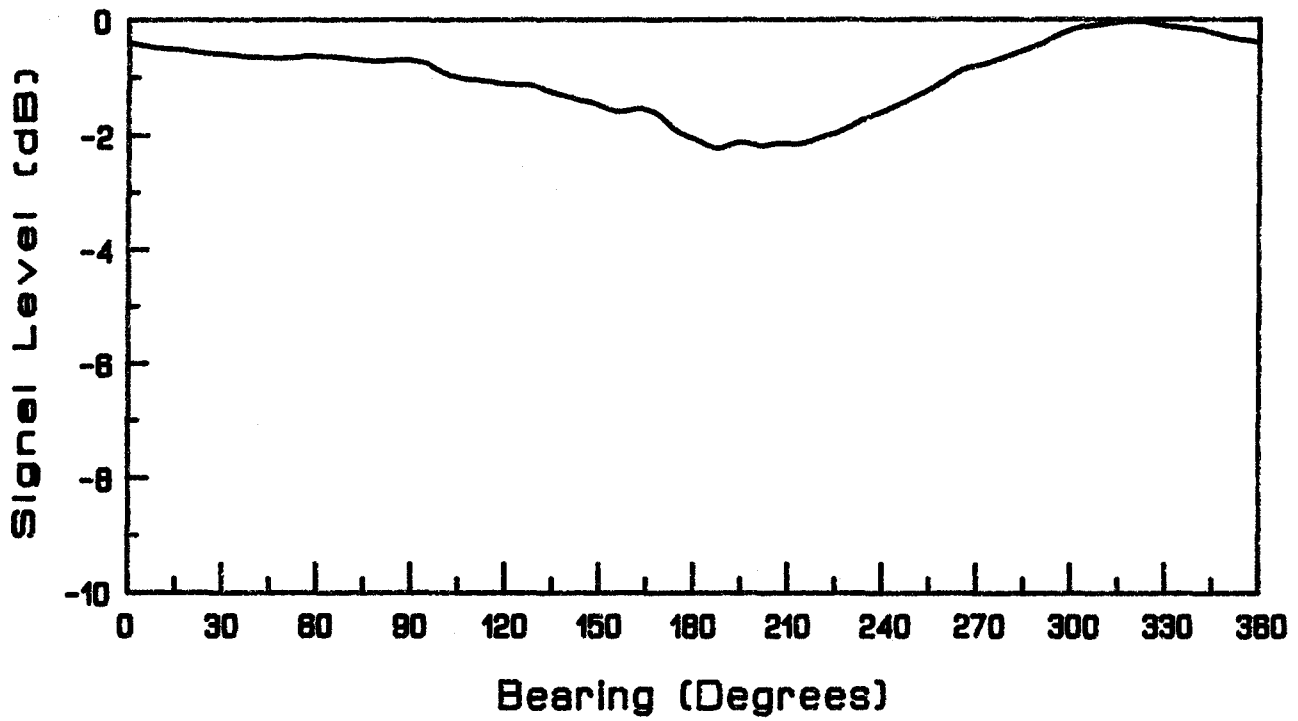


Active Whip Antenna Pattern At 13.50 MHz

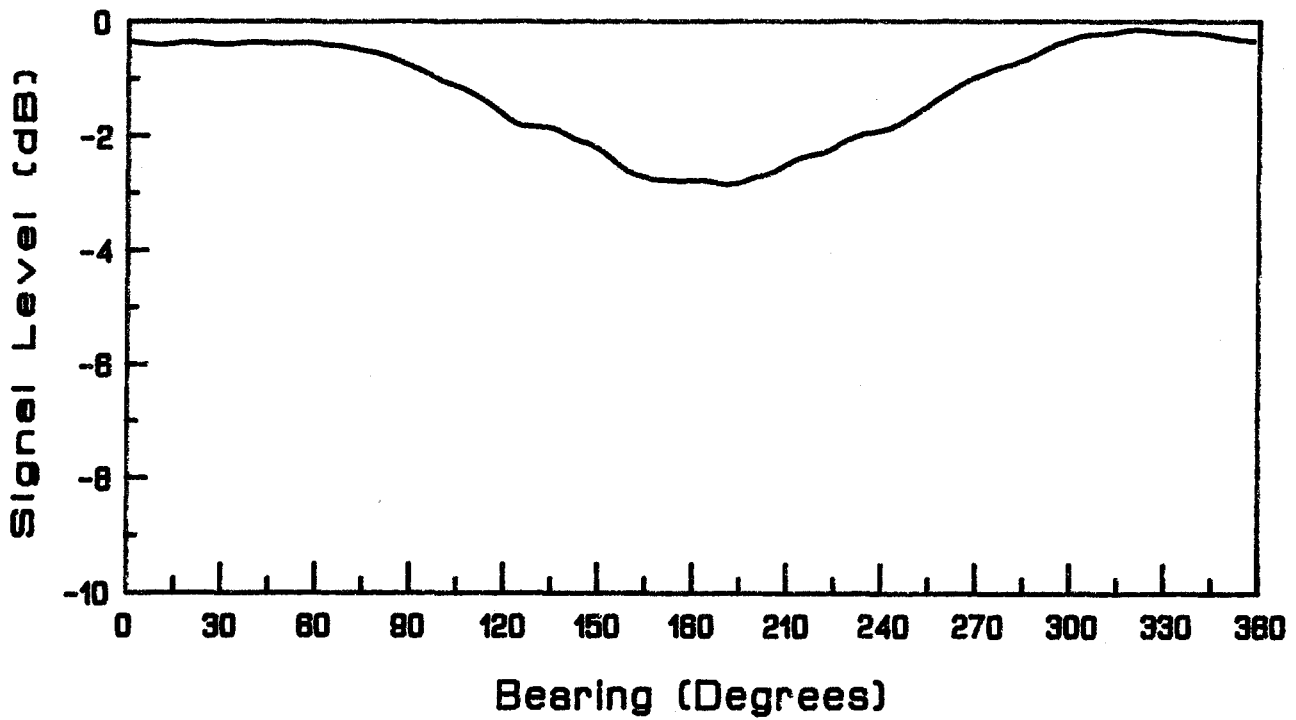


Active Whip Antenna Pattern At 15.50 MHz

Figure A-8 (Cont.)

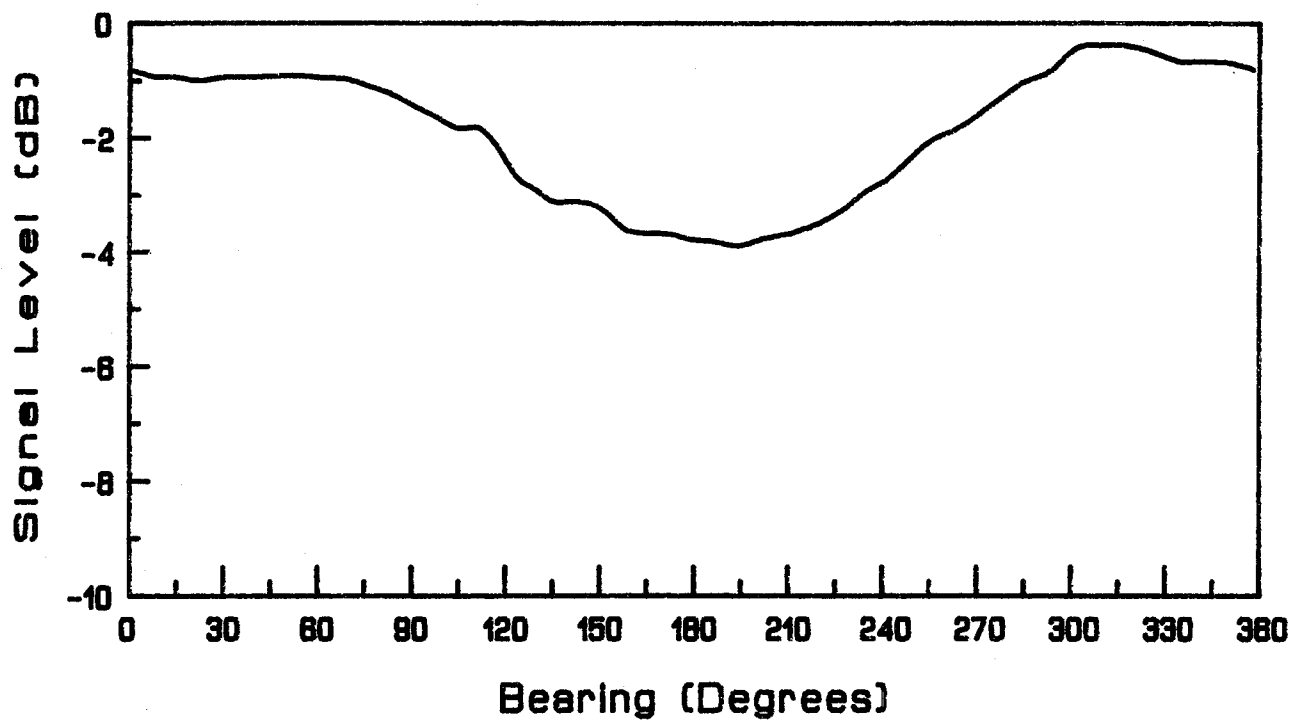


Active Whip Antenna Pattern At 17.50 MHz

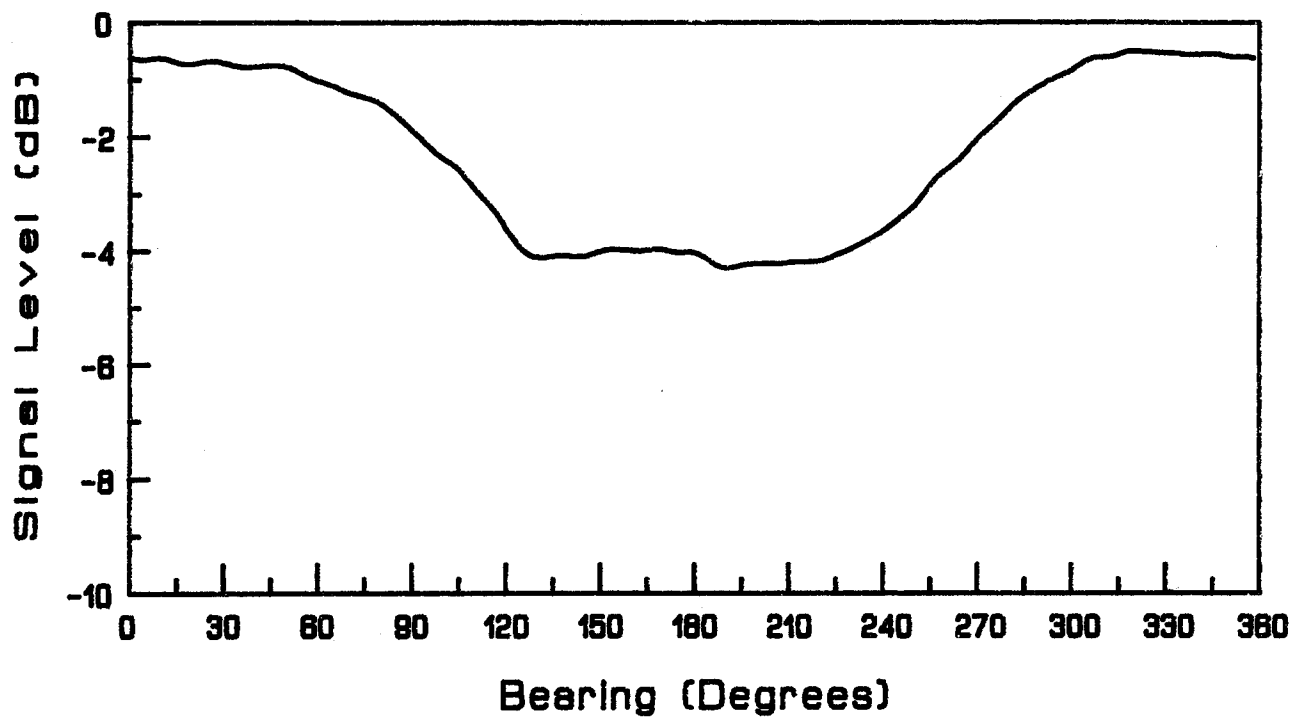


Active Whip Antenna Pattern At 19.50 MHz

Figure A-8 (Cont.)

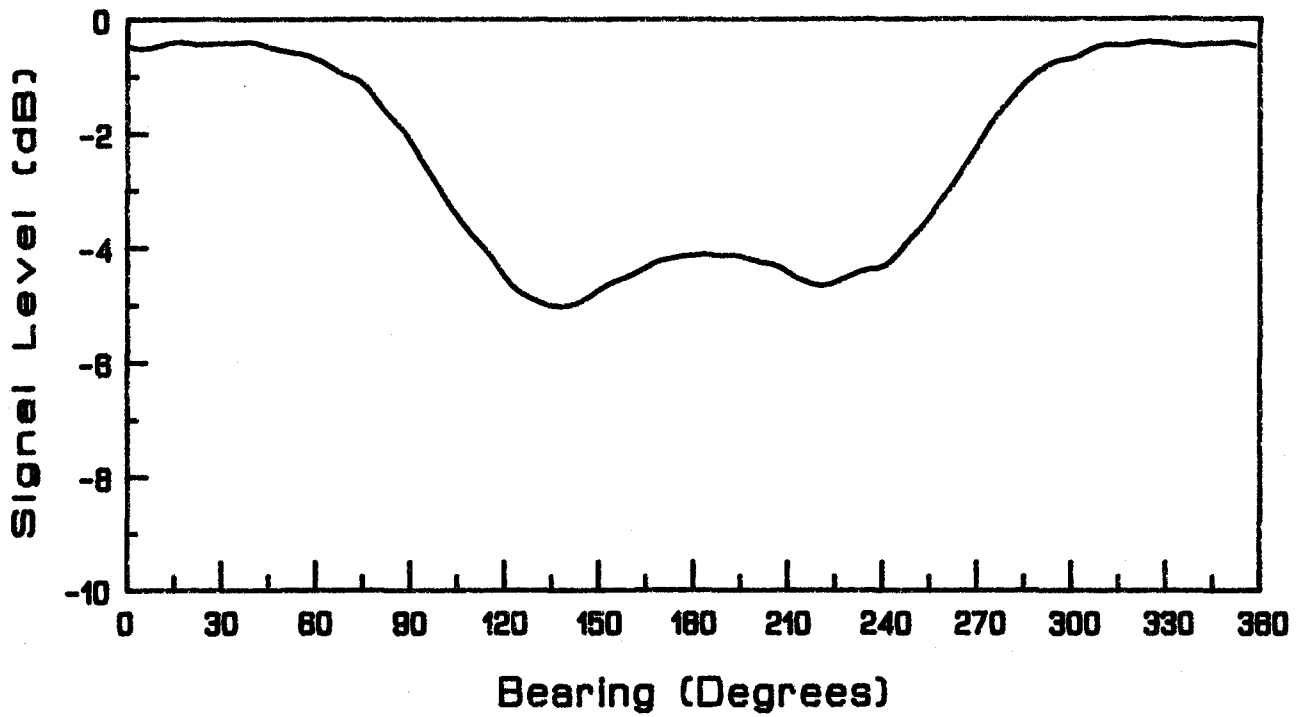


Active Whip Antenna Pattern At 21.50 MHz

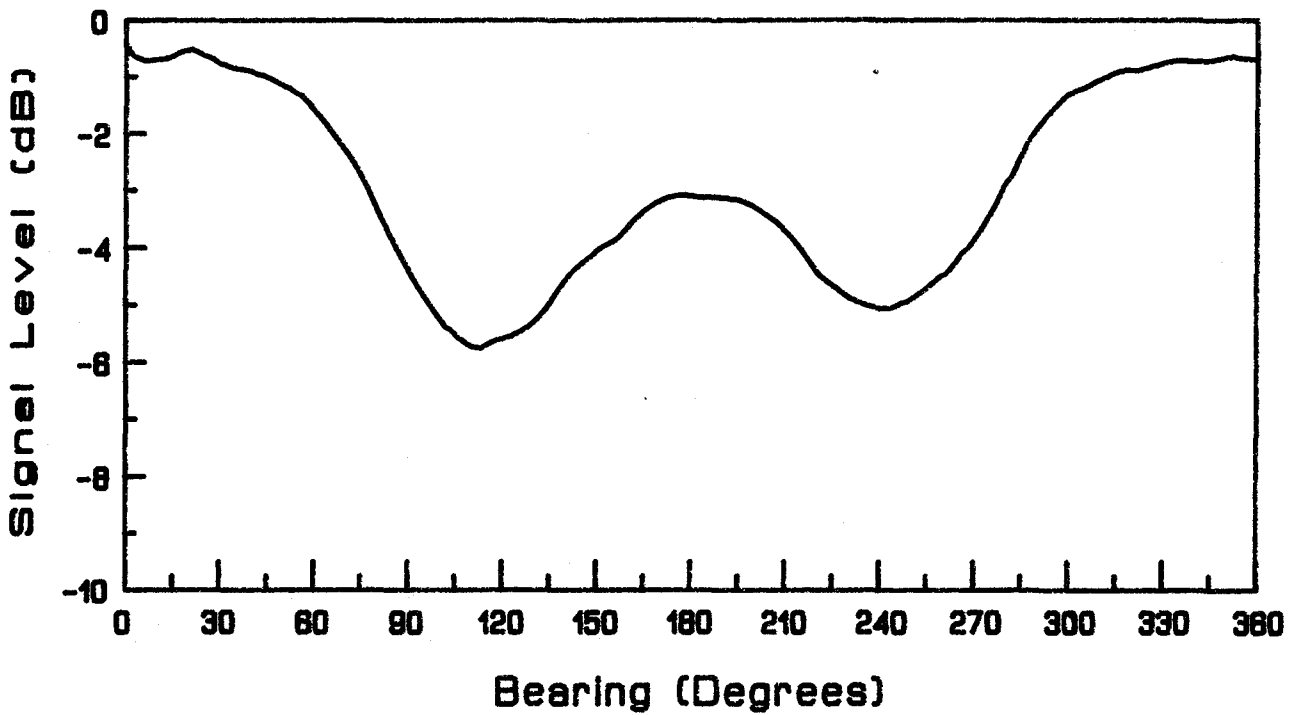


Active Whip Antenna Pattern At 23.50 MHz

Figure A-8 (Cont.)

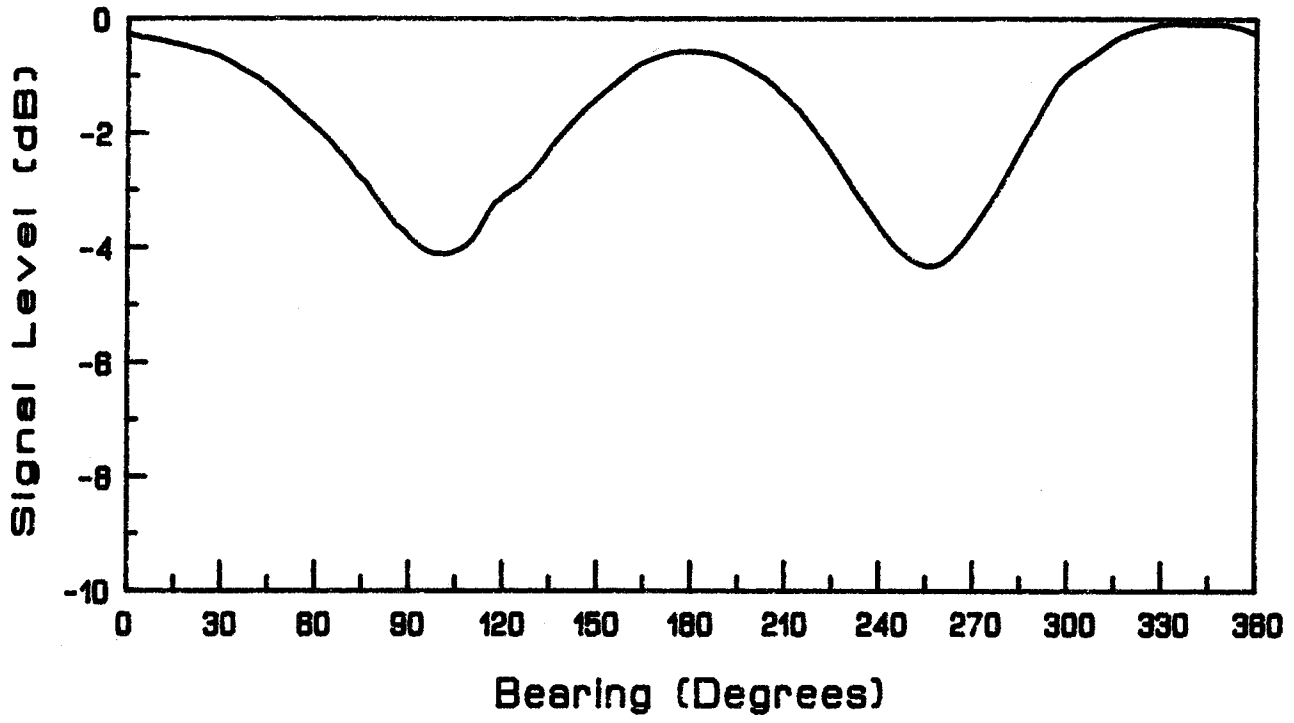


Active Whip Antenna Pattern At 25.50 MHz

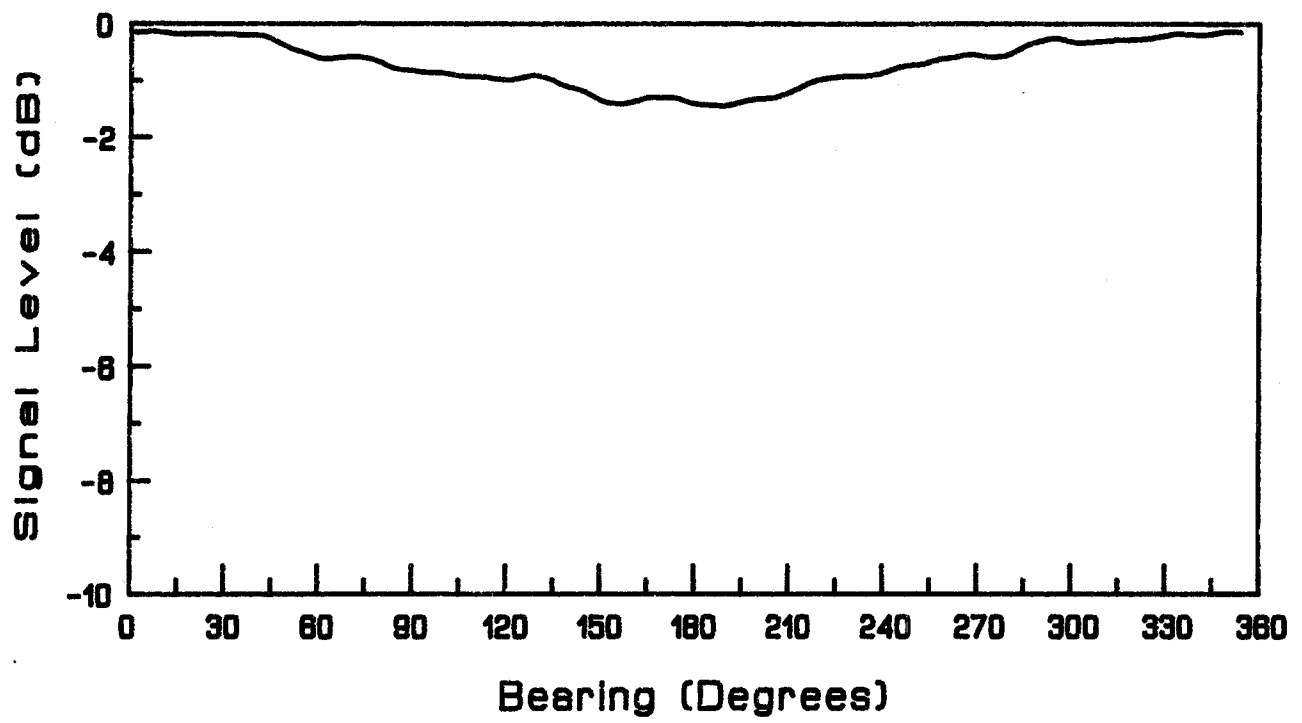


Active Whip Antenna Pattern At 28.00 MHz

Figure A-8. (Cont.)

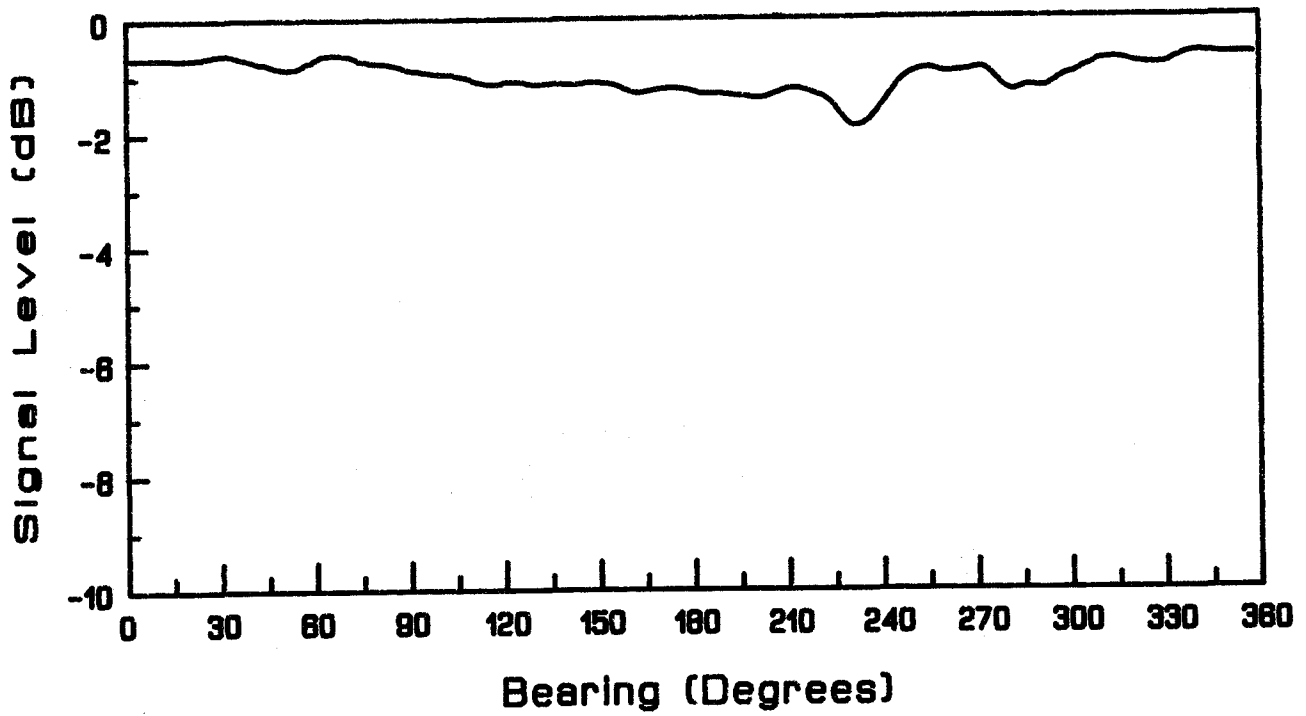


Active Whip Antenna Pattern At 30.15 MHz

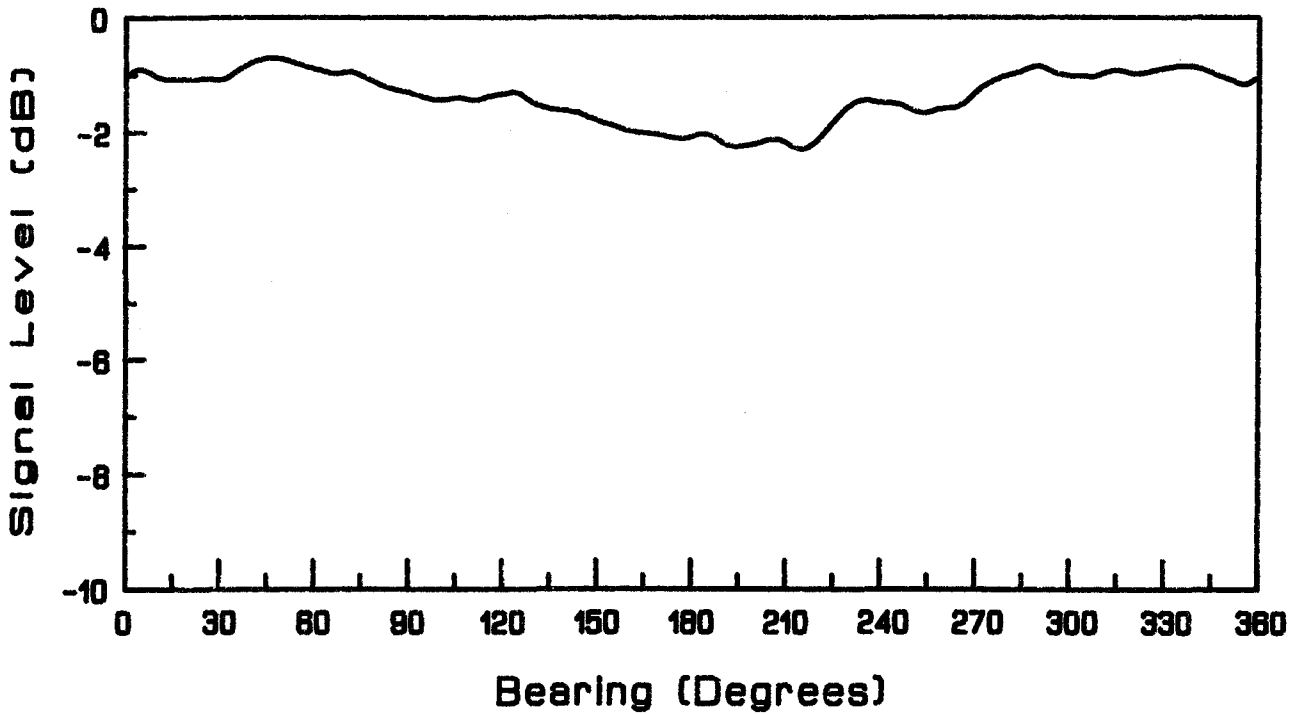


Active Whip Antenna Pattern At 2.85 MHz

Figure A-8. (Cont.)

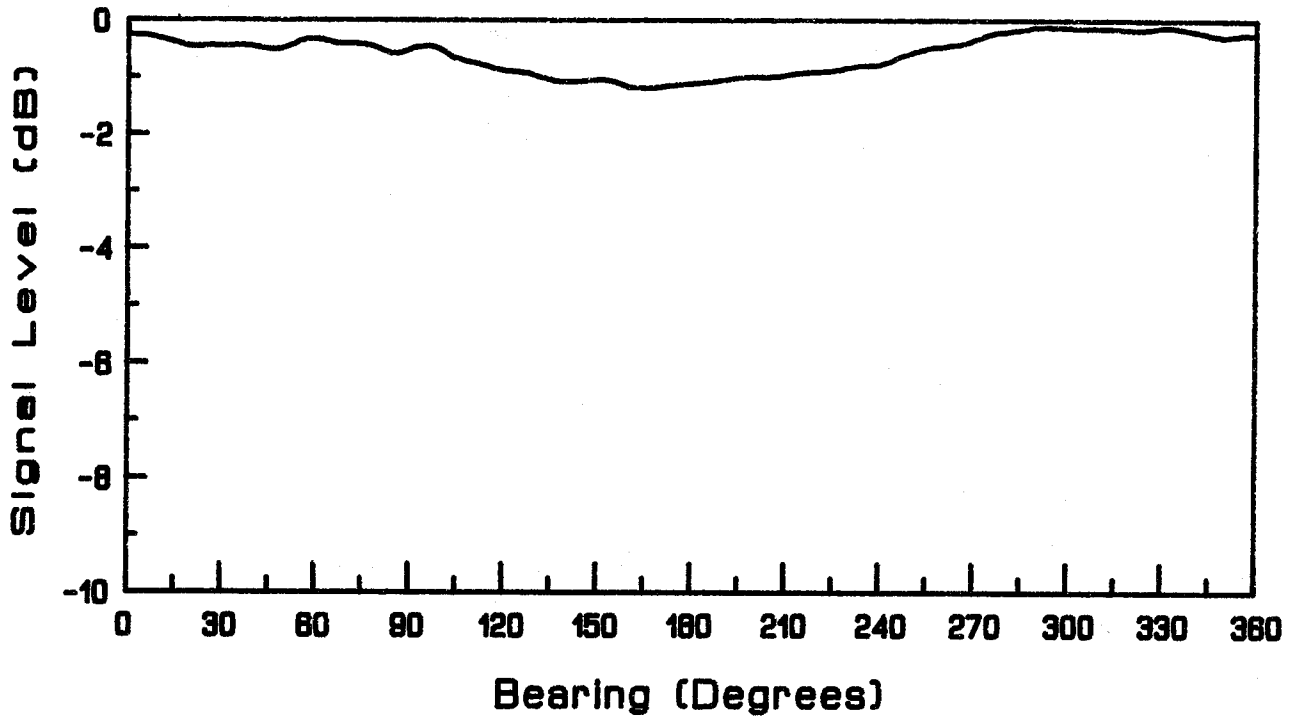


Passive Whip Antenna Pattern At 5.25 MHz

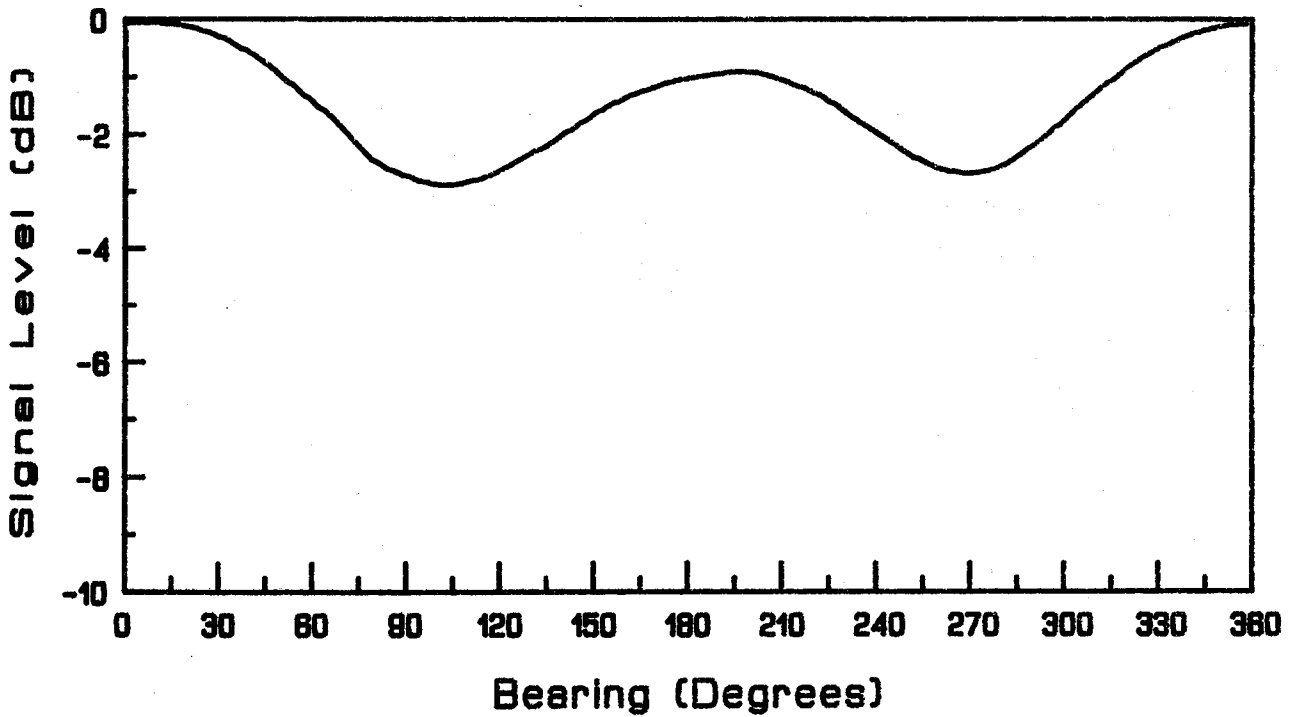


Passive Whip Antenna Pattern At 7.50 MHz

Figure A-9. Pattern measurements of a passive antenna mounted on a van for 5 to 28 MHz.



Passive Whip Antenna Pattern At 11.30 MHz



Passive Whip Antenna Pattern At 28.00 MHz

Figure A-9. (Cont.)

separate the desired signal from the interfering signals, the frequency agility to receive many discrete frequencies in a short time, and measurement of the antenna output voltage at each of the frequencies. The parameters describing the operation of the analyzer, and the resultant measurements were sent to a single board computer that controlled the recording and evaluation of the data. An ASCII terminal provided operator interface to the computer.

APPENDIX B: GROUND CONSTANTS MEASUREMENT

B.1 Introduction

In order to make some immediate assessment of wave-tilt measurements, a manually-operable wave-tilt test fixture was designed and constructed. A limited amount of data were gathered during December 1983 and January 1984 at sites in the large, flat field to the south of the Department of Commerce Radio building in Boulder, Colorado.

The manual measurement fixture employed a rotatable receiver/antenna unit and depended on the system operator to rotate the antenna by hand. In order to assess the receiver's signal level the operator viewed, from a distance, a digital multimeter attached to the receiver's signal strength meter. This was accomplished by means of high power binoculars.

Figure B-1 shows a diagram of the receiver/antenna and rotation assembly (front view). Figure B-2 shows a diagram of the overall test system including the transmitter and receiver systems. A wooden test stand was built to support the receiver/antenna rotation assembly about 2.1 m (7 ft) above the ground and is shown in Figure B-3. A large protractor was attached to the stand and facilitated antenna orientation angle measurements.

Photographs of the actual receiver test system are shown in Figures B-4 through B-8. Except for a few small screws and nails, the test stand and rotation assembly consisted of wood, and other dielectric materials to minimize disruption of the electric field near the receiver system during a wave-tilt measurement.

B.2 Operation

Measurements were made in the IRAC-assigned frequency bands (see Section 2). Because interference from nearby unwanted transmitters could have masked the minimum electric field strength measurement portion of the wave-tilt technique, it was important to find a "quiet" test frequency within each band.

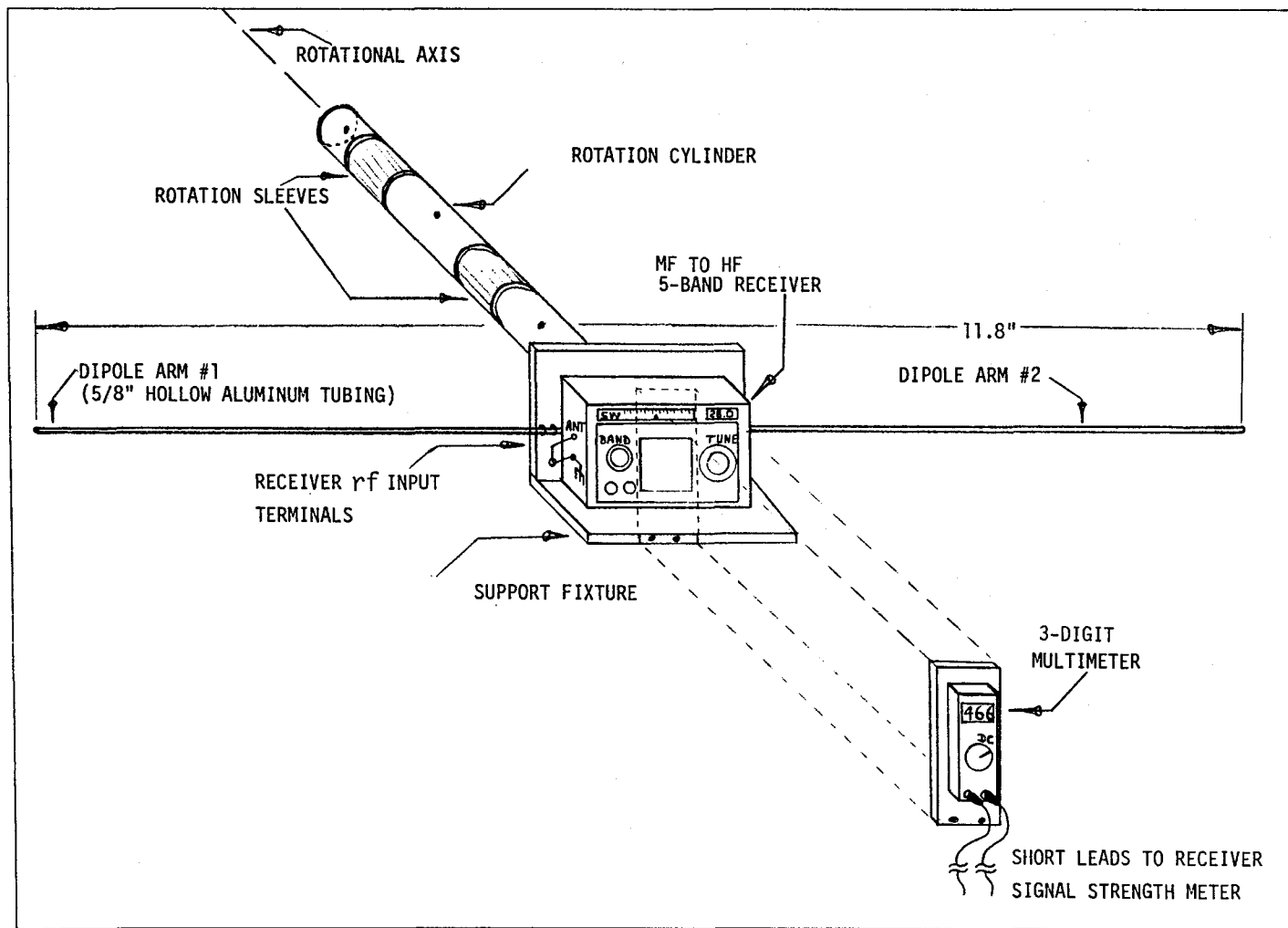


Figure B-1. Receiver/antenna and rotation assembly.

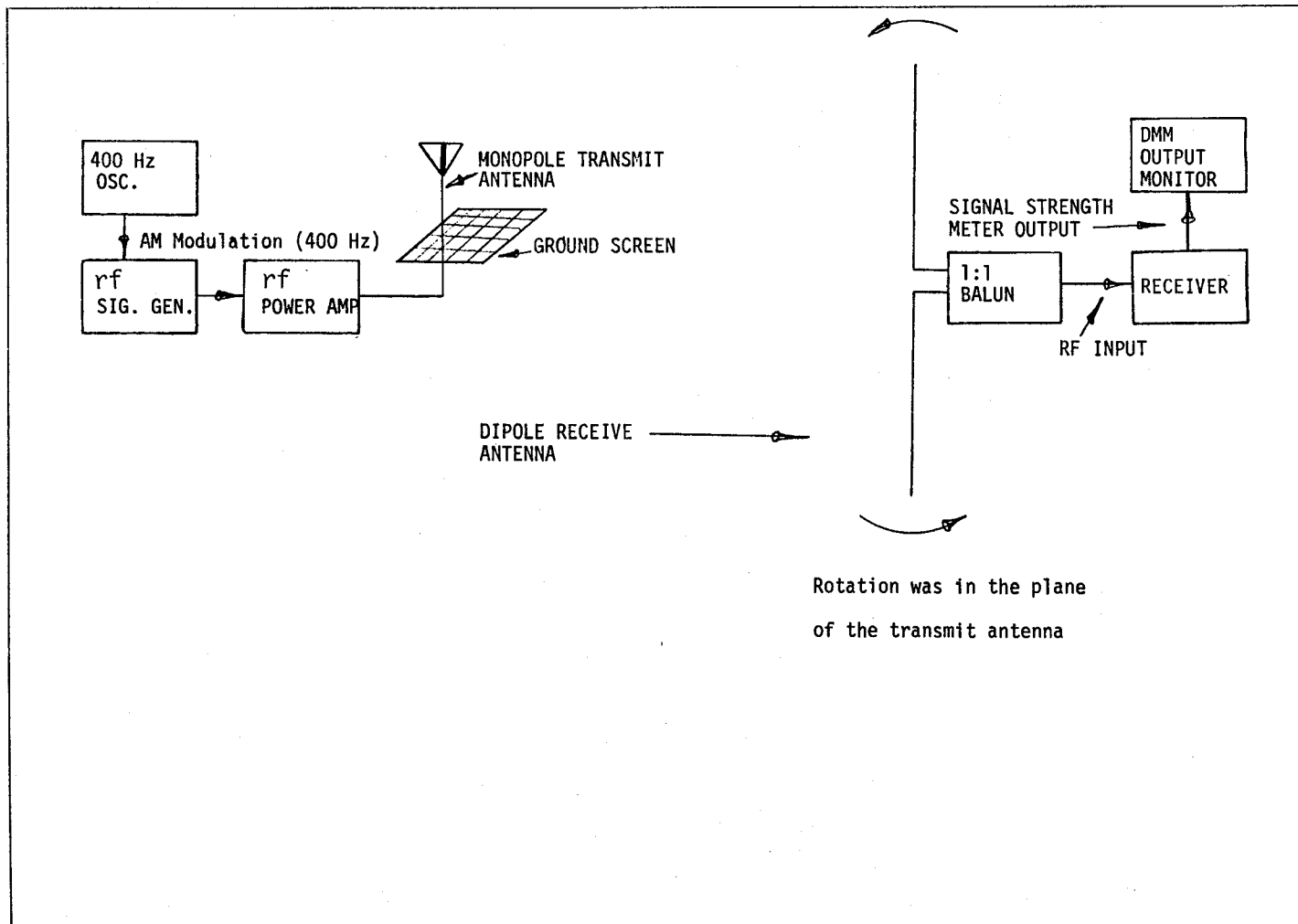


Figure B-2. Overall wave-tilt measurement system.

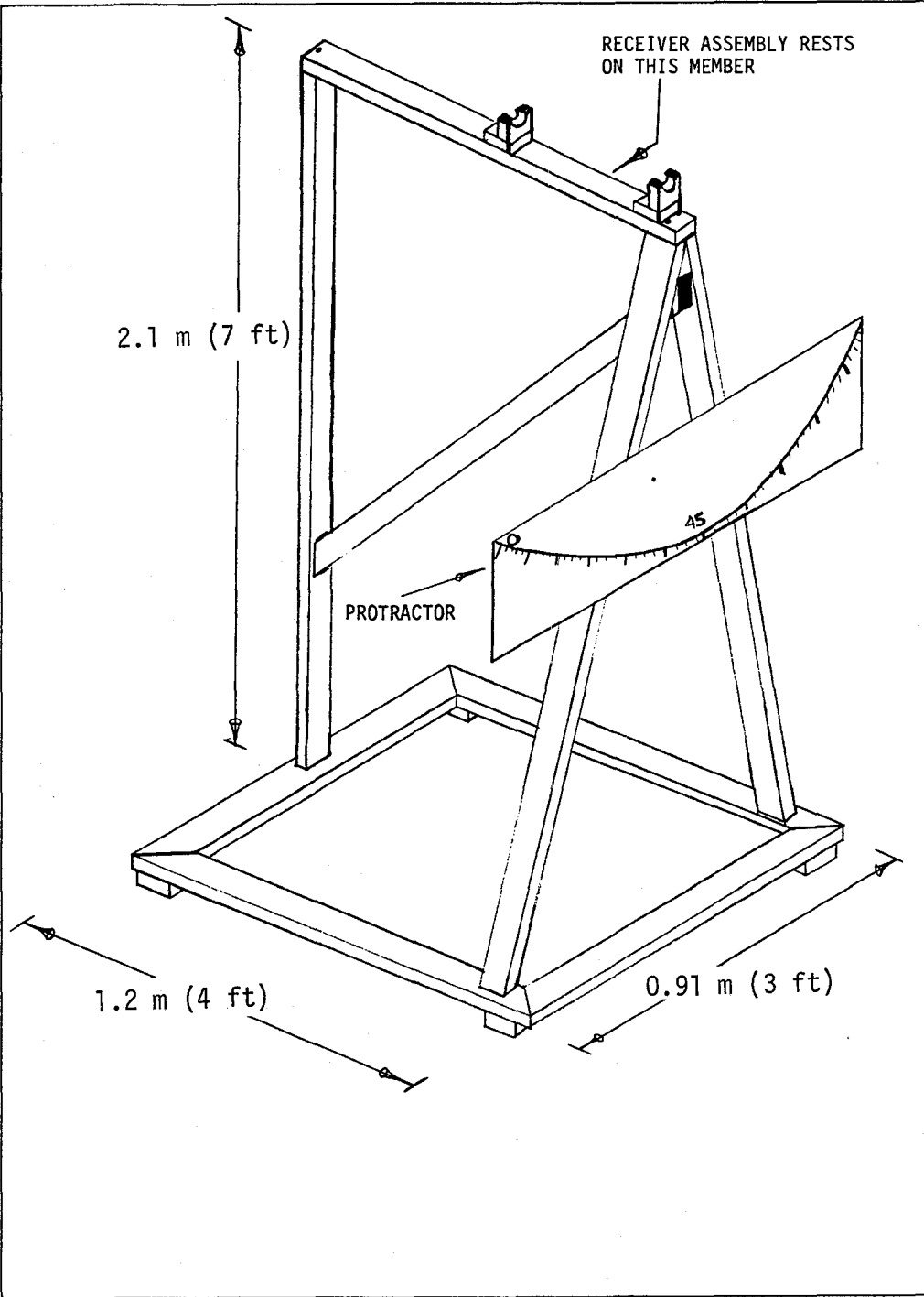


Figure B-3. Receiver test stand.



Figure B-4. Photograph of receiver and digital multimeter.



Figure B-5. Photograph of wave-tilt system--front view with antenna oriented for minimum E-field measurement.



Figure B-6. Photograph of wave-tilt system--front view with antenna oriented for maximum E-field measurement.

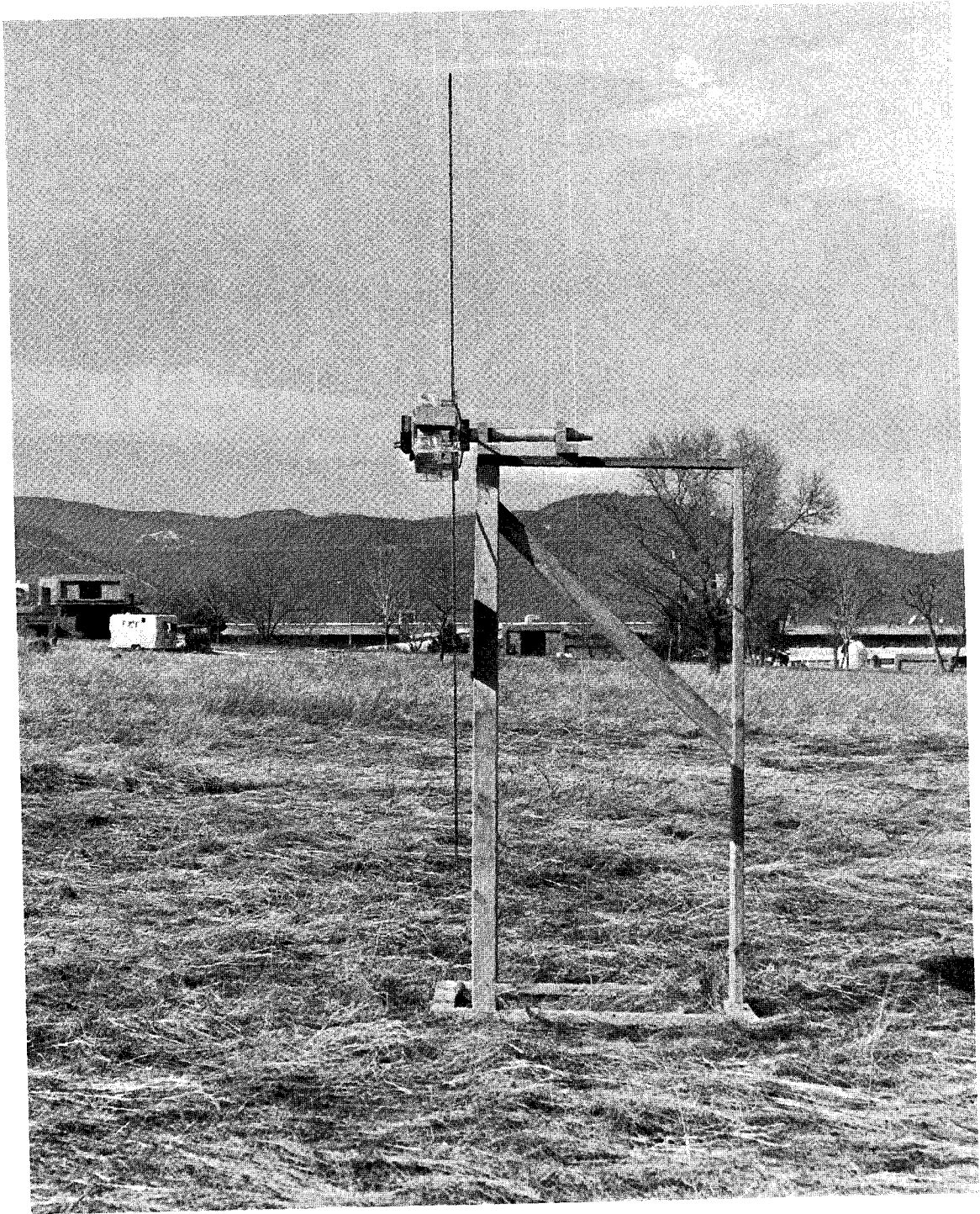


Figure B-7. Photograph of wave-tilt system--side view.

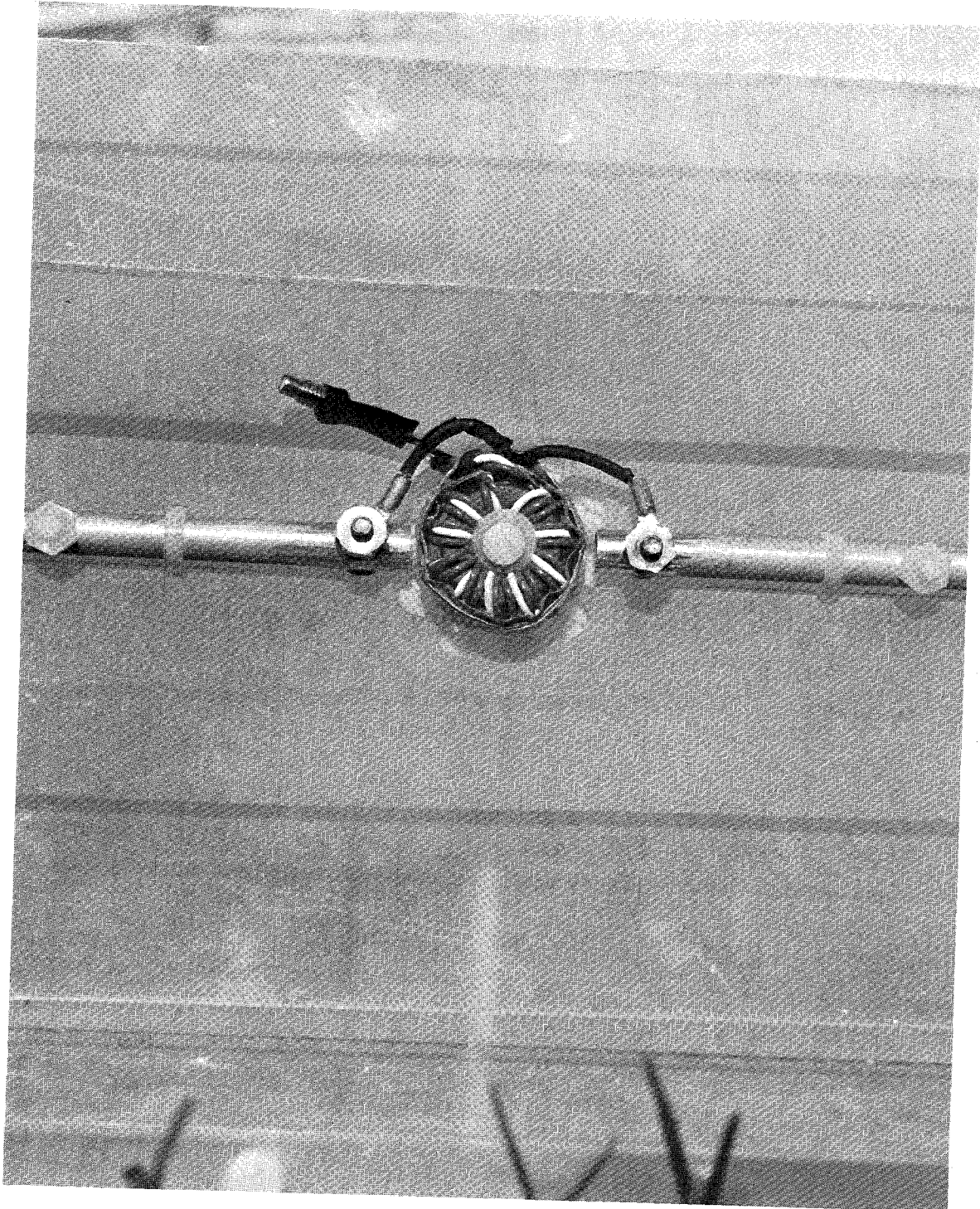


Figure B-8. Photograph of receiver antenna and matching balun.

The test frequencies were determined by operating the receiver with the desired transmitter turned off. The frequencies used were 28, 11.54, 7.5, and 5.25 MHz.

Operation of the receiver/antenna system involved manual rotation of the antenna to locate and record the maximum and minimum electric field strengths (interpreted as a voltage reading from the receiver's signal strength meter) and the antenna tilt angle.

Operation of the transmitter required setting up a desired cw signal frequency, adding some optional reference modulation, and adjusting transmitter power up or down to deliver a signal level compatible with the operating range of the receiver.

B.3 Equipment Description

This wave-tilt measurement technique required the following equipment:

- 1) SIGNAL SOURCE operable over desired test frequencies (3-30 MHz)--modulation capabilities optional.
- 2) RF POWER AMPLIFIER.
- 3) MONOPOLE TRANSMITTER ANTENNA (adjustable height).
- 4) GROUND SCREEN to improve wave launching at transmitter.
- 5) RECEIVER tuneable to desired test frequencies (3-30 MHz).
- 6) DIPOLE RECEIVING ANTENNA, two lengths of 1.6 cm (5/8 in) OD aluminum tubing.
- 7) DIGITAL MULTIMETER with a 0-999 mV scale.

B.3.1 Antenna Design

Weight considerations called for light aluminum tubing as the receiver pickup elements. Hollow tubing with a 1.6 cm (5/8 in) outer diameter (OD) was chosen. Two arms were cut to a length of about 1.8 m (5.9 ft) each corresponding to one-quarter wavelength at about 21 MHz--an intermediate frequency of interest. Because the aluminum tubing was thin, the antenna's bandwidth was not as great as it would have been with "fat" arms considered in the preliminary design described in Appendix C. Hence, exact matching of the antenna to the receiver was not important because relative signal strengths, not absolute, were desired.

Figure B-9 [Jasik (1961)] shows the effects of armlength and outer diameter on the dipole antenna's input impedance. A 3.6 m (11.8 ft) dipole

For the dipole antenna, double the resistance and reactance. "A" equals one-half dipole length; for an antenna with A equal to one wavelength, the antenna length equals 360 degrees. "D" equals the antenna's diameter.

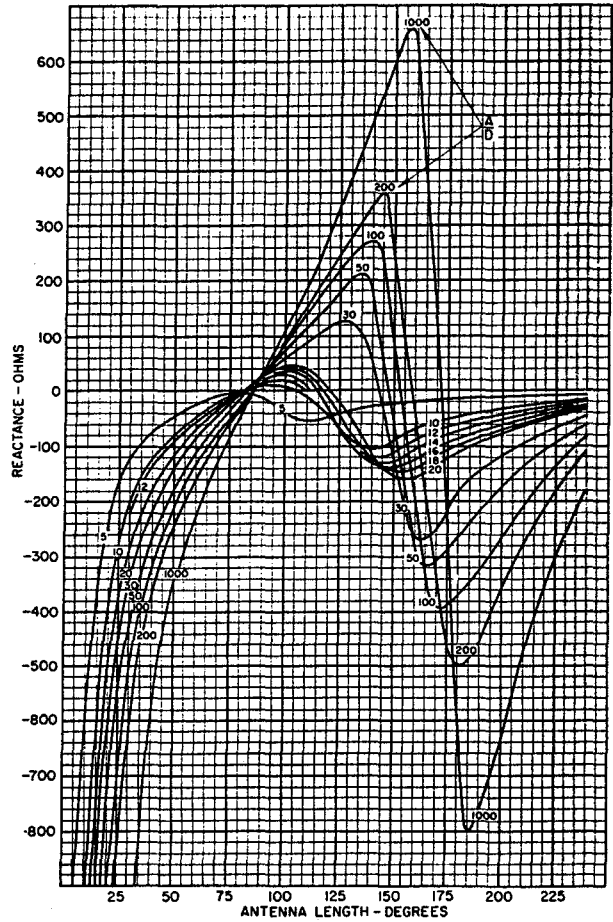
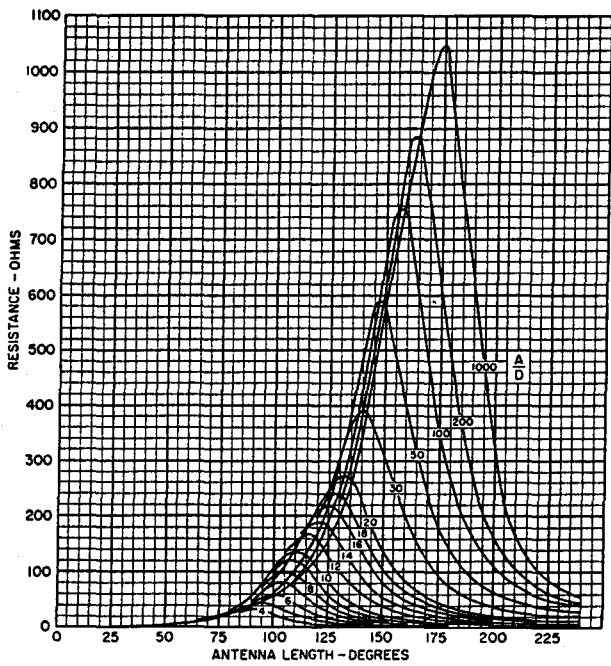


Figure B-9. Antenna resistance and reactance for a monopole above a ground plane [reprinted with permission from the Antenna Engineering Handbook, Jasik, H., Figures 3-3 and 3-4, McGraw-Hill Book Company (1961)].

with 1.6 cm (5/8 in) OD has an A/D ratio of 113. At 28 MHz the antenna length is 60.4 deg; thus, the expected impedance is about $4-j270$ ohms. At 5.25 MHz the impedance becomes about $1-j2700$ ohms.

Because the receiver input was unbalanced, a 1:1 balun (American Radio Relay League, 1969) was placed between the balanced dipole and the receiver rf input terminals as shown in Figures B-10 and B-11.

During measurements the dipole was rotated in a vertical plane containing the transmitter and receiver antennas. Slight friction in the rotation assembly kept the antenna orientation stationary during the measurement process.

B.3.2 Receiver Design

The receiver was a multiband shortwave type with three shortwave bands, 3.9 to 10 MHz, 11.5 to 20 MHz, and 20 to 28 MHz. The receiver had a usable dynamic range of about 44 dB if both the low and high AM sensitivities of the unit were employed. Experience showed best results were obtained in the field if the receiver was left in the high or low sensitivity mode and transmitter power altered to deliver a signal level compatible with the operating range of the receiver. When the AM sensitivity switch was untouched, usable dynamic range was reduced to about 24 dB. Wave-tilt measurements were made at 28, 11.54, 7.5, and 5.25 MHz. These frequencies were found to have minimal amounts of interference from other sources. This insured measurement of the transmitted signal and not interference, especially during measurement of the minimum signal level.

Signal strength at the receiver was interpreted as the voltage measured across the receiver's own signal strength meter. By calibrating the receiver with a known input signal level and recording how the signal strength meter responded, we could interpolate the actual input signal levels to the receiver during the wave-tilt measurement. Figure B-12 shows a block diagram of the receiver and the monitoring points at the receiver's signal strength meter (called out as "A" and "B" on the diagram). Figures B-13 through B-16 show the receiver calibration results for the test frequencies 28, 11.54, 7.5 and 5.25 MHz, respectively.

The telescopic antenna included with the receiver was removed and the receiver was wrapped with a layer of aluminum foil in an attempt to minimize undesired signal pickup by receiver electronics.

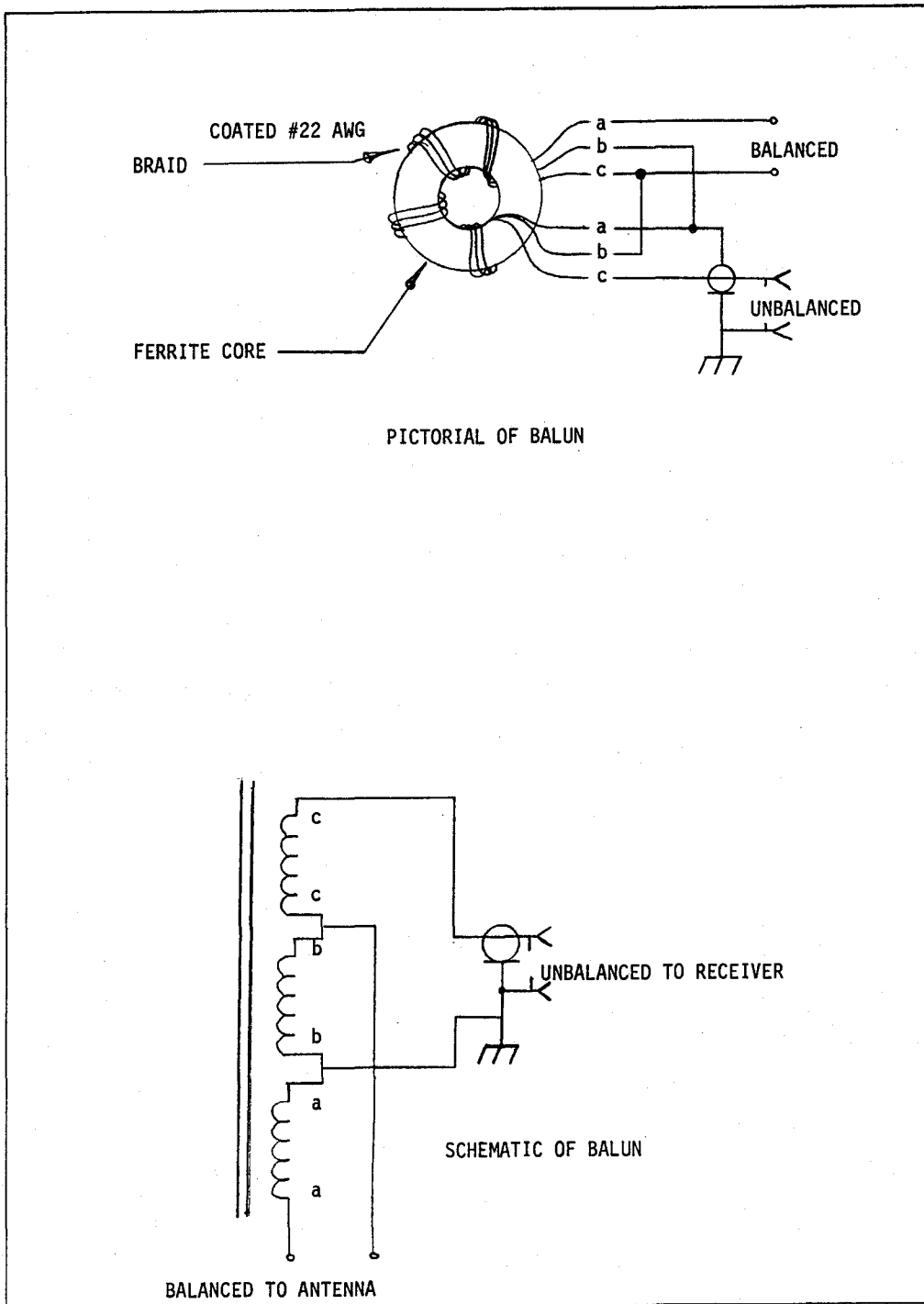


Figure B-10. Receiver antenna matching balun [reprinted with permission from the Radio Amateur's Handbook, Figure 13-11C, ARRL (1969)].

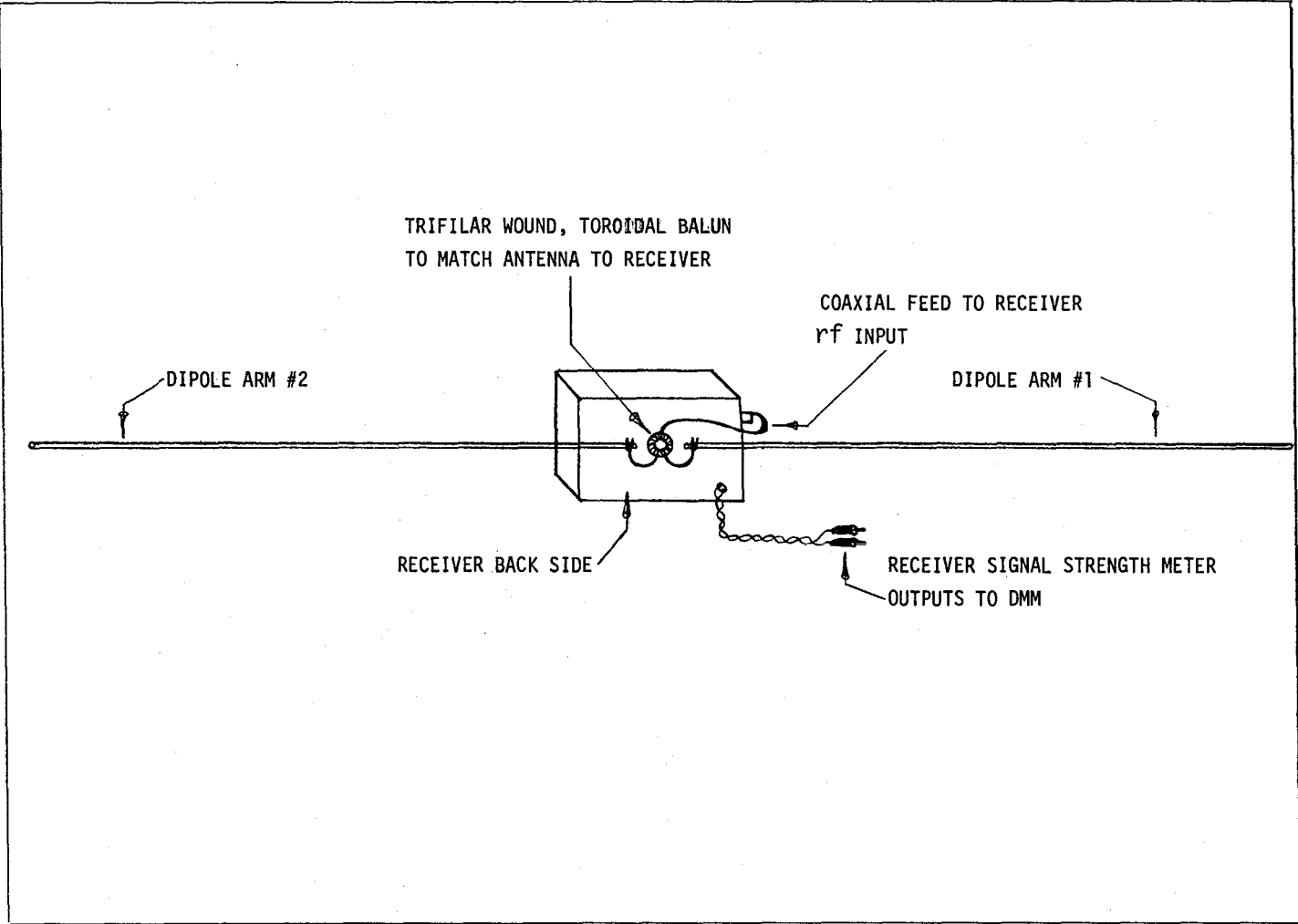


Figure B-11. Receiver antenna and matching balun.

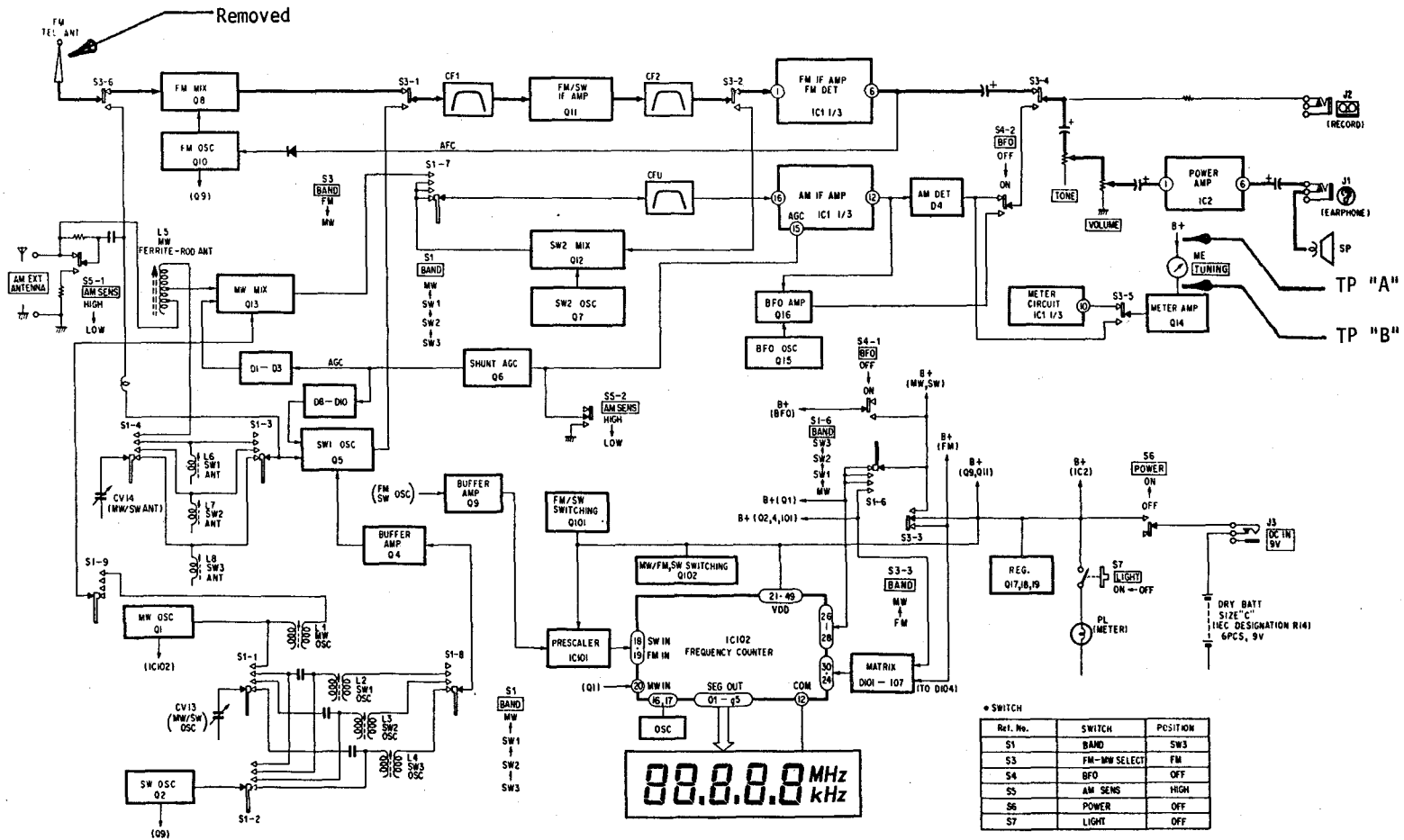


Figure B-12. Receiver block diagram [reprinted with permission from the Sony Corporation, Audio Group, Park Ridge, NJ (1982)].

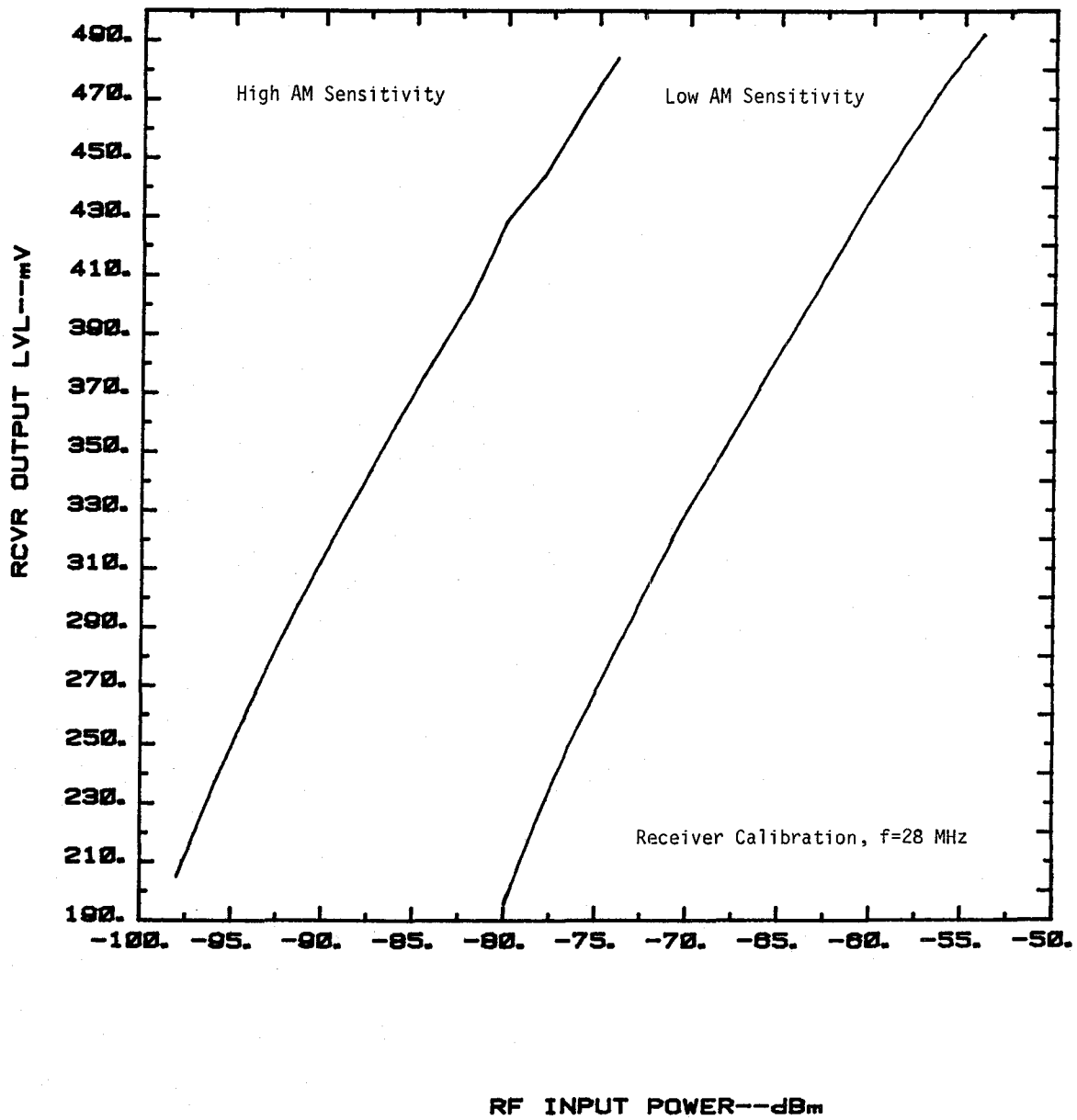


Figure B-13. Receiver calibration curve for 28 MHz.

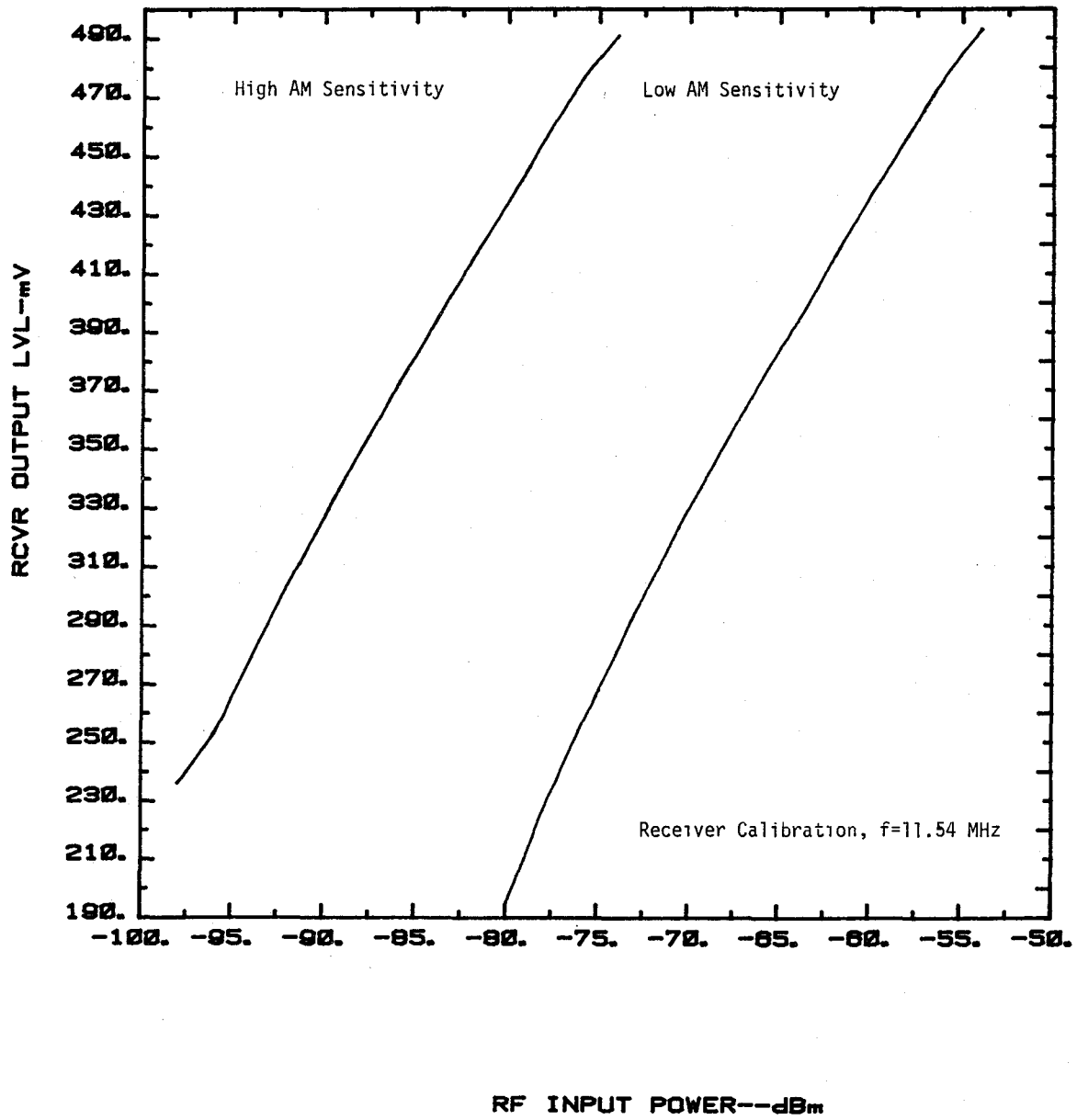


Figure B-14. Receiver calibration curve for 11.54 MHz.

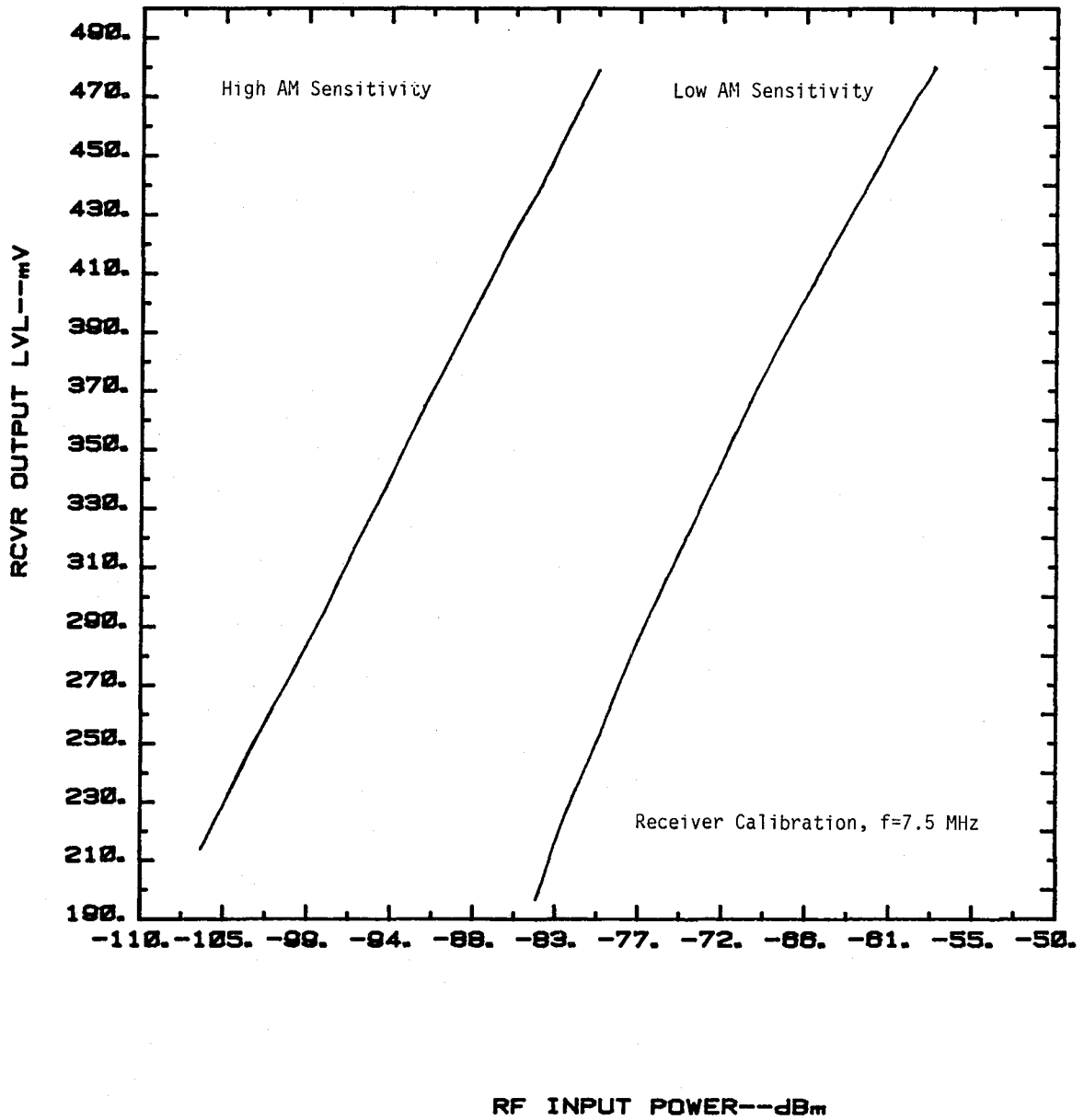


Figure B-15. Receiver calibration curve for 7.5 MHz.

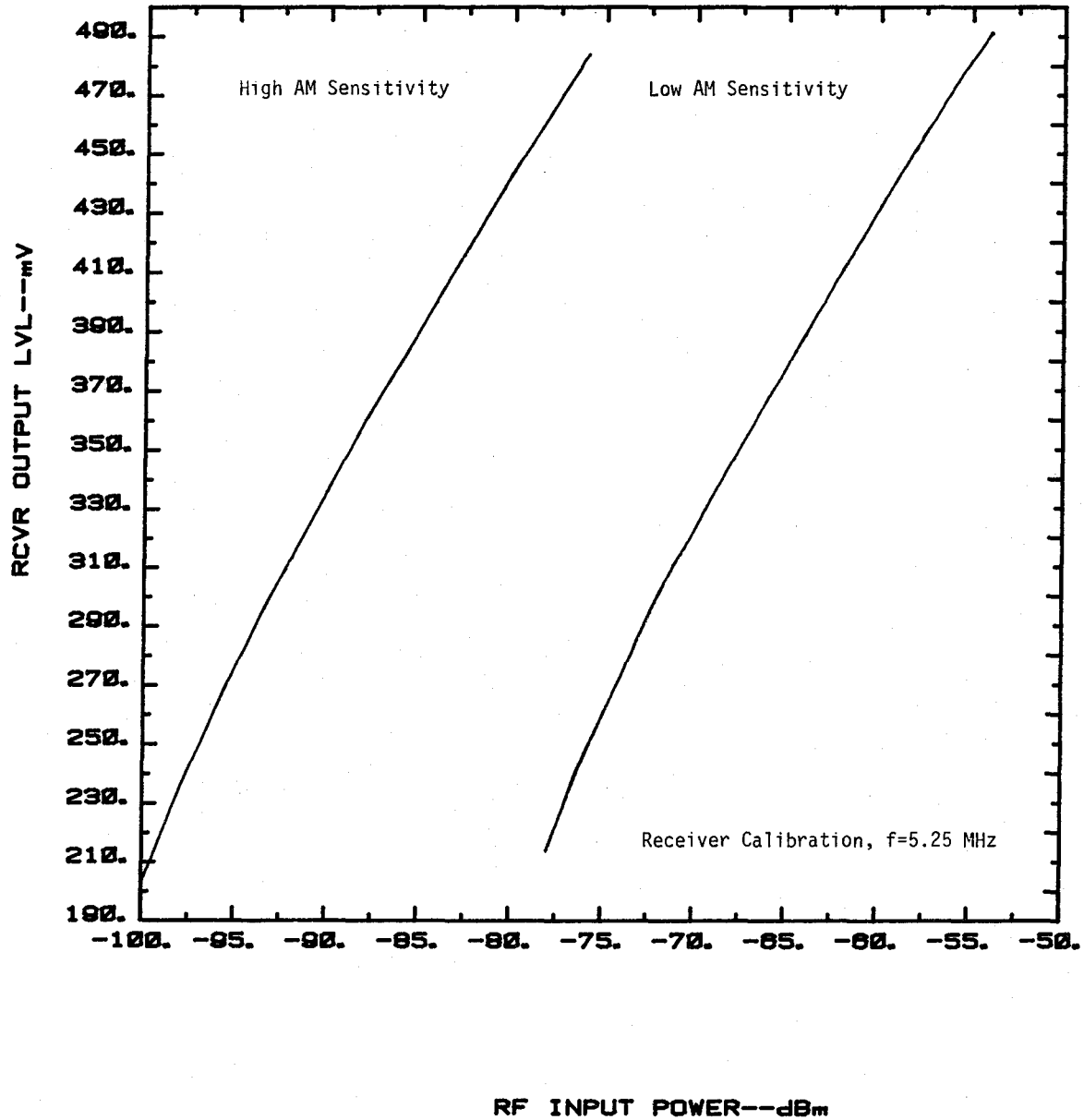


Figure B-16. Receiver calibration curve for 5.25 MHz.

B.3.3 Transmitter and Transmitter Antenna

The transmitter consisted of an rf signal source driving an rf amplifier. External AM modulation was provided by a 400 Hz oscillator to help tune the receiver to the desired frequency. The amplified rf was fed to a vertical monopole resting on a wire mesh ground screen. The monopole was adjusted in height to be about a quarter-wavelength at 28 MHz. The rf source had fixed attenuation steps of 10 dB which were used to produce power levels appropriate for good reception at the receiver site. A photograph of the transmitter antenna is shown in Figure B-17.

B.3.4 Power Supplies

The receiver required 9 V dc provided by six size "C" batteries and the DMM (digital multimeter) required 9 V dc provided by one transistor battery.

B.4 Measurement Process

The reader is referred to Eaton (1976) for background on the wave-tilt measurement technique and theory.

During a typical wave-tilt measurement the receiver dipole antenna was rotated in small increments (about 0.5 deg) in the plane containing the receiver and transmitter antennas. This was continued until the minimum voltage level (within receiver's operating range) was read on the digital multi-meter (DMM). It was assumed that the dipole antenna was now aligned with the minor axis of the electric field ellipse. Observations of the DMM were taken about 15 m (50 ft) away from the receiver and were made with the observer crouched low to the ground to minimize disturbances to the local electric field. Note that the transmitter power level was adjusted to permit operation of the receiver in its calibrated metering range.

Typically the antenna orientation was between 75 and 85 deg away from the normal to the local terrain when the minimum was located. All antenna angle measurements were made relative to the normal of the surface terrain beneath the receiver, not the gravitational vertical. When the wooden blocks on the antenna support frame all rested firmly on the ground, the 45 deg mark on the protractor could be taken as the normal to the local surface terrain. Hence, tilt angles were measured directly from the protractor scale by noting the angle of the dipole arm on the protractor relative to the 45 deg mark.



Figure B-17. Photograph of transmitter antenna in open field to the south of the Department of Commerce Radio Building in Boulder, CO.

Experience showed the minimum field orientation to be quite well defined and easy to locate. Conscientiousness in measuring yielded half a degree of accuracy in locating the minimum, albeit it was a time-consuming process without a stepper motor.

Once the minimum voltage was ascertained and the antenna orientation angle recorded, the antenna was rotated 90 deg and the maximum voltage level was noted from the distant viewing location. It was assumed that the dipole was now aligned with the major axis of the electric field ellipse. The tilt angle of the dipole was recorded, and all measurements were repeated with the dipole rotated through 180 degrees in order to eliminate certain instrumentation errors. To read the maximum voltage level, it was frequently necessary to reduce the transmitter level by some known amount, say 20 dB from that used for measuring the minimum voltage level, in order that the receiver continued to operate in the calibrated meter range.

Experience showed the maximum field orientation was rather undefined. Hence, if the receiver was within about 2 deg of the true maximum, an accurate signal strength value was ascertainable. An accurate 90 deg rotation from the signal strength minimum was required to measure tilt angles, though.

The equations used to make the ground constant calculations are discussed in Section 6 and rely on some important conditions being met:

- 1) The wave-tilt method should not be used just after a change in the composition of the terrain, i.e., after a sudden change in permittivity and conductivity as at a coastline (Eaton, 1976).
- 2) The ground in the vicinity of the test area should be flat and homogeneous (Eaton, 1976).
- 3) There should be no local obstacles (such as trees, buildings, or other obstructions) to cause disturbance to the measured field (Eaton, 1976).
- 4) It is advisable to make receiver measurements at distances large compared to the antenna dimensions at high frequencies (CCIR, 1982; Gething et al., 1965).

The following is a sample calculation of ϵ_r and σ from measured wave-tilt data:

At 28 MHz one field site yielded a tilt angle, θ , of 15 deg (relative to the terrain normal), a minimum DMM voltage of 335 mV (high AM sensitivity), and a maximum DMM voltage of 384 mV (high AM sensitivity). Transmitter power was reduced 30 dB to make the maximum voltage measurement. From Figure B-9, 335 mV refers to a power level of -87.25 dBm and 384 mV refers to a power

level of -83.25 dBm. Hence, P_{\min} was -87.25 dBm and P_{\max} was -83.25 dBm + 30 dB = -53.25 dBm. To obtain r , which is the ratio of the electric field strengths, E_{\max} and E_{\min} , the ratio of the square roots of the power levels, P_{\min} and P_{\max} , (converted to watts) was taken. The value of r then was 0.019.

With r and θ known, formulas 1 and 2 from Section 6 were used to arrive at $\epsilon_r = 13.7$ and $\sigma = 3.2$ mS/m.

To assess measurement errors associated with the wave-tilt method consider the rectangle of uncertainty labeled "U" superimposed on Figure 47. The rectangle applies to the data point discussed in the example above where the tilt angle, θ , was 15 degrees and the axial ratio, r , was 0.019. In practice voltages leading to the axial ratio were easily read to within ± 1.5 mV and tilt angles to within ± 1.0 degrees. These uncertainties lead to a rectangle of uncertainty with a length of 2 degrees and a width of 0.003. The rectangle indicates the spread of uncertainty in the stated values of relative permittivity and conductivity.

B.5 References

- American Radio Relay League (1969), Loads and Balancing Devices, The Radio Amateur's Handbook, Edition 46, pp. 349-351.
- CCIR (1982), Electrical characteristics of the surface of the earth, Recommendation 527-1, Propagation in Non-Ionized Media, Vol. V, CCIR XVth Plenary Assembly, Geneva.
- Eaton, J. L. (1976), The Wave-tilt Method of Measuring Electrical Ground Constants in the L.F. and M.F. Bands, BBC Research Department Technical Report BBC-RD-1976/15, June.
- Gething, P. J. D., A. D. Morgan, E. G. Shepherd, and D. V. Tibble (1965), Wave-tilt measurements of ground properties, Electronics Letters, No. 1, June, pp. 106-107.
- Jasik, H. (1961), Antenna Engineering Handbook, First Edition (McGraw-Hill Book Co., Inc., New York, NY), Chapter 3.
- Sony Corporation (1982), Audio Group, Service Manual No. 9-950-846-11, pp. 5-6.

APPENDIX C: AUTOMATED GROUND CONSTANTS MEASUREMENT INSTRUMENTATION

C.1 Introduction

This appendix describes elements of the wave-tilt measurement system originally proposed for automated ground constant determinations. The system is a more ambitious version of the manual fixture described in Appendix B and includes computer control along with improvements to system bandwidth. While this system was never fully implemented, the description is provided for future reference.

Operation of the receiver antenna unit still includes tilting the antenna and measuring and recording the minimum and maximum field strengths as well as the tilt angle. This data is carried via optical fiber to a nearby computer for processing. The receiver antenna is mounted atop a support stand with a shaft through the antenna mount to allow for rotation. All circuitry, including the receiver, and power supplies are contained inside the hollow dipole receiver antenna. The antenna support and receiver antenna are on a trailer bed attached to a van containing the processing equipment. A stepper motor and controller located at the trailer base is used to rotate the antenna. Additional gearing is used between the stepper motor and the antenna to provide a smaller step angle for measurement purposes. This will be discussed in detail in a later section.

A basic, overall diagram of the receiver unit is shown in Figure C-1. Note the trailer, wheels, axle, etc., are nonmetallic to avoid disturbing the fields. A fiber optic link is used to direct the controller of the stepper motor which in turn allows the motor to rotate the antenna. A set of gears and pulley is located between the stepper motor and the antenna to provide gear reduction. This way, a particular step of the motor creates a proportionally smaller step of the antenna.

The circuitry used to accept and transport the data from the antenna is located in a hollow compartment at the center of the antenna. The circuitry includes a receiver, an A/D converter, a sequential logic unit, a clock, and a universal asynchronous receiver/transmitter chip (UART). Data then is converted into light pulses using an RS-232 compatible optical fiber link. Pulses sent from the computer, via optical fiber to the circuitry, signal the converter when to take measurements. Each part of the receiver unit will be discussed in more detail in the following sections.

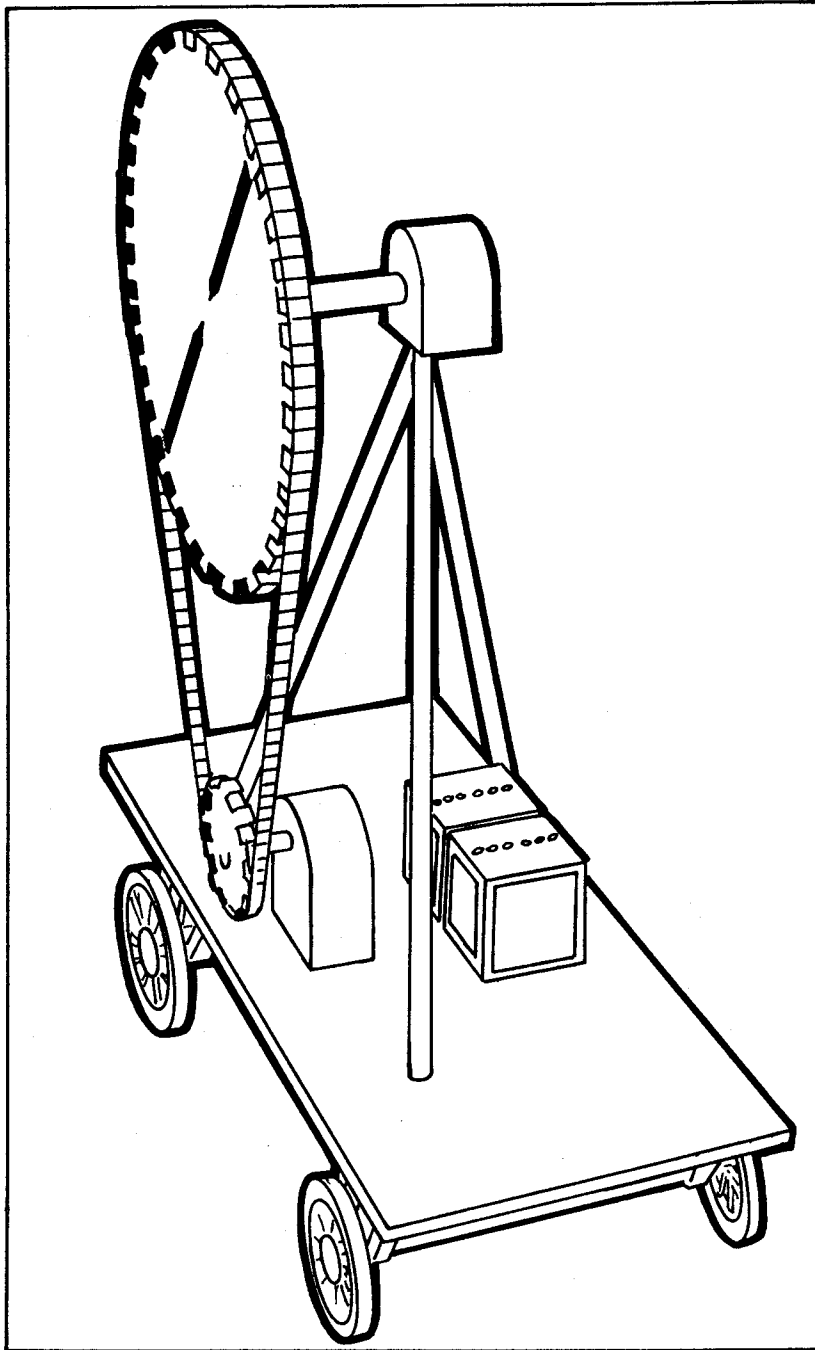


Figure C-1. Diagram of automated receiver for wave-tilt measurements.

C.2 Antenna Design

The receiver antenna consists of a 2.44 m (8 ft) cylindrical dipole antenna. A sketch of the antenna mounted on its gear assembly is shown in Figure C-2. Ideally the antenna would be an isolated antenna in space over the ground whose ground constants are to be measured by the wave-tilt technique. This means there should be no transmission lines, electronics, power cables, or data cables leading up to the antenna. The reason for this requirement is that these external components influence the fields the antenna is attempting to measure. To approach the ideal system, the receiver, the analog-to-digital converter, the fiber optics components, and their associated power supply batteries are all housed inside of the antenna at its center. The only cable that is external to the antenna is the fiber optic cable, which is nonmetallic. The fiber optics are used to communicate with the antenna from the on-site computer.

The circuitry housing as well as the dipole arms are made of aluminum. By making the arms "fat," the antenna's bandwidth is increased over that of the thin antenna described in Appendix B. The dipole is 2.44 m (8 ft) in length, which at 30 MHz is one-quarter wavelength. The arms are made of 5 cm (2 in) OD tubing. Figure B-9 shows the effect on the dipole antenna's input impedance when the antenna length to diameter ratio and the wavelength are varied. A 2.44 m (8 ft) dipole with a diameter of 5 cm (2 in) has an A/D ratio of 24. At 30 MHz, the antenna length is 45 deg; thus the expected input impedance is $2-j280$ ohms. At 3 MHz, the impedance becomes $1-j3000$ ohms.

The biconical antenna offers several advantages over the dipole (see Figure C-3 for a sketch of the biconical antenna). It has a broader bandwidth than the dipole and it offers more room inside the antenna for the associated electronics. Figure C-4 shows the experimental data for biconical antenna input impedance versus antenna shape and wavelength. For the biconical dipole shown in Figure C-3, the input impedance is $40-j40$ ohms at 30 MHz; a definite improvement over the dipole. At 3 MHz, the impedance becomes $2-j600$ ohms.

If an unbalanced transmission line is used between the antenna terminals and the receiver's input terminals, then a balun is required to match or balance the currents on the dipole's two arms. With the receiver inside of the dipole, the two arms are connected by a balanced transmission line directly to the receiver's input.

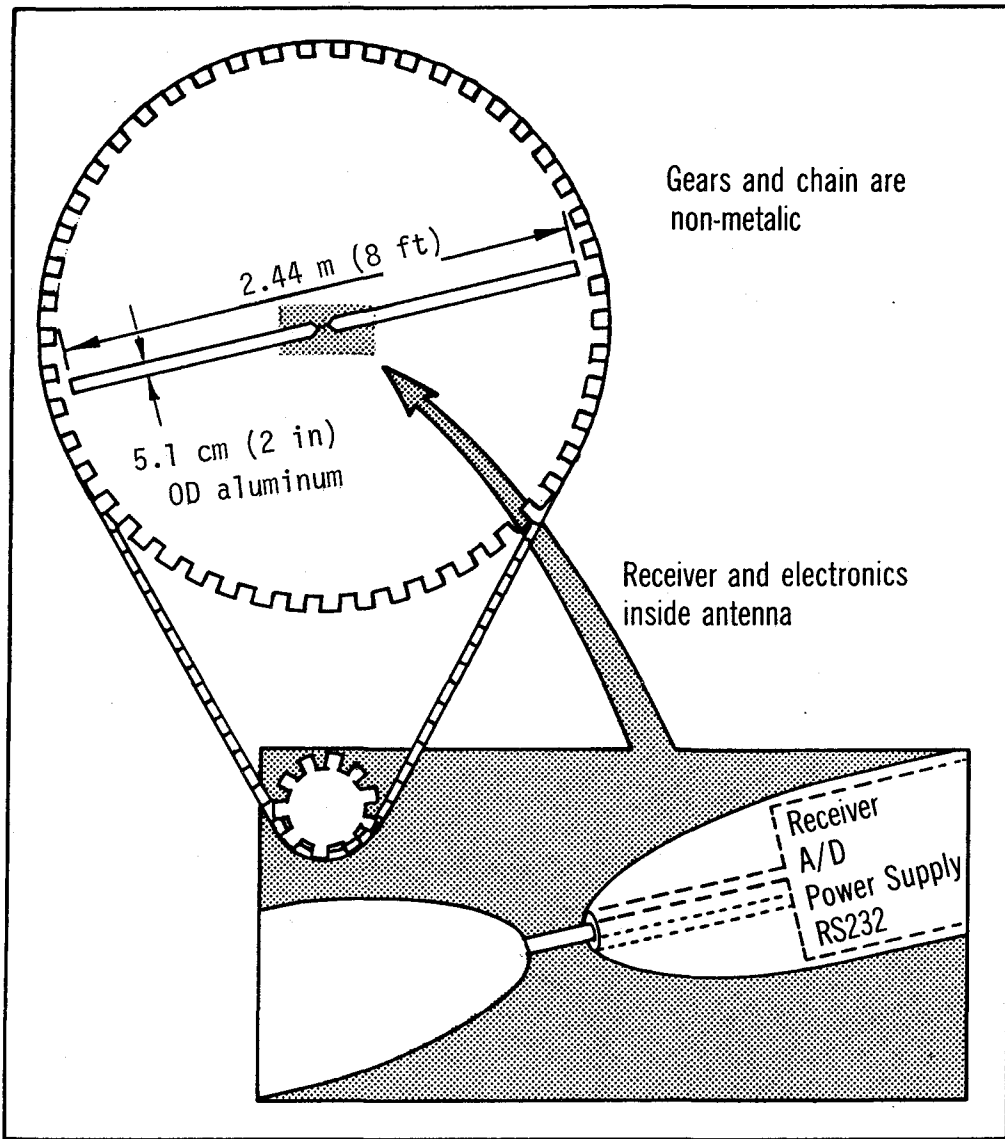


Figure C-2. Cylindrical dipole receiver antenna mounted on gear assembly.

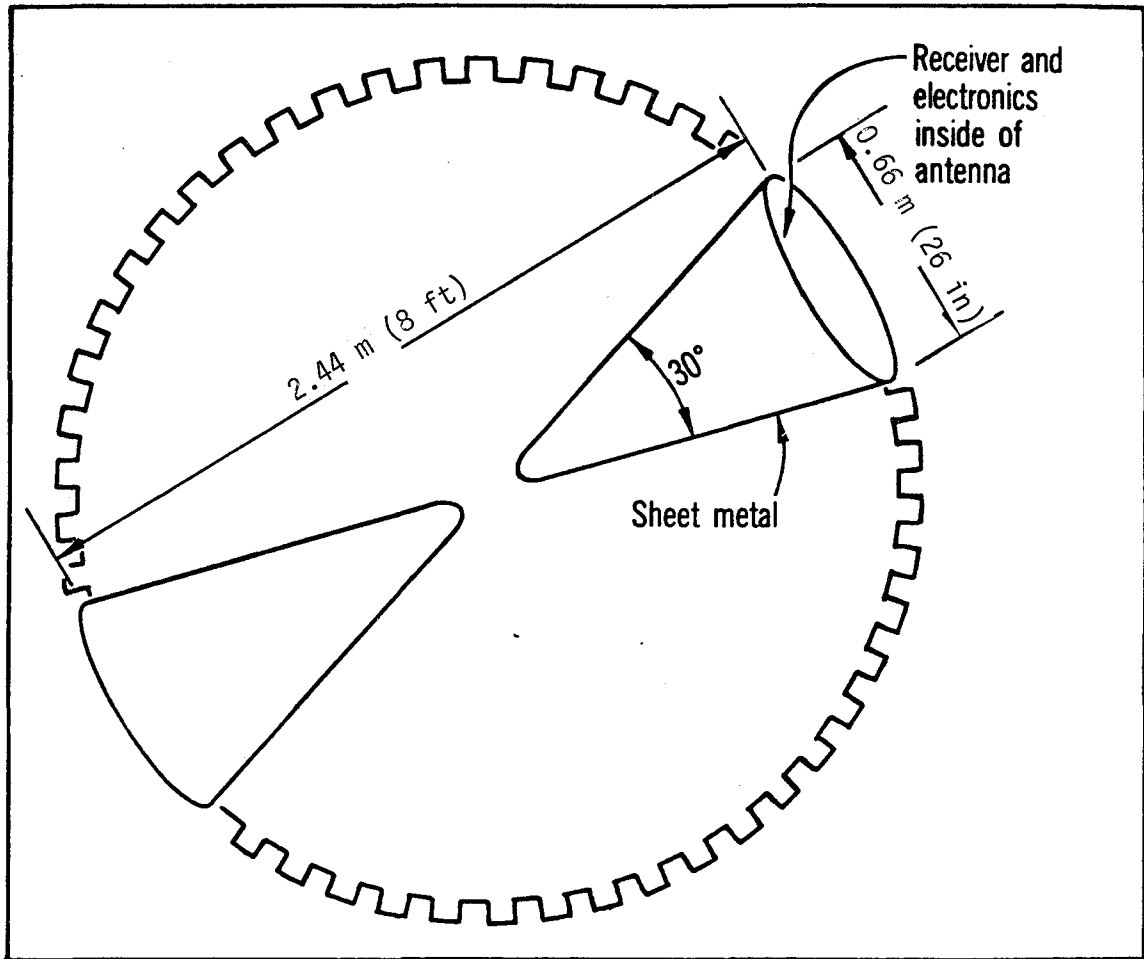
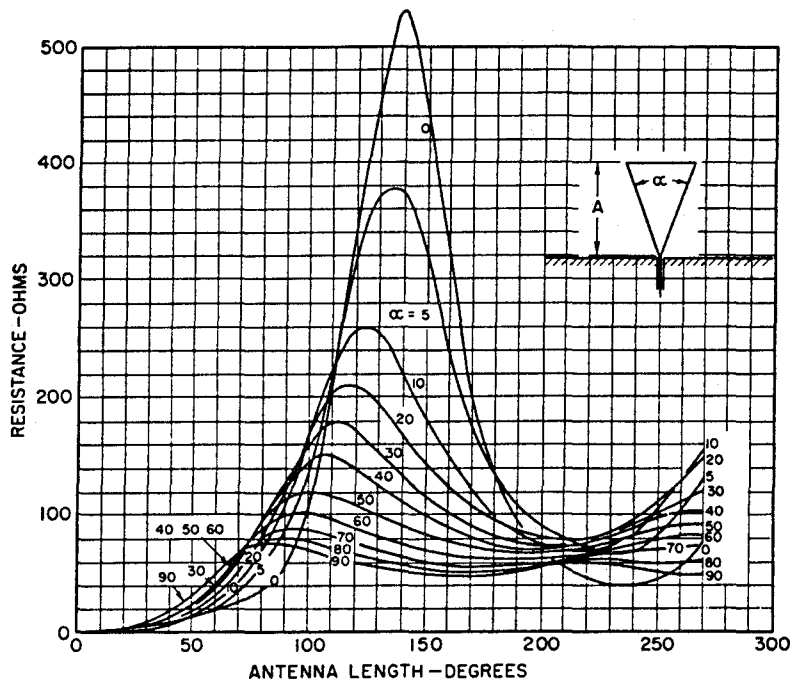
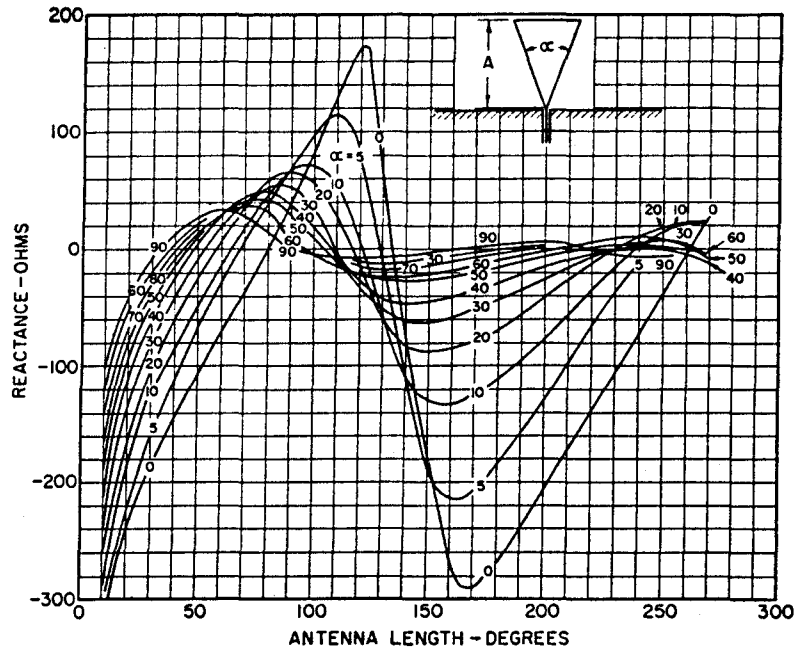


Figure C-3. Biconical dipole receiver antenna mounted on gear assembly.



For a biconical dipole antenna, double the resistance and reactance.

Figure C-4. Antenna resistance and reactance for a conical monopole above a ground plane [reprinted with permission from the Antenna Engineering Handbook, Jasik, H., Figures 3-13, McGraw-Hill Book Company (1961)].

C.3 Receiver Design

The receiver is as described in Appendix B, Section B.3.2, with one exception: it has a usable dynamic range of at least 60 dB. This insures the ability to measure the difference between the maximum and minimum received signal strength as the dipole is rotated during the wave-tilt measurement. Transmitter output level remains constant at all times.

C.4 Analog-to-Digital Conversion

The analog voltage from the receiver's signal strength meter is converted to a digital signal and sent to the on-site computer for processing. The analog-to-digital (A/D) circuit uses a 12 bit analog-to-digital converter chip to perform the conversion. The 12 bits are read as two 8-bit words. The first word consists of the four least significant bits of the 12-bit value followed by four 0's. The second word contains the eight most significant bits of the 12-bit value. The two data words are then converted to serial format by a universal asynchronous receiver/transmitter (UART) chip. The output of the UART is made RS-232 compatible with a voltage level shifter chip.

The circuit block diagram is shown in Figure C-5. The control signals for the A/D conversion and UART are generated by a sequential circuit. The first of these is the line CD. The sequential circuit will halt in its present state (of eight possible states) whenever the CD line goes low. This feature is used to start the sequential circuit in a known state when the power is first turned on. The circuit remains in this condition until it is triggered by the rising edge of a pulse from the external input. To control pulse widths, the rising edge triggers a one-shot circuit that produces a 25 μ s pulse. This pulse initiates the A/D conversion process. When the conversion is complete, a pulse STS is generated. This signal is used to bring the CD line high, after which the sequential circuit executes the transfer through its states. The other input signal is TRE, which is the transmitting holding resistor empty signal. The UART will bring this line low when it is in the process of transmitting a word. The sequential circuit monitors this line and if it sees the line go low, it will halt in one of two states to allow the UART to finish transmitting before the next word is loaded into the transmitting holding register. Thus, the speed of the circuit is limited only by the rates at which the UART can transmit data. The maximum

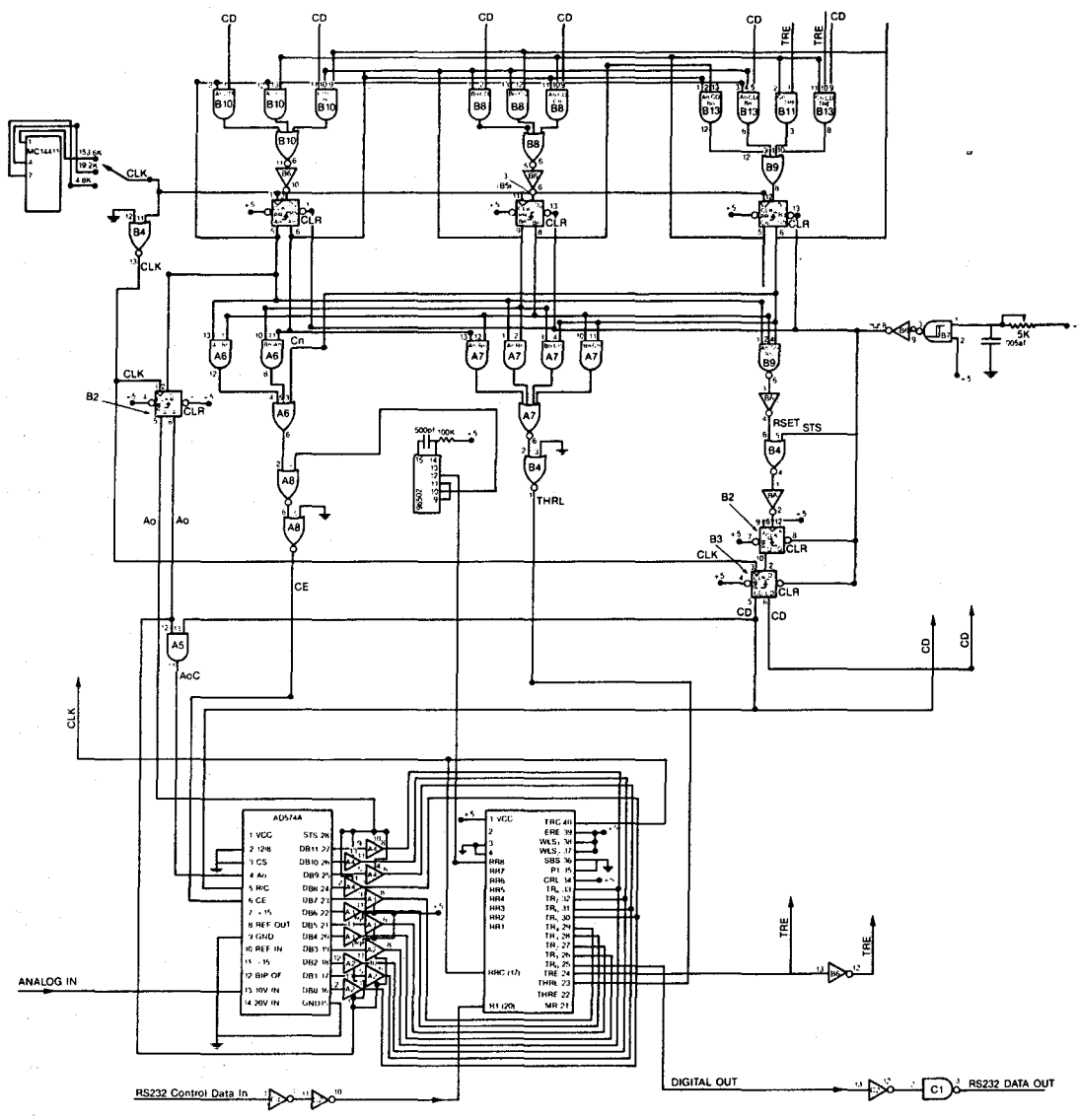


Figure C-5. Analog-to-Digital converter block diagram.

clock frequency the UART can tolerate is 800 KHz. The sequential circuit and the UART use the same clock.

C.5 Fiber Optic Link

To avoid metallic signal-carrying lines near the antenna, a non-metallic fiber optic line is used to carry the digitized signal-strength data to the on-site computer. The fiber optic link consists of two RS-232 signal level-to-optical converters along with a fiber optic cable as shown in Figure C-6. One unit will be located at the computer and the other at the antenna. An outdoor 50 micron four-fiber cable is used for transmission between the two connectors.

Digital signal strength data are at RS-232 voltage levels upon first entering the fiber optic system and are then converted to light pulses. The light pulses are transmitted on the cable and converted back to RS-232 voltage levels at the computer end. The fiber optic system allows full duplex operation. After a command to convert signal strength data is sent by the computer to the receiver over the fiber optic cable, the receiver performs the conversion and immediately puts the data on the cable for processing by the computer.

A second fiber optic system is used to send commands from the computer to the stepper motor controller.

C.6 Power Supplies

The multiband receiver requires 9 V dc, the fiber optic system requires 12 V dc, and the IC circuitry requires +15 V dc and -15 V dc. The batteries are housed inside the aluminum center of the antenna. The stepper motor and its controller require a 24 V dc, 6 A supply. This can be a rechargeable battery pack that sits next to the controller.

C.7 Antenna Rotation Control

The rotation and positioning of the antenna is under computer control and is accomplished by using a stepper motor and controller. The controller receives commands from the computer via a fiber optic cable. The goal is to locate the dipole starting in a horizontal position to begin the measurements. Then in half-degree increments the dipole is rotated through 360 deg while the computer records the received signal at each increment. The

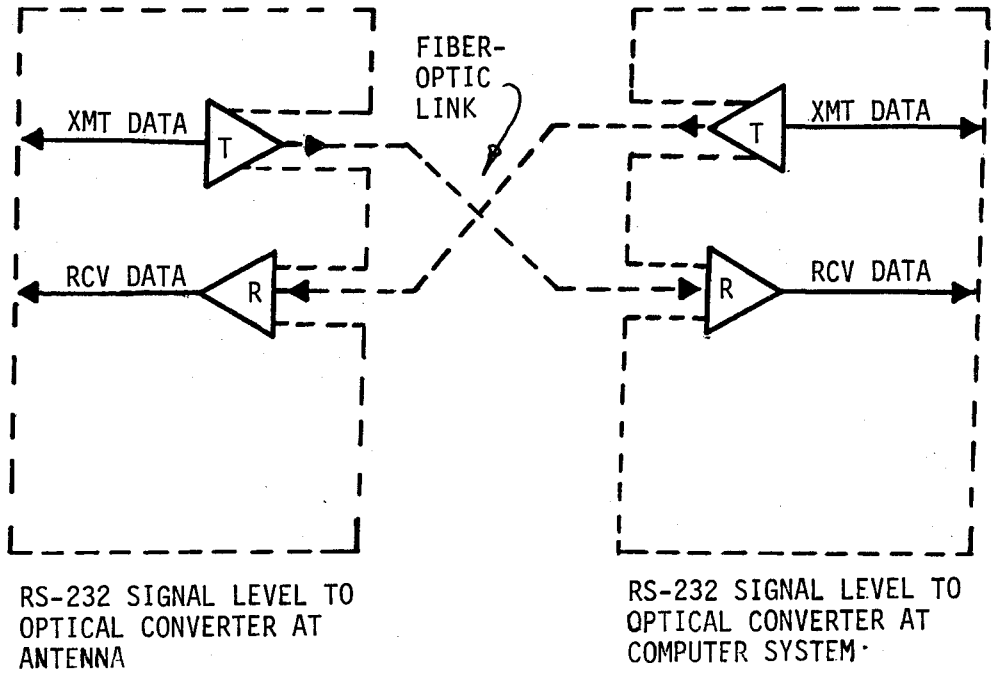


Figure C-6. Fiber-optic link block diagram.

stepper motor, controller, and gearing are set up to allow the desired half degree increment and the stepper motor holding torque is chosen such that the antenna structure is held in position during a signal strength measurement. The gears and drive chain are nonmetallic.

C.8 Program Control and Data Reduction

The antenna position control and the commands for data transfer are under program control by a portable computer system. The computer is housed in a van at least 10 wavelengths away from the antenna structure so that the van does not interfere with the measurements. As data is taken, it is reduced and checked for reasonableness given the location and ground conditions.

C.9 References

Jasik, H. (1961), Antenna Engineering Handbook, First Edition (McGraw-Hill Book Co., Inc., New York, NY), Chapter 3.

APPENDIX D: MONOPULSE RECEIVER

To enable system measurements to greater distances and weaker signal strengths, a receiver was developed employing digital monopulse techniques. A theoretical noise figure improvement in excess of 20 dB is expected.

The transmitter is phase modulated by a pseudorandom digital sequence to generate biphase signals. The receiver then duplicates this pseudo-random sequence for control of its biphase modulation in a synchronous detector. The result is an output to the computer of an analog signal that can be digitized and further processed. This system is a monopulse probe and ideally would produce a single pulse representing the continuous wave (cw) signal but in practice the pulse is distorted by multipath signals as well as propagation anomalies across the signal path.

The overall block diagrams are shown in Figures D-1 and D-2. Wide-band, low-noise amplifiers are used in the rf portions of the receiver to provide a very low noise figure with high dynamic range. The gain of this first stage is just large enough to overcome the losses in the first converter while the maximum power level at the 1 dB compression point is high to maintain a high receiver dynamic range. Wide bandwidth of the input amplifier and first converter has an inherent advantage of not restricting the usable operating range of the receiver. The actual operating frequency is determined by the local oscillator (LO) frequency injected from the front panel.

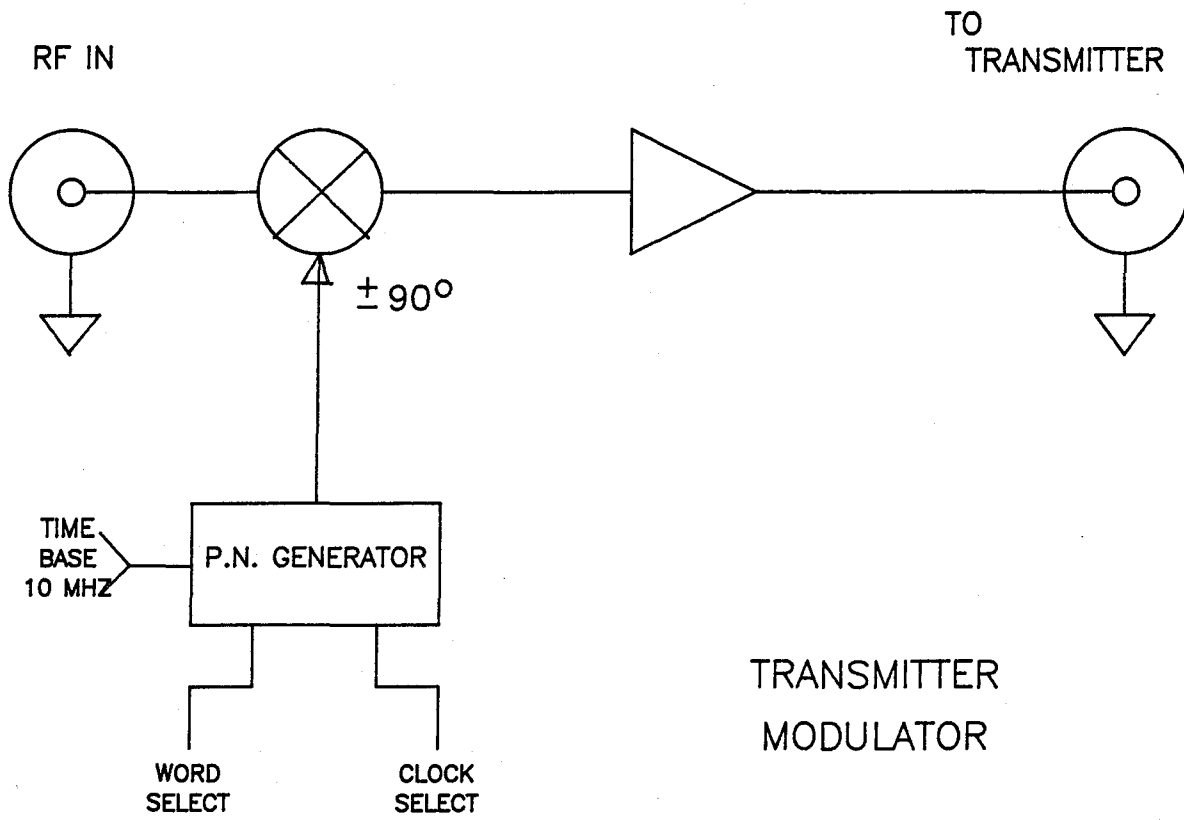


Figure D-1. Block diagram of the pseudorandom noise transmitter.

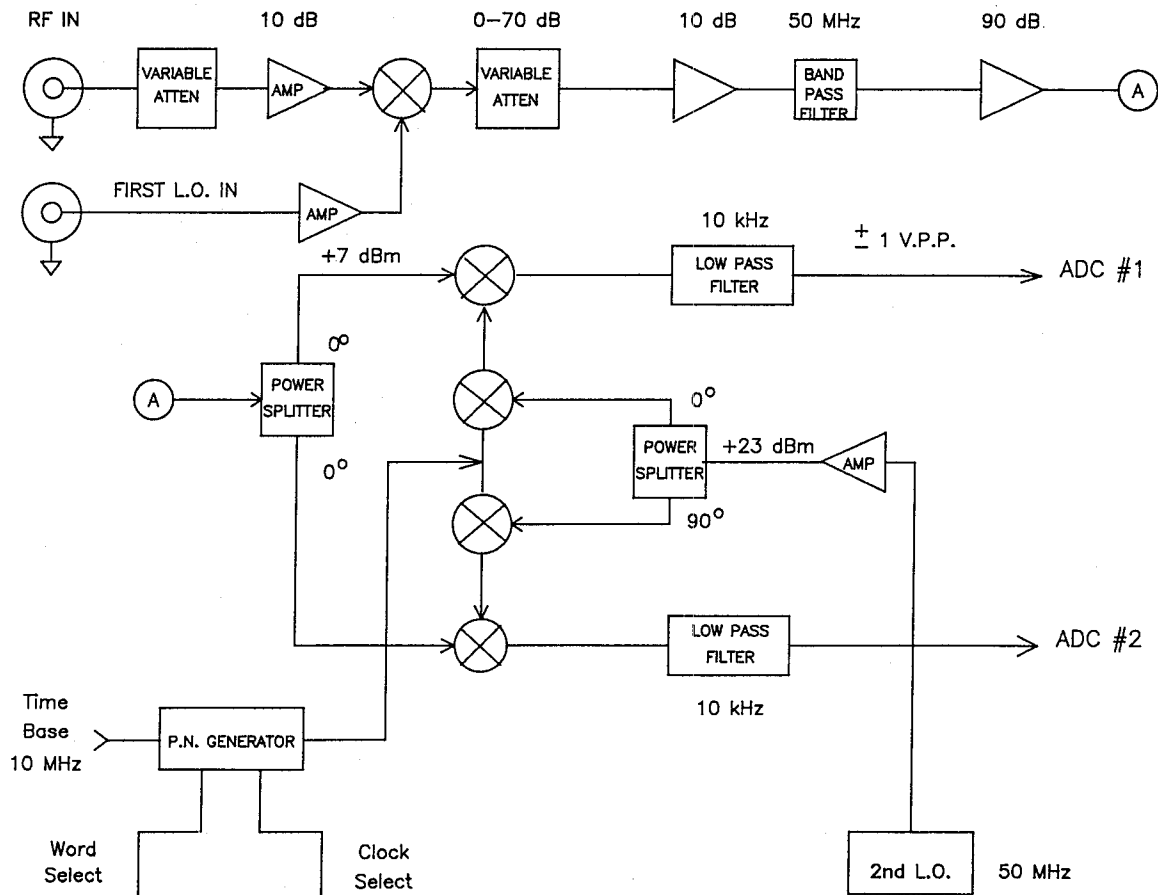


Figure D-2. Block diagram of the pseudorandom noise receiver.

The Intermediate Frequency (IF) amplifier is made up of a string of cascaded hybrid amplifiers to give a total available gain of 70 dB. A low noise amplifier is again used as the first stage in order to maintain a low noise figure. This stage feeds a filter, to restrict the bandwidth of the IF amplifier, and an attenuator, to allow control of the IF gain. With a high level output stage, the IF amplifier has a resulting 1 dB saturation level of +25 dBm. The overall dynamic range of the receiver is from -110 dBm to -10 dBm or 100 dB total.

The phase detector stage is designed using high level, balanced mixers to provide several functions without the need for active stages. Phase splitting, phase switching, detection, and quadrature output are accomplished while requiring only high level drive from the beat frequency oscillator (BFO) at a fixed frequency of 50 MHz.

The BFO is a x5 multiplier stage from the 10 MHz standard frequency output from the LO synthesizer. Its residual 10 MHz harmonics are at a level of 50 dB down from the 50 MHz output. Amplifiers in the 50 MHz chain boost the BFO level to +25 dBm required to maintain high dynamic range in the receiver.

Signal output is filtered with matched 1 kHz low-pass filters in the in-phase (I) and quadrature phase (Q) detected outputs. From here the signals go to the A/D inputs to the computer for processing of the received signals. Analog special-function devices are included in the output stage of the detector to provide the sum-of-squares output for monitoring and testing.

Digital functions are provided on a digital logic board. Included are selectable word lengths of 31, 63, 127, and 255 bit word lengths, and selectable data rates of 1 MHz, 100 kHz, and 10 kHz. A phase-lock loop provides the scan offset of either 1 kHz or 100 Hz. A special frequency divider is provided for oscilloscope synchronization to the P N word.

BIBLIOGRAPHIC DATA SHEET

1. PUBLICATION NO. NTIA Report 84-151		2. Gov't Accession No.	3. Recipient's Accession No.
4. TITLE AND SUBTITLE Measurements and Predictions of HF Ground Wave Radio Propagation over Irregular, Inhomogeneous Terrain		5. Publication Date July 1984	
*Continued: 7. AUTHOR(S) J. E. Adams, J. C. Carroll, E. A. Costa, D. R. Ebaugh, Jr., J. R. Godwin, E. J. Haakinson,		6. Performing Organization Code ITS.S4	
8. PERFORMING ORGANIZATION NAME AND ADDRESS U.S. Department of Commerce National Telecommunications & Information Administration Institute for Telecommunication Sciences Boulder, CO 80303		9. Project/Task/Work Unit No. 9104526	
11. Sponsoring Organization Name and Address Defense Nuclear Agency Washington, DC 20305		10. Contract/Grant No.	
		12. Type of Report and Period Covered	
		13.	
14. SUPPLEMENTARY NOTES			
15. ABSTRACT (A 200-word or less factual summary of most significant information. If document includes a significant bibliography or literature survey, mention it here.) Measurements of radio propagation path loss were made over four paths in the 3 to 30 MHz band. The paths were of lengths up to 45 km in the Boulder, CO, area. They ranged from smooth to mountainous terrain, from open areas with few or no man-made structures to suburban areas with building heights up to three stories, and from open spaces with little vegetation to heavily forested regions. On one path, measurements were made with and without snow cover. The measurements were made in the daytime and because of the short paths, the primary mode of propagation was ground wave. Measurements of the ground constants at each of the four measurement frequencies were made at the transmitter site using the wave-tilt measurement technique. (Continued next page)			
* D. H. Layton, and D. Smith			
16. Key Words (Alphabetical order, separated by semicolons) Key words: HF ground wave; predictions and measurements; HF antenna with ground screen measurements; HF antenna on mobile measurements; propagation path loss; ground constants measurement; wave-tilt technique; irregular, inhomogeneous terrain			
17. AVAILABILITY STATEMENT <input checked="" type="checkbox"/> UNLIMITED. <input type="checkbox"/> FOR OFFICIAL DISTRIBUTION.		18. Security Class. (This report) Unclassified	20. Number of pages 140
		19. Security Class. (This page) Unclassified	21. Price:

15. ABSTRACT (Cont.)

One objective of gathering the HF propagation data was to compare the measurement results with ground wave propagation predictions made by a computer program that used the path profile, ground constants, and frequency as prediction parameters. The results of the predictions and the comparisons with the measured data are discussed.

Another objective of the measurement project was to describe the measurement technique and procedure in sufficient detail so that similar measurements could be made by others. The measurements were made with a fixed transmitter and mobile receiver and data collection system. Since measurements were made continuously while the receive van was in motion, position location information was determined by recording the vehicle's speedometer shaft rotation. Antenna gain measurements were made and are presented for the transmit antenna on a partial ground screen and for the receive antenna mounted on a van.